The Dissertation Committee for Feng Yan Certifies that this is the approved version of the following dissertation:

Biochemical and Spectroscopic Studies of (*S*)-2-Hydroxypropylphosphonic Acid Epoxidase in Fosfomycin Biosynthesis

Committee:

Hung-wen Liu, Supervisor

Eric V. Anslyn

Dean R. Appling

Brent L. Iverson

Christian P. Whitman

Biochemical and Spectroscopic Studies of (*S*)-2-Hydroxypropylphosphonic Acid Epoxidase in Fosfomycin Biosynthesis

by

Feng Yan, B.S.

Dissertation

Presented to the Faculty of the Graduate School of

The University of Texas at Austin

in Partial Fulfillment

of the Requirements

for the Degree of

Doctor of Philosophy

The University of Texas at Austin

December 2004

Biochemical and Spectroscopic Studies of (*S*)-2-Hydroxypropylphosphonic Acid Epoxidase in Fosfomycin Biosynthesis

Publication No._____

Feng Yan, Ph.D.

The University of Texas at Austin, 2004

Supervisor: Hung-wen Liu

Fosfomycin, produced by a few strains of *Streptomyces*, is a clinically useful antibiotic against both gram-positive and gram-negative bacteria. The unique structure of fosfomycin, characterized by a carbon-phosphorous bond and an epoxide ring, has attracted many attentions to its biosynthetic pathway. (*S*)-2-hydroxylpropanylphosphonic acid epoxidase (HppE) catalyzes the last step in the pathway, conversion of a secondary alcohol, (*S*)-2-hydroxylpropanylphosphonic acid ((*S*)-HPP), to the final epoxide product. This is a completely new enzymatic reaction in contrast to many other biological epoxidation reactions that usually involve olefin oxidation. It is worth noting that the oxygen atom in the hydroxyl group of (*S*)-HPP is retained during the ring closure.

The previous studies of HppE have led to the discovery of a novel biological epoxidation system, (*S*)-HPP + NADH + O_2 + $H^+ \rightarrow$ fosfomycin + NAD^+ + $2H_2O$. The further biochemical and EPR spectral analyses suggested that HppE is a new type of mononuclear non-heme iron-dependent enzyme carrying a 2-His-1-carboxylate triad iron-binding motif. In addition to three amino acid ligands, both phosphonate and hydroxyl groups of (*S*)-HPP also coordinate to the iron center in the enzyme-substrate complex. The bidentate substrate-binding mode is presumably responsible for the strict regiospecificity and stereospecificity in the HppE-catalyzed epoxidation.

A catecholate-to-Fe^{III} charge transfer complex was identified in the HppE active site, by UV-visible absorption and resonance Raman spectroscopies. The catechol is derived from a hydroxylated amino acid residue, Tyr105, as a product of the self-catalytic hydroxylation. The oxidation of Try105 to DOPA is a side reaction that occurs only in the absence of substrate, and the presence of DOPA has no apparent effects on the epoxidase activity of HppE.

Mechanistic information of HppE has been continuously garnered by EPR spectral analysis. Using NO as a dioxygen analogue and a probe for ferrous center, the first step of the catalytic cycle has been revealed to be the reduction of substrate-bound iron center from its ferric state to ferrous state by FMN/NADH. Besides, the presence of a spin-coupled adduct of protein-centered radical and ferric center has been supported by experimental evidence. However, it is still not clear whether the “hidden” radical plays any roles in HppE catalysis.

Table of Contents

List of Tables

List of Figures

Chapter 1: Background and Significance

1.1 THE ANTIBIOTIC FUNCTION OF FOSFOMYCIN

In 1929, Alexander Fleming discovered the antibacterial properties of penicillin and opened the era of antibiotics. Since then, a great variety of antibiotics have been developed and are widely used in fighting numerous bacteria that cause infections and diseases. A useful antibiotic must target reactions and/or structures within the bacteria (prokaryotic cells) that are different from the hosting organisms (eukaryotic cells). The most common targets are the processes and/or organelles involved in cell wall synthesis, protein synthesis, and DNA replication.

1.1.1 Cell Wall Biosynthesis

On the basis of the procedure developed by Christian Gram in 1884, in which heat-fixed cells are successively treated with the crystal violet dye and iodine, and then destained with either ethanol or acetone, bacteria are labeled as either Gram-negative or Gram-positive depending on whether or not they take up gram stain. Gram-positive bacteria take up the stain because they possess a mono-layered cell wall, while Gram-negative bacteria possess at least two structurally distinct layers and thus do not absorb dye. Both types of bacteria have a cell wall made up of covalently linked polysaccharide and polypeptide chains called peptidoglycan, which provides strength and shape to the bacterial cell, and allows bacteria to withstand the osmotic pressure generated by its hyperosmolar cytoplasm. The polysaccharide component of peptidoglycan

consists of linear chains of alternating β(1,4)-linked *N*-acetylglucosamine (NAG) and *N*-acetyl-muramic acid (NAM) (Figure 1-1). The lactyl side chain of the repeating NAG-NAM disaccharide unit forms an amide bond with a pentapeptide. These peptide subunits are cross-linked so that the overall structure is an interwoven network that surrounds the cell.

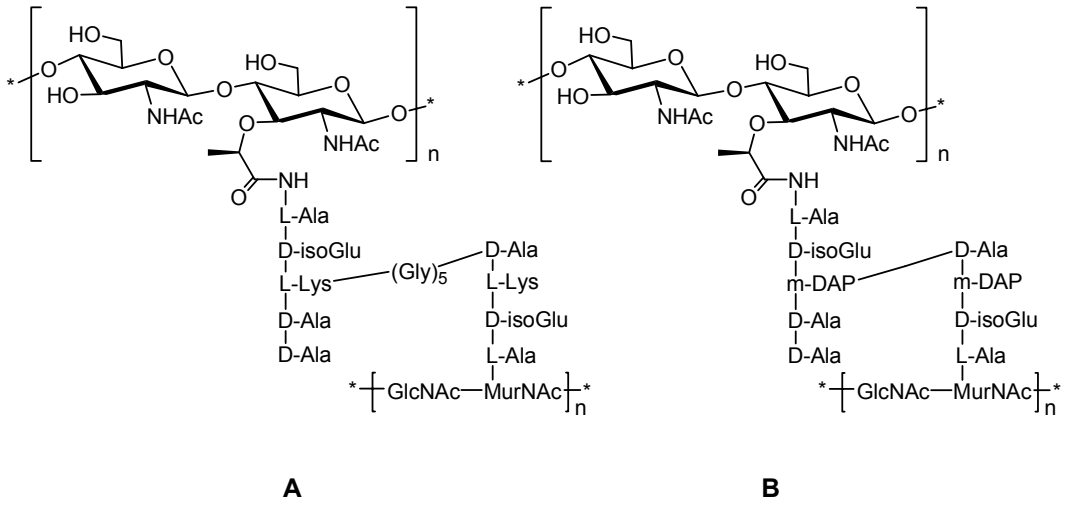

Figure 1-1. The peptidoglycan structures of Gram-positive (A) and Gram-negative (B) bacteria.

Peptidoglycan synthesis occurs in three distinct stages (Figure 1-2). The first stage, the formation of cell wall building blocks, UDP-acetylmuramyl-pentapeptide (UDP-MurNAc-pentapeptide), takes place in the cytoplasm. This stage is initiated by the conversion of uridine tri-phosphate (UTP) and *N*-acetylglucosamine α-1-P (GlcNAc-1-P, **1-1**) to UDP-GlcNAc (**1-2**). The second enzyme, UDP-GlcNAc-3-enolpyruvyl-transferase catalyzes the coupling of a pyruvate enol ether moiety from phosphoenolpyruvate (PEP) to UDP-GlcNAc.

The newly formed UDP-GlcNAc-enolpyruvate (**1-3**) is then reduced by a NADPH-dependent reductase giving rise to the first key intermediate, UDP-*N*-acetylmuramic acid (UDP-MurNAc, **1-4**). In the subsequent steps, three amino acids and a preformed dipeptide D-alanyl-D-alanine are added sequentially to the carboxyl group of the muramic acid residue to form UDP-MurNAc-pentapeptide (**1-5**).

The second stage of peptidoglycan synthesis occurs in the membrane since all the enzymes involved in this stage are membrane-bound. MurNAc-pentapeptide is first transferred to a lipophilic carrier in the cytoplasmic membrane by a pyrophosphate bridge, followed by the coupling of *N*-acetylglucosamine from UDP-GlcNAc. The nascent product of these reactions is GlcNAc-β-(1,4)-MurNAc-(pentapeptide)-P-P-phospholipid. Subsequent transformations result in the addition of five glycines to the ε-amino group of lysine. In the next step, the modified disaccharide-pentapeptide is cleaved from its lipophilic carrier in the membrane and covalently linked to the GlcNAc end of a saccharide-peptide that is already attached to the bacterial membrane. At the same time, phospholipid will be regenerated and enter the next cycle to react with another product (**1-5**) of stage I.

The third and final stage of peptidoglycan synthesis takes place outside the cell. It involves the polymerization of the subunits and attachment of these units to the growing peptidoglycan chain. The new peptidoglycan is attached to the preexisting cell wall peptidoglycan by a transpeptidase reaction that crosslinks

peptide chains from two polymers, one end of which must possess a D-alanyl-D-alanine terminus.

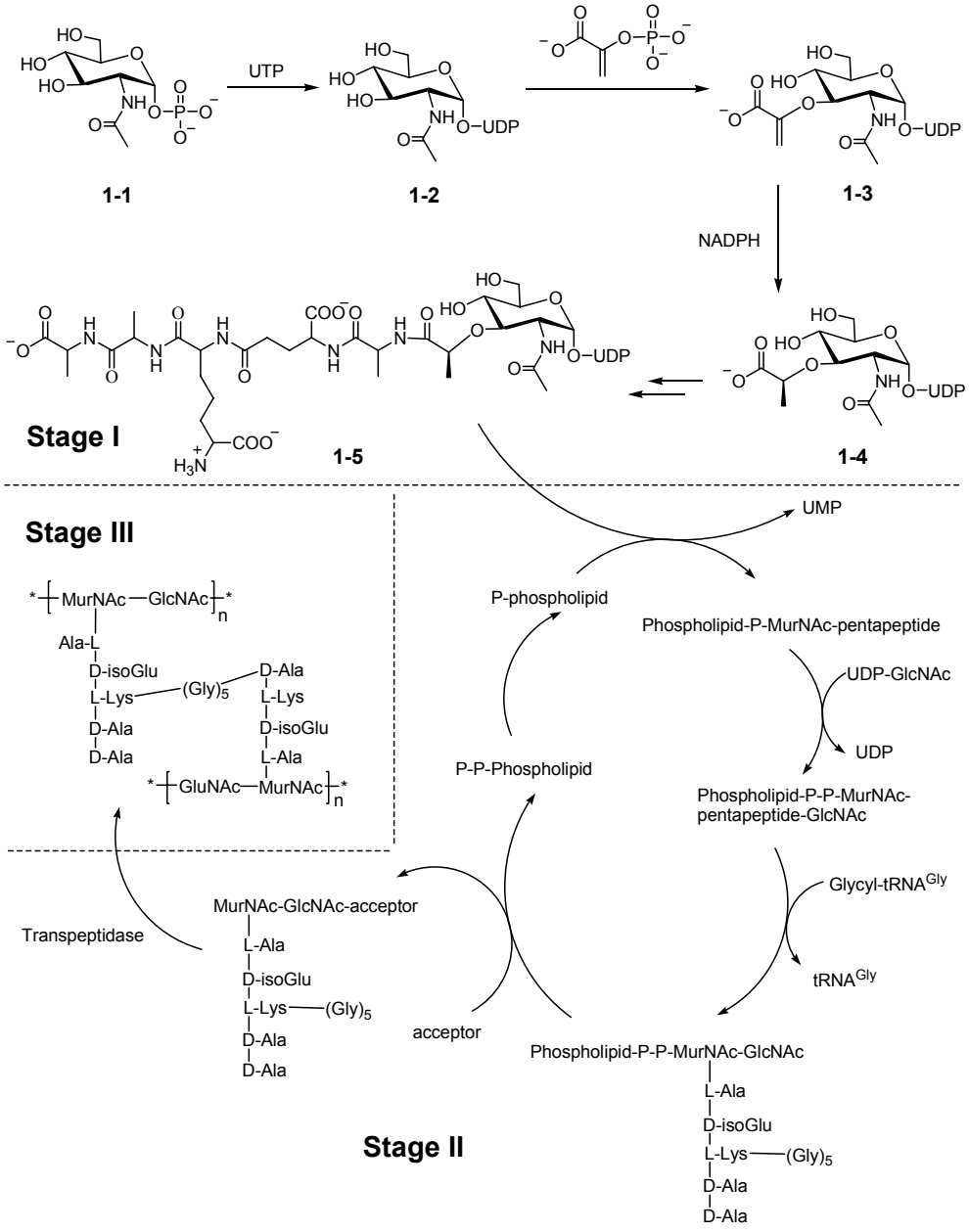

Figure 1-2. The peptidoglycan biosynthesis in Gram-positive bacteria.

1.1.2 The Antibiotic Function of Fosfomycin

The antibiotics that interfere the cell wall peptidoglycan biosynthesis have been proven effective in preventing bacterial growth. Without the restraining influence of the cell wall, the high osmotic pressure inside the cell will lead to the burst of the inner and/or outer membranes of bacteria. The antibiotics that are capable of inhibiting the synthesis of peptidoglycan include fosfomycin, cycloserine, bacitracin, β-lactams, and vancomycin.

Fosfomycin is a broad-spectrum antibiotic produced by some strains of *Streptomyces* (*1, 2*). The target of fosfomycin is UDP-GlcNAc-3-*O*-enolpyruvyl-transferase (MurA), which catalyzes the first committed step of peptidoglycan biosynthesis, namely, the transfer of enolpyruvate from PEP to UDP-GlcNAc (**1-2**), releasing inorganic phosphate as a by-product (Figure 1-2) (*3, 4*). MurA is conserved across both gram-positive and gram-negative bacterial species but has no mammalian counterparts. MurA is an essential enzyme in that its deletion from bacterial genome has been proven lethal (*5*). The mechanism of inhibition of MurA by fosfomycin has been well characterized, in which fosfomycin acts as an analogue of PEP, a cosubstrate of MurA (Figure 1-3). The negatively charged phosphonate moiety is important for anchoring fosfomycin in the active site of MurA with a proper orientation. The subsequent nucleophilic attack by the enzymatic active site Cys115 results in the ring opening of fosfomycin epoxide and the formation of a covalent adduct between MurA and fosfomycin (Figure 1-3) (*6, 7*). Since the C-P bond of fosfomycin is chemically inert, the resulting adduct is fairly stable. This is the mode of action in which fosfomycin

irreversibly inhibits the catalytic function of MurA. Because fosfomycin is not a close structural mimic of PEP, the antibiotic has no or little effect on the functions of many other PEP-dependent enzymes. This explains why fosfomycin has low toxicity toward mammals.

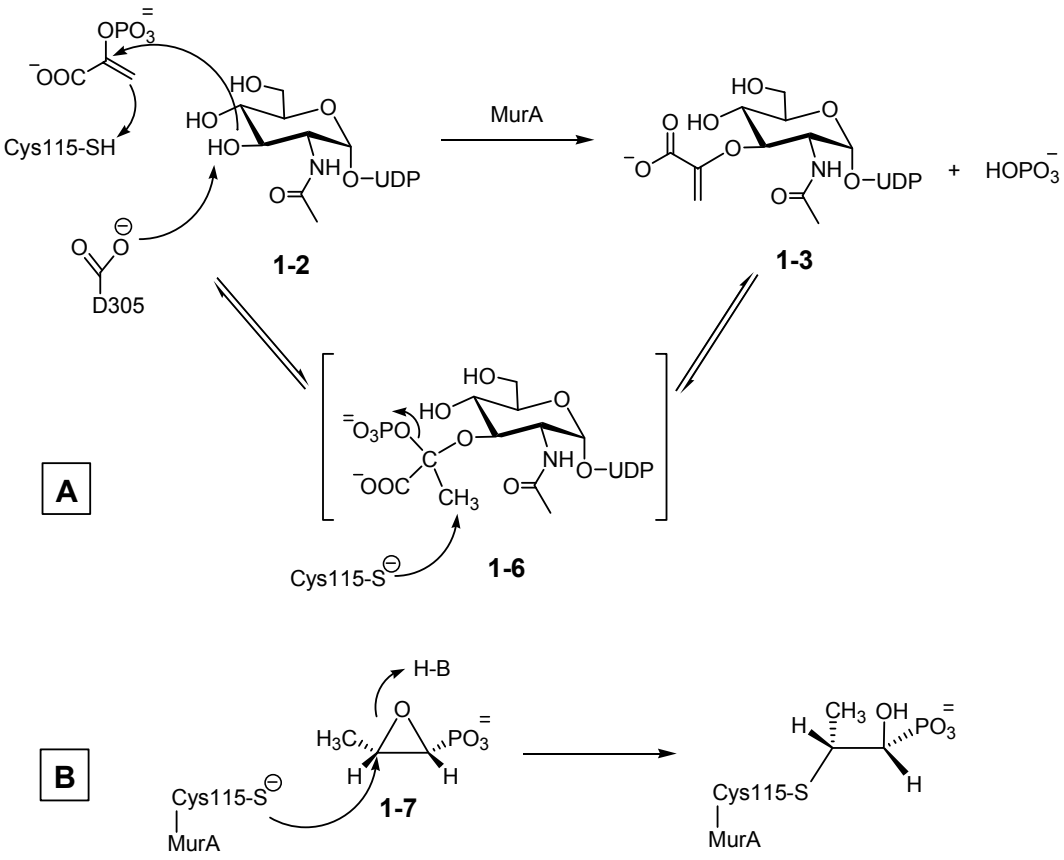

Figure 1-3. The catalytic mechanism of MurA (**A**) and the mechanism of MurA inactivation by fosfomycin (**B**).

Fosfomycin utilizes two uptake systems to gain entry into microorganisms: the L-α-glycerophosphate and the hexose phosphate transport systems (*8*). Because of the difference in the uptake of fosfomycin, bacteria exhibit various

levels of sensitivity to fosfomycin. Most resistant strains are found to be defective in one of the transport systems (*9, 10*). Besides decreased antibiotic uptake, resistance to fosfomycin can be achieved by several other mechanisms, e.g., enzymatic modification of the antibiotic (*11*) and overexpression of MurA (*12*). In addition, MurA containing a Cys115Asp mutation was found to be catalytically active but resistant to fosfomycin (*6*).

1.2 FOSFOMYCIN BIOSYNTHESIS

Structurally, fosfomycin belongs to a steadily growing family of natural products containing a C-P bond (*13*). Members of this family, such as fosfomycin (**1-7**), aminoethylphosphonic acid (AEP, **1-8**), and bialaphos (**1-9**), are all derived from phosphoenolpyruvate (PEP, **1 -10**) (*14*). The C-P bonds in

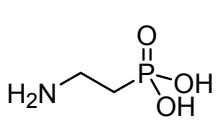

1-8

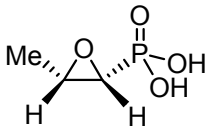

1-7

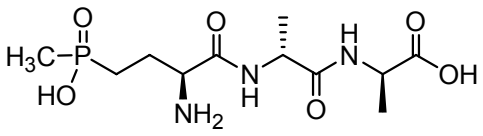

1-9

these compounds are formed through an intramolecular rearrangement reaction catalyzed by PEP mutase, resulting in the conversion of PEP (**1-10**) to phosphopyruvate (PnPy, **1-11**) (Figure 1-4) (*15-17*). Since the equilibrium between PEP and PnPy highly favors the cleavage of the C-P bond, the decarboxylation catalyzed by a second enzyme, PnPy decarboxylase, which converts PnPy (**1-10**) to phosphonoacetaldehyde (PnAA, **1-12**), provides the driving force to shift the equilibrium to favor the C-P bond formation (*18*).

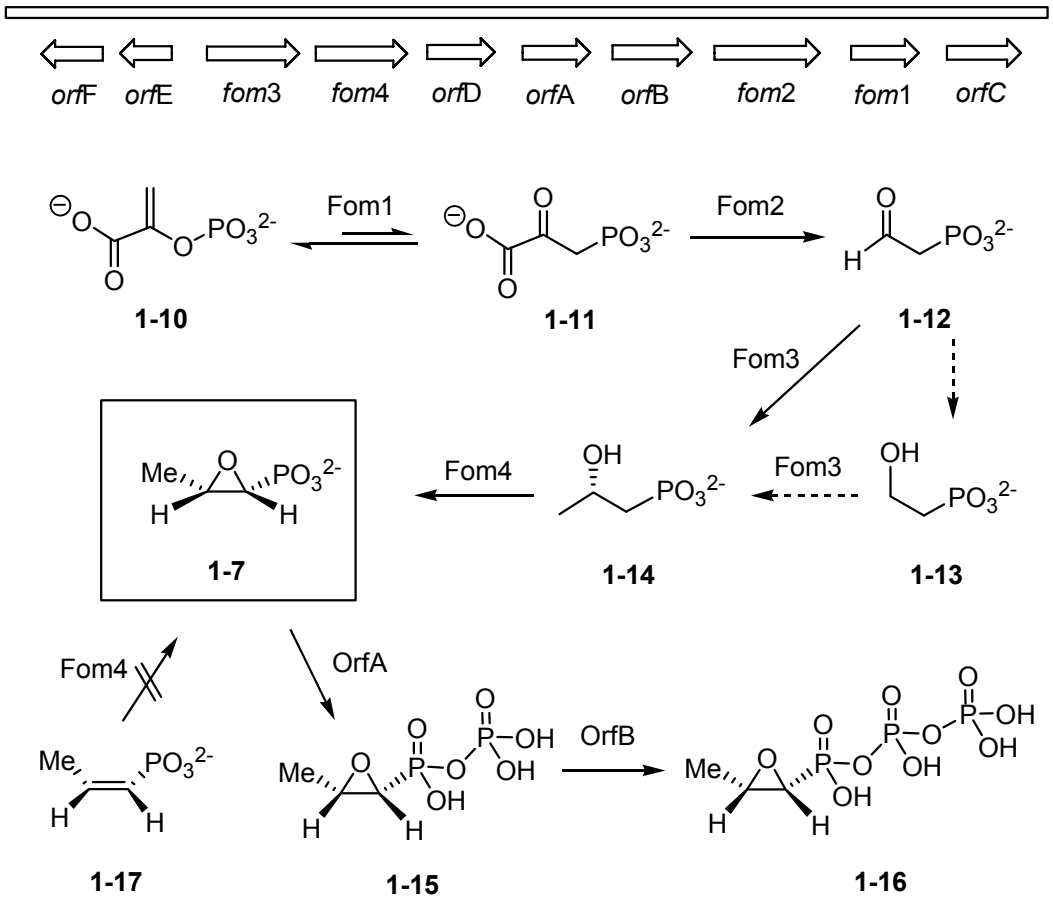

Figure 1-4. The gene cluster and pathway of fosfomycin biosynthesis in *Streptomyces wedmorensis*.

1.2.1. Fosfomycin Biosynthetic Pathway

Recently, the entire fosfomycin biosynthetic gene cluster has been cloned from *Streptomyces wedmorensis* (Figure 1-4) (*18*), and part of the gene cluster *from Pseudomonas syringae* has also been isolated (*19*). Ten genes have been identified in the gene cluster from *S. wedmorensis*. Accordingly, the biosynthesis of fosfomycin has also been proposed to involve at least four steps

(Figure 1-4) (*18*). In contrast to the early transformations involved in C-P bond formation that have been well established and characterized, little is known about the remaining steps of the biosynthesis of fosfomycin.

To explore the later stages of fosfomycin biosynthesis, a mutant of fosfomycin producing strain, NP-7, was constructed, in which the second step in the biosynthetic pathway is blocked. In the absence of self-produced PnAA (**1-12**), this mutant strain can convert hydroxyethylphosphonic acid (HEP, **1-13**) (*20*) and 2-hydroxypropylphosphonic acid (HPP, **1-14**) (*21*), respectively, to fosfomycin. Interestingly, no fosfomycin was produced upon feeding *cis*-propenylphosphonic acid (PPOH, **1-17**) to the strain (*21*). On the basis of these findings, a methylation step and an epoxidation step were proposed as part of a minimum pathway to complete fosfomycin biosynthesis (Figure 1-4).

As indicated by the radiolabeling experiments, the 2-methyl group of fosfomycin is derived from methionine (*22*). The identity of the methyl source has been confirmed by utilizing another mutant strain of *S. wedmorensis*, A-16, which lacks the ability to synthesize cobalamin (*23*). A-16 can convert PnAA (**1-12**) or its equivalent HEP (**1-13**) to fosfomycin in the presence of endogenous cobalamin, by incorporating [$^{14}CH_3$]-group from [$^{14}CH_3$]methylcobalamin into fosfomycin (*23*). This result strongly supports the presence of a methyltransferase that is dependent on methylcobalamin for its activity and catalyzes the addition of a methyl group to a two-carbon intermediate in fosfomycin biosynthetic pathway. This two-carbon intermediate may either be PnAA (**1-12**) or HEP (**1-13**).

After the above steps, an epoxidation reaction is necessary to produce fosfomycin. In nature, most epoxide rings are generated via oxidation of the corresponding alkenes by either heme-dependent cytochrome P450s (*24, 25*) or non-heme iron-dependent monooxygenases (*26*). However, all attempts to convert PPOH (**1-17**) to fosfomycin by mutant NP-7 failed. Instead, NP-7 can produce fosfomycin upon feeding with HPP (**1-14**) (*21*). Further evidence supporting HPP as the immediate precursor for fosfomycin was provided by Hammerschmidt *et al.* (*27, 28*). When *S. fradiae* was fed with ^{18}O-labeled HEP (**1-13**) in their experiments, ^{18}O was found to be incorporated into fosfomycin.

The function of two more genes, *orfA* and *orfB*, in the fosfomycin biosynthesis gene cluster from *S. wedmorensis* have recently been established as self-resistance genes (*29*). The encoded proteins of these two genes inactivate fosfomycin by adding one phosphate group at a time to the phosphonate group to give a biologically inert product, **1-16**.

1.2.2. Methyltransferase (Fom3)

Four genes have been tentatively assigned to encode the putative enzymes responsible for the four proposed steps (Figure 1-4). The assignments of genes *fom1* and *fom2* to encode the enzymes involved in C-P bond formation have been biochemically verified. The gene product of *fom3* is believed to be responsible for the methylation step.

As previously stated, methylcobalamin is likely the methyl source for the methylation reaction catalyzed by Fom3, a putative methyltransferase (*23*). As the carbonyl carbon of PnAA (**1-12**) is electrophilic, it is unlikely the methyl

source is a methyl cation supplied by *S*-adenosyl-L-methionine (SAM), which is the most common methyl donor in biological systems. Instead, the methylation reaction might involve a methyl anion or even a methyl radical derived from methylcobalamin. A similar case can be found in the formation of the second C-P bond in bialaphos biosynthesis (Figure 1-5). There are experimental evidence showing that this P-methylation is also dependent on methylcobalamin as the methyl donor (*30*). Since the phosphorus atom of the phosphinate group is electrophilic, its methylation may also proceed via a similar radical or anionic methyl transfer mechanism.

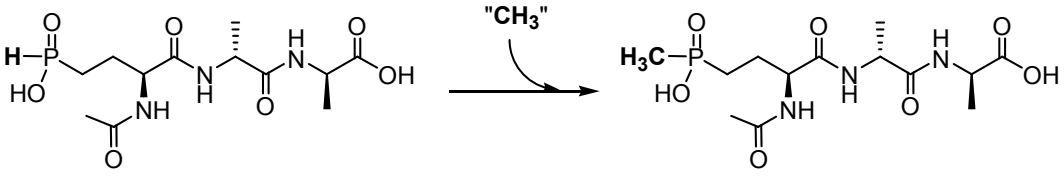

Figure 1-5. P-methylation reaction in bialaphos biosynthesis.

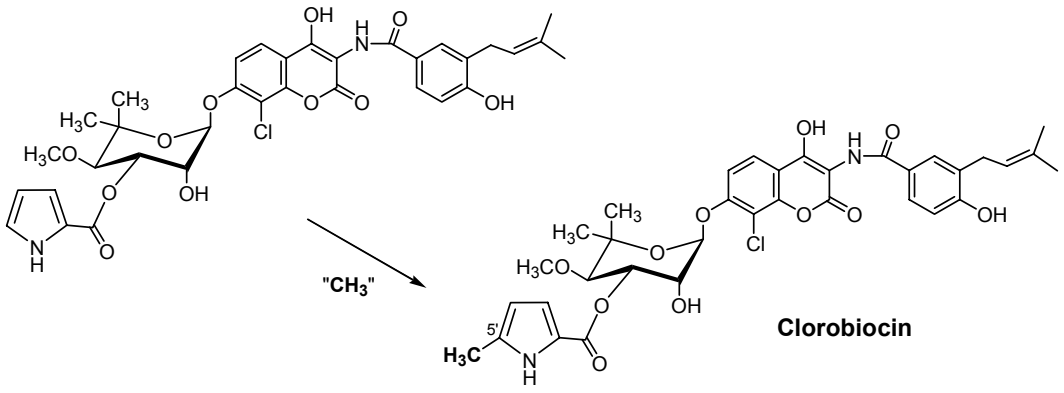

Figure 1-6. Methylation reaction in clorobiocin biosynthesis.

According to a recently reported protein sequence analysis (*31*), Fom3 enzyme contains not only a cobalamin-binding domain but also a radical SAM iron-sulfur binding domain. Along with the new finding, a group of sequence homologous methyltransferases were identified as well. Other than the aforementioned P-methylase in bialaphos biosynthesis, the so-called BchE-like/methyltransferase subgroup includes fortimicin KL1 methyltransferase (*32*) and CloN6 in clorobiocin biosynthesis (Figure 1-6) (*33*). Interestingly, the 5'-site of pyrrole ring is actually nucleophilic, which is opposite to the methylation sites in the cases of fosfomycin and bialaphos biosynthesis. This means that the CloN6-catalyzed methylation reaction may favor a methyl cation over a methyl anion as the methyl source. If we assume that all these enzymes proceed via a similar mechanism, the most likely scenario should be the transfer of a methyl radical from methylcobalamin.

A relevant enzymatic methylation system that may provide inspirations in understanding the above unprecedented type of methyltransferases is cobalamin-dependent methionine synthase (MetH). MetH catalyzes the final step in the *de novo* biosynthesis of methionine in *Escherichia coli*, formation of methionine (**1-19**) by a methyl transfer to homocysteine (**1-18**) from methylcobalamin (**1-24**) (Figure 1-7) (*34*). To regenerate methylcobalamin, a methyl group is transferred from methyltetrahydrofolate (CH_3-H_4folate) (**1-20**) to cob(I)alamin (**1-22**), forming methylcobalamin and H_4folate (**1-21**). Methionine synthase is a modular enzyme that binds CH_3-H_4folate (**1-20**), homocysteine (**1-18**), methylcobalamin (**1-24**), and SAM (**1-25**) in each of its four modules. During

catalytic turnover, a methyl cation is formally transferred from methylcobalamin (**1-24**) to the homocysteine (**1-18**) thiolate while another methyl cation is transferred from CH_3-H_4folate (**1-20**) to cob(I)alamin (**1-22**). Occasionally, cob(I)alamin (**1-22**) is oxidized to cob(II)alamin (**1-23**), which is inactive and needs to be converted to methylcobalamin (**1-24**) by a reductive methylation involving electron transfer from reduced flavodoxin and methyl group donation from SAM (**1-25**).

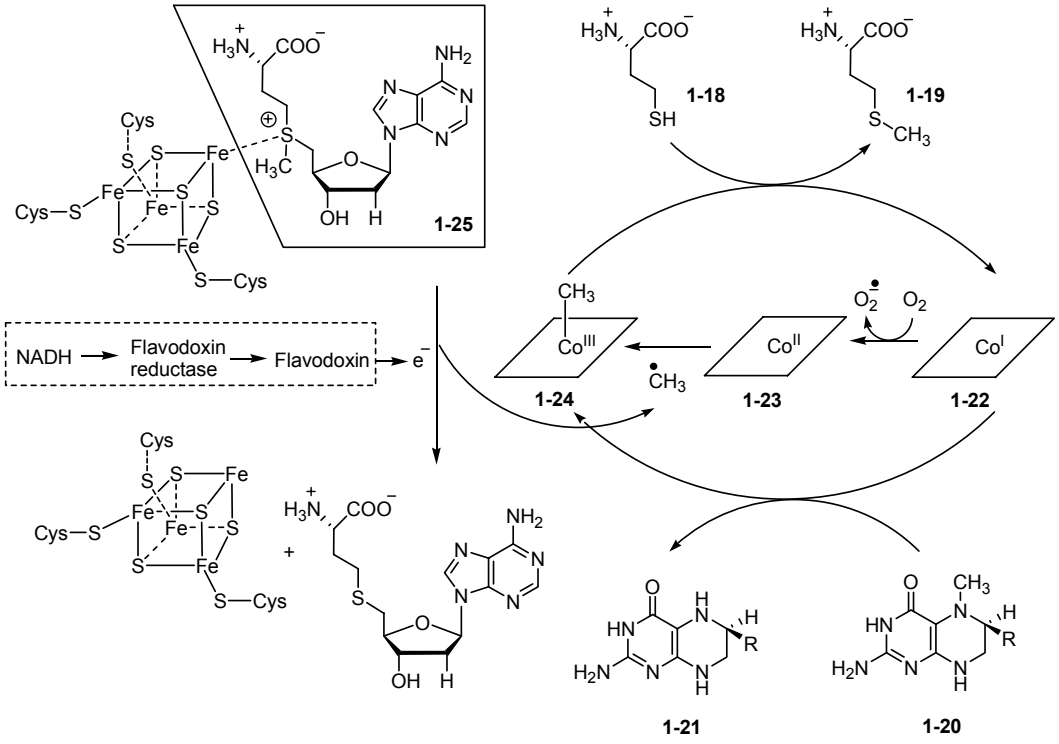

Figure 1-7. The hypothetic catalytic model of methionine synthase.

Combining all the information above, we attempt to propose a common catalytic mechanism for the enzymes in the BchE-like/methyltransferase subgroup. The mechanism is based on a radical methyl transfer from

methylcobalamin (**1-24**) to substrate radical that is pre-generated by radical SAM chemistry, forming cob(II)alamin (**1-23**) and product (X-CH_3). Similarly, the regeneration of methylcobalamin (**1-24**) needs another radical methyl transfer from SAM (**1-25**) to cob(II)alamin (**1-23**). This catalytic model takes advantage of the dual function of SAM to generate radical on substrate and to regenerate methylcobalamin. Both functions of SAM have been seen in several enzyme catalytic systems.

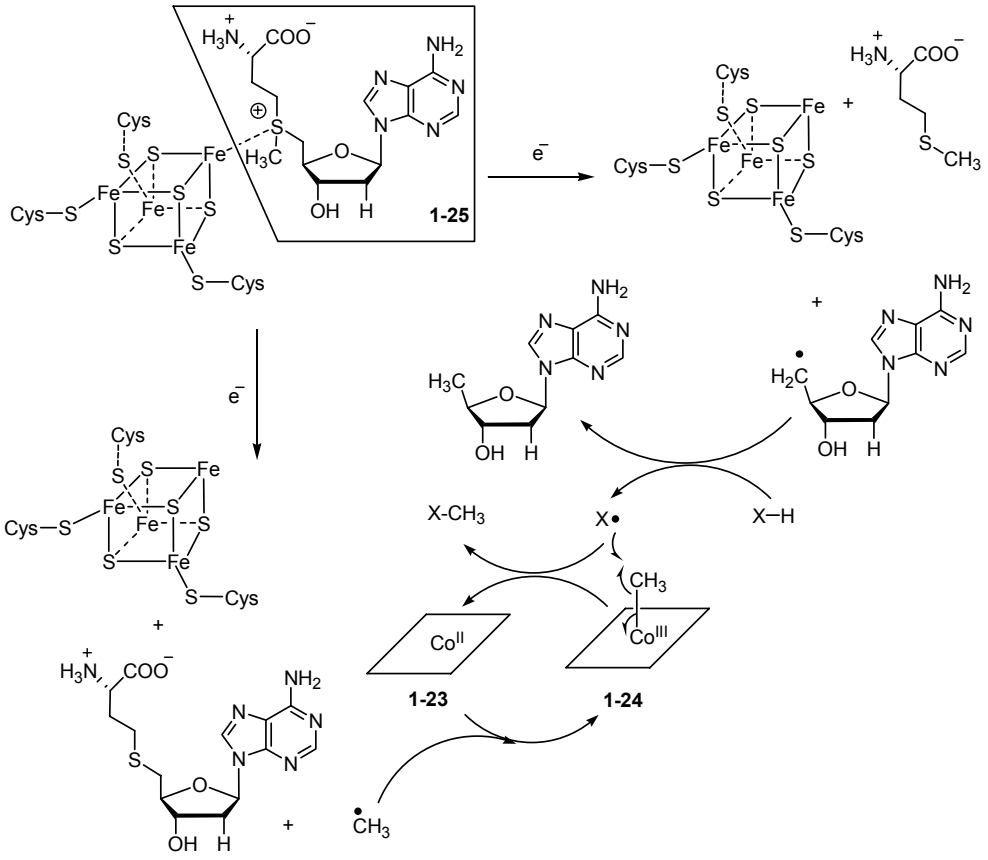

Figure 1-8. The hypothetic catalytic model of the putative enzymes dependent on both cobalamin and SAM for their activities.

1.2.3. Epoxidase (Fom4)

The final step in the proposed fosfomycin biosynthetic pathway is epoxidation. The gene *fom4* from *Streptomyces wedmorensis* encodes the epoxidase responsible for this reaction. In a separate effort, a *fom4* homolog, *orf*3, was also identified in the fosfomycin biosynthetic gene cluster from *Pseudomonas syringae* PB-5123 (*19*). Fom4 has been our primary research focus in studying fosfomycin biosynthesis. Since the isolated Fom4 was only an apoprotein, a considerable amount of work has been devoted to find conditions for reconstitution of the enzyme activity and to confirm its identity as the desired epoxidase (*35, 36*). Through this effort, Fom4 has been verified as the desired 2-hydroxypropylphosphonic acid epoxidase (HppE) that takes (*S*)-HPP (**1-14**) as the preferred substrate. The purified enzyme is capable of catalyzing the epoxidation reaction *in vitro* in the presence of an exogenous electron mediator, such as FMN. Preliminary characterization of HppE has established it as an NADH dependent mononuclear non-heme iron dependent enzyme.

In nature, the most common enzymatic epoxidation is olefin epoxidation. The responsible enzymes are either heme enzymes such as cytochrome P450s (*24, 25*) or non-heme iron enzymes such as methane monooxygenase (MMO) (*26*). Among them, P450s represent the largest group of natural epoxidases. The general mechanism of P450-catalyzed epoxidation is almost the same as that of heme monooxygenases (Figure 1-9) (*24*).

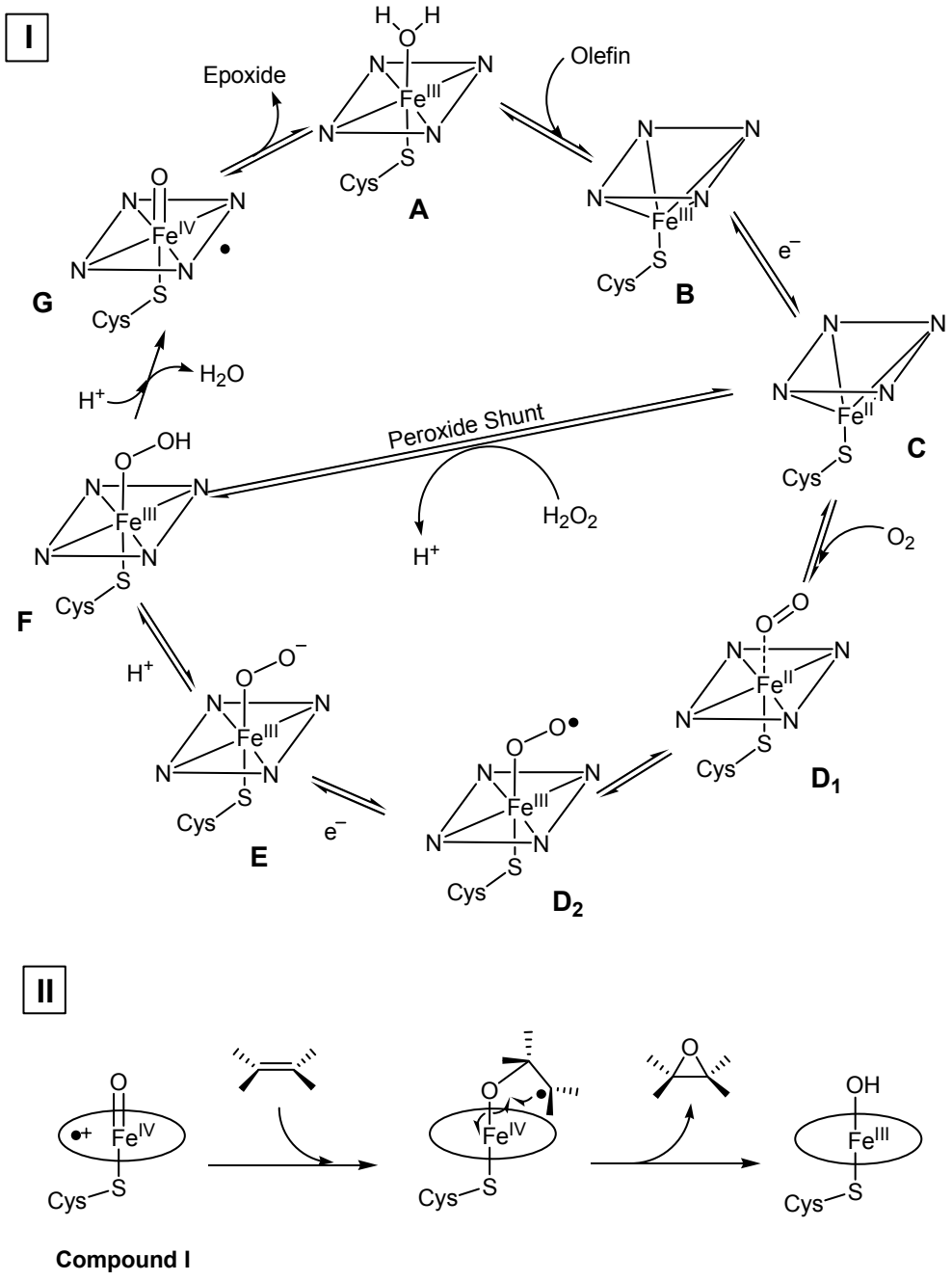

Figure 1-9. The catalytic model of olefin epoxidation catalyzed by P450s.

The resting state (**A**) is a six-coordinate low-spin ferric state with water (or hydroxide) as the exchangeable distal ligand trans to the proximal cysteine. The addition of olefin substrate results in a five-coordinate high-spin ferric state (**B**) with a vacant coordination site available for dioxygen binding. Accompanied with the conversion of enzymatic ferric iron from low to high spin is a significant increase in the redox potential, which facilitates the reduction of ferric ion generating a five-coordinate high-spin deoxyferrous state (**C**). Dioxygen binds to the ferrous center to form Fe^{II}-dixoygen (**D_1**) and Fe^{III}-superoxide (**D_2**) complexes in equilibrium. The second electron transfer is the rate-limiting step in the cycle, leading to the formation of Fe^{III}-hyperoxide (**E**) complex or its protonated equivalent Fe^{III}-hyperoxy complex (**F**). Upon further protonation of the distal oxygen in complex **F**, the O-O bond breaks heterolytically, generating the hypothetic compound I, the oxoferryl ($O=Fe^{IV}$) porphyrin radical cation complex (**G**). For some P450 enzymes, H_2O_2 can react with ferric center to directly form **F** and its immediate product, **G** (compound I). This shortcut is called "peroxide shunt". It is generally accepted that the highly oxidative intermediate **G** is used to oxidize olefins to generate epoxides. Currently, there are at least two possible mechanisms that are used to describe the process of olefin epoxidation by **G**, stepwise mechanism (Figure 1-9 **II**) and concerted mechanism (not shown).

The ability to activate and transfer molecular oxygen into organic molecules is not restricted to the cytochrome P450 family. Some non-heme monooxygenases such as methane monooxygenase (MMO) are also able to

catalyze epoxidation reactions. The natural function of MMO is to convert methane to methanol in methanotrophic bacteria (*37*). MMO can also hydroxylate a wide range of substrates, including alkanes (*38*). MMO catalytic system consists of three separate protein components, a hydroxylase (MMOH), a reductase (MMOR) and a component B protein (MMOB). The central component is MMOH that contains a binuclear non-heme iron in the active site responsible for its activity of dioxygen activation and substrate oxidation.

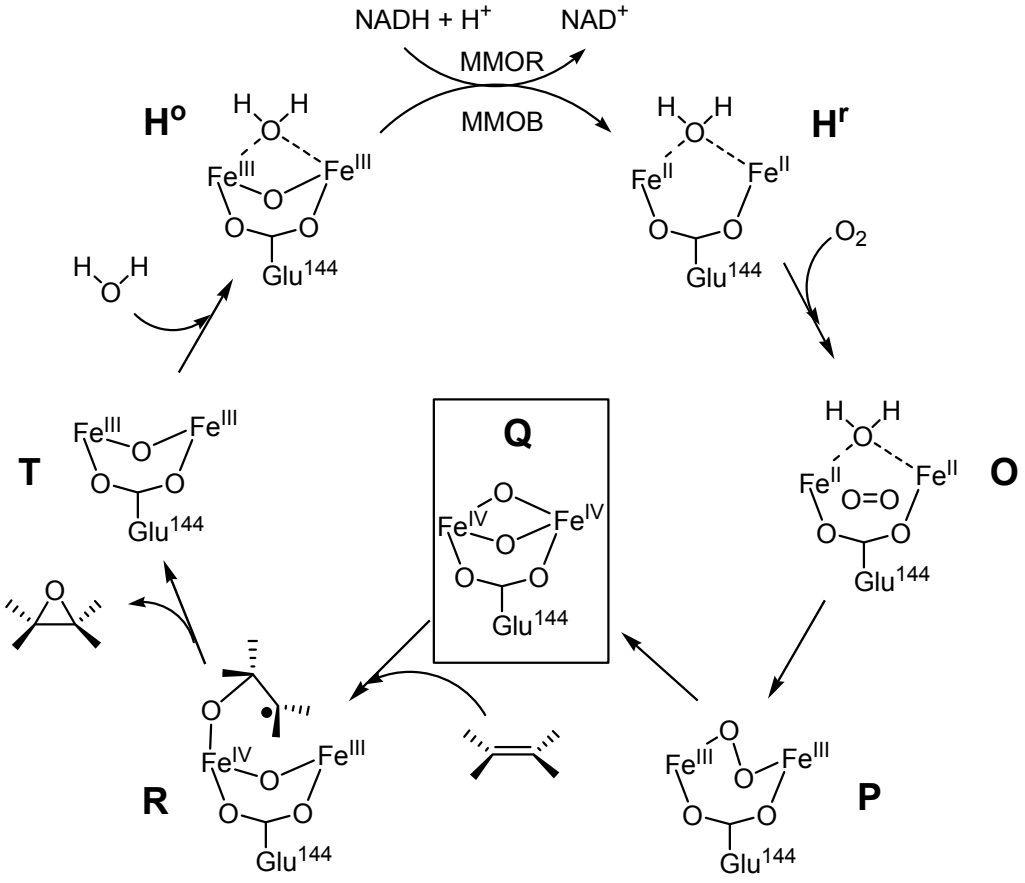

Figure 1-10. The catalytic model of olefin epoxidation catalyzed by MMO.

The established catalytic cycle of MMO starting with the resting state ($\mathbf{H^o}$), involves initial reduction by two electrons from MMOR and NADH to the reduced form $\mathbf{H^r}$ (Figure 1-10) (*39*). In the following step, dioxygen binds in the MMOH active site (**O**) and then oxidizes $\mathbf{H^r}$ to the intermediate **P**. As a result of further oxidation, a transient chromophoric species, intermediate **Q**, is formed. **Q** can be considered as the equivalent of compound I (**G**) in MMO non-heme iron catalytic system. It has been suggested to be the activated form of MMOH and the oxidative species responsible for substrate oxidation. Although the stepwise radical-based epoxidation mechanism by MMO is preferred and presented in Figure 1-10, other mechanistic alternates are also possible.

In contrast to the above alkene epoxidation catalyzed by P450s and MMO, alcohol epoxidation catalyzed by HppE is a rare case in nature. To date, there is only one precedent of such an epoxidation reaction, which is catalyzed by hyoscyamine 6β-hydroxylase (H6H) in the biosynthesis of scopolamine (**1-29**) (Figure 1-11) (*40, 41*). However, H6H belongs to the α-ketoglutarate dependent oxygenase family. Besides its epoxidase activity in conversion of both 6-hydroxyhyoscyamine (**1-27**) and dehydrohyoscyamine (**1-28**) to scopolamine (**1-29**), H6H can also catalyze the hydroxylation of hyoscyamine (**1-26**) to form 6β-hydroxyhyoscyamine (**1-27**) (Figure 1-11). Furthermore, the amino acid sequence analysis of HppE and H6H fails to show any sequence homology. These apparent differences between HppE and H6H strongly imply that these two epoxidation reactions would proceed through different mechanisms.

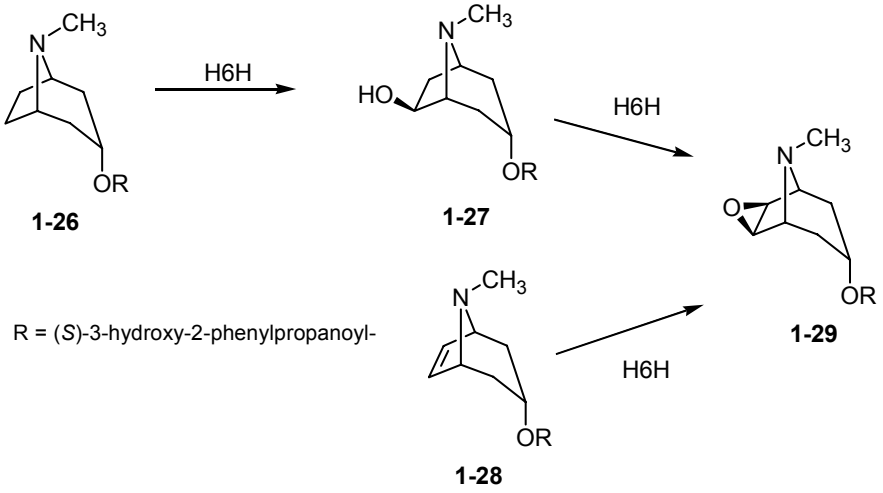

Figure 1-11. The hydroxylation and epoxidation reactions catalyzed by hyoscyamine 6β-hydroxylase.

Clearly, the alcohol epoxidation in the final step of fosfomycin biosynthesis catalyzed by HppE is unique among all enzymatic epoxidation reactions. Since HppE belongs to the family of mononuclear non-heme iron-dependent enzymes, it must share some common structural and functional characteristics with other enzymes of the family. Thus, learning knowledge of other mononuclear non-heme iron enzymes may shed light on the catalysis of HppE.

1.3 MONONUCLEAR NON-HEME IRON ENZYMES

Non-heme iron enzymes are known to catalyze a range of oxidative reactions more diverse than those associated with heme enzymes (*42, 43*). Depending on the type of reaction they catalyze and the cofactor(s) they need for their catalytic activities, they can be divided into a few categories (Table 1-1).

Except that intradiol dioxygenases and lipoxygenases are dependent on ferric ion, all other enzymes require ferrous ion for their activities. In the following sections, a brief review of each of the mononuclear non-heme iron enzymes listed in Table 1-1 is presented dealing in particular with their particular structural and catalytic features.

1.3.1. Lipoxygenase

Lipoxygenases (LOs) are a group of enzymes that catalyze regio- and stereospecific hydroperoxidation of 1,4-diene units in fatty acids (**1-30**) (*44, 45*). The produced hydroperoxide compounds (**1-33**) play important regulatory roles in animals (*44*) and plants (*45*). The X-ray structures of lipoxygenases show a clear picture of the enzymatic metal active site (*46*) (Figure 1-12). The iron center is coordinated with five amino acid ligands in a distorted octahedral geometry. The iron ligands in soybean LOs is slightly different from those in rabbit LOs (Figure 1-12, **I** vs. **II**). As shown in the proposed catalytic cycle (Figure 1-12, **III**), hydrogen abstraction is the key step in the whole reaction. Ferric hydroxide is believed to be the species that homolytically cleaves the C-H bond and creates a substrate radical (**1-31**) (*47*). The pentadienyl radical intermediate (**1-31**) then reacts with dioxygen giving rise to an organic superoxide radical intermediate (**1-32**). The reaction is completed with the formation of the hydroperoxide product and the oxidation of iron from ferrous state to ferric state. Under anaerobic conditions, the pentadienyl radical intermediate (**1-31**) could diffuse out of enzyme active site and react with each other. In support of the proposed mechanism, the resulting dimer has been experimentally detected (*48*).

Reaction Type	Representative enzyme	Catalytic reaction
Hydroperoxidation	lipoxygenase	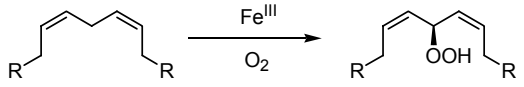
Intradiol dioxygenation	protocatechuate 3,4-dioxygenase	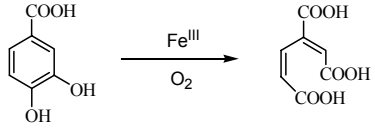
Extradiol dioxygenation	catechol 2,3-dioxygnease	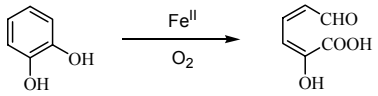
Pterin-dependent hydroxylation	phenylalanine hydroxylase	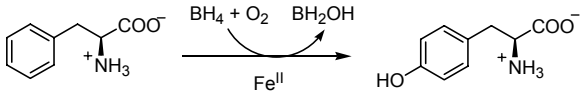
α-ketoglutarate-dependent oxidation	clavaminate synthase	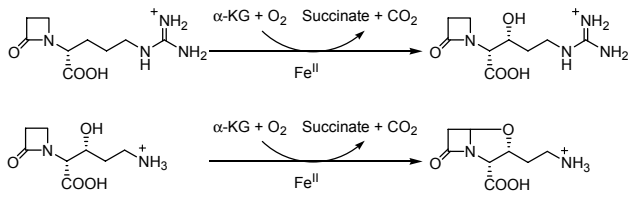
Four-electron oxidative ring closure	isopenicillin *N*-synthase	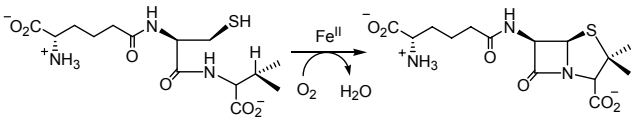
Ascorbate two-electron oxidation	1-amino-cyclopropane carboxylic acid oxidase	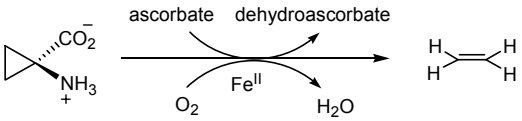
cis-hydroxylation	phthalate dioxygenase	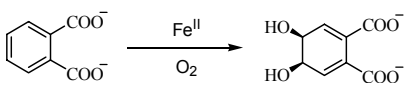

Table 1-1 Mononuclear non-heme iron enzymes and their reactions.

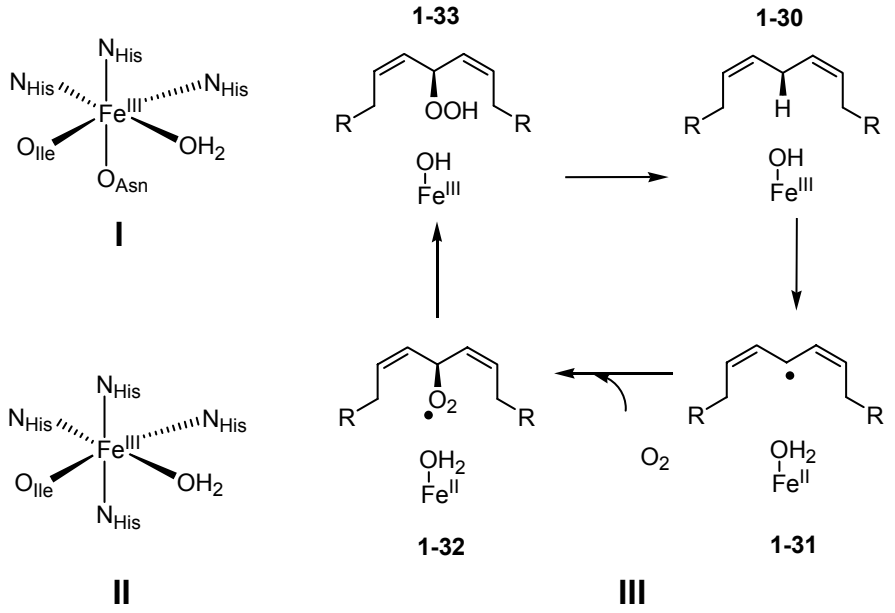

Figure 1-12. Lipoxygenase active site structure (**I**. Soybean LOs; **II**. Rabbit LOs) and the proposed hydroperoxidation mechanism.

1.3.2. Intradiol Cleaving Catechol Dioxygenase

The catechol dioxygenases are part of the bacterial machinery for aromatic ring degradation. They catalyze the oxidative cleavage of the aromatic ring of catechol and its derivatives (*49*). Catechol dioxygenases can be divided into two classes, intradiol and extradiol cleaving dioxygenases. The difference between them can be easily told by their names. Briefly, intradiol dioxygenases cleave the C-C bond of enediol unit while extradiol dioxygenases cleave the C-C bond adjacent to the enediol unit (Figure 1-13).

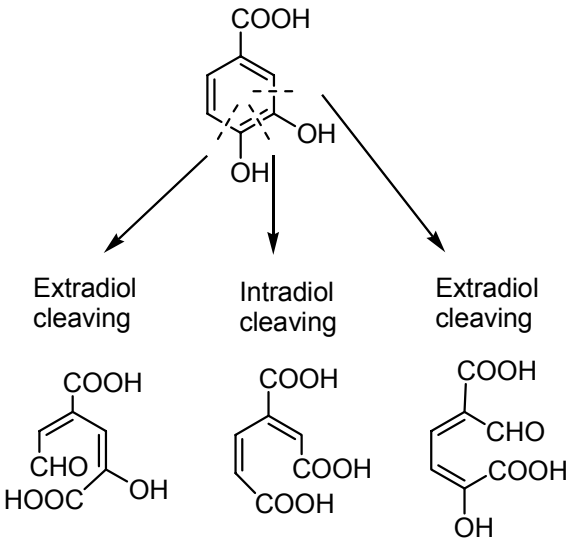

Figure 1-13 Product distribution of intradiol and extradiol dioxygenases.

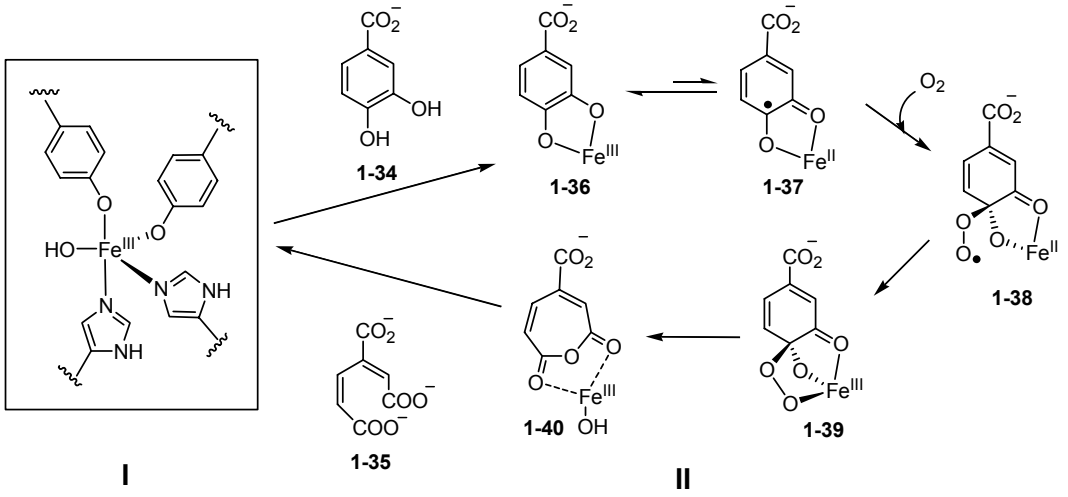

Figure 1-14 Intradiol cleaving catechol dioxygenases: active site structure (**I**) and proposed catalytic mechanism (**II**).

Intradiol cleaving dioxygenases utilize a mononuclear non-heme ferric ion for substrate binding and catalysis. The representative enzyme of this class is protocatechuate 3,4-dioxygenase (PCD). PCD has a trigonal-bipyramidal iron core in the active site that consists of two histidines, two tyrosines, and a hydroxide ion (*50*) (Figure 1-14, **I**). Both the axial and equatorial tyrosine ligands contribute the ligand-to-metal charge transfer (LMCT) bands, 500 nm and 450 nm, to the UV-vis absorption spectrum of the enzyme (*51*). These LMCT transitions give a characteristic red-brown color to the enzyme. When its substrate, protocatechuate (PCA, **1-34**), binds to the metal center, a new broad low-energy band appears around 600 nm, which has been assigned to another LMCT transition from the catecholate-to-Fe^{III} charge transfer complex (**1-36**) (*52*). Given that ferric ion cannot activate dioxygen, the key step in the proposed mechanism is the formation of an Fe^{II}-bound semiquinone intermediate (**1-37**). The intermediate **1-37** then binds dioxygen (**1-38**) to form a tri-bridged Fe^{III}-peroxy complex (**1-39**). The aromatic C-C bond cleavage is another key step, in which an anhydride (**1-40**) is formed via a Criegee rearrangement. Hydrolysis of the anhydride (**1-40**) gives the final ring-cleaved product (**1-35**). In an alternative mechanism, the Fe^{III}-peroxy complex (**1-39**) is proposed to proceed through a dioxetane rather than the anhydride intermediate (**1-40**) (*49*). However, the much less than 100% incorporation of oxygen atom in the final product from isotope-labeled dioxygen makes the former mechanism involving the anhydride intermediate a favorable one (*53*).

1.3.3. Extradiol Cleaving Catechol Dioxygenase

Catalyzing very similar types of catechol cleavage reactions, extradiol and intradiol dioxygenases are actually very different. Instead of using a ferric ion in their catalysis, the extradiol cleaving catechol dioxygenases, represented by 2,3-dihydroxybiphenyl 1,2-dioxygenase (1,2-DHBD), catechol 2,3-dioxygenase (2,3-CTD), and protocatechuate 4,5-dioxygenase (4,5-PCD), have a ferrous ion in their active site (*54*). Moreover, all of these enzymes have a common metal-binding motif, a 2-His-1-carboxylate facial triad (*54, 55*) (Figure 1-15 **I**).

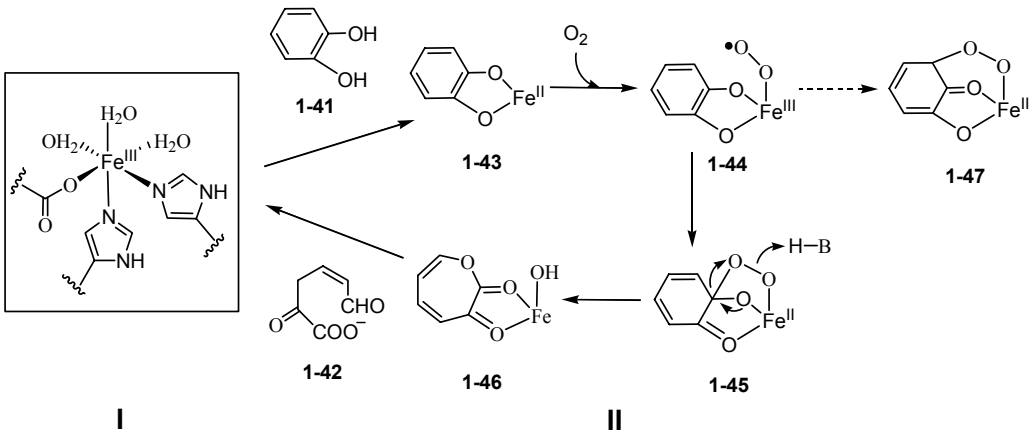

Figure 1-15 Extradiol cleaving catechol dioxygenases: active site structure (**I**) and proposed catalytic mechanism (**II**).

Like their intradiol counterpart, extradiol dioxygenases start the catalysis with the formation of an iron-catecholate complex (**1-43**). Since the extradiol dioxygenases have a ferrous active site, the enzyme substrate binary complexes have no visible colors. It is also because of the ferrous center, dioxygen can easily bind to the enzyme active site and be activated, generating a Fe(III)-

superoxide intermediate (**1-44**). Very similar to the intermediate **1-39** in the catalysis of intradiol dioxygenases (Figure 1-14), a tri-bridged iron peroxy intermediate (**1-45**) is also proposed (*49*). In the following step, the intermediate **1-45** undergoes a Criegee rearrangement that breaks down the aromatic ring by inserting an oxygen atom to it. It is worthy of noting that the Criegee rearrangements proposed in the catalytic cycles of intradiol and extradiol dioxygenases are different. The acyl group is transferred to the proximal oxygen atom in bound peroxy in the intradiol cleaving mechanism. In contrast, it is the alkenyl group that is transferred in the extradiol cleaving mechanism. The distinction between these two mechanisms is proposed to account for the different ring cleavage regiochemistry (**1-35** vs. **1-42**). There is an alternative way to explain the difference, in which another tri-bridged peroxy complex (**1-47**) is formed in place of complex **1-45**. Subsequent acyl transfer-based Criegee rearrangement should lead to the same product (**1-42**). However, in the crystal structure of enzyme-substrate-NO ternary complex (*56*), the dioxygen mimic NO seems to have access only to the C2 position rather than the C3 position on the aromatic ring, which is incompatible with the intermediacy of **1-47**. As a result, the alternative mechanism is disfavored.

1.3.4. Pterin-dependent Aromatic Amino Acid Hydroxylases

Pterin-dependent aromatic amino acid hydroxylases include phenylalanine (PheH), tyrosine (TyrH), and tryptophan (TrpH) hydroxylases (*57*). Like the above extradiol cleaving catechol dioxygenases, they are also dependent on Fe^{II} for activities. The metal binding ligands for these enzymes have been

established to consist of two histidines and one glutamate (*58*). The hydroxylation of aromatic amino acids is a two-electron redox reaction. To fully reduce dioxygen, however, requires four electrons in total. The other two electrons are provided by tetrahydrobiopterin (BH_4, **1-48**). The reaction is highly ordered. The binding of either aromatic amino acid substrate (**1-49**) or BH_4 (**1-48**) does not perturb the hexa-coordinated active site. Only when substrate and BH_4 are both bound, the resulting ternary complex becomes penta-coordinated, as indicated by the crystal structure of the ternary complex of PheH, BH_4 and substrate analogue (*59*). This structural change that results in an open coordinate site for dioxygen binding is presumed to facilitate the attack on pterin by dioxygen. Following O_2 attack is the formation of an Fe^{II}-O-O-pterin intermediate (**1-50**), which then heterolytically cleaves to yield 4a-hydroxy-BH_4 (**1-51**) and Fe^{IV}=O. The oxoferryl (Fe^{IV}=O) species has not been experimentally observed yet. However, it is believed to be responsible for substrate hydroxylation, because the pterin-dependent enzymes can carry out sulfoxidation, epoxidation, and benzylic hydroxylation that are usually associated with Fe^{IV}=O/porphyrin radical intermediate of cytochrome P450 (*57*). Arene hydroxylation is often accompanied by NIH shift (2-H/D shift, Figure 1-16), which is due to the formation of a cationic intermediate during the oxo atom transfer (**1-53**). The formation of the intermediate **1-50** and its subsequent heterolysis are the center of the proposed mechanism. The isotope-labeling studies revealed nearly quantitative incorporation of ^{18}O from $^{18}O_2$ in both 4a-

hydroxy-BH_4 (**1-51**) (*60*) and the hydroxylated product (**1-54**) (*61*). The result implicitly supports the proposed mechanism (Figure 1-16).

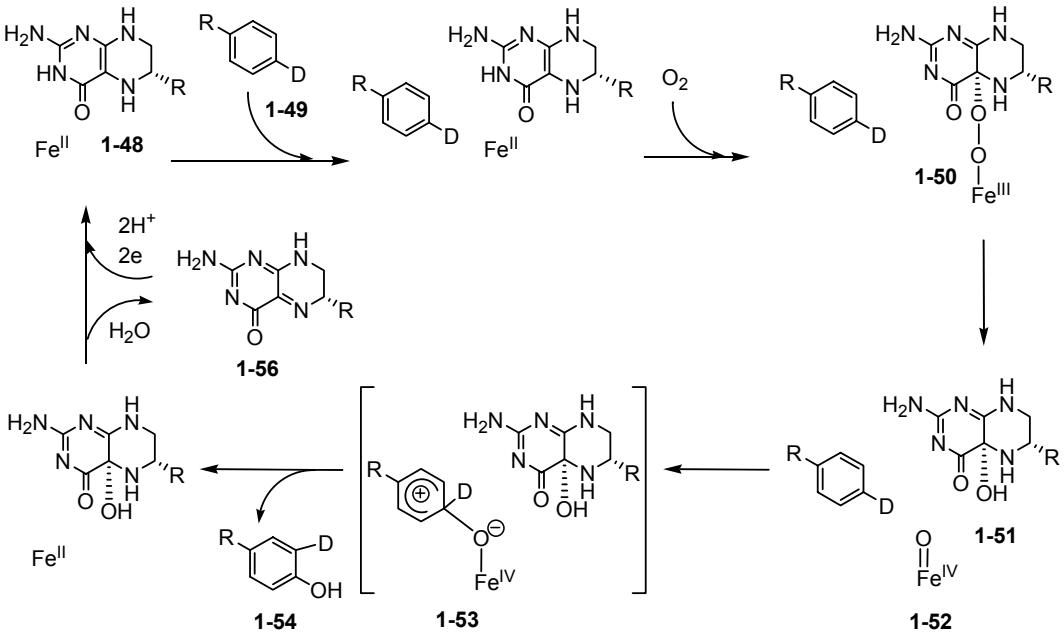

Figure 1-16 The proposed catalytic mechanism of pterin-dependent aromatic amino acid hydroxylases.

1.3.5. α-Keto Acid-dependent Dioxygenases

Enzymes that require an α-keto acid as a cosubstrate comprise the largest group of mononuclear nonheme iron-dependent enzymes (*62*). Like pterin-dependent hydroxylation, α-keto acid-dependent oxidation also needs totally four electrons to fully reduce dioxygen. Besides two electrons generated from substrate oxidation, α-keto acid donates the other two electrons. Again, enzymes in this subfamily all have a 2-His-1-carboxylate iron-binding motif in their active site (*55*). Their catalytic functions rely on the ferrous center for dioxygen

activation. A good example that illustrates the great catalytic diversity of this subfamily of enzymes is clavaminate synthase (CAS). Dependent on α-ketoglutarate (α-KG), CAS catalyzes three different types of reactions, hydroxylation, cyclization and desaturation (Table 1-1). In each of the reactions, the substrate turnover is coupled with the oxidative cleavage of an α-KG molecule.

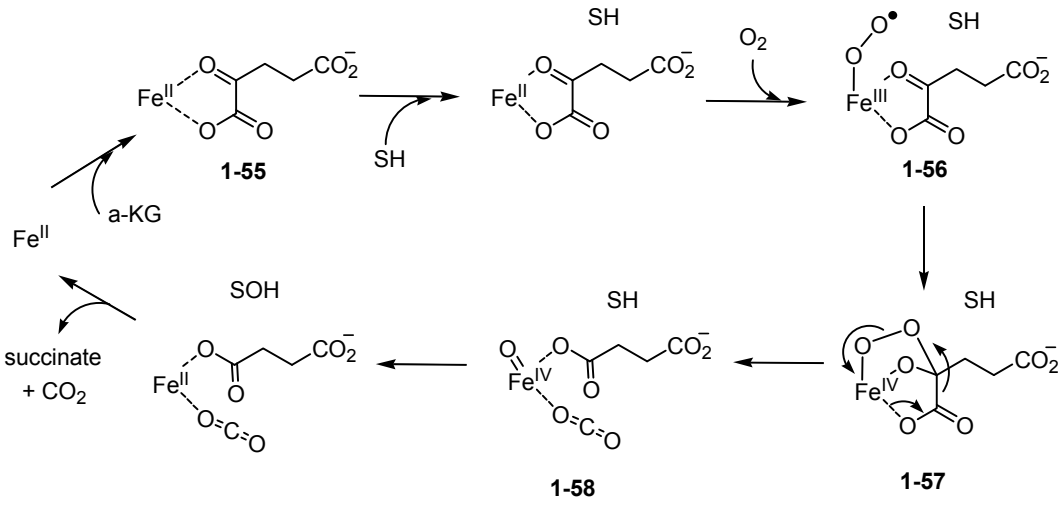

Figure 1-17 The proposed catalytic mechanism of α-keto acid-dependent hydroxylases.

From the mechanistic point of view, α-keto acid-dependent dioxygenases are probably the best-studied class of mononuclear non-heme iron enzymes. When α-keto acid binds to the enzymatic ferrous center in a bidentate pattern (**1-55**, Figure 1-17), a typical metal-to-ligand charge transfer (MLCT) band appears in the UV-vis absorption spectrum of the binary complex (*63*). Accompanying with substrate binding, the ferrous center becomes penta-coordinated leaving one site open for dioxygen binding (*64*). The molecular oxygen would then bind to

the ferrous center at the open site to form an Fe^{III}-superoxo radical anion intermediate (**1-56**). In the next step, the iron-bound activated dioxygen attacks the α-keto carbon, giving rise to a tri-bridged intermediate (**1-57**), which is reminiscent of the structurally similar intermediates **1-39** (Figure 1-14) and **1-45** (Figure 1-15) in earlier discussions. The following Criegee rearrangement with an acyl transfer results in the decarboxylation of α-keto acid, and, more importantly, the generation of an Fe^{IV}-oxo species (**1-58**). The involvement of this high valent iron-oxo intermediate (**1-58**) in the catalytic cycle has long been speculated and was strongly supported by a recent rapid freeze-quench Mössbauer study (*65*). The experimentally trapped intermediate shows characteristic spectral features of Fe^{IV} and is catalytically competent capable of taking hydrogen atom from substrate (*66*). This is the first time that such an intermediate is spectroscopically observed. Some enzymes in this class can catalyze olefin epoxidation, sulfoxidation, and N-demethylation, a typical reactivity pattern of reminiscent of cytochrome P450s (*67*), which also supports the participation of the Fe^{IV}-oxo species in the catalytic mechanism of α-keto acid-dependent enzymes. In the postulated two-step process of substrate hydroxylation, the hydrogen atom is first abstracted by the Fe^{IV}-oxo species, which is followed by oxygen rebound. However, it is worthy of noting that P450 uses the Fe^{III}/Fe^{V}=O couple, while the α-keto acid-dependent enzymes use the Fe^{II}/Fe^{IV}=O couple. For enzymes that catalyze cyclization and desaturation like CAS, the oxygen rebound step in the hydroxylation reaction is replaced with a ring closure or a second hydrogen-abstraction reaction.

Similar to the proposed catalytic cycles of pterin-dependent hydroxylases (Figure 1-16), the reactions catalyzed by α-keto acid-dependent enzymes can also be divided into two half-reactions. The first half-reaction is to form an oxoferryl oxidative species at the expense of α-keto acid, while the second half is to use the oxoferryl species to oxidize substrate. The presence of substrate is essential to couple these two half-reactions. In the absence of substrate, uncoupled oxidation of cofactors often led to side reactions, such as protein self-modification (*68, 69*).

1.3.6. IPNS and ACCO

Isopenicillin N synthase (IPNS) and 1-aminocyclopropane-1-carboxylate oxidase (ACCO) are both mononuclear nonheme iron enzymes that are biologically important. IPNS is a bacterial enzyme that catalyzes the formation of antibiotics isopenicillin N from δ-(L-α-aminoadipoyl)-L-cysteinyl-D-valine (ACV), while ACCO is a plant enzyme that produces plant hormone ethylene to regulate plant growth (Table 1-1). Although they both share the sequence $HX(D/E)X_mHX_nRXS$ that is highly conserved among all α-keto acid-dependent enzymes (*55*), their catalyses are completely independent of any α-keto acid. Both of their reactions involve the four-electron redox chemistry. For IPNS, all four electrons are originated from substrate, ACV, while for ACCO, ACC degradation provides two electrons and ascorbate provides the other two.

Thanks to the recent advances in crystallographic study, a great deal of structural and mechanistic information that would otherwise be hard to obtain has become available. The crystal structure of Fe^{II}-IPNS-ACV-NO adduct not only

confirmed the direct coordination between Cys thiolate of ACV and the ferrous center (**1-59**), but also showed the position of NO, a dioxygen analogue, relative to the cysteinyl β-carbon (*70*). This information provided the structural evidence for the first hydrogen abstraction step by an Fe^{III}-superoxide species in the proposed mechanism of IPNS (Figure 1-18). This step leads to the formation of a Cys thioaldehyde (**1-61**), and an Fe^{III}-hydroperoxy intermediate. The next step features a heterolytic cleavage of the O-O bond forming the Fe^{IV}-oxo intermediate coupled with a nucleophilic attack of the amino group at thioaldehyde to close the β-lactam ring (**1-62**). The second ring-closure step is reminiscent of a typical cyclization mediated by an oxoferryl species, which starts with the abstraction of the valinyl C_3-H, followed by C_3-S bond formation, generating the thiazolidine ring in the final product, isopenicillin N (IPN, **1-63**).

Using a variety of substrate analogues, the proposed mechanism has been tested. The presence of Fe^{IV}-oxo in the catalytic cycle is supported by the alternative activity of IPNS in sulfoxidation and double bond epoxidation (*71*).

Like IPNS, ACCO is also a nonheme iron enzyme with the $HX(D/E)X_mHX_nRXS$ sequence motif conserved in many α-KG dependent enzymes but does not require α-KG for activity. Instead, the enzyme requires carbon dioxide (or carbonate) as a catalytic activator, in addition to the essential cosubstrates, dioxygen and ascorbate. Its crystal structure that was available only weeks ago identified a 2-His-1-carboxylate iron-binding motif (*72*). ENDOR study using ^{15}N- and ^{17}O-labeled alanine has demonstrated a bidentate binding pattern for ACC, in which both its amino and carboxylate groups

coordinate the active site iron (**1-65**) (*73*). In the same study, ACC (**1-64**) and NO were also found to bind simultaneously. Taken with the previous finding that ascorbate binding is competitive with NO, these observations led to the proposed catalytic cycle in Figure 1-19.

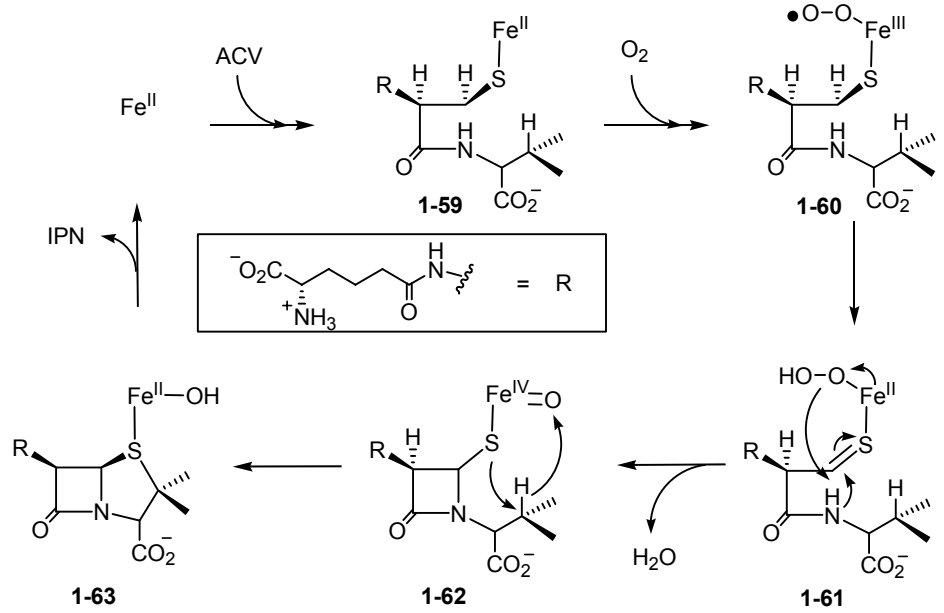

Figure 1-18 The proposed catalytic mechanism of IPNS.

1.3.7. Rieske Dioxygenases

Rieske dioxygenases catalyzes the first step in the biodegradation of aromatic compounds, the *cis*-dihydroxylation of arenes. These enzymes contain a unique Rieske-type [2Fe-2S] cluster that consists of a 2His (on one iron), 2Cys (on the other iron) coordination pattern (*74*) (**1-70**). This coordination pattern is distinct from the more common 4Cys ligation pattern found in plant ferredoxins iron sulfur cluster. Rieske dioxygenases are multi-component enzymes

comprising of an oxygenase component responsible for dioxygen activation and substrate hydroxylation, and a reductase component responsible for electron transfer from exogenous NADPH to the oxygenase component.

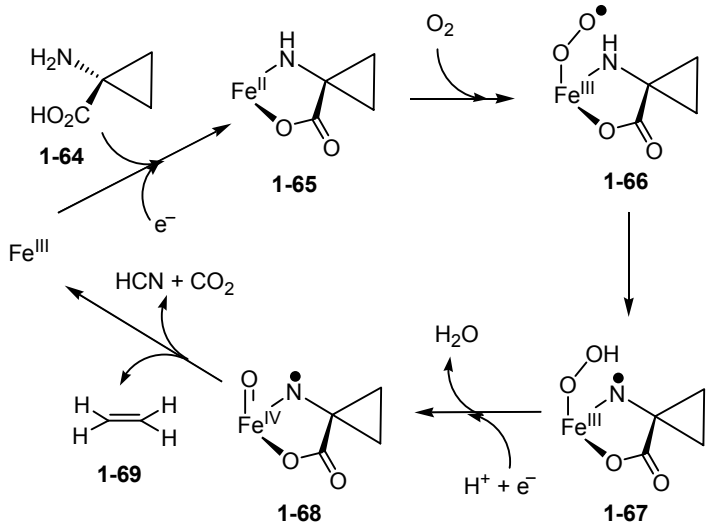

Figure 1-19 The proposed catalytic mechanism of ACCO.

As the representative enzyme of this class, naphthalene 1,2-dioxygenase (NDO) has been well studied both structurally and mechanistically. The crystal structure of its oxygenase component shows a mononuclear non-heme iron bound to a distinct 2-His-1-carboxylate motif (*74*) (**1-71**), which is highlighted by a

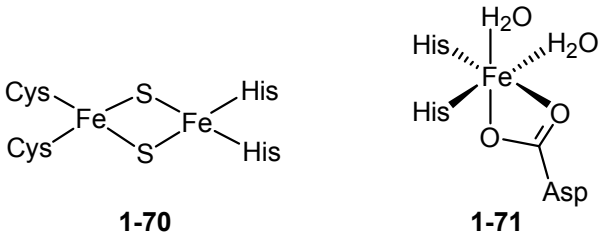

bidentate carboxylate ligand. This mononuclear iron center has a neighboring Rieske iron-sulfur cluster, both of which are essential to NDO activity.

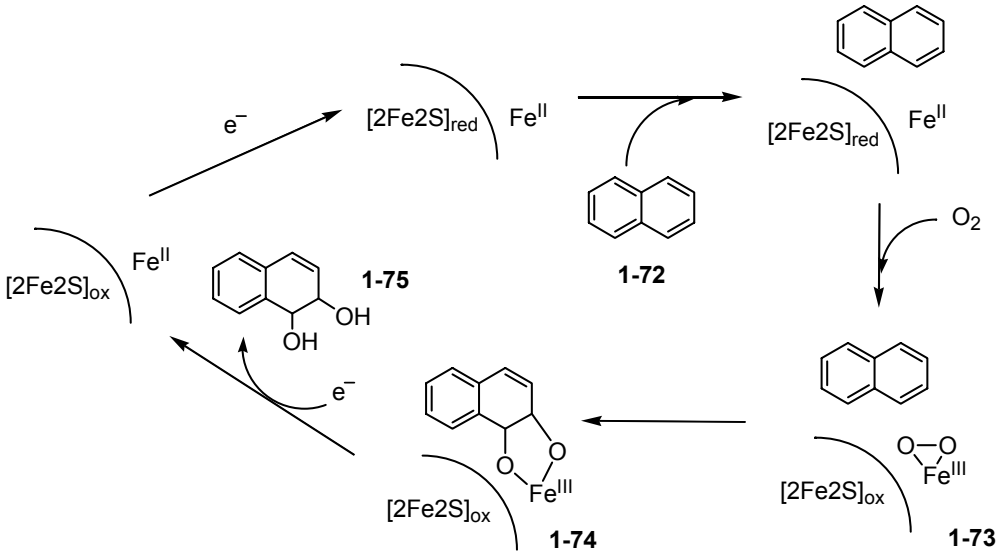

Figure 1-20 The proposed catalytic mechanism of Rieske dioxygenase.

The recently resolved crystal structures of NDO-O_2 adduct, in the absence and in the presence of substrate, naphthalene (**1-72**), marks the first structural characterization of a non-heme enzyme dioxygen adduct (*75*). The dioxygen is bound to the iron center in a very unusually side-on mode (**1-73**), instead of an end-on mode. Given that the *cis*-dihydroxylated product (**1-75**) also binds to the iron center in a bidentate manner (**1-74**), as shown in the crystal structure of enzyme-product complex (*76*), a catalytic cycle can be proposed by lining up all these known structures. As depicted in Figure 1-20, the reaction involves dioxygen activated to generate **1-73** followed by arene dihydroxylation to form **1-75**. The Rieske cluster mediates electron transfer from the reductase component

to the oxygenase active site, using NADPH as the ultimate electron source. At the end stage of the catalytic cycle, both non-heme iron center and Rieske cluster are in their oxidized forms. To release the product (**1-75**) and regenerate the redox cofactors, an electron is transferred to non-heme ferric ion. The subsequent electron transfer that reduces Rieske center renders the enzymatic active site ready for the next cycle of catalysis.

1.4 THESIS STATEMENT

The focus of this dissertation is to study HppE, the enzyme catalyzing the last step of fosfomycin biosynthesis. The transformation catalyzed by HppE is an unique epoxidation, because its substrate is a secondary alcohol rather than an alkene, which is much more common in other biological epoxidation reactions. In contrast to other natural epoxidases, which are either heme-based cytochrome P450s or binuclear non-heme iron enzymes, HppE is a novel type of mononuclear non-heme iron enzyme. The only similar case is found in the scopamine biosynthesis, where a mononuclear non-heme iron-dependent 6β-hydroxylase (H6H) can also convert an alcohol substrate to an epoxide product. However, H6H is an α-KG dependent enzyme while HppE is independent of α-KG but instead relies on NADH for two exogenous electrons essential to its epoxidation.

Previously, Dr. Pinghua Liu has successfully reconstituted the epoxidase activity of HppE using recombinant enzyme originally from *Streptomyces wedmorensis*. This dissertation focuses on further structural and mechanistic studies of the epoxidation reaction catalyzed by HppE. The work towards better understanding of HppE itself and its catalysis involves many collaborative efforts.

The dissertation describes the exploration of the reaction sequence (Chapter 2), the metal-couple protein radical (Chapter4), the active site structure (Chapter 5), and the substrate binding (Chapter 6) by EPR, which were conducted in collaboration with Dr. John D. Lipscomb at the University of Minnesota and Dr. Aimin Liu at University of Mississippi Medical Center. The identification and characterization of a green chromophore in the modified HppE, covered in Chapter 3, was undertaken in collaboration with Dr. Mark P. Mehn and Dr. Lawrence Que at the University of Minnesota.

The results obtained from the studies depicted in this dissertation firmly established that HppE is unique among all known mononuclear non-heme iron enzymes. It requires no organic coenzyme or metal cluster and its activity is independent of pterin, α-KG and ascorbate. Instead, its catalysis consumes a stoichiometric amount of NADH with molecular oxygen. Our data reveal that HppE is in a class of its own within the mononuclear non-heme iron enzyme superfamily and the reaction catalyzed by HppE is beyond the scope encompassed by common biological epoxidation and C-O bond formation reactions.

1.5 REFERENCE

1. Hendlin, D., Stapley, E. O., Jackson, M., Wallick, H., Miller, A. K., Wolf, F. J., Miller, T. W., Chaiet, L., Kahan, F. M., Foltz, E. L., Woodruff, H. B., Mata, J. M., Hernandez, S., and Mochales, S. (1969) "Phosphonomycin, a new antibiotic produced by strains of *streptomyces*" *Science 166*, 122-123.
2. Christensen, B. G., Leanza, W. J., Beattie, T. R., Patchett, A. A., Arison, B. H., Ormond, R. E., Kuehl, F. A., Jr., Albers-Schonberg, G., and Jardetzky, O. (1969) "Phosphonomycin: structure and synthesis" *Science 166*, 123-125.

3. Kahan, F. M., Kahan, J. S., Cassidy, P. J., and Kropp, H. (1974) "The mechanism of action of fosfomycin (phosphonomycin)" *Ann. N. Y. Acad. Sci. 235*, 364-386.

4. Kim, D. H., Tucker-Kellogg, G. W., Lees, W. J., and Walsh, C. T. (1996) "Analysis of fluoromethyl group chirality establishes a common stereochemical course for the enolpyruvyl transfers catalyzed by EPSP synthase and UDP-GlcNAc enolpyruvyl transferase" *Biochemistry 35*, 5435-5440.

5. Brown, E. D., Vivas, E. I., Walsh, C. T., and Kolter, R. (1995) "MurA (MurZ), the enzyme that catalyzes the first committed step in peptidoglycan biosynthesis, is essential in *Escherichia coli*" *J. Bacteriol. 177*, 4194-4197.

6. Kim, D. H., Lees, W. J., Kempsell, K. E., Lane, W. S., Duncan, K., and Walsh, C. T. (1996) "Characterization of a Cys115 to Asp substitution in the *Escherichia coli* cell wall biosynthetic enzyme UDP-GlcNAc enolpyruvyl transferase (MurA) that confers resistance to inactivation by the antibiotic fosfomycin" *Biochemistry 35*, 4923-4928.

7. Marquardt, J. L., Brown, E. D., Lane, W. S., Haley, T. M., Ichikawa, Y., Wong, C. H., and Walsh, C. T. (1994) "Kinetics, stoichiometry, and identification of the reactive thiolate in the inactivation of UDP-GlcNAc enolpyruvoyl transferase by the antibiotic fosfomycin" *Biochemistry 33*, 10646-10651.

8. Dette, G. A., Knothe, H., Schèonenbach, B., and Plage, G. (1983) "Comparative study of fosfomycin activity in Mueller-Hinton media and in tissues" *J. Antimicrob. Chemother. 11*, 517-524.

9. Kojo, H., Shigi, Y., and Nishida, M. (1980) "FR-31564, a new phosphonic acid antibiotic: bacterial resistance and membrane permeability" *J. Antibiot. 33*, 44-48.

10. Tsuruoka, T., Miyata, A., and Yamada, Y. (1978) "Two kinds of mutants defective in multiple carbohydrate utilization isolated from in vitro fosfomycin-resistant strains of *Escherichia coli* K--12" *J. Antibiot. (Tokyo) 31*, 192-201.

11. García, P., Arca, P., and Evaristo Suárez, J. (1995) "Product of fosC, a gene from Pseudomonas syringae, mediates fosfomycin resistance by using ATP as cosubstrate" *Antimicrob. Agents. Chemother. 39*, 1569-1573.

12. Horii, T., Kimura, T., Sato, K., Shibayama, K., and Ohta, M. (1999) "Emergence of fosfomycin-resistant isolates of Shiga-like toxin-producing *Escherichia coli* O26" *Antimicrob. Agents. Chemother. 43*, 789-793.

13. Seto, H., and Kuzuyama, T. (1999) "Bioactive natural products with carbon-phosphorus bonds and their biosynthesis" *Nat. Prod. Rep. 16*, 589-596.

14. Liu, S., Lu, Z., Jia, Y., Dunaway-Mariano, D., and Herzberg, O. (2002) "Dissociative phosphoryl transfer in PEP mutase catalysis: structure of the enzyme/sulfopyruvate complex and kinetic properties of mutants" *Biochemistry 41*, 10270-10276.

15. Seidel, H. M., Freeman, S., Seto, H., and Knowles, J. R. (1988) "Phosphonate biosynthesis: isolation of the enzyme responsible for the formation of a carbon-phosphorus bond" *Nature 335*, 457-458.

16. McQueney, M. S., Lee, S. L., Swartz, W. H., Ammon, H. L., Mariano, P. S., and Dunaway-Mariano, D. (1991) "Evidence for an intramolecular, stepwise reaction pathway for PEP phosphomutase catalyzed phosphorus-carbon bond formation" *J. Org. Chem. 56*, 7121-7130.

17. Nakashita, H., Watanabe, K., Hara, O., Hidaka, T., and Seto, H. (1997) "Studies on the biosynthesis of bialaphos. Biochemical mechanism of C-P bond formation: discovery of phosphonopyruvate decarboxylase which catalyzes the formation of phosphonoacetaldehyde from phosphonopyruvate" *J. Antibiot. (Tokyo) 50*, 212-219.

18. Hidaka, T., Goda, M., Kuzuyama, T., Takei, N., Hidaka, M., and Seto, H. (1995) "Cloning and nucleotide sequence of fosfomycin biosynthetic genes of *Streptomyces wedmorensis*" *Mol. Gen. Genet. 249*, 274-280.

19. Kuzuyama, T., Seki, T., Kobayashi, S., Hidaka, T., and Seto, H. (1999) "Cloning and expression in *Escherichia coli* of 2-hydroxypropylphosphonic acid epoxidase from the fosfomycin-producing organism, *Pseudomonas syringae* PB-5123" *Biosci. Biotechnol. Biochem. 63*, 2222-2224.

20. Imai, S., Seto, H., Sasaki, T., Tsuruoka, T., Ogawa, H., Satoh, A., Inouye, S., Niida, T., and Otake, N. (1985) "Studies on the biosynthesis of bialaphos (SF-1293). 6. Production of *N*-acetyl-demethylphosphinothricin and *N*-acetylbialaphos by blocked mutants of *Streptomyces hygroscopicus* SF-1293 and their roles in the biosynthesis of bialaphos" *J. Antibiot. 38*, 687-690.

21. Seto, H., Hidaka, T., Kuzuyama, T., Shibahara, S., Usui, T., Sakanaka, O., and Imai, S. (1991) "Studies on the biosynthesis of fosfomycin. 2.

Conversion of 2-hydroxypropyl-phosphonic acid to fosfomycin by blocked mutants of *Streptomyces wedmorensis*" *J. Antibiot. (Tokyo) 44*, 1286-1288.

22. Rogers, T. O., and Birnbaum, J. (1974) "Biosynthesis of fosfomycin by *Streptomyces fradiae*" *Antimicrob. Agents. Chemother. 5*, 121-32.

23. Kuzuyama, T., Hidaka, T., Kamigiri, K., Imai, S., and Seto, H. (1992) "Studies on the biosynthesis of fosfomycin. 4. The biosynthetic origin of the methyl group of fosfomycin" *J. Antibiot. (Tokyo) 45*, 1812-1814.

24. Ortiz de Montellano, P. R. (1995) *Cytochrome P450: Structure, Mechanism, and Biochemistry*, Plenum Press, New York.

25. Sono, M., Roach, M. P., Coulter, E. D., and Dawson, J. H. (1996) "Heme-Containing Oxygenases" *Chem. Rev. 96*, 2841-2887.

26. Lange, S. J., and Que, L., Jr. (1998) "Oxygen activating nonheme iron enzymes" *Curr. Opin. Chem. Biol. 2*, 159-172.

27. Hammerschmidt, F. (1991) "Biosynthesis of natural products with a phosphorus-carbon bond. Part 8. On the origin of the oxirane oxygen atom of fosformycin in *Streptomyces fradiae*" *J. Chem. Soc., Perkin Trans. 1*, 1993-1996.

28. Hammerschmidt, F. (1991) "Markierte vertreter eines möglichen zwischen-produkts der biosynthese von fosfomycin in *Streptomyces fradiae*: darstellung von (*R*,*S*)-(2-hydroxypropyl)-, (*R*,*S*)-, (*R*)-, (*S*)-(2-hydroxy-[1,1-$^{2}H_{2}$]propyl)- und (*R*,*S*)-(2-[^{18}O]hydroxypropyl)phosphonsäure." *Monatsh. Chem.*, 389-393.

29. Kuzuyama, T., Kobayashi, S., O'Hara, K., Hidaka, T., and Seto, H. (1996) "Fosfomycin monophosphate and fosfomycin diphosphate, two inactivated fosfomycin derivatives formed by gene products of fomA and fomB from a fosfomycin producing organism *Streptomyces wedmorensis*" *J. Antibiot. (Tokyo) 49*, 502-504.

30. Kamigiri, K., Hidaka, T., Imai, S., Murakami, T., and Seto, H. (1992) "Studies on the biosynthesis of bialaphos (SF-1293) 12. C-P bond formation mechanism of bialaphos: discovery of a P-methylation enzyme" *J. Antibiot. (Tokyo) 45*, 781-787.

31. Sofia, H. J., Chen, G., Hetzler, B. G., Reyes-Spindola, J. F., and Miller, N. E. (2001) "Radical SAM, a novel protein superfamily linking unresolved steps in familiar biosynthetic pathways with radical mechanisms: functional characterization using new analysis and information visualization methods" *Nucleic Acids Res. 29*, 1097-1106.

32. Kuzuyama, T., Seki, T., Dairi, T., Hidaka, T., and Seto, H. (1995) "Nucleotide sequence of fortimicin KL1 methyltransferase gene isolated from *Micromonospora olivasterospora*, and comparison of its deduced amino acid sequence with those of methyltransferases involved in the biosynthesis of bialaphos and fosfomycin" *J. Antibiot. (Tokyo) 48*, 1191-1193.

33. Westrich, L., Heide, L., and Li, S. M. (2003) "CloN6, a novel methyltransferase catalysing the methylation of the pyrrole-2-carboxyl moiety of clorobiocin" *Chembiochem 4*, 768-773.

34. Ludwig, M. L., and Matthews, R. G. (1997) "Structure-based perspectives on B_{12}-dependent enzymes" *Annu. Rev. Biochem. 66*, 269-313.

35. Liu, P., Murakami, K., Seki, T., He, X., Yeung, S.-M., Kuzuyama, T., Seto, H., and Liu, H.-w. (2001) "Protein purification and function assignment of the epoxidase catalyzing the formation of fosfomycin" *J. Am. Chem. Soc. 123*, 4619-4620.

36. Liu, P., Liu, A., Yan, F., Wolfe, M. D., Lipscomb, J. D., and Liu, H.-w. (2003) "Biochemical and spectroscopic studies on (*S*)-2-hydroxypropylphosphonic acid epoxidase: a novel mononuclear non-heme iron enzyme" *Biochemistry 42*, 11577-11586.

37. Lipscomb, J. D. (1994) "Biochemistry of the soluble methane monooxygenase" *Annu. Rev. Microbiol. 48*, 371-399.

38. Colby, J., Stirling, D. I., and Dalton, H. (1977) "The soluble methane mono-oxygenase of *Methylococcus capsulatus* (Bath). Its ability to oxygenate *N*-alkanes, *N*-alkenes, ethers, and alicyclic, aromatic and heterocyclic compounds" *Biochem. J. 165*, 395-402.

39. Wallar, B. J., and Lipscomb, J. D. (1996) "Dioxygen activation by enzymes containing binuclear non-heme iron clusters" *Chem. Rev. 96*, 2625-2657.

40. Hashimoto, T., and Yamada, Y. (1987) "Purification and characterization of hyoscyamine 6 beta-hydroxylase from root cultures of *Hyoscyamus niger* L. Hydroxylase and epoxidase activities in the enzyme preparation" *Eur. J. Biochem. 164*, 277-285.

41. Hashimoto, T., Matsuda, J., and Yamada, Y. (1993) "Two-step epoxidation of hyoscyamine to scopolamine is catalyzed by bifunctional hyoscyamine 6β-hydroxylase" *FEBS Lett. 329*, 35-39.

42. Solomon, E. I., Brunold, T. C., Davis, M. I., Kemsley, J. N., Lee, S.-K., Lehnert, N., Neese, F., Skulan, A. J., Yang, Y.-S., and Zhou, J. (2000)

"Geometric and electronic structure/function correlations in non-heme iron enzymes" *Chem. Rev. 100*, 235-349.

43. Costas, M., Mehn, M. P., Jensen, M. P., and Que, L., Jr. (2004) "Dioxygen Activation at Mononuclear Nonheme Iron Active Sites: Enzymes, Models, and Intermediates" *Chem. Rev. 104*, 939-986.

44. Ford-Hutchinson, A. W., Gresser, M., and Young, R. N. (1994) "5-Lipoxygenase" *Annu. Rev. Biochem. 63*, 383-417.

45. Gardner, H. W. (1991) "Recent investigations into the lipoxygenase pathway of plants" *Biochim. Biophys. Acta. 1084*, 221-239.

46. Boyington, J. C., Gaffney, B. J., and Amzel, L. M. (1993) "The three-dimensional structure of an arachidonic acid 15-lipoxygenase" *Science 260*, 1482-6.

47. Solomon, E. I., Zhou, J., Neese, F., and Pavel, E. G. (1997) "New insights from spectroscopy into the structure/function relationships of lipoxygenases" *Chem. Biol. 4*, 795-808.

48. Garssen, G. J., Vliegenthart, J. F., and Boldingh, J. (1972) "The origin and structures of dimeric fatty acids from the anaerobic reaction between soya-bean lipoxygenase, linoleic acid and its hydroperoxide" *Biochem. J. 130*, 435-442.

49. Bugg, T. D. H., and Winfield, C. J. (1998) "Enzymic cleavage of aromatic rings: mechanistic aspects of the catechol dioxygenases and later enzymes of bacterial oxidative cleavage pathways" *Nat. Prod. Rep. 15*, 513-530.

50. Ohlendorf, D. H., Weber, P. C., and Lipscomb, J. D. (1987) "Determination of the quaternary structure of protocatechuate 3,4-dioxygenase from *Pseudomonas aeruginosa*" *J. Mol. Biol. 195*, 225-227.

51. Davis, M. I., Orville, A. M., Neese, F., Zaleski, J. M., Lipscomb, J. D., and Solomon, E. I. (2002) "Spectroscopic and electronic structure studies of protocatechuate 3,4-dioxygenase: nature of tyrosinate-Fe(III) bonds and their contribution to reactivity" *J. Am. Chem. Soc. 124*, 602-614.

52. Elgren, T. E., Orville, A. M., Kelly, K. A., Lipscomb, J. D., Ohlendorf, D. H., and Que, L., Jr. (1997) "Crystal structure and resonance Raman studies of protocatechuate 3,4-dioxygenase complexed with 3,4-dihydroxyphenylacetate" *Biochemistry 36*, 11504-11513.

53. Mayer, R. J., and Que, L., Jr. (1984) "^{18}O studies of pyrogallol cleavage by catechol 1,2-dioxygenase" *J. Biol. Chem. 259*, 13056-13060.

54. Han, S., Eltis, L. D., Timmis, K. N., Muchmore, S. W., and Bolin, J. T. (1995) "Crystal structure of the biphenyl-cleaving extradiol dioxygenase from a PCB-degrading *pseudomonas*" *Science 270*, 976-980.

55. Hegg, E. L., and Que, L., Jr. (1997) "The 2-His-1-carboxylate facial triad--an emerging structural motif in mononuclear non-heme iron(II) enzymes" *Eur. J. Biochem. 250*, 625-629.

56. Sato, N., Uragami, Y., Nishizaki, T., Takahashi, Y., Sazaki, G., Sugimoto, K., Nonaka, T., Masai, E., Fukuda, M., and Senda, T. (2002) "Crystal structures of the reaction intermediate and its homologue of an extradiol-cleaving catecholic dioxygenase" *J. Mol. Biol. 321*, 621-636.

57. Fitzpatrick, P. F. (1999) "Tetrahydropterin-dependent amino acid hydroxylases" *Annu. Rev. Biochem. 68*, 355-381.

58. Flatmark, T., and Stevens, R. C. (1999) "Structural Insight into the Aromatic Amino Acid Hydroxylases and Their Disease-Related Mutant Forms" *Chem. Rev. 99*, 2137-2160.

59. Andersen, O. A., Flatmark, T., and Hough, E. (2002) "Crystal structure of the ternary complex of the catalytic domain of human phenylalanine hydroxylase with tetrahydrobiopterin and 3-(2-thienyl)-L-alanine, and its implications for the mechanism of catalysis and substrate activation" *J Mol Biol 320*, 1095-108.

60. Dix, T. A., Bollag, G. E., Domanico, P. L., and Benkovic, S. J. (1985) "Phenylalanine hydroxylase: absolute configuration and source of oxygen of the 4a-hydroxytetrahydropterin species" *Biochemistry 24*, 2955-2958.

61. Siegmund, H. U., and Kaufman, S. (1991) "Hydroxylation of 4-methylphenylalanine by rat liver phenylalanine hydroxylase" *J. Biol. Chem. 266*, 2903-2910.

62. Hausinger, R. P. (2004) "FeII/α-ketoglutarate-dependent hydroxylases and related enzymes." *Crit. Rev. Biochem. Mol. Biol. 39*, 21-68.

63. Pavel, E. G., Zhou, J., Busby, R. W., Gunsior, M., Townsend, C. A., and Solomon, E. I. (1998) "Circular Dichroism and Magnetic Circular Dichroism spectroscopic studies of the non-heme ferrous active site in clavaminate synthase and its interaction with α-ketoglutarate cosubstrate" *J. Am. Chem. Soc. 120*, 743-753.

64. Zhang, Z., Ren, J., Harlos, K., McKinnon, C. H., Clifton, I. J., and Schofield, C. J. (2002) "Crystal structure of a clavaminate synthase-Fe(II)-2-oxoglutarate-substrate-NO complex: evidence for metal centered rearrangements" *FEBS Lett. 517*, 7-12.

65. Price, J. C., Barr, E. W., Tirupati, B., Bollinger, J. M., Jr., and Krebs, C. (2003) "The first direct characterization of a high-valent iron intermediate in the reaction of an α-ketoglutarate-dependent dioxygenase: A high-spin Fe(IV) complex in taurine/α-ketoglutarate dioxygenase (TauD) from *Escherichia coli*" *Biochemistry 42*, 7497-7508.

66. Price, J. C., Barr, E. W., Glass, T. E., Krebs, C., and Bollinger, J. M., Jr. (2003) "Evidence for hydrogen abstraction from C1 of taurine by the high-spin Fe(IV) intermediate detected during oxygen activation by taurine: α-ketoglutarate dioxygenase (TauD)" *J. Am. Chem. Soc. 125*, 13008-13009.

67. Thornburg, L. D., Lai, M. T., Wishnok, J. S., and Stubbe, J. (1993) "A non-heme iron protein with heme tendencies: an investigation of the substrate specificity of thymine hydroxylase" *Biochemistry 32*, 14023-14033.

68. Ryle, M. J., Liu, A., Muthukumaran, R. B., Ho, R. Y. N., Koehntop, K. D., McCracken, J., Que, L., Jr., and Hausinger, R. P. (2003) "O_2- and α-ketoglutarate-dependent tyrosyl radical formation in tauD, an α-keto acid-dependent non-heme iron dioxygenase" *Biochemistry 42*, 1854-1862.

69. Liu, A., Ho, R. Y., Que, L., Jr., Ryle, M. J., Phinney, B. S., and Hausinger, R. P. (2001) "Alternative reactivity of an α-ketoglutarate-dependent iron(II) oxygenase: enzyme self-hydroxylation" *J. Am. Chem. Soc. 123*, 5126-5127.

70. Roach, P. L., Clifton, I. J., Hensgens, C. M., Shibata, N., Schofield, C. J., Hajdu, J., and Baldwin, J. E. (1997) "Structure of isopenicillin N synthase complexed with substrate and the mechanism of penicillin formation" *Nature 387*, 827-30.

71. Burzlaff, N. I., Rutledge, P. J., Clifton, I. J., Hensgens, C. M., Pickford, M., Adlington, R. M., Roach, P. L., and Baldwin, J. E. (1999) "The reaction cycle of isopenicillin N synthase observed by X-ray diffraction" *Nature 401*, 721-4.

72. Zhang, Z., Ren, J. S., Clifton, I. J., and Schofield, C. J. (2004) "Crystal structure and mechanistic implications of 1-aminocyclopropane-1-carboxylic acid oxidase-the ethylene-forming enzyme" *Chem. Biol. 11*, 1383-1394.

73. Rocklin, A. M., Tierney, D. L., Kofman, V., Brunhuber, N. M. W., Hoffman, B. M., Christoffersen, R. E., Reich, N. O., Lipscomb, J. D., and Que, L., Jr. (1999) "Role of the nonheme Fe(II) center in the biosynthesis of the plant hormone ethylene" *Proc. Natl. Acad. Sci. USA 96*, 7905-7909.

74. Kauppi, B., Lee, K., Carredano, E., Parales, R. E., Gibson, D. T., Eklund, H., and Ramaswamy, S. (1998) "Structure of an aromatic-ring-hydroxylating dioxygenase-naphthalene 1,2-dioxygenase" *Structure 6*, 571-586.

75. Karlsson, A., Parales, J. V., Parales, R. E., Gibson, D. T., Eklund, H., and Ramaswamy, S. (2003) "Crystal structure of naphthalene dioxygenase: side-on binding of dioxygen to iron" *Science 299*, 1039-1042.

76. Carredano, E., Karlsson, A., Kauppi, B., Choudhury, D., Parales, R. E., Parales, J. V., Lee, K., Gibson, D. T., Eklund, H., and Ramaswamy, S. (2000) "Substrate binding site of naphthalene 1,2-dioxygenase: functional implications of indole binding" *J. Mol. Biol. 296*, 701-712.

Chapter 2: Initial Characterization of HppE

2.1 INTRODUCTION

(*S*)-2-hydroxypropylphosphonic acid epoxidase (HppE) from *Streptomyces wedmorensis* catalyzes the final step of the biosynthesis of fosfomycin (**2-1**, (1*R*,2*S*)-1,2-epoxypropylphosphonic acid) using (*S*)-2-hydroxy-propylphosphonic acid ((*S*)-HPP, **2-2**) as the substrate (Figure 2-1) (*1-3*). In contrast to most epoxide rings in nature, which are generated via oxidation of the corresponding alkenes by heme-dependent cytochrome P450s (*4, 5*) or non-heme iron-dependent monooxygenases (*6*), the epoxide functionality in fosfomycin is converted from a secondary alcohol, (*S*)-HPP (**2-2**), rather than an alkene, *cis*-propenylphosphonic acid (**2-3**) (*7*). In addition, the hydroxyl oxygen of HPP (**2-2**) has been found to be retained in fosfomycin (*8*). Thus far, there has been only one other known enzyme that can convert an secondary alcohol to an epoxide, which is hyoscyamine 6β-hydroxylase (H6H) in scopamine biosynthesis (9). However, H6H can also take the corresponding alkene as substrate and convert it to epoxide (10). The unique substrate specificity that HppE exhibits is another good indication that its catalytic mechanism must be distinct from above other natural epoxidases.

The original clone of HppE was constructed by Drs. Haruo Seto and Tomohisa Kuzuyama at Tokyo University using *fom4* gene from fosfomycin biosynthesis gene cluster of *S. wedmorensis* (*1*). Using HppE produced by heterologously expressing this clone in *E. coli*, Dr. Pinghua Liu successfully

reconstituted its epoxidase activity for the first time *in vitro* (Figure 2-1) (*2*). The *in vitro* reconstitution of the enzymatic epoxidation is based on a four-electron reduction of O_2 to H_2O, in which two electrons are provided by the substrate, (*S*)-HPP (**2-2**), and the other two electrons are supplied by an exogenous reductant, NAD(P)H. The key component responsible for the enzymatic catalysis is a mononuclear non-heme iron that can facilitate activation of dioxygen and/or substrate. To make the overall reaction more efficient, an electron mediator is needed to transfer electron from NAD(P)H to the enzyme active site. This electron mediator should be a reductase protein also from *S. wedmorensis*. However, efforts in searching for the reductase have thus far been unsuccessful. Fortunately, FMN was found to be an effective alternate and has been used as the substitute for the reductase.

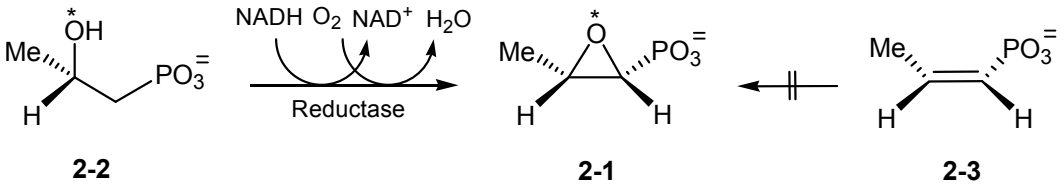

2-2 **2-1** **2-3**

Figure 2-1 The epoxidation reaction catalyzed by HppE *in vitro*.

HppE produced from the original clone contained a N-terminal His_6-tag that was attached to the enzyme to ease protein purification. However, the metal binding affinity of His_6-tag is a potential problem in studying the iron-dependent catalytic function of HppE. To avert the potential complications associated with the presence of His_6-tag, Dr. Pinghua Liu constructed a new clone to produce non-tagged HppE in *E. coli*. Since the His_6-tag was removed, the previous

protein purification procedure based on Ni-NTA affinity chromatography was replaced by a multi-step purification protocol including ammonium sulfate precipitation and DEAE column chromatography (*2*). However, a considerable degree of iron loss from HppE was observed under new purification conditions. To restore the catalytically essential iron ion in the as-purified HppE, a few more modifications were made to improve the purification procedure. First, EDTA and DTT were added to the purification buffers to remove all iron from enzyme, so the as-purified HppE was totally free of any iron ions (*3*). The apo-protein was reconstituted with more than one equivalent of $Fe^{II}(NH_4)_2(SO_4)_2$ under aerobic conditions and then passed over a gel filtration column to remove adventurously bound iron. The subsequent iron titration analysis verified that the ratio of protein to iron is close to 1:1. In contrast to the HppE with His_6-tag, the newly purified and reconstituted HppE exhibited significant enhancement in its epoxidase activity (*11*).

As previously discussed in Chapter 1, mononuclear non-heme iron enzymes can be classified in two categories, Fe^{II}- and Fe^{III}-dependent. The former class includes the majority of mononuclear non-heme iron enzymes, e.g. the extradiol cleaving catechol dioxygenases, α-keto acid-dependent oxidases and oxygenases, pterin-dependent hydroxylases, Rieske-type dioxygenases, the ethylene forming enzyme, and isopenicillin N synthase (*12*). While these enzymes catalyze a wide variety of reactions, their proposed mechanisms all involve a high valent iron-oxo species as the oxidant in the course of an overall four-electron reduction of dioxygen to water (*13*). An organic co-substrate, such

as ascorbate, tetrahydropterin, or α-ketoglutarate (α-KG), is often required to provide the additional electrons to complete the four-electron redox cycle (*14-17*). Alternatively, an iron-sulfur cluster, such as that built into the Rieske-type dioxygenases (*18*), can also be used to mediate electron transfer from NADH. Unlike members in this class of enzymes, which are aided by an organic co-substrate or a Rieske center in oxygen activation, HppE has no built-in iron-sulfur cluster and is ascorbate-, pterin-, and α-KG-independent. On the other hand, the members of the Fe^{III}-dependent class are very few, solely represented by lipoxygenases and intradiol cleaving catechol dioxygenases, and their catalyses involve Fe^{III}-dependent substrate activation more than oxygen activation (*12*). Although the Fe^{III}-reconstituted HppE was used to establish the in vitro enzymatic epoxidation system (*2*), neither the mechanism of lipoxygenases nor that of the intradiol cleaving catechol dioxygenases can be applied to HppE. Clearly, the reaction catalyzed by HppE is beyond the scope encompassed by common biological epoxidation and C-O bond formation reactions. Thus, HppE should be in a class of its own within the mononuclear non-heme iron enzyme superfamily.

This chapter begins with the expression and purification of the recombinant HppE from *S. wedmorensis*, followed by experiments to characterize the purified enzyme. As all the basic properties of HppE were confirmed to be the same as previously reported, the enzyme was then subjected to EPR spectral analysis. The EPR study showed that the enzymatic ferric center is reduced to its ferrous state by FMN/NADH in the presence of substrate. The EPR results strongly imply an Fe^{II}-dependent catalytic mechanism of HppE.

2.2 MATERIALS AND METHODS

General. The *E. coli* strain BL21(DE3) for protein expression was obtained from Novagen (Madison, WI). The plasmid pPL1001 containing the HppE gene (*fom4*) was constructed by Dr. Pinghua Liu using pET24b(+) expression vector from Novagen (*3*). DNA minipreps were performed using Qiaprep® spin miniprep kit from Qiagen (Valencia, CA). Culture medium ingredients were purchased from Difco (Detroit, MI). Protein concentrations were determined by the procedure of Bradford using bovine serum albumin as the standard (*19*). All chemicals were analytical grade or the highest quality commercially available. Biochemicals including fosfomycin disodium salt standard were purchased from Sigma (St. Louis, MO), unless noted otherwise. The catalytic inhibitor of HppE, (*S*)-1-difluoro-2-hydroxypropylphosphonate ((*S*)-FHPP, **2-4**), was chemically synthesized by Dr. Zongbao Zhao (*20*).

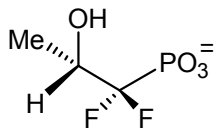

2-4

The NMR spectra were acquired on a Varian Unity 300 spectrometer and chemical shifts (δ in ppm) are given relative to those for Me_4Si (for ^1H and ^{13}C) and aqueous 85% H_3PO_4 (external, for ^{31}P), with coupling constants reported in hertz (Hz). The UV-vis absorption spectra were recorded on a HP 8453A diode array or a Beckman DU 650 spectrophotometer.

Heterologous Expression of fom4 in E. coli. An overnight culture of *E. coli* BL21(DE3)/pPL1001 grown at 37 °C in LB medium supplemented with kanamycin (50 μg/mL) was used, in a 200-fold dilution, to inoculate 6 L of the same medium supplemented with 0.1 mM $Fe^{II}(NH_4)_2(SO_4)_2$. When the OD_{600}

reached 0.4 - 0.6, the incubation temperature was lowered to 18 °C and then IPTG was added to a final concentration of 0.1 mM to induce gene expression. After incubation for an additional 15 - 20 h at 18 °C, cells were harvested by centrifugation (5,000 *g*, 10 min) at 4 °C, washed with Tris·HCl buffer (20 mM, pH 7.5), collected again by centrifugation (8,000 *g*, 15 min), and stored at - 80 °C for future use. The typical yield was 6 g of wet cells per liter of culture.

Purification of Recombinant HppE. All purification operations were carried out at 4 °C except for the FPLC step, and all buffers were degassed and saturated with nitrogen before use. Thawed cells were resuspended in 5 fold (w/v) of lysis buffer (20 mM Tris·HCl, pH 7.5, 0.1 mM DTT; 1 mM EDTA was included to remove trace amount of iron ion when necessary) and subjected to 8 × 30 s ultrasonic bursts, with 2 min cooling interval between each blast. Cellular debris was removed by centrifugation at 30,000 *g* for 25 min. The supernatant was fractionated by $(NH_4)_2SO_4$ and the 30-65% $(NH_4)_2SO_4$ precipitate was collected. The protein pellet was resuspended in a minimal amount of dialysis buffer (Tris·HCl 20 mM, pH 7.5, 0.18 M KCl). The resulting protein solution was dialyzed against 2 L of the same buffer for 4 h with two buffer changes.

The dialysate was applied to a DEAE-Sepharose CL-6B column (5 × 17 cm) pre-equilibrated with the dialysis buffer (20 mM Tris·HCl, pH 7.5, 0.18 M KCl). The elution was then continued with a linear gradient of KCl from 0.18 to 0.3 M in 20 mM Tris·HCl buffer, pH 7.5 (2 L total volume). The flow rate was 2 mL/min and fractions of 15 mL were collected throughout the gradient elution. The fractions containing HppE, as determined by SDS-PAGE, were pooled,

concentrated to about 10 mL by ultrafiltration on an Amicon concentrator using an YM 10 membrane (Millipore, Bedford, MA), and desalted by dialyzing against 20 mM Tris·HCl buffer, pH 7.5.

The protein from last step was further purified at room temperature by FPLC equipped with a Mono Q HR 10/10 (Amersham Biosciences, Uppsala, Sweden) using the solvent systems A (20 mM Tris·HCl buffer, pH 7.5) and B (A plus 0.6 M NaCl). The elution profile included a linear gradient of 0 to 60% B from 0 to 25 min, followed by a linear gradient of 60 to 100% B from 25 to 26 min, and concluded with a 5 min wash at 100% B. The flow rate was 3 mL/min and the detector was set at 280 nm. A sharp peak with a retention time of about 19 min was collected, concentrated by ultrafiltration as described before, desalted with 20 mM Tris·HCl buffer (pH 7.5), and stored at -80 °C.

Polyacrylamide Gel Electrophoresis. The subunit molecular mass and the purity of the protein samples were assessed by SDS-PAGE. The separation gel and the stacking gel for electrophoresis were 12% and 4%, respectively. Prior to electrophoresis, protein samples were mixed with 10 μL of loading buffer (62.5 mM Tri-HCl buffer, pH 6.8, containing 10% glycerol, 2% SDS, 5% β-mercaptoethanol, and 0.0025% bromophenol blue) and heated in boiling water for 5 min except for the His_6-tagged proteins. For proteins with either N- or C-terminal His_6-tag, the corresponding mixtures were incubated at 37 °C for 10 min. Electrophoresis was run in 25 mM Tris·HCl buffer containing 192 mM glycine, and 0.1% SDS (pH 8.3) at 25 mA. Gels were stained with Coomassie blue and destained with acetic acid/ethanol/water (15:29:165 by volume). Protein

standards for SDS-PAGE include α-lactalbumin (14 kDa), trypsinogen (24 kDa), carbonic anhydrase (29 kDa), glyceraldehyde-3-phosphate dehydrogenase (36 kDa), egg albumin (45 kDa), and bovine serum albumin (66 kDa).

Molecular Mass Determination. The molecular mass of HppE was determined by size exclusion chromatography performed on a Pharmacia FPLC Superdex 200 HR 10/30 column with 20 mM Tris·HCl, 0.15 M NaCl, pH 7.5 at a flow rate of 0.8 mL/min. Calibration of the column was achieved using the following protein standards (Sigma): cytochrome C (14.2 kDa), carbonic anhydrase (29 kDa), egg albumin (45 kDa), bovine serum albumin (66 kDa). The void volume (V_0) of the column was measured using blue dextran. A linear fit to a plot of the molecular weight versus V_e/V_0 was used to estimate the native molecular mass (M_r) of protein sample.

Preparation of Reconstituted HppE. The original reconstitution strategy was initiated with dilution of concentrated as-purified apo-HppE (usually 1 - 2 mM in 20 mM Tris·HCl, pH 7.5) in ddH_2O to a final concentration of 1 mg/mL. The protein solution was mixed with $Fe^{II}(NH_4)_2(SO_4)_2$ to an enzyme/iron ratio of 1:2 - 2.5 and stirred at 4 °C in air for 30 min. The excess or weakly bound Fe was removed by a G-10 column (2.5 × 75 cm). The elution was run at 5-6 mL/min with Tris·HCl buffer (20 mM, pH 7.5). The green fractions (5-mL fractions) were collected, concentrated, and the final concentration was determined by A_{280} (1 OD ~ 0.7 mg). The reconstituted epoxidase was aliquoted and stored at –80 °C.

This reconstitution protocol was modified for samples subjected to biophysical studies. Briefly, the apo-HppE was mixed with $Fe^{II}(NH_4)_2(SO_4)_2$ in a ratio of 1:1 and then exposed to pure O_2 for 0.5 - 1 h. The reconstituted enzyme was used directly in the EPR studies without further purification (e.g. G-10).

Iron Titration. Protein samples for iron titration analysis (1 mL each) were mixed with 500 μL of reagent A (1:1 of 4.5% $KMnO_4$:1.2 N HCl) and incubated at 60 °C for 2 h. To these samples were added 100 μL of reagent B (8.8 g of ascorbic acid, 9.7 g of ammonium acetate, 80 mg of ferrozine, 80 mg of neocuprione, ddH_2O to 25 mL total volume) followed by immediate vortexing. The samples were read at 562 nm after the color was fully developed by a 1 h incubation period at room temperature.

Preparation of HppE Substrate. The substrates of HppE in its enantiomerically pure forms were chemically synthesized. To a solution of diethyl 2-oxopropylphosphonate (**2-5**, 3.3 g, 17 mmol) in anhydrous tetrahydrofuran (THF, 100 mL) was added $NaBH_4$ (1.5 g, 40 mmol). The reaction mixture was stirred at room temperature for 3 h. The product, diethyl 2-hydroxypropylphosphonate (**2-6**), was extracted by chloroform (100 mL) and washed with 1 M HCl (100 mL × 3). After the extract had been dried by $MgSO_4$ powder, the chloroform was evaporated. To the colorless oil left in the flask were added vinyl acetate (40 mL), isopropyl ether (60 mL) and lipase from *Pseudomonas fluorescens* (Amano Enzymes Inc., Nagoya, Japan, 1 g). The reaction mixture was shaken at 30 °C, and the progress was monitored by NMR

until the ratio between the acetylated and unacetylated compounds reached 1:1. The acetylated product, diethyl (*R*)-2-acetoxypropylphosphonate (**2-7**), was separated from the unreacted diethyl (*S*)-2-hydroxypropylphosphonate (**2-8**) by silica gel chromatography using ethyl acetate as solvent.

To the isolated acetylated compound (**2-7**) was added NH_3 (5 mL, 2M solution in MeOH). The solution was stirred at room temperature for 24 h and the desired product, diethyl (*R*)-2-hydroxypropylphosphonate (**2-9**), was purified by chromatography on silica gel using mixed solvent of ethyl acetate and ethanol.

The enantiomers of diethyl 2-hydroxypropylphosphonate (**2-8** and **2-9**, 0.7 g, 3.5 mmol each) were separately added with trimethylsilyl bromide (TMSBr, 2 g, 13 mmol) in dichloromethane (4 mL). The reaction solution was stirred for 24 h at room temperature. After dichloromethane was removed, the residue was vigorously stirred with 5 mL of water for 10 min. The aqueous layer was neutralized with NH_4HCO_3, washed with chloroform, and then lyophilized.

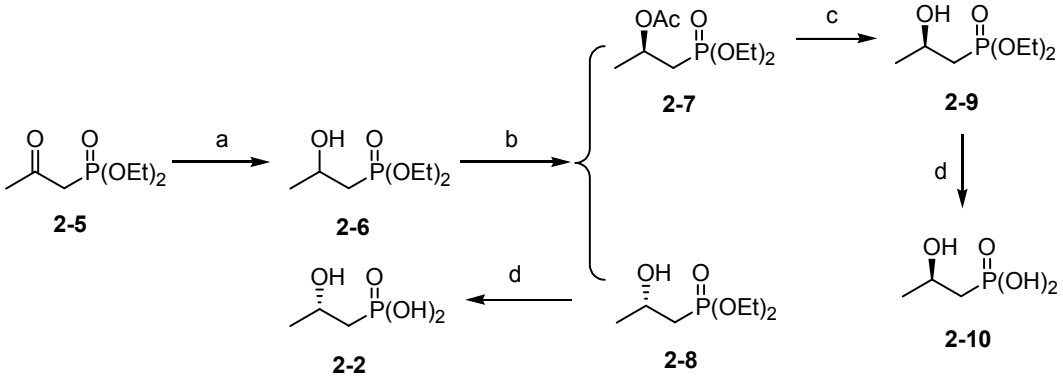

Figure 2-2. Synthetic scheme for (*S*)-2-hydroxypropyl phosphonic acid (**2-2**) and (*R*)-2-hydroxypropyl phosphonic acid (**2-10**). Reagents and conditions: a) $NaBH_4$/THF; b) lipase/vinyl acetate/isopropyl ether; c) NH_3/MeOH; d) TMSBr/CH_2Cl_2.

The spectral data of the final products, (*S*)-2-hydroxypropylphosphonic acid (**2-2**) and (*R*)-2-hydroxypropylphosphonic acid (**2-10**) are the same: ^{1}H NMR (300 MHz, D_2O) δ 3.80 (1H, m, *J* = 6.5, 2-H), 1.39 (2H, dd, *J* = 18.0, 6.6, 15.3, 1-H), 0.97 (3H, d, *J* = 6.5, 3-H); ^{13}C NMR (300 MHz, D_2O) δ 65.0 (d, *J* = 2.0, C-2), 37.9 (d, *J* = 132.0, C-1), 22.1 (C-3); ^{31}P NMR (300 MHz, D_2O) δ 19.9 (s).

NMR Assay. In order to directly determine the percentage of HPP conversion to fosfomycin catalyzed by HPP epoxidase, an NMR assay was developed. A typical assay mixture (100 μL) contained 10.5 mM (*S*)-HPP (**2-2**), 21.6 μM HppE, 21.8 mM NADH and 60 μM E_3 in 20 mM Tris·HCl buffer, pH 7.5. The reaction was carried out at room temperature with vigorous shaking and was quenched at an appropriate time by adding EDTA to a final concentration of 100 mM, followed by freezing with liquid nitrogen. The frozen sample was thawed immediately before NMR analysis. The amount of fosfomycin produced was determined based on integration of the appropriate NMR peaks. Spectral data of fosfomycin (**2-1**): ^{1}H NMR (300 MHz, D_2O) δ 3.03 (1H, m, *J* = 5.0, 2-H), 2.57 (1H, d, *J* = 5.0, 14.0, 1-H), 1.21 (3H, d, *J* = 5.5, 3-H); ^{13}C NMR (300 MHz, D_2O) δ 54.2 (s, C-2), 54.3 (d, *J* = 176.0, C-1), 13.2 (C-3); ^{31}P NMR (300 MHz, D_2O) δ 10.9 (s).

EPR Spectroscopy. EPR first derivative spectra of HppE were collected at X-band microwave frequency with 100-kHz field modulation on a Bruker Elexsys E500 spectrometer. A calibrated frequency counter and a Bruker ER035M NMR Gauss meter were used for the *g*-value determinations. The cryo-temperature measurements were achieved with an Oxford Instruments ESR-

10 continuous flow liquid helium cryostat and a digitalized temperature controller. Spin quantitation was performed by double integration of the corresponding spectra recorded under non-saturating conditions at 20 K using a Cu-EDTA standard (1 mM) for calibration. The EPR parameters were obtained using an EPR program written by Dr. Frank Neese (*21*) and were further verified in Bruker SimFonia.

The isolated, Fe^{II}-loaded (reduced) and Fe^{III}-reconstituted (oxidized) HppE were individually mixed with (*S*)-HPP (**2-2**) and/or FMN/NADH and then examined by EPR spectroscopy at 2 - 50 K. To prevent interference from oxidation by the air, the majority of the samples were prepared under strict anaerobic conditions. Oxygen was then removed by repeated cycles of vacuuming and argon flushing from all samples prior to NO exposure. The anaerobic solutions of purified enzyme, (*S*)-HPP, $Fe^{II}(NH_4)_2(SO_4)_2$, FMN, and NADH were made ready prior to mixing with each other. The solutions were transferred through gas-tight Hamilton syringes and the mixings took place in the EPR tubes under the protection of argon. Only the samples of Fe^{III}-reconstituted HppE, alone and with substrate, were prepared in the air.

In the nitric oxide (NO) experiments, the stricter anaerobic conditions were required. Oxygen was removed from all samples prior to NO exposure. NO gas was quantitatively introduced to the samples in EPR tubes through a gas-tight Hamilton syringe under the protection of argon. The samples were slowly chilled by liquid nitrogen for later EPR analysis.

2.3 RESULTS

Expression and Purification of Recombinant HppE. Wild-type HppE from *S. wedmorensis* was expressed using *E. coli* BL21(DE3)/pPL1001 constructed by Dr. Pinghua Liu and purified according to a previously reported procedure (*2*). As shown in SDS-PAGE (Figure 2-3), the desired protein was isolated in nearly homogeneous form after ammonium sulfate fractionation and two anion exchange chromatographic steps (DEAE-Sepharose and FPLC-Mono Q).

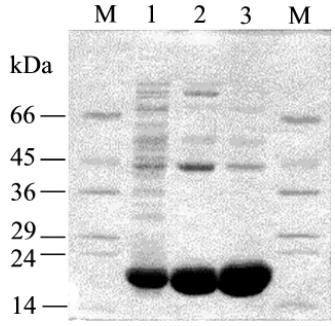

Figure 2-3. The SDS-PAGE gel of HppE purification. Lanes: M, Molecular weight markers: α-lactalbumin (14 kDa), trypsinogen (24 kDa), carbonic anhydrase (29 kDa), glyceraldehyde-3-phosphate dehydrogenase (36 kDa), egg albumin (45 kDa), and bovine serum albumin (66 kDa); 1, 35-60% $(NH_4)_2SO_4$ precipitate; 2, after DEAE-Sepharose column, 3, after FPLC-Mono Q column.

The subunit molecular mass of 21,208.9 Da, assessed by MALDI mass spectroscopy, correlates well with the predicted value of 21,210 Da calculated from the deduced amine acid sequence. The purified recombinant HppE exists as a homo-tetramer having a mass of 89 kDa as determined by gel filtration chromatography. Due to the inclusion of EDTA and DTT in the protein

purification procedure, the purified HppE is essentially free of iron. Indeed, iron titration analysis revealed less than 0.05% iron per monomer in the as-isolated HppE. The apo-HppE was found inactive in the epoxidase activity assay. After it was reconstituted with iron *in vitro*, the holo-enzyme regained its activity to produce fosfomycin (**2-1**) from (*S*)-HPP (**2-2**).

The Electronic Absorption Spectrum of HppE. When the isolated HppE was reconstituted with $Fe^{II}(NH_4)_2(SO_4)_2$ under anaerobic conditions, the resulting protein was colorless. However, when this sample was exposed to air, it slowly turned green in color. The optical spectrum of this green protein exhibits a broad band around 650 – 700 nm with a molar absorption coefficient of approximately 450 $(M \text{ of } Fe)^{-1} \cdot cm^{-1}$ (Figure 2-4). This absorption is likely due to a ligand–to–metal charge transfer (LMCT) transition. Detailed characterization of this chromophore will be reported in Chapter 3.

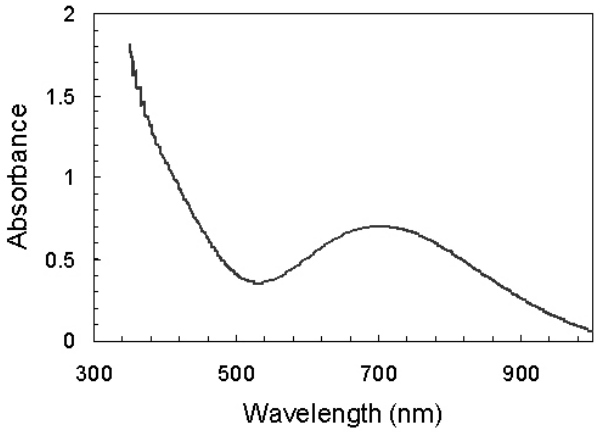

Figure 2-4. The electronic absorption spectrum of reconstituted HppE. Protein concentration is 1.4 mM.

EPR Characterization of Reconstituted HppE. As mentioned above, HppE as isolated contains little iron and thus is effectively EPR-silent. Stoichiometric addition (1.0 Fe/per enzyme monomer) of $Fe^{II}(NH_4)_2(SO_4)_2$ to the as-isolated HppE under anaerobic conditions led to an Fe^{II}-loaded holo-protein. As expected, the Fe^{II}-loaded HppE is EPR-inactive. Upon oxidation, the EPR spectrum of the oxidized sample displays a set of resonance at g = 4.29, 5.28, and 8.59, that is indicative of a mononuclear non-heme ferric center with d^5 electronic configuration of S = 5/2 and E/D of 0.145 (Figure 2-5A).

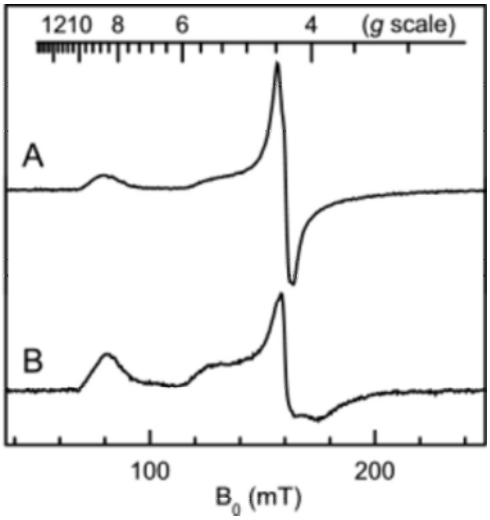

Figure 2-5. EPR spectra of reconstituted HppE. (A) 250 μM reconstituted (oxidized) HppE; (B) 250 μM reconstituted (oxidized) HppE in the presence of 10× excess of (*S*)-HPP. Instrumental parameters: temperature, 2 K; microwave frequency, 9.6 GHz; microwave power, 0.6 mW; modulation amplitude, 5 G; time constant, 0.02 s; sweep rate, 50 G/s.

The S = 5/2 EPR signal is sensitive to the binding with (*S*)-HPP (**2-2**) (Figure 2-5B). The broadening and splitting of the middle Kramer's doublet (g =

4.29) in the presence of (*S*)-HPP (**2-2**) suggest that the substrate binds to or near the iron center. Spin quantitation reveals that the total EPR-active ferric species accounts for about 0.7 iron per enzyme monomer, suggesting a large fraction of the Fe center is diamagnetic. It should be noted that an isotropic g = 4.3 component (S = 5/2) may also exist and be superimposed to the middle doublet of the signal with E/D of 0.145. Nevertheless, this component reflects only a minor fraction of the total Fe and may be ascribed to adventitiously bound ferric ion.

EPR Characterization of Fe^{II}-HppE Nitrosyl Complex. To assess whether the EPR-inactive iron in the reconstituted HppE are still in ferrous state, nitric oxide was added to the EPR sample. Since NO is known to complex with non-heme ferrous ion to produce species with electronic spin S = 3/2, the resulting EPR spectrum is expected to be different. Surprisingly, the EPR spectrum of reconstituted HppE (Figure 2-5A) is unaffected upon the addition of NO up to 1–5 times excess than the enzyme (data not shown). The absence of an EPR-active NO adduct with S = 3/2 signature argues against the presence of a large fraction of ferrous ion in the oxidized HppE. To test if the reduced iron center of HppE is accessible to nitric oxide, the NO experiment was also performed with the Fe^{II}-loaded enzyme. It was found that anaerobic addition of NO to this sample led to the formation of at least two major S = 3/2 species from the diamagnetic Fe^{II} protein (Figure 2-6A). In addition, a signal derived from a small amount of ferric ion is also discernible, a phenomenon likely due to the carrying over from the native protein. The spin quantitation of all EPR-active components in this sample is close to the full content of the total iron.

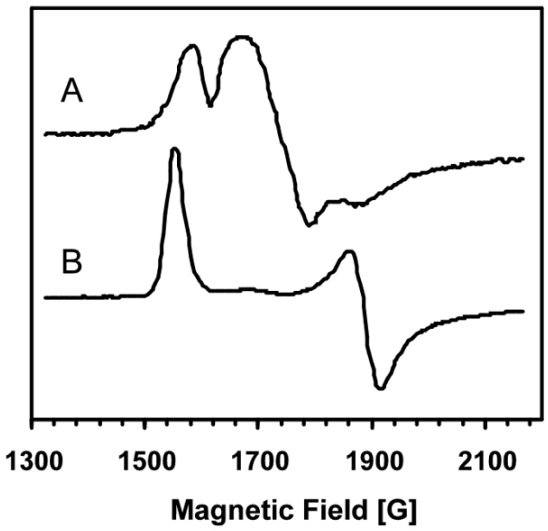

Figure 2-6 EPR spectra of Fe^{II}-HppE nitrosyl complexes. (A) 250 μM Fe^{II}-loaded HppE in the presence of NO; (B) the ternary complex of Fe^{II}-loaded HppE, substrate (10-fold excess over active sites) and NO. Instrumental parameters are the same as those in Figure 2-5.

As shown in Figure 2-6A, an Fe^{II}-NO adduct has *g* values at 3.94 and 4.16 (and 1.99), with an E/D value of 0.055. This species is highly temperature sensitive and becomes less pronounced when temperature rises from 2 K to 10 or 20 K (data not shown). The resonance of another Fe^{II}-NO complex is much broader and has a doublet splitting with spectral features at 3.57 and 4.36 (and 1.99) (E/D = 0.013). Spectral simulations (Figure 2-7) show that the E/D = 0.055 signal (Figure 2-7C) and the E/D = 0.013 signal (Figure 2-7D) account for about half of the iron, respectively. The relative concentration of the two Fe^{II}-nitrosyl centers can be varied. This may be ascribed to the NO diffusion consistency in EPR tubes during sample preparations at various protein concentrations. These results clearly demonstrate that the ferrous center of the

reduced HppE can react with the dioxygen analogue, NO. Since no Fe^{II}-nitrosyl adduct was detected in the oxidized enzyme treated with NO, one may conclude that the iron in the oxidized epoxidase is primarily at its ferric state. The data have revealed the presence of heterogeneity of the Fe center in both the reduced and oxidized epoxidase, each consisting of two or more components. The nature of the EPR-inactive fraction of the ferric center and the underlying reason for the heterogeneity of the Fe centers at both reduced and oxidized forms are intriguing.

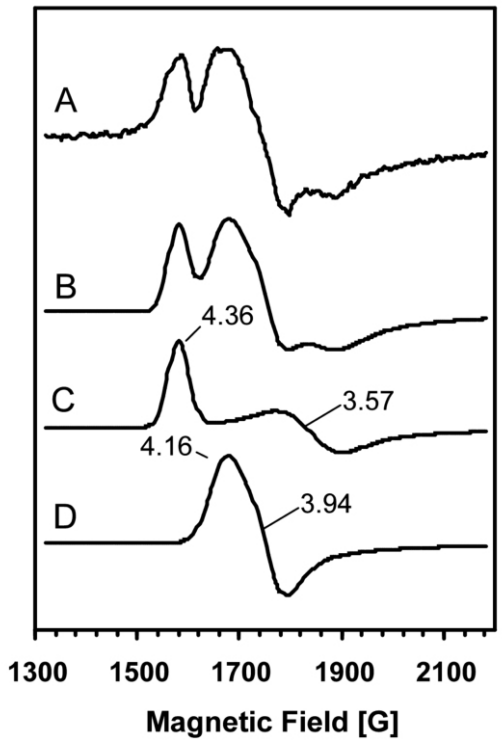

Figure 2-7 Simulations of EPR spectra of Fe^{II}-HppE nitrosyl complexes. (A) Experimental spectrum in Figure 2-6A, (B) Simulated spectrum combining C (50%) and D (50%), (C) Simulated spectrum of the EPR signal with E/D = 0.055, (D) Simulated spectrum of the EPR signal with E/D = 0.013. Important *g* values are given in spectra.

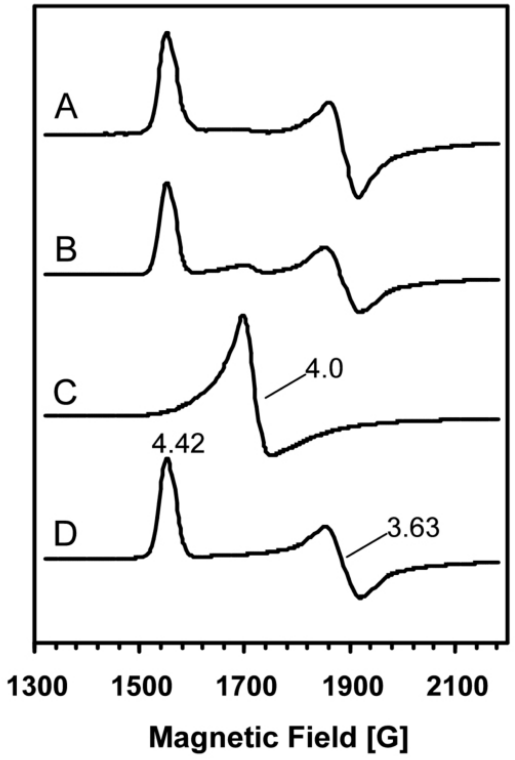

Figure 2-8 Simulations of EPR spectra of Fe^{II}-HppE·substrate nitrosyl complexes. (A) Experimental spectrum in Figure 2-6B, (B) Simulated spectra combining C (95%) and D (5%), (C) Simulated spectrum of the EPR signal with E/D = 0.066, (D) Simulated spectrum of the EPR signal with E/D = 0. Important *g* values are given in spectra.

As shown in the spectrum B of Figure 2-6, addition of (*S*)-HPP to the Fe^{II}-HppE nitrosyl complex results in a significant change in the EPR spectrum. Most of the heterogeneity that characterizes the ferric complex and the nitrosyl complex of the substrate free enzyme disappears and a single species predominates with *g* values of 4.42, 3.63 and 1.97, and E/D value of 0.066. Spectral simulations (Figure 2-8) show that the dominant E/D = 0.066 signal

(Figure 2-8C) is responsible for 95% of the iron center in the spectrum B of Figure 2-6. An extremely minor species (g = 4.0, E/D = 0) was also identified (Figure 2-8D), which accounts for about 5% of the whole spectrum (Figure 2-6B). Quantitation of the spectrum by double integration shows that nearly all the iron centers bind substrate and NO. These results suggest that substrate binds near, and perhaps directly to, the ferrous active site, and in doing so organizes the metal center so that effectively only one species is present.

During nitrosyl EPR sample preparation, the order of additions of substrate and NO was found not critical. However, protein precipitation often occurred when more than enough NO gas was introduced to Fe^{II}-HppE·substrate complex. Sometimes, the precipitated protein could be resuspended after gentle shaking. However, the effects on EPR spectra caused by protein precipitation were irreversible. For example, totally different EPR spectra were obtained by measuring these denatured samples (Figure 2-9D). Most of the spectra consist of two major signals, as predicted by spectral simulations in Figure 2-8 (simulated spectra C and D). These two signals are supposed to correspond to native and denatured forms of the Fe^{II}-HppE·substrate nitrosyl complex. The ratio of the signal intensities may reflect the degree of denaturation of the protein induced by excess NO gas (Figure 2-9A-D).

The Reaction Sequence. In order to determine the reaction sequence, a set of experiments was carried out with NO, a molecular oxygen analogue. The EPR spectrum of the oxidized HppE is unaffected by the anaerobic addition of NO to the sample (data not shown). Since no Fe^{II}-nitrosyl adduct was detected

in the oxidized enzyme treated with NO, one may conclude that the iron in the oxidized epoxidase is primarily at its ferric state.

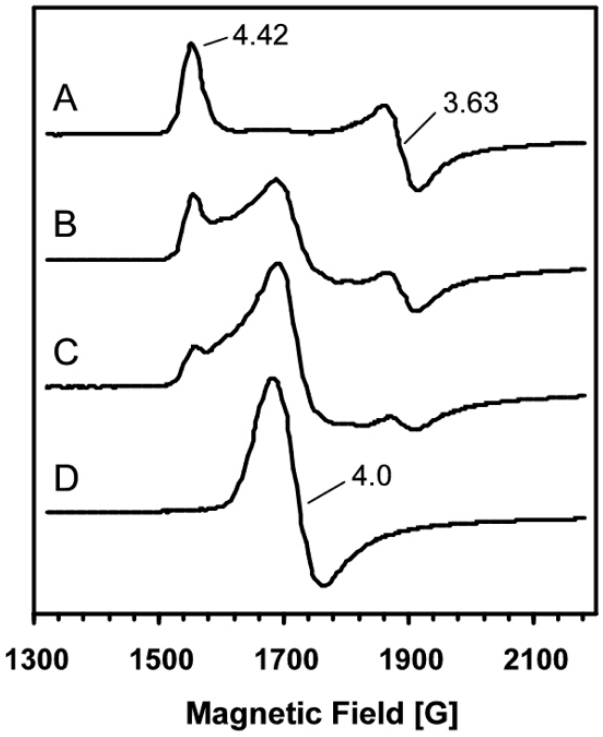

Figure 2-9 EPR spectra of Fe^{II}-HppE with substrate in the presence of increasing amounts of NO (A $\rightarrow$ D). Instrumental parameters are the same as those in Figure 2-5. Important *g* values are given in spectra.

Anaerobically addition of NADH/FMN, a reducing system used for *in vitro* reconstitution of the epoxidase activity of HppE, to the reconstituted HppE had no effects on the corresponding EPR signals (Figure 2-5A *vs.* Figure 2-10A). Neither did the addition of NO to the mixture of enzyme, substrate, and NADH/FMN lead to any change of its EPR spectrum (Figure 2-10B).

Interestingly, mixing of (*S*)-HPP (**2-2**) and NADH/FMN together with the reconstituted HppE rendered the majority of the ferric signals disappear. An immediate explanation is that the ferric center was reduced to the EPR-silent ferrous state by NADH/FMN in the presence of substrate. The introduction of NO gas to the sample soon verified the above hypothesis by visualizing the otherwise invisible ferrous ion. A new signal with *g* values of 4.42 and 3.63 appeared in the EPR spectrum (Figure 2-10C), which is reminiscent of that of the Fe^{II}-HppE·substrate nitrosyl complex (Figure 2-6B). When these two spectra are closely compared, it becomes apparent that they are nearly identical (Figure 2-11). Clearly, the ferric ion reduced by NADH/FMN in the presence of substrate and the ferrous ion detected when complexed with NO are the same iron center, but in different oxidation states. Given the substantial effects of substrate binding on the environment of the active site iron (Figure 2-5 and Figure 2-6) and on its redox potential (Figure 2-10), it is very likely that (*S*)-HPP directly coordinates to the iron center in HppE. The reduction of the ferric center of HppE by NADH/FMN has also been observed in the presence of the alternative substrate, (*R*)-HPP, and the inhibitor, (*S*)-FHPP, (data not shown), and thus strongly supports the hypothesis of direct coordination of substrate to the iron center.

Along with the signal of the $S = 3/2$ Fe^{II}-nitrosyl adduct, a radical-like signal also emerged at $g = 2$ region in the same EPR spectrum (Figure 2-10C). Although the identity of the $S = 1/2$ free radical signal has not yet been determined, it is likely derived from a substrate-based radical. This series of

experimental results demonstrated that the reducing system only reacts with the E·S binary complex but not the enzyme alone. The iron-binding pattern of both enantiomers of HPP may play an important role in regulating the redox potential of the iron center.

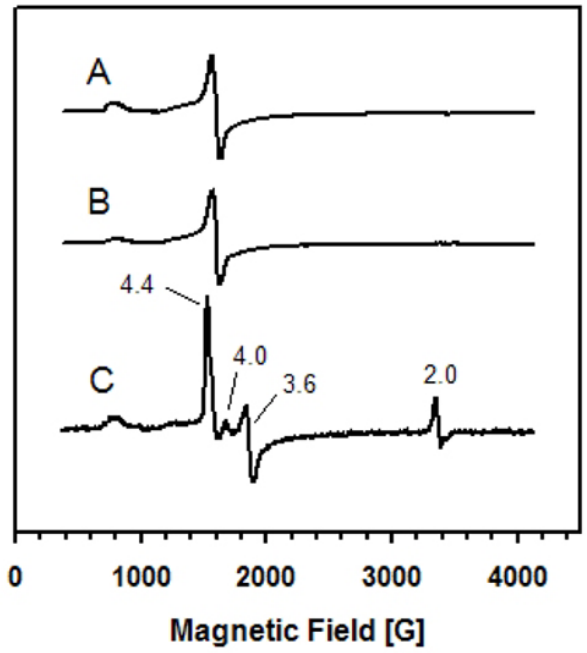

Figure 2-10 EPR spectra of reconstituted HppE in the presence of FMN/NADH. (A) Reconstituted HppE + FMN/NADH; (B) Reconstituted HppE + FMN/NADH + NO; (C) Reconstituted HppE + FMN/NADH + NO + substrate. Instrumental parameters are the same as those in Figure 2-5. Important *g* values are given in spectra.

2.4 DISCUSSION

The expression, purification and *in vitro* activity reconstitution of HppE have shown the dependence of its catalysis on iron. Through *in vitro* iron reconstitution, the as-isolated apo-HppE was found to bind nearly an equivalent of

ferric ion per enzyme monomer and then become active to catalyze epoxidation reaction. In contrast to the heme-containing proteins that have a strong characteristic band in the blue region (~ 400 nm) of their optical absorption spectra, which is known as Soret band, the similar optical features were missing in the spectrum of reconstituted HppE (Figure 2-4) (*4*). The lacking of Soret band clearly indicates that HppE relies on a non-heme iron in its active site, instead of a heme iron, for catalysis. Thus, HppE is a new member of the family of mononuclear non-heme iron-dependent enzymes.

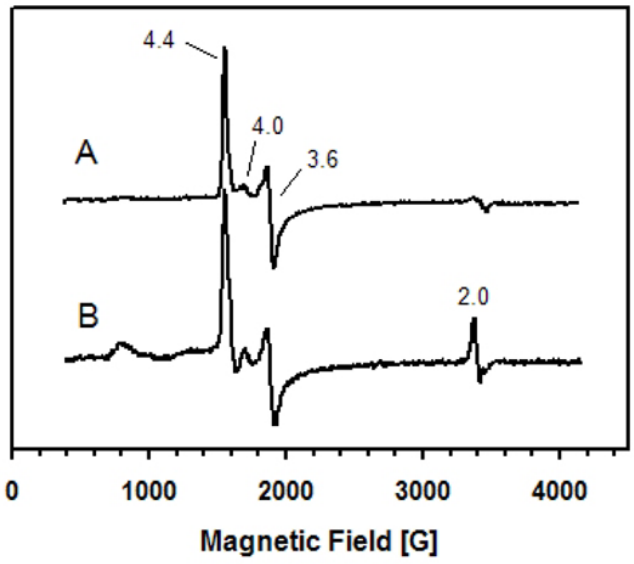

Figure 2-11 Comparison of EPR spectra. (A) Fe^{II}-HppE + (*S*)-HPP + NO (Figure 2-6B); (B) the reconstituted HppE + FMN/NADH + (*S*)-HPP + NO (Figure 2-10C). Important *g* values are given in spectra.

EPR spectroscopy is a powerful tool to study proteins containing transition metals. Many non-heme iron enzymes have been analyzed by this spectroscopic

technique and a great deal of structural and mechanistic information has thus been obtained (*12, 13*). As a new mononuclear non-heme iron enzyme that catalyzes a unique epoxidation reaction, HppE was also subjected to EPR spectral analysis. The EPR spectra of HppE in its oxidized and reduced forms are typical for a non-heme iron-containing enzyme. Upon substrate binding, the spectral features were significantly affected, suggesting that the substrate may bind directly to the iron or closely nearby. The most interesting finding from these EPR analyses is that FMN/NADH cannot reduce the ferric center of HppE unless the substrate is also added. This observation strongly suggests that substrate binding has a significant impact on the active site iron of HppE, not only on its spectral features but also on its redox potential.

Since the epoxidation reaction catalyzed by HppE involves the full reduction of dioxygen to water, it is necessary for the iron center to be in its ferrous state for the dioxygen activation step in the catalytic cycle. The reduction of ferric center of HppE by FMN/NADH provides the means to produce the catalytically necessary ferrous center. On the basis of our experimental results, a minimal reaction sequence can be formulated as shown in Figure 2-12. These few steps constitute the early stage of the enzymatic epoxidation, in which HppE and its iron center, substrate, dioxygen and electron donor are all made ready for the subsequent chemical steps of catalysis. The $S = 3/2$ Fe^{II}-HppE·(*S*)-HPP nitrosyl complex that gave rise to the homogeneous EPR signal in Figure 2-6B may be the best representative of this catalytically ready stage.

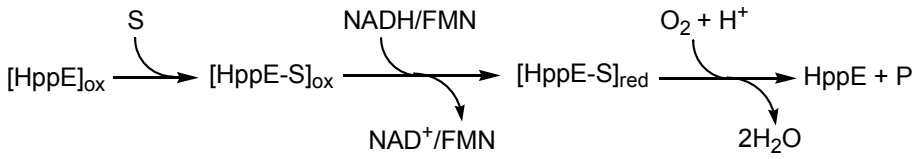

Figure 2-12 The minimal reaction sequence in the early stage of HppE catalysis.

The reaction sequence proposed above is analogous to the beginning steps in the catalytic mechanism of cytochrome P450s (Figure 1-9, **A** → **D$_1$**). In the catalysis of P450s, dioxygen is then activated by reacting with the heme ferrous center and receiving exogenous electrons to form the hypothetic compound I (**G**), an Fe^V species that is presumably responsible for the substrate oxidation (*4*). It is generally believed that Fe^V is a highly unstable species and thus exists in the form of Fe^{IV}-oxo with a porphyrin radical cation. However, no porphyrin ring is present in non-heme iron enzymes to stabilize Fe^V. Alternatively, Fe^{IV} intermediates are more commonly accepted in the mechanisms proposed for mononuclear non-heme iron enzymes. Some Fe^{IV} centers have been experimentally identified in enzymes and model compounds (*22, 23*). As a new mononuclear non-heme iron enzyme, HppE is assumed to rely on a similar Fe^{IV} intermediate rather than a less stable Fe^V intermediate in its catalytic mechanism. On the other hand, HppE resembles P450s owing to its dependence on NADH as the electron source and the requirement of a reductase as the electron transfer mediator. Using this reductase/NADH reduction system, electrons can be transferred in a step-wise manner. In contrast, a large number of mononuclear

non-heme iron enzymes rely on cosubstrates like α-KG and pterin that can only donate two electrons together at one time.

Recently, Hammerschmidt and co-workers reported that (1*S*, 2*S*)-1,2-epoxypropylphosphonic acid (**2-11**) may be a co-metabolite of fosfomycin (**2-1**), and both of them are products of the oxidation of (*S*)-HPP (**2-2**) by HppE (*24*). Several mechanisms can be envisioned to account for the above observations. The most likely mechanism involves a substrate radical intermediate as shown in Figure 2-13. Thus, the formation of *trans*-epoxide may be a result of the rotation around C_1-C_2 bond at the α-C radical (**2-12**) stage. It should be mentioned here that HppE converts not only **2-2** to **2-1**, but also the *R*-isomer of HPP (**2-10**) to 2-oxopropylphosphonic acid (**2-14**) with nearly equal efficiency (*20*). The oxidation of the (*R*)-isomer of HPP by HppE is believed to involve the formation of a carbon-centered β-ketyl radical (**2-13**), which is distinct from the α-radical intermediate proposed for the catalysis of (*S*)-HPP (**2-2**) (Figure 2-13).

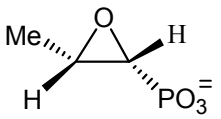

2-11

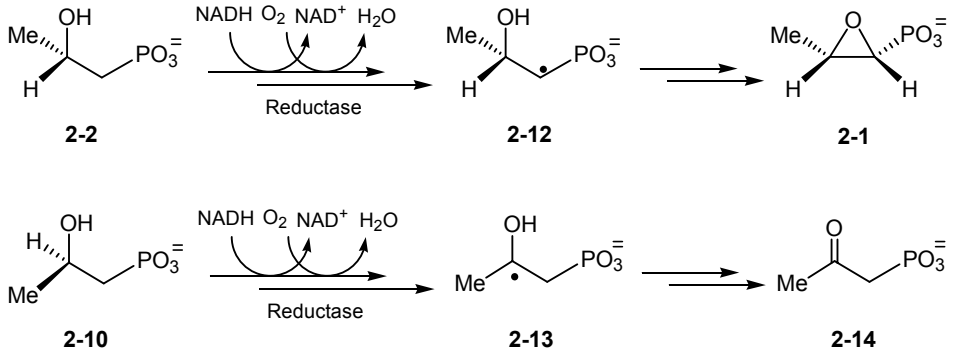

Figure 2-13 The proposed substrate radical intermediates in the conversions of both enantiomers of HPP catalyzed by HppE (*20*).

On the basis of above discussion, an Fe^{IV} intermediate and a substrate-based radical intermediate have thus been proposed to be part of the catalytic cycle of HppE. The steps involving formation of these intermediate as well as the earlier established beginning steps involving substrate binding, iron reduction and dioxygen activation, constitute a nearly complete cycle of enzymatic epoxidation. Now, the question comes down to the key chemical steps in the reaction, the formation of the substrate radical intermediate via hydrogen abstraction, and the formation of the final product via epoxide ring closure. Hydrogen abstraction is probably the most important step in enzymatic epoxidation since the regiospecificity and stereospecificity of the reaction are supposedly determined in this step. It is currently unclear which iron-oxygen oxidative species is responsible for the abstraction of the hydrogen atom from the substrate. After dioxygen docks on the non-heme iron center of HppE, it would evolve into at least four distinct species Fe^{III}-superoxy (**2-15**), Fe^{III}-peroxy (**2-16a**), Fe^{III}-hydroperoxy (**2-16b**), and Fe^{IV}-oxo (**2-17**), depending on how many

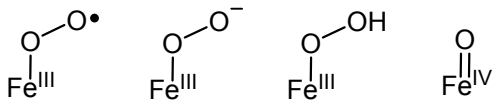

2-15 **2-16a** **2-16b** **2-17**

electrons and protons are transferred to the iron-oxygen adduct. Among them, Fe^{IV}-oxo (**2-17**) is the most reactive species and thus is commonly proposed to play the hydrogen abstracting role. As a general oxidative species, Fe^{IV}-oxo is also able to perform other oxidative tasks including sulfoxidation, *N*-demethylation and olefin epoxidation (*13*). However, it has been known that

HppE cannot convert an alkene like **2-3** to its corresponding epoxide product like fosfomycin (**2-1**) (*7*). Therefore, relative to other iron-oxygen reactive species, Fe^{IV}-oxo (**2-17**) is less likely responsible for the C-H bond cleavage in the HppE reaction. The Fe^{III}-peroxy (**2-16a**) and Fe^{III}-hydroperoxy (**2-16b**) species only differ by one proton. To abstract a hydrogen atom from the substrate, they have to undergo a homolytic cleavage of the O-O bond to form the next stable intermediate, Fe^{IV}-oxo, and release a molecule of water for **2-16b** or a hydroxide ion for **2-16a**. Apparently, it is more thermodynamically favorable for Fe^{III}-hydroperoxy (**2-15b**) to take the hydrogen atom. Fe^{III}-superoxy (**2-15**) has not often been proposed for C-H activation because the C-H bonds in substrates are generally stronger than the terminal O-H bond in Fe^{III}-hydroperoxy. In another word, there will be little energy gain by breaking a C-H bond and forming an O-H bond. Therefore, even if the hydrogen atom were abstracted by Fe^{III}-superoxy (**2-15**), the process will most likely end in equilibrium and need the subsequent steps involving cleavage of the O-O bond and formation of the Fe^{IV}-oxo species (**2-17**) to provide the driving forces to shift the equilibrium toward completion. In summary, the hydrogen abstraction mechanisms via different iron-oxygen intermediates are illustrated in Figure 2-14.

Since the formation of an Fe^{IV}-oxo intermediate along with a substrate radical is very likely the outcome of the hydrogen abstraction step in enzymatic epoxidation, as indicated by Figure 2-14, the epoxide ring closure must be accomplished by a radical induced C-O bond formation. The homolytic

cleavage of the Fe-O bond provides an electron to regenerate the ferric center of HppE. The complete catalytic cycle is illustrated in the Figure 2-15.

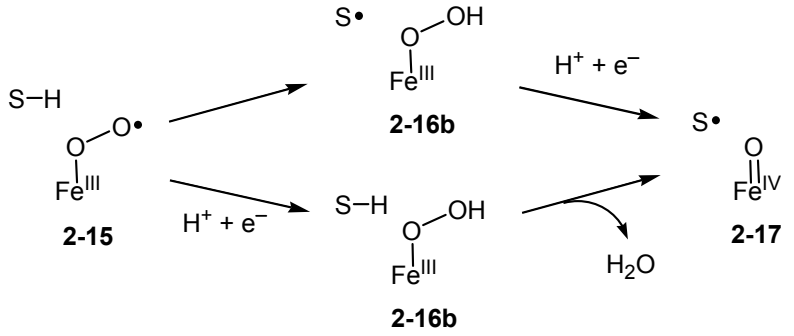

Figure 2-14 The proposed mechanisms of hydrogen abstraction in HppE catalysis.

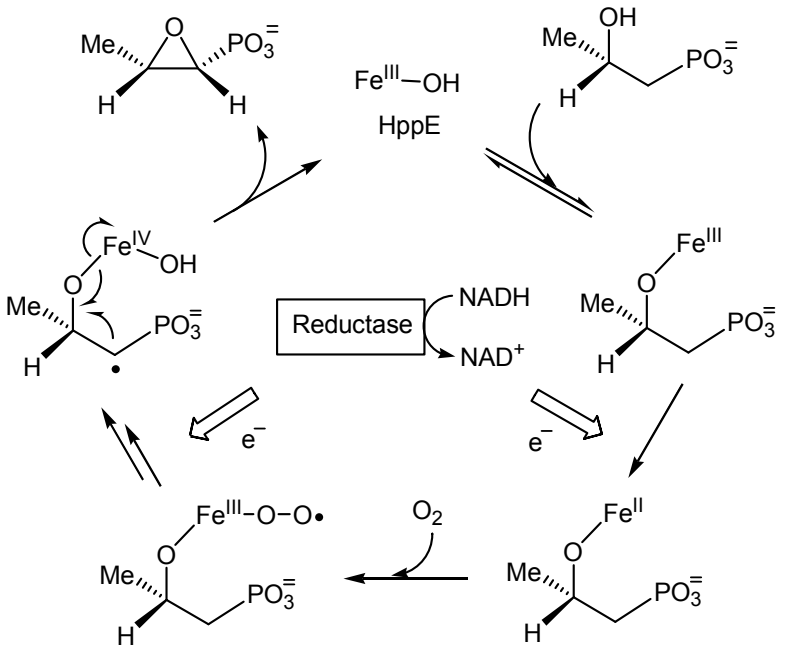

Figure 2-15 Proposed mechanism of HppE-catalyzed epoxidation reaction.

The proposed mechanism starts with HppE in its ferric state, the assumed resting state of the enzyme. Its ferric center is first bound with (*S*)-HPP, and then reduced to the ferrous state by receiving an electron from NADH mediated by the reductase. The resulting substrate-bound ferrous center binds dioxygen and activates it to form some reactive iron-oxygen species. The direct coordination of (*S*)-HPP (**2-2**) to iron center of HppE is strongly hinted by the EPR results, and is important for facilitating electron flow between substrate and iron-oxygen intermediates in the following steps. Abstraction of an α-H of (*S*)-HPP (**2-2**), by either Fe^{III}-superoxy (**2-15**) or Fe^{III}-hydroperoxy (**2-16b**) as previously discussed (Figure 2-14), is followed by a radical induced homolytic cleavage of the Fe–O bond. Accompanying the product formation, the iron center is reduced back to its resting ferric state.

2.5 REFERENCE

1. Hidaka, T., Goda, M., Kuzuyama, T., Takei, N., Hidaka, M., and Seto, H. (1995) "Cloning and nucleotide sequence of fosfomycin biosynthetic genes of *Streptomyces wedmorensis*" *Mol. Gen. Genet. 249*, 274-280.
2. Liu, P., Murakami, K., Seki, T., He, X., Yeung, S. M., Kuzuyama, T., Seto, H., and Liu, H. (2001) "Protein purification and function assignment of the epoxidase catalyzing the formation of fosfomycin" *J. Am. Chem. Soc. 123*, 4619-4620.
3. Liu, P., Liu, A., Yan, F., Wolfe, M. D., Lipscomb, J. D., and Liu, H. W. (2003) "Biochemical and spectroscopic studies on (*S*)-2-hydroxypropylphosphonic acid epoxidase: a novel mononuclear non-heme iron enzyme" *Biochemistry 42*, 11577-11586.
4. Ortiz de Montellano, P. R. (1995) *Cytochrome P450: Structure, Mechanism, and Biochemistry*, Plenum Press, New York.
5. Sono, M., Roach, M. P., Coulter, E. D., and Dawson, J. H. (1996) "Heme-containing oxygenases" *Chem. Rev. 96*, 2841-2887.

6. Lange, S. J., and Que, L., Jr. (1998) "Oxygen activating nonheme iron enzymes" *Curr. Opin. Chem. Biol. 2*, 159-172.

7. Seto, H., Hidaka, T., Kuzuyama, T., Shibahara, S., Usui, T., Sakanaka, O., and Imai, S. (1991) "Studies on the biosynthesis of fosfomycin. 2. Conversion of 2-hydroxypropyl-phosphonic acid to fosfomycin by blocked mutants of *Streptomyces wedmorensis*" *J. Antibiot. (Tokyo) 44*, 1286-1288.

8. Hammerschmidt, F. (1991) "Biosynthesis of natural products with a phosphorus-carbon bond. Part 8. On the origin of the oxirane oxygen atom of fosformycin in *Streptomyces fradiae*" *J. Chem. Soc., Perkin Trans. 1*, 1993-1996.

9. Hashimoto, T., and Yamada, Y. (1987) "Purification and characterization of hyoscyamine 6 β-hydroxylase from root cultures of *Hyoscyamus niger* L. Hydroxylase and epoxidase activities in the enzyme preparation" *Eur. J. Biochem. 164*, 277-285.

10. Hashimoto, T., Matsuda, J., and Yamada, Y. (1993) "Two-step epoxidation of hyoscyamine to scopolamine is catalyzed by bifunctional hyoscyamine 6 β-hydroxylase" *FEBS Lett. 329*, 35-39.

11. Liu, P. (2001) Ph.D. dissertation, "Insights into the enzymes in fosfomycin biosynthesis: mechanistic studies of HPP epoxidase" *Department of Chemsitry*, *The University of Minnesota*, *Minneapolis*, 77.

12. Solomon, E. I., Brunold, T. C., Davis, M. I., Kemsley, J. N., Lee, S.-K., Lehnert, N., Neese, F., Skulan, A. J., Yang, Y.-S., and Zhou, J. (2000) "Geometric and electronic structure/function correlations in non-heme iron enzymes" *Chem. Rev. 100*, 235-349.

13. Costas, M., Mehn, M. P., Jensen, M. P., and Que, L., Jr. (2004) "Dioxygen activation at mononuclear nonheme Iron active sites: enzymes, models, and intermediates" *Chem. Rev. 104*, 939-986.

14. Prescott, A. G., and Lloyd, M. D. (2000) "The iron(II) and 2-oxoacid-dependent dioxygenases and their role in metabolism" *Nat. Prod. Rep. 17*, 367-383.

15. Rocklin, A. M., Tierney, D. L., Kofman, V., Brunhuber, N. M. W., Hoffman, B. M., Christoffersen, R. E., Reich, N. O., Lipscomb, J. D., and Que, L., Jr. (1999) "Role of the nonheme Fe(II) center in the biosynthesis of the plant hormone ethylene" *Proc. Natl. Acad. Sci. USA 96*, 7905-7909.

16. Fitzpatrick, P. F. (1999) "Tetrahydropterin-dependent amino acid hydroxylases" *Annu. Rev. Biochem. 68*, 355-381.

17. Kappock, T. J., and Caradonna, J. P. (1996) "Pterin-dependent amino acid hydroxylases" *Chem. Rev. 96*, 2659-2756.

18. Gibson, D. T., and Parales, R. E. (2000) "Aromatic hydrocarbon dioxygenases in environmental biotechnology" *Curr. Opin. Biotechnol. 11*, 236-243.

19. Bradford, M. M. (1976) "A rapid and sensitive method for the quantitation of microgram quantities of protein utilizing the principle of protein-dye binding" *Anal. Biochem. 72*, 248-254.

20. Zhao, Z., Liu, P., Murakami, K., Kuzuyama, T., Seto, H., and Liu, H. W. (2002) "Mechanistic studies of HPP epoxidase: configuration of the substrate governs its enzymatic fate" *Angew. Chem. Int. Ed. 41*, 4529-4532.

21. Neese, F., Zumft, W. G., Antholine, W. E., and Kroneck, P. M. H. (1996) "The purple mixed-valence CuA center in nitrous-oxide reductase: EPR of the ^{63}Cu-, ^{65}Cu-, and Both ^{65}Cu- and ^{15}N histidine-enriched enzyme and a molecular orbital interpretation" *J. Am. Chem. Soc. 118*, 8692-8699.

22. Rohde, J. U., In, J. H., Lim, M. H., Brennessel, W. W., Bukowski, M. R., Stubna, A., Münck, E., Nam, W., and Que, L., Jr. (2003) "Crystallographic and spectroscopic characterization of a nonheme Fe(IV)-O complex" *Science 299*, 1037-1039.

23. Price, J. C., Barr, E. W., Tirupati, B., Bollinger, J. M., Jr., and Krebs, C. (2003) "The first direct characterization of a high-valent iron intermediate in the reaction of an α-ketoglutarate-dependent dioxygenase: A high-spin Fe(IV) complex in taurine/α-ketoglutarate dioxygenase (TauD) from *Escherichia coli*" *Biochemistry 42*, 7497-7508.

24. Woschek, A., Wuggenig, F., Peti, W., and Hammerschmidt, F. (2002) "On the transformation of (*S*)-2-hydroxypropylphosphonic acid into fosfomycin in *Streptomyces fradiae*--a unique method of epoxide ring formation" *Chembiochem 3*, 829-835.

Chapter 3: Self-catalytic Hydroxylation of HppE

3.1 INTRODUCTION

As a newly identified mononuclear non-heme iron enzyme, HppE is clearly in a class of its own within this family of enzymes. Unlike most other members of this superfamily, which utilize an organic co-substrate or the Rieske center to aid in oxygen activation (*1-5*), HppE has no built-in iron-sulfur cluster and is ascorbate-, pterin-, and α-KG-independent. Instead, its catalytic turnover consumes a stoichiometric amount of NADH using molecular oxygen as the oxidant (*6, 7*). A reductase, whose identity remains elusive, is also required to mediate electron transfer from NADH to the epoxidase. The reaction catalyzed by HppE is beyond the scope currently encompassed by common biological epoxidation and C-O bond formation reactions. It converts a secondary alcohol, an unusual substrate of natural enzymatic epoxidation, to an epoxide. More interestingly, the alcoholic oxygen is retained in the product. Therefore, the overall epoxidation reaction is actually a dehydrogenation reaction.

In our earlier studies (*7*), we have found that the heterologously expressed HppE is an apo-protein. This tetrameric enzyme can be reconstituted with $Fe^{II}(NH_4)_2(SO_4)_2$ to a 1:1 ratio of iron per enzyme monomer. The anaerobically reconstituted Fe(II)-enzyme is colorless, but it develops a green color upon air exposure in the absence of substrate (*7*). Inspired by the possibility that the green chromophore may be related to the unique catalytic property of HppE, lots of efforts have been devoted to determine the identity of this green chromophore

and to study its biogenesis. In collaboration with Dr. Mark P. Mehn and Dr. Lawrence Que at the University of Minnesota, we have characterized this chromophore by quinone staining and resonance Raman spectroscopic techniques. This chapter describes the evidence collected through the collaborative efforts, uncovering an Fe^{III}-catecholate complex as the chromophoric core, and Tyr105 as the most likely site of post-translational modification to dihydroxyphenylalanine (DOPA). Also included are the possible mechanisms of DOPA formation and the implications on the catalytic mechanism of HppE.

3.2 MATERIALS AND METHODS

General. HppE was purified from *E. coli* BL21(DE3)/pPL1001 according to the published procedure (*7*). The enzyme activity was determined as previously described (*7*). DNA sequencing was carried out by the Core Facility of the Institute for Cellular and Molecular Biology, University of Texas at Austin. All reagents and solvents were purchased from commercial sources and were used without further purification unless otherwise noted. Biochemicals were purchased from Sigma (St. Louis, MO). Labeled water (95% ^{18}O) and labeled oxygen (99% ^{18}O) were obtained from ICON, Inc (Summit, NJ).

Preparation of HppE Mutants. Site-directed mutagenesis of the HppE gene (*fom4*) was carried out using QuickChange™ Site-directed Mutagenesis Kit from Strategene (La Jolla, CA). The oligonucleotide primers used for mutagenesis were custom-made by Invitrogen (Carlsbad, CA), which are, for the Y103/105F double mutant, pFYF7: 5′-CAACGTCGACTACTTCGTCTTCAAC-TGTCTCGTCC-3′, and pFYF8: 5′-GGACGAGACAGTTGAAGACGAAGTAG-

TCGACGTTG-3′. The nucleotide primers for the C107A single mutant to be used in mass spectral study are pFYC1: 5′-CTACGTCTACAACGCTCTC-GTCCGCACC-3′, and pFYC2: 5′-GGTGCGGACGAGAGCGTTGTAGACGTA-G-3′. Mutant plasmids were constructed by PCR amplification of the HppE gene from pPL1001 using the above primers under the following conditions: (1) 14 cycles at 95 °C for 30 s, 55 °C for 1 min, and 68 °C for 10 min; (2) 1 cycle at 72 °C for 10 min. The PCR template in each sample was digested with *Dpn*I at 37 °C for 1 h and the recombinant plasmid was then used to transform *E. coli* XL1-blue supercompetent cells. After their sequences were confirmed by DNA sequencing, these mutant plasmids were used to transform *E. coli* BL21(DE3) competent cells for expression. The mutant proteins were purified according to the same procedure used for the wild type HppE. After reconstitution with $Fe^{II}(NH_4)_2(SO_4)_2$, the excess metals were removed by a G-10 column. The resultant proteins were stored at – 80 °C. Single mutants Y102F, Y103F and Y105F were constructed by Dr. Zongbao Zhao (*8*).

Preparation of HppE with Various Extents of Modification. To verify the role of iron in self-modification of HppE, the enzyme was expressed in iron-depletion (ID) medium (*9*) that contained 45.4 mM phosphate buffer, pH 7.3, 7.57 mM $(NH_4)_2SO_4$, 0.4% glucose, 610 μM L-leucine, 406 μM $MgSO_4$, 50 μM EDTA, 5 μM $CaCl_2$, 0.6 M $ZnCl_2$, 60 μM $CuSO_4$, 0.6 μM $MnCl_2$, 0.75 μM $CoC1_2$, 5.9 μM thiamin dichloride, and 50 μg/mL kanamycin. The phosphate buffer, $(NH_4)_2SO_4$, glucose, and leucine solutions were all filtered through Corning sterile syringe filters with 0.22 μm membrane (Corning, NY) prior to media

preparation. The expression and purification of HppE from iron-depletion medium (ID-HppE) were carried out by the same procedures as previously reported for HppE from LB medium (LB-HppE) (*7*). Since the growth of cells in the ID medium is slower than that in the LB medium, extended growth time was required.

To examine the effects of iron content in the growth media on the extent of posttranslational modification, HppE was also expressed in ID media supplemented with 0.1, 0.01, 0.001 and 0.0001 mM of $Fe^{II}(NH_4)_2(SO_4)_2$, which were named as low iron media 1 to 4 (LI1 – LI4), respectively. The produced enzymes (LI1-HppE - LI4-HppE) were purified according to the procedure established for LB-HppE (*7*). The extent of self-hydroxylation was analyzed by NBT quinone staining and electronic absorption spectroscopy.

NBT Staining and NBT/glycinate Solution Test. The wild type HppE produced in different media and its mutants were subjected to 15% SDS-PAGE and transblotted onto a nitro-cellulose membrane at 100 V for 1 h using a transfer buffer (25 mM Tris base, 192 mM glycine, 20% methanol). Detection of the presence of quinoid structure was performed according to a procedure of Paz *et al.* (*10*) by immersing the membrane in a solution of 0.24 mM nitroblue tetrazolium and 2 M potassium glycinate, pH 10, for 45 min. After the membrane was rinsed with H_2O, the stained bands were recorded.

NBT/glycinate solution test is based on the same principle as NBT staining but designed for quantitative purpose. In this test, samples were directly mixed with the solution of 0.24 mM nitroblue tetrazolium and 2 M potassium

glycinate, pH 10. After 1 h incubation, the quinone contents in these samples were determined on the basis of the intensity of purple color developed, measured at 560 nm by a UV-vis spectrometer.

Preparation of HppE Samples for Raman Spectral Studies. The apo-enzyme used for resonance Raman studies was prepared by adjusting the apo-HppE solution in 50 mM Tris·HCl buffer (pH 7.5) to a final concentration of 15-20 mg/mL. The apo-protein sample was made anaerobic by repeated cycles of vacuum and purging with argon, and then transferred to the spinning cell (~150 μL) used for Raman study. The Fe^{II}-HppE sample was prepared by reconstituting the apo-enzyme with 1 equivalent (relative to HppE subunit) of $Fe^{II}(NH_4)_2(SO_4)_2$ in H_2O. This colorless protein solution was exposed to dioxygen for at least 30 min, during which time a green color developed. The protein sample was then concentrated prior to filling the spinning cell. The $H_2{}^{18}O$ samples were prepared by the same procedure except the apo-HppE was lyophilized and reconstituted with $Fe^{II}(NH_4)_2(SO_4)_2$ in $H_2{}^{18}O$ (95% ^{18}O).

Spectroscopic Studies. Electronic absorption spectra were obtained on a HP 8453 diode array spectrometer. EPR first derivative spectra were recorded at X-band microwave frequency with 100-kHz field modulation on a Bruker Elexsys E500 spectrometer following the same protocol reported in Chapter 2. Resonance Raman spectra were collected on an Acton AM-506 spectrometer (1200 groove grating) using a Kaiser Optical holographic super-notch filter with a Princeton Instruments liquid N_2 cooled (LN-1100PB) CCD detector with a 4 cm^{-1} spectral resolution. The laser excitation lines were obtained with a Spectra

Physics 2030-15 argon ion laser and a 375B CW dye (Rhodamine 6G), or a Spectra Physics BeamLok 2060-KR-V krypton ion laser. The Raman frequencies were referenced to indene, and the entire spectral range of 400-1700 nm was obtained by collecting spectra at 2-3 different frequency windows and splicing the spectra together. All data were referenced to the non-resonance enhanced 1005 cm^{-1} band assigned to a phenylalanine ring mode prior to splicing to avoid artifacts (*11*). Raman spectra of HppE were obtained at room temperature by 90º scattering from a spinning cell. Curve fits (Gaussian functions) and baseline corrections (polynomial fits) were carried out using Grams/32 Spectral Notebase Version 4.04. Excitation profiles were constructed by comparing peak area to the non-resonance enhanced vibration at 1005 cm^{-1}.

Epoxidase Activity Assay. A new assay was developed which contains 70 μM enzyme, 70 μM $Fe^{II}(NH_4)_2(SO_4)_2$, 15 mM (*S*)-HPP, 60 μM FMN, 22.5 mM NADH in 20 mM Tris·HCl buffer, pH 7.5 (totally 200 μL). The reaction was carried out at room temperature with vigorous shaking and then quenched by the addition of 40 μL of EDTA (0.5 M). The reaction mixture was kept on ice for immediate NMR analysis or frozen at – 80 °C and thawed shortly before analysis. The enzyme activity was calculated based on the integration of the ^{31}P NMR peaks assigned to product (δ 10.9) and substrate (δ 19.9). A sample of the wild-type HppE was run in parallel as the standard in comparing enzyme activity of different mutants.

In vitro Self-hydroxylation. As-purified apo-proteins were diluted with ddH_2O to 1 mg/mL and were aerobically incubated with an equivalent of

$Fe^{II}(NH_4)_2(SO_4)_2$ and ten equivalents of ascorbate at 4 °C for 1 h. The mixtures were concentrated by Amicon concentrator with a membrane pore size of 10 kDa (Millipore, Bedford, MA). The final protein concentrations were between 10-20 mg/mL. The extent of self-hydroxylation was analyzed by NBT quinone staining and UV-vis absorption spectroscopy as previously described.

Preparation of HppE Samples for Mass Spectral Analysis. The samples to be submitted for mass spectral analysis were prepared in forms of both gel slice and powder. To prepare samples in gel, the as-purified LB-HppE and ID-HppE were subjected to SDS-PAGE. The desired protein bands were cut from the gel and incubated in dd H_2O. To prepare samples in powder, the as-purified proteins were lyophilized and the resulting white powder was collected in eppendorf tubes. To reduce the potential interference from protein dimerization via disulfide bond formation, the purified C107A mutant was also prepared and sent for analysis. All samples were shipped to our collaborator Dr. Yu-Ju Chen at the Institute of Chemistry of Academia Sinica (Taiwan, ROC). There, the protein samples were digested by trypsin prior to injection.

3.3 RESULTS

Optical Properties of HppE. Both apo-HppE and anaerobically reconstituted Fe^{II}-HppE are nearly transparent above 300 nm (data not shown). However, upon exposure to molecular oxygen, a green chromophore is formed with visible absorption maxima at 680 and 430 nm within 1 h (Figure 3-1). Similar chromophores have been observed in tyrosine hydroxylase complexed with various catecholamines (λ_{max} at 420 and 700 nm, ε_{720} = 1900 $M^{-1}cm^{-1}$/Fe)

(*12*), in ribonucleotide reductase R2 DOPA208 mutant (λ_{max} at 460 and 720 nm, ε_{720} = 2500 $M^{-1}cm^{-1}$ per R2 subunit) (*13*), and in the iron-substituted zinc-dependent recombinant phosphomannose isomerase (PMI) (λ_{max} at 420 and 680 nm ; ε_{680} = 2100 $M^{-1}cm^{-1}$ /Fe) (*14*). These features are all characteristic of a ferric center with a chelated catecholate and arise from the catecholate-to-Fe^{III} charge transfer transitions (*15, 16*). However, the Fe-HppE chromophore has a significantly lower extinction coefficient (ε_{680} = 450 $M^{-1}cm^{-1}$) than those observed for proteins listed above and model complexes (ε = 1500-2500 $M^{-1}cm^{-1}$) (*17*), suggesting only partial formation of the chromophore in HppE. Another example is taurine/α-KG dioxygenase (TauD) which, along with its cofactor α-KG, reacts slowly with oxygen in the absence of its substrate taurine. This reaction results in the hydroxylation of a nearby tyrosine residue to give rise to a green-brown Fe^{III}-catecholate chromophore with λ_{max} at 550 nm and a low extinction coefficient (ε = 460 $M^{-1}cm^{-1}$) (*18*).

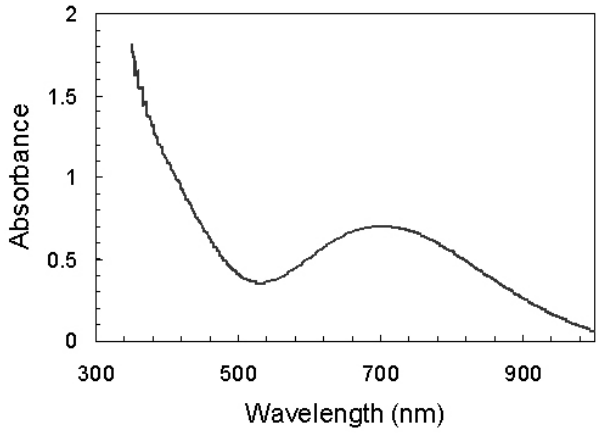

Figure 3-1. Electronic absorption spectrum of reconstituted HppE. Protein concentration is 1.4 mM.

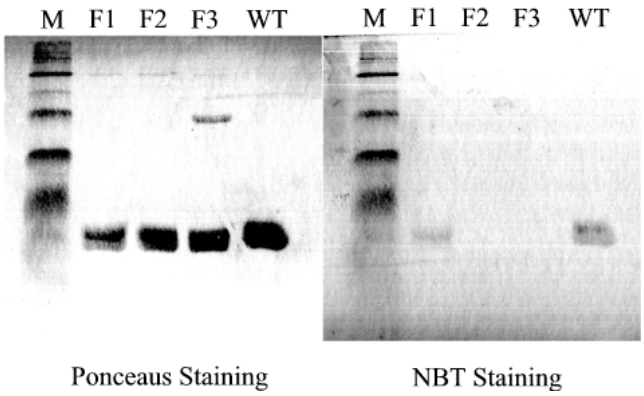

Figure 3-2 Ponceaus (left) and NBT (right) staining of the wild type HppE and its mutants: lane M, marker bands; lane F1, HppE-Y102F; lane F2, HppE-Y103F; lane F3, HppE-Y105F; lane WT, wild type HppE. The extra band in lane F3 is likely the dimer of HppE-Y105F.

Detection of the Catecholate Residue in HppE by Quinone Staining. Evidence for such a catecholate moiety in HppE was obtained by subjecting the isolated HppE to Paz's quinone-staining reagents including glycine and nitroblue tetrazolium (NBT) (*10*). It has been shown that under basic conditions, quinone cofactors, such as pyrroloquinoline quinone (PQQ), can oxidize glycine. The reduced quinone can then react with dioxygen to generate superoxide, which in turn oxidizes NBT to formazan to give a blue-purple color. Besides PQQ, other quinonoid compounds, such as 1,2,4-trihydroxybenzene, menadione, and DOPA, are also sensitive to this NBT/glycinate staining method. As shown in Figure 3-2, HppE is clearly sensitive to the quinone staining treatment. The fact that HppE without reconstitution is strongly stained by NBT/glycinate (see Figure 3-2, lane WT) not only provides evidence for the presence of a catecholate moiety, but also serves as an initial hint for its formation as an *in vivo* post-translational event.

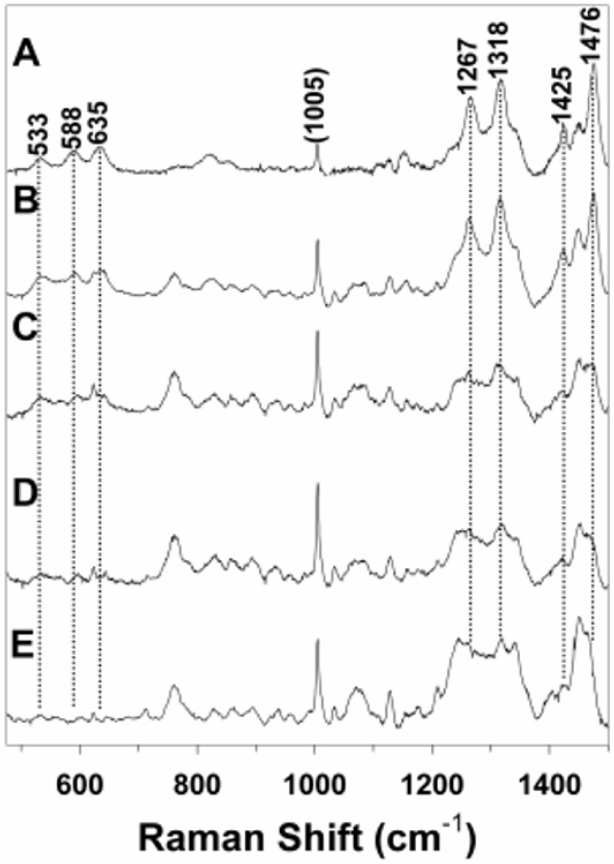

Figure 3-3 Resonance Raman spectra of HppE and its mutants. (A) Wild type HppE + Fe^{II} + O_2, (B) HppE-Y102F + Fe^{II} + O_2, (C) HppE-Y103F + Fe^{II} + O_2, (D) HppE-Y105F + Fe^{II} + O_2, and (E) apo HppE, obtained using 632.8 nm laser excitation with 90º scattering geometry from a spinning cell at room temperature. The spectra are not shown at the same vertical scale (note changes in the intensity of the 1005 cm^{-1} band associated with the Phe residues in the enzyme that serves as an internal calibrant of protein concentration).

Resonance Raman Studies of HppE. To ascertain whether the HppE chromophore consists of a catecholate ligand, the reconstituted HppE was subjected to resonance Raman analysis by laser excitation into the green chromophore. The spectrum of the reconstituted protein displays a number of

resonance-enhanced features at 533, 588, 635, 1267, 1318, 1425, and 1476 cm^{-1} (Figure 3-3). This spectrum could be observed with laser wavelengths at 514.5 nm and above, but a high fluorescence background obscured the spectrum when excitation was performed at wavelengths below 514.5 nm. Excitation profiles for selected bands are shown in the inset of Figure 3-4.

By comparison with the thoroughly investigated resonance Raman features of Fe^{III}-phenolate and Fe^{III}-catecholate chromophores in both model complexes and enzymatic systems (*15-17*), those observed for HppE are characteristic of an Fe^{III}-catecholate complex but distinct from those of an Fe^{III}-phenolate complex (Table 3-1). The latter displays a different pattern of vibrations from those observed for the oxidized HppE, in particular, the presence of only a single ν_{Fe-O} mode in the 560-640 cm^{-1} range, as well as a δ_{C-H} mode at ~1160 cm^{-1} (*15-17, 19*). Most of the bands in the region of 1200-1500 cm^{-1} observed for HppE are assignable to aromatic ring deformation modes with predominant ν_{C-C} stretching character, and closely match those observed for the ferric-catecholate complexes of phenylalanine hydroxylase (*17*), tyrosine hydroxylase (*19*) and ribonucleotide reductase R2 DOPA208 mutant (*20*) (see Table 3-1). The enhanced vibrational modes between 500–700 cm^{-1}, which are associated with the metal-ligand vibrations (ν_{Fe-O}), are the most significant signals for the identification of the iron-catecholate chromophore (*21*). The peaks at 635 and 588 cm^{-1} can be assigned to the Fe–O stretches at C-4 and C-3 of the DOPA catecholate ring, respectively, and the feature at 533 cm^{-1} arises from the chelate mode of a bidentate iron-catecholate species (*17, 19, 20*). Thus, the

resonance Raman spectrum of HppE is fully consistent with the presence of an iron-catecholate chromophore.

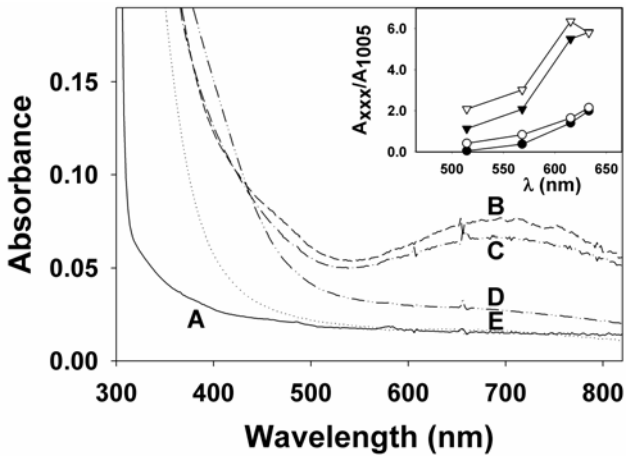

Figure 3-4 Electronic absorption spectra of apo and reconstituted HppE. Protein concentrations are 0.15 mM. (A) apo-HppE; (B) HppE + Fe^{II} + O_2; (C) HppE-Y102F + Fe^{II} + O_2; (D) HppE-Y103F + Fe^{II} + O_2; (E) HppE-Y105F + Fe^{II} + O_2. Inset: resonance Raman excitation profiles for the Fe-reconstituted WT HppE. The spectra were obtained on a 1 mM sample in a spinning cell at room temperature (90° scattering geometry). Only profiles for the bands at 592 (●), 635 (❍), 1319 (▼), and 1475 (▽) cm^{-1} are shown for clarity. The 1005 cm^{-1} phenylalanine vibration was used as the internal standard and the areas of the peaks were determined by curve fitting.

Determination of the Site of Modification by Site-Directed Mutagenesis. The catecholate moiety in HppE presumably arises from the hydroxylation of a tyrosine residue. Interestingly, sequence alignment of HppE from *Streptomyces wedmorensis* and *Pseudomonas syringae* reveals only three conserved tyrosine residues, Y102, Y103, and Y105 (Figure 3-5).

Sample	Raman frequencies (cm^{-1})									Reference
HppE + Fe^{II} + $^{16}O_2$	533	588	635		1267	1318	1425	1476		(*8*)
HppE + Fe^{II} + $^{18}O_2$	532	587	635		1267	1319	1425	1477		(*8*)
HppE + Fe^{II} + $^{16}O_2$ + $H_2{}^{18}O$	534	588	636		1266	1317	1425	1476		(*8*)
HppE + Fe^{II} + Asc + $^{16}O_2$	531	591	636		1264	1315	1425	1478		(*8*)
HppE + Fe^{II} + Asc + $^{18}O_2$	525	570	633		1261	1315	1424	1478		(*8*)
RNR R2 DOPA-208	512	592	619	1143	1263	1319	1350	1475	1569	(*20*)
RNR R2 [3-^{18}O, 4-^{16}O]DOPA-208	499	584	617	1143	1263	1319	1350	1475	1569	(*20*)
Phe Hydroxylase + catecholate	531		621	1151	1257	1313		1470	1568	(*17*)
Tyr Hydroxylase DOPA	528	592	631		1275	1320	1425	1475		(*19*)
Tyr Hydroxylase [3-^{18}O, 4-^{16}O]DOPA	522	580	629		1271	1320	1425	1475		(*19*)
Tyr Hydroxylase [3-^{18}O, 4-^{18}O]DOPA	509	578	619		1266 (broad)	1320	1423	1473		(*19*)
Phosphomannose Isomerase DOPA-287		591	631		1266	1330	1428	1482		(*14*)
TauD DOPA-73	545		612	1141	1261	1318/1346	1424	1482		(*18*)
$[Fe^{III}$(salen)(catecholate)$]^-$	511		614		1260	1324		1473		(*16*)
$[Fe^{III}(catecholate)_3]^{3-}$	533		622		1267	1327		1487		(*21*)

Table 3-1 Resonance Raman vibrations of ferric-catecholate complexes in proteins and models.

```
S. wendomorensis      MSNTKTASTG FAELLKDRRE QVKMDHAALA SLLGETPETV AAWENGEGGE   50
P. syringae           M–DVRTLAVG KAH-LEALLA TRKM---TLE HLQDVRHDAT QVYFDGLEHL   45
Consensus             M....T...G .A..L..... ..KM....L. .L........ .....G....   50

S. wendomorensis      LTLTQLGRIA HVLGTSIGAL TPPAGNDLDD GVIIQMPDER PILKGVRDNV  100
P. syringae           QNVAQY--LA IPLSEFFVGQ TQ---SDLDD GVKIARRNGG FKREEIRGGV   90
Consensus             ....Q....A ..L..... T.....DLDD GV.I...... ......R..V  100

S. wendomorensis      DYYVYNCLVR TKRAPSLVPL VVDVLTDNPD DAKFNSGHAG NEFLFVLEGE  150
P. syringae           HYYTYEHLVT TNQDPGLMAL RLDLHSDDEQ PLRLNGGHGS REIVYVTRGA  140
Consensus             .YY.Y..LV. T...P.L..L ..D...D... ....N.GH.. .E...V..G.  150

S. wendomorensis      IHMKW-GDKE NPKEALLPTG ASMFVEEHVP HAFTAAKGTG SAKLIAVNF-  198
P. syringae           VRVRWVGDND ELKEDVLNEG DSIFILPNVP HSFTNHVGGA KSEIIAINYG  190
Consensus             ....W.GD.. ..KE..L..G .S.F....VP H.FT...G.. ....IA.N..  200
```

Figure 3-5 Sequence alignment of HppE isolated from *Streptomyces wedmorensis* and *Pseudomonas syringae*. The three conserved tyrosines are boxed.

Site-directed mutagenesis of each tyrosine to phenylalanine has thus been carried out to determine which of the three conserved tyrosine residues is involved in the formation of the chromophore. The reconstituted Y102F mutant enzyme is green in color and has a visible as well as a resonance Raman spectrum comparable to those of the wild type enzyme (Figures 3-4C and 3-3B), so Y102 can be ruled out as the site of modification. On the other hand, the reconstituted Y103F and Y105F mutant enzymes show little evidence for the green chromophore in their visible spectra (Figures 3-4D, E), and their Raman spectra are comparable to that observed for apo-HppE (Figures 3-3C, D, and E). Thus, either Y103 or Y105 can be the precursor of DOPA in HppE. This conclusion is corroborated by parallel quinone staining experiments. As shown in Figure 3-2, both the wild type (lane WT) and Y102F (lane F1) HppE are stained, but not Y103F (lane F2) and Y105F (lane F3) mutant enzymes. Interestingly, while the

Y102F and Y103F enzymes maintain about 100% of the activity of the wild type enzyme, the relative activity of Y105F enzyme is considerably reduced to less than 30%. Clearly, Tyr105 is a key residue, which must play an important role in the activation of dioxygen required for the enzymatic activity of HppE.

Post-translational DOPA Formation in vivo and/or in vitro. To gain more information about this post-translational modification event, more Raman experiments were performed using HppE samples reconstituted with isotopic tracers, for instance under $^{18}O_2$ atmosphere in $H_2{}^{16}O$, and under $^{16}O_2$ atmosphere in $H_2{}^{18}O$. Neither notable broadening nor significant isotopic shifting of the peaks was observed in any of the tested samples (see Table 3-1 and Figures 3-6A-C). The absence of isotope incorporation in these samples confirms that formation of DOPA in HppE is not an artifact of *in vitro* reconstitution but an *in vivo* post-translational event.

However, when reconstitution was carried out under $^{18}O_2$ atmosphere in the presence of ascorbate (10 equivalents), the green chromophore increased in intensity and isotope shifts for several Raman peaks were observed (Figures 3-6D and E). The change at 591 cm^{-1} is most apparent, with the appearance of the new peak at 570 cm^{-1} (Table 3-1). This peak can be attributed to the ^{18}O downshift of the 591 cm^{-1} peak, which corresponds to the Fe^{III}-OAr stretch at C-3 of the DOPA ring, owing to ^{18}O incorporation. The feature at 531 cm^{-1} assigned to the iron-catecholate chelate mode also downshifts by 6 cm^{-1} and broadens significantly to a width twice as large as that observed in the $^{16}O_2$ sample. Downfield shifts of 3 cm^{-1} are also observed for the Fe-O_4 mode at 636 cm^{-1} and

the ring deformation mode at 1264 cm^{-1}. These isotopic shifts are reminiscent of those observed in the spectrum of tyrosine hydroxylase when complexed with dopamine specifically labeled at the 3-position of the aromatic ring (Table 3-1) (*19*).

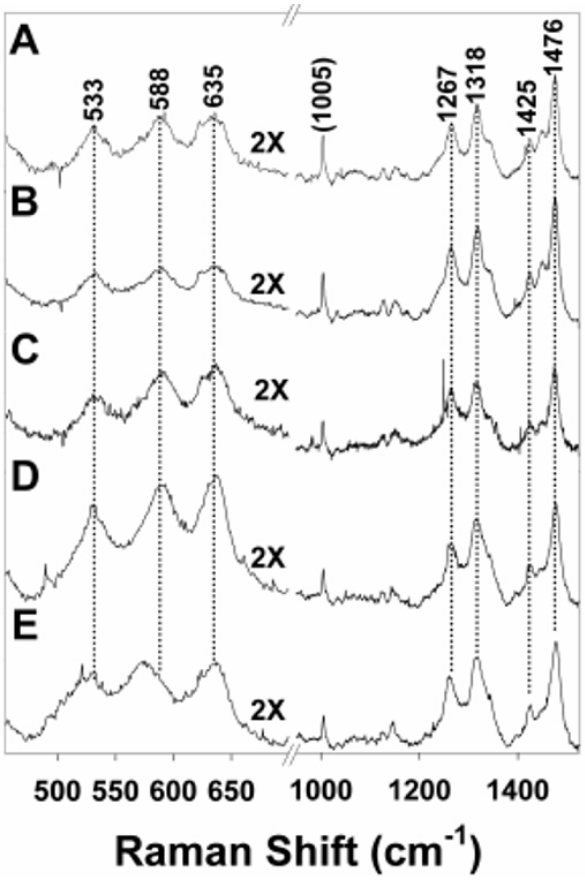

Figure 3-6 Resonance Raman spectra of the reconstituted HppE reconstituted in the presence of oxygen isotopes. (A) HppE + Fe^{II} + $^{16}O_2$, (B) HppE + Fe^{II} + $^{18}O_2$, (C) HppE + Fe^{II} + $^{16}O_2$ + $H_2{}^{18}O$, (D) HppE + Fe^{II} + $^{16}O_2$ and 10 equivalents of ascorbate, and (E) HppE + Fe^{II} + $^{18}O_2$ and 10 equivalents of ascorbate. The vertical scale in the lower region has been magnified to two times that of the upper region for clarity. A greater number of accumulations were acquired for the $H_2{}^{18}O$ sample.

These results clearly indicate that HppE is capable of catalyzing tyrosine self-hydroxylation when provided with sufficient electrons for oxygen activation. However, due to the tight binding between ascorbate and the iron center to form an aborted complex, HppE reconstituted under such conditions is catalytically inactive.

Reconstitution of Mutant Proteins in the Presence of Ascorbate. Taking advantage of the newly discovered oxygenase activity of HppE, the Y103F, Y105F, and Y103F/Y105F mutant proteins were also subjected to aerobically reconstitution with $Fe^{II}(NH_4)_2(SO_4)_2$ in the presence of ascorbate (10 equivalents) to further differentiate between Tyr103 and Try105 as the site of modification. After one-hour incubation, the Y103F mutant protein became green in color and its electronic absorption spectrum clearly revealed the formation of the green chromophore with the maximum wavelength at 680 nm (ε_{680} = 360 $M^{-1}cm^{-1}$, Figure 3-7A). In contrast, much less green chromophore was produced from the Y105F mutant under the same conditions (ε_{680} = 200 $M^{-1}cm^{-1}$, Figure 3-7B). The spectrum of the wild-type HppE at the same concentration is also included (ε_{680} = 450 $M^{-1}cm^{-1}$, Figure 3-7D) for comparison. These observations strongly indicate that Tyr105 is the preferred site of modification. However, the fact that the absorption at longer wavelength remains visible for the reconstituted Y105F mutant suggests that hydroxylation at the near-by Tyr103 can occur when Tyr105 is mutated to a less reactive phenylalanine. This hypothesis is supported by the finding that the Y103F/Y105F double mutant showed no sign of modification under the same reconstitution conditions (Figure 3-7C).

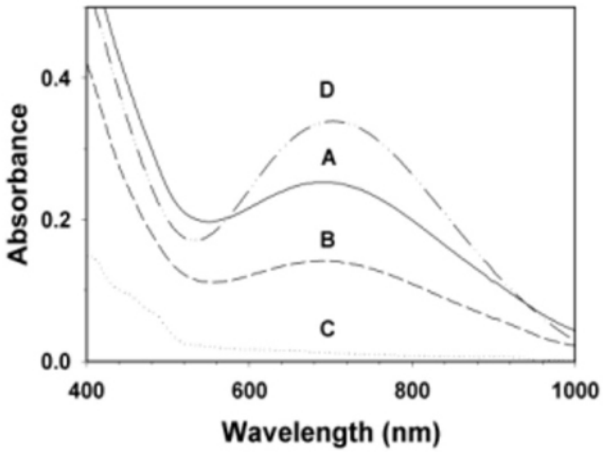

Figure 3-7 Electronic absorption spectra of WT and mutants HppE aerobically reconstituted with Fe^{II} and ascorbate. (A) HppE-Y103F, (B) HppE-Y105F, (C) HppE-Y103F/Y105F, and (D) WT HppE, 0.6 mM each, were reconstituted with an equivalent of $Fe^{II}(NH_4)_2(SO_4)_2$ and ten equivalents of ascorbate in 20 mM Tris•HCl buffer, pH 7.5.

The Relationship Between Epoxidase Activity and Self-Hydroxylation. The earlier studies have shown that the self-modification of HppE is an *in vivo* posttranslational event and that it can be imitated *in vitro* under proper conditions. The critical role of iron in the *in vitro* self-modification inspired the attempt to express an unmodified form of HppE in iron-depletion growth medium (ID-HppE). The purified ID-HppE was thoroughly analyzed and confirmed to be free of self-modification. The aerobically reconstituted ID-HppE was yellow in color and its electronic absorption spectrum exhibited no optical features associated with the green chromophore (Figure 3-8). In consistence, none of the fingerprint bands of the Fe^{III}-catecholate LMCT complex (533, 588 and 635 cm^{-1}) was visible in the resonance Raman spectrum of the reconstituted ID-HppE

(Figure 3-9A). All of these data, together with the negative result from the NBT staining analysis of ID-HppE (Figure 3-10, Lane 1), strongly indicate that HppE generated under the above conditions is unmodified and support an essential role played by iron in the self-modification process.

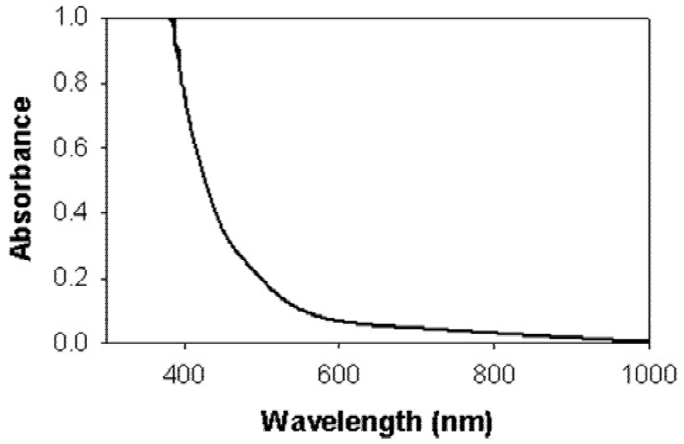

Figure 3-8 The electronic absorption spectrum of the reconstituted ID-HppE. Protein concentration is 1.4 mM.

The next important question is whether this DOPA residue has a catalytic role in enzymatic epoxidation. The availability of ID-HppE provided a great opportunity to address this question. When ID-HppE was incubated with FMN/NADH, (*S*)-HPP and $Fe^{II}(NH_4)_2(SO_4)_2$, fosfomycin was generated at a rate comparable to that catalyzed by LB-HppE, showing no significant difference in catalytic activity between modified and unmodified HppE. The fact that no obvious sign of modification was detected in ID-HppE throughout the reaction (Figure 3-10, Lane 2) is another strong line of evidence against the catalytic relevance of the DOPA residue. It should be noted that under the nearly

identical conditions except for the absence of (*S*)-HPP, ID-HppE was extensively modified as indicated by the strong purple band in the NBT stained membrane (Figure 3-10, Lane 3). The distinct outcomes under similar incubation conditions clearly demonstrated that epoxidation and self-hydroxylation are two competing reactions and substrate binding is the key factor in determining the reaction course. It appears that the epoxidation reaction is preferred over self-hydroxylation when (*S*)-HPP is bound in the enzyme active site. Accordingly, Tyr105 residue has access to the active site iron center only in the absence of substrate.

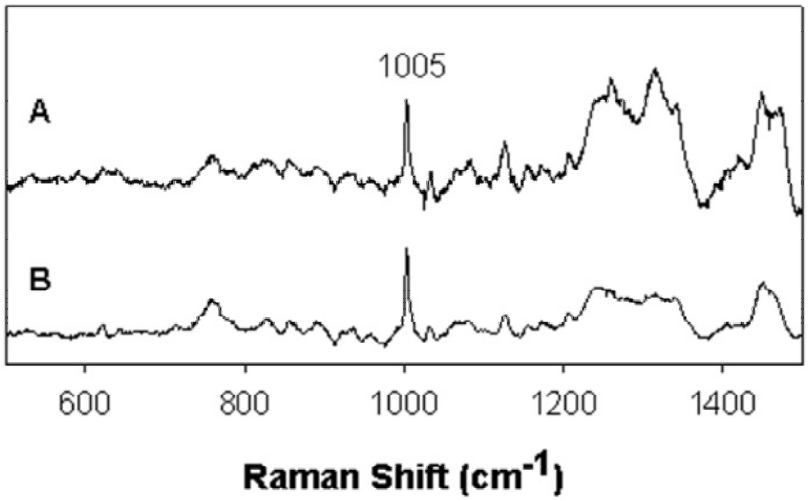

Figure 3-9 Resonance Raman spectra of reconstituted ID-HppE. (A) ID-HppE + Fe^{II} + O_2, (B) apo ID-HppE. (Note: the phenylalanine band at 1005 cm^{-1} is labeled as an internal standard.)

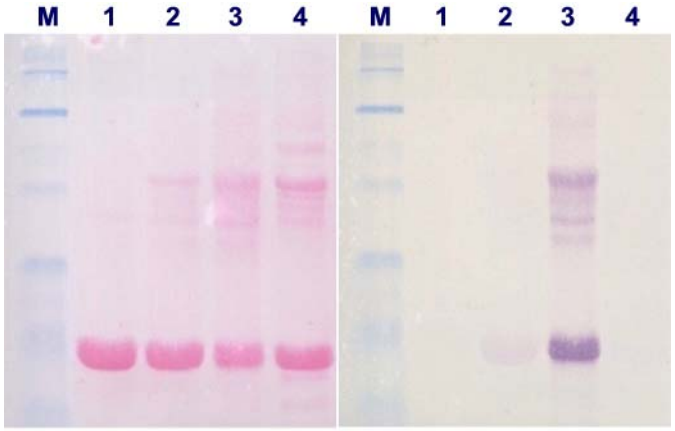

#	ID-HppE	FMN/NADH	(*S*)-HPP	Fe^{2+}	Activity Assay
1	+	-	-	-	-
2	+	+	+	+	+
3	+	+	-	+	-
4	+	+	+	-	-

Figure 3-10 The relationship between epoxidase activity and self-hydroxylation. Above: Ponceau S and NBT stained membranes (M, protein marker); Below: The components of sample 1 - 4. (Note: the higher molecular weight bands are due to oxidative cross-linking between individual HppE monomers by air.)

Apparently, studies of ID-HppE failed to establish a direct correlation between the epoxidase activity of HppE and its active site DOPA residue. To further analyze the effects of self-modification on the epoxidase activity of HppE, the wild type enzyme was expressed in a series of low iron (LI) media as described in the experimental procedure. The enzymes purified from these media, named as LI1-HppE to LI4-HppE, were analyzed by electronic absorption spectroscopy and the quantitative NBT/glycinate solution assay. The results, as

expected, showed that the extent of self-modification is proportional to the iron concentration in the expression media. As illustrated in Figure 3-11 and Table 3-2, with the iron concentration increased from 0.0001 mM in the LI4 medium to 0.1 mM in the LI1 medium, the experimental data of A_{280} and NBT assay in Table 3-2 that are indicative of the quantity of the enzyme-based DOPA also escalated. However, the trend of proportionality was less apparent in the epoxidase activity of enzymes. Instead, their activities are all in a narrow range, with small fluctuations mainly due to experimental errors (Table 3-2), suggesting that the enzyme-based DOPA has little effects on the catalytic activity of HppE.

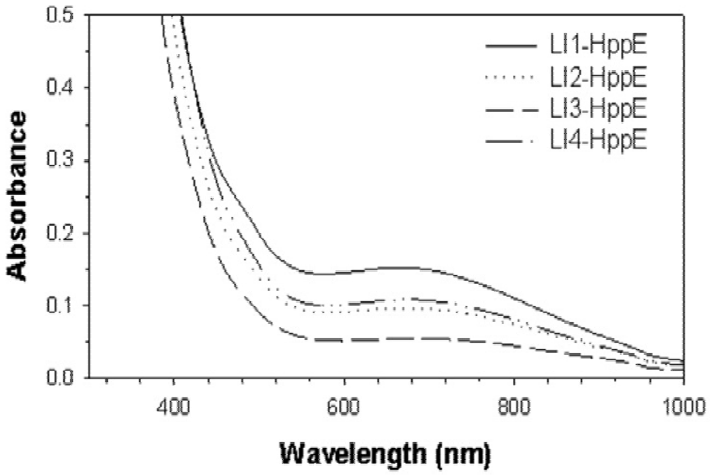

Figure 3-11 The electronic absorption spectra of reconstituted LI-HppEs. Protein concentrations are 1.0 mM.

	LI4-HppE	LI3-HppE	LI12-HppE	LI1-HppE
[Fe] in Medium (mM)	0.0001	0.001	0.01	0.1
A_{680} (%)	11	29	65	100
NBT assay (%)	3	15	42	100
Activity (%)	100	116	124	100

Table 3-2. The properties of HppE produced in low iron media (LI-HppEs). (Note: for better comparison, the experimental results are converted to percentages relative to the values of LI1-HppE.)

EPR Spectral Analysis of ID-HppE. ID-HppE was reconstituted with $Fe^{II}(NH_4)_2(SO_4)_2$ and (*S*)-HPP under anaerobic conditions. The enzyme-substrate complex was then added NO gas under the protection of argon. The EPR spectrum of the Fe^{II}-ID-HppE·(*S*)-HPP nitrosyl complex is shown in Figure 3-12, which is nearly identical to the previously reported EPR spectrum of Fe^{II}-LB-HppE·(*S*)-HPP nitrosyl complex (*7*). According to the spectral simulations in Chapter 2, they both comprise two $S = 3/2$ signals, corresponding to two different types of Fe^{II}-nitrosyl centers. The only difference between these two spectra is the ratio of the intensities of two signals. As previously postulated (Chapter 2), the signal accounting for the majority of the iron in ID-HppE (g = 4.42, 3.63, E/D = 0.066) is arisen from a catalytically competent enzyme-substrate complex, while the minor signal (g = 4.0) may arise from a denatured inactive form of HppE. Thus, the EPR results also confirmed the catalytic competence of the unmodified ID-HppE.

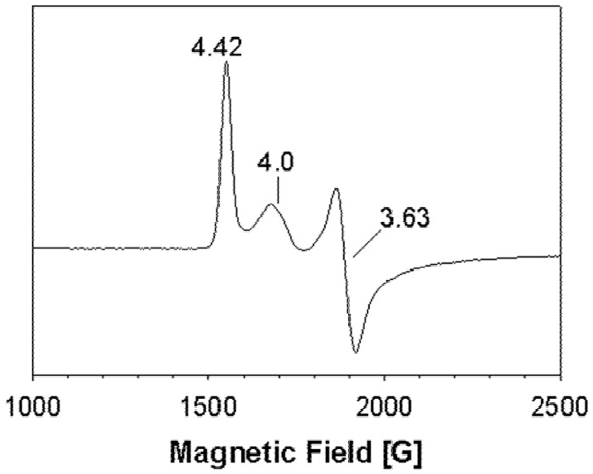

Figure 3-12 EPR spectrum of Fe^{II}-ID-HppE·(*S*)-HPP nitrosyl ternary complex. Substrate is 10-fold excess over active sites. Instrumental parameters: temperature 2 K, microwave frequency 9.6 GHz, microwave power 0.6 mW, modulation amplitude 5 G, time constant 0.02 s, and a sweep rate of 50 G/s.

Determination of the Site of Modification by Mass Spectral Analysis. The initial efforts to analyze posttranslational modification by mass spectroscopy had been hampered by low yield of modification. Only recently, results from a joint effort with Dr. Chen at Academia Sinica by mass spectral analysis have confirmed Tyr105 as the primary modification site (Data not shown).

3.4 DISCUSSION

An increasing number of proteins that are post-translationally modified to contain a DOPA residue have been discovered in recent years. Many DOPA-containing proteins are found in liver flukes or in adhesive plaques of mussels where their DOPA residues play important roles in metal chelation facilitating the

iron uptake (*22, 23*). There are also examples where DOPA formation occurs in enzymes. Such a post-translational modification is well documented for the F208Y mutant of the ribonucleotide reductase (RNR) R2 protein from *E. coli*, where the newly introduced tyrosine residue (Tyr208) near the diiron active site is hydroxylated both *in vitro* and *in vivo* to DOPA (*9*). The crystal structure of this mutant protein indeed showed a diiron core with a bidentate catecholate ligand (DOPA208) to one of the ferric ions that gives rise to its unusual blue color. A tyrosine residue (Tyr287) in the active site of the zinc-dependent recombinant phosphomannose isomerase (PMI) can also be hydroxylated to DOPA in the overexpressed cells to generate a green chromophore when the zinc center is replaced by iron (*14*). Similarly, Tyr73 is converted to DOPA in the α-KG-dependent non-heme iron enzyme TauD to generate a green chromophore when the enzyme reacts with O_2 in the presence of α-KG co-substrate, but in the absence of its substrate taurine (*18*). By a combination of site-directed mutagenesis and resonance Raman spectral analysis in this study, we have established HppE as a new member of this select group of proteins with hydroxylated tyrosine residues. The site of modification in HppE is most likely at Tyr105.

Several of the DOPA forming enzymes mentioned above as well as tyrosine hydroxylase belong to a family of mononuclear non-heme iron enzymes with the recurring 2-His-1-carboxylate facial triad in their active sites (*24, 25*). Sequence comparisons suggest that HppE likely utilizes the combination of H138, H180, and E142 as ligands to the iron center, thus making it another plausible

addition to this family of oxygen activating enzymes. But the reaction it catalyzes is unusual, entailing an oxidative dehydrogenation of HPP to form fosfomycin such that the alcohol oxygen of the substrate becomes the epoxide ring oxygen in the product. The lack of any oxygen incorporation from O_2 into the epoxide product is somewhat unexpected, as metalloenzyme-catalyzed epoxidation typically results in the incorporation of an oxygen atom from O_2. However, our observation that HppE can carry out the hydroxylation of a tyrosine residue to DOPA in the presence of ascorbate with incorporation of an oxygen atom from O_2 suggests that it may share a common mechanism for oxygen activation with other mononuclear non-heme iron enzymes (*24*).

The mechanism of substrate hydroxylation catalyzed by non-heme iron enzymes typically involves a high valent iron-oxo species produced at the expense of two exogenous electrons in each catalytic cycle. For tyrosine hydroxylase, the two electrons are provided by the tetrahydropterin cofactor, and for α-KG-dependent enzymes like TauD, the two electrons are derived from the α-KG co-substrate (*24*). While the resultant Fe^{IV}-oxo species is considered the reactive intermediate responsible for tyrosine oxidation in both cases, the actual mechanism of oxygen incorporation into DOPA may not be the same. For tyrosine hydroxylase where tyrosine is an external substrate, a cationic cyclohexadiene intermediate, perhaps from an arene oxide, is proposed to be the product of the initial oxygen addition (Figure 1-16) (*5*). Evidence supporting this concerted oxygen-transfer mechanism includes the occurrence of a NIH shift in the subsequent rearrangement to yield DOPA, and the exclusive incorporation

of an oxygen atom from dioxygen into the DOPA structure (*5*). In contrast, for self-hydroxylation of TauD where the substrate (Tyr73) is an internal active site residue, the reaction proceeds via a tyrosyl radical intermediate, whose formation is associated with the reduction of the Fe^{IV}-oxo to an Fe^{III}-hydroxo species, with exclusive incorporation of an oxygen atom from water into the DOPA that is formed (*18*). An oxygen atom from water was also incorporated into a hydroxylated Trp residue in another α-KG-dependent mononuclear non-heme iron containing dioxygenase, TfdA (*26*), and into a DOPA residue of RNR R2 F208Y mutant (*20*) by presumed involvement of an Fe^{IV}-oxo species.

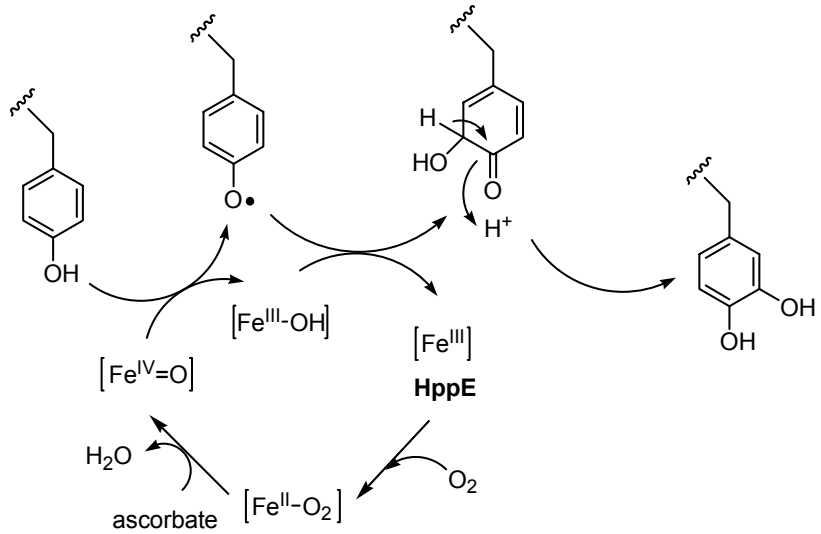

Figure 3-13 Schematic illustration of the self-hydroxylation mechanism of HppE.

The self-hydroxylation of HppE may follow a similar path as the above enzymes. An Fe^{IV}-oxo intermediate may be formed with the influx of two reducing equivalents from ascorbate in place of tetrahydropterin or α-ketoglutarate into the Fe^{II}-O_2 adduct (Figure 3-13). Tyrosine hydroxylation may

then occur as a $2e^-$-oxidation as proposed for tyrosine hydroxylase (*5*) or in two $1e^-$-steps as demonstrated for TauD self-hydroxylation (*18*).

However, tyrosine hydroxylase, TauD, and TfdA utilize either tetrahydropterin or α-KG bound at the active site as the two-electron source, while HppE instead uses an external reductant, either ascorbate for the *in vitro* formation of DOPA or NADH for the catalyzed epoxide formation. This requirement for an external reductant resembles that for another class of non-heme iron enzymes with a 2-His-1-carboxylate motif, the Rieske dioxygenases that catalyze *cis*-dihydroxylation of arenes, where the two electrons from NADH are introduced in $1e^-$-aliquots during the catalytic cycle (*1, 24*). There is recent strong evidence in the Rieske dioxygenase mechanism for an Fe^{III}-OOH intermediate that derives from the one-electron reduction of an initial Fe^{II}-O_2 adduct (Figure 1-20) (*27, 28*). This peroxo intermediate is proposed to either attack the substrate directly or may evolve first to an Fe^{IV}-oxo species that then carries out the oxidation. HppE self-hydroxylation may also be envisioned to occur by such a pathway (Figure 3-14).

The third mechanism is a derivative of the mechanism proposed for epoxidation reaction catalyzed by HppE (Figure 2-13 and 2-14). Instead of the Fe^{III}-peroxo or Fe^{IV}-oxo intermediates, the mechanism uses the Fe^{III}-superoxide species to initiate oxidation of the Tyr residue. As the supporting evidence will be presented in Chapter 4, the proposed mechanism will also discussed later in the same chapter (Figure 4-12).

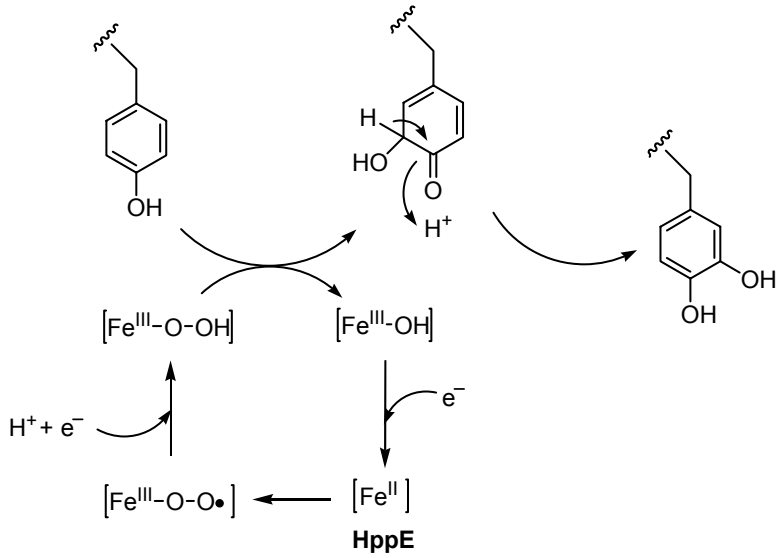

Figure 3-14 Schematic illustration of the self-hydroxylation mechanism of HppE.

The discovery of the modified DOPA structure in HppE raised an issue regarding its role in enzyme catalysis. Our studies using an unmodified form of HppE (ID-HppE) showed that there is no correlation between DOPA residue and the catalytic activity of HppE. The conclusion was further supported by the EPR spectral analysis of ID-HppE. The previously reported homogeneous EPR spectrum that is presumably indicative of a catalytically competent complex was also observed for ID-HppE complexed with Fe^{II}, (*S*)-HPP and nitric oxide. Thus far, no obvious effects of self-modification have been detected on the epoxidase activity of HppE. In fact, self-hydroxylation and epoxidation were found to be competitive. Binding of substrate appears to be the switch controlling two different reaction pathways. The presence of substrate turns on the epoxidation reaction while its absence leads to the self-hydroxylation reaction.

In summary, the combined spectroscopy and mutagenesis results have identified a ferric-catecholate complex as the chromophore for the green color of HppE. More importantly, strong evidence indicates that DOPA formation in HppE is a self-hydroxylation reaction. It is thus clear that HppE can act as an oxygenase and an activated dioxygen species is responsible for the self-hydroxylation. The discovery of this new activity of HppE has significant mechanistic implications since by extension, the same reactive intermediates may be involved in the catalytic mechanism for fosfomycin formation. The catalytic cycles illustrated in Figures 3-13 and 3-14 can easily be adapted to HppE-catalyzed epoxidation reaction, which may require the same oxidant (either the Fe^{IV}=O species in Figure 3-13 or the Fe^{III}-OOH species in Figure 3-14) to carry out the $2e^-$-oxidation of substrate in one-electron steps, parallel to the alkane hydroxylation mechanisms proposed for cytochrome P450 (*29*) and nonheme iron oxygenases (*24*). More studies are currently in progress to uncover details of the DOPA formation mechanism relevant to that of HppE-catalyzed epoxidation. Insight gained from study of this unique non-heme iron-dependent enzyme will certainly enhance our understanding of this important and growing enzyme family.

3.5 REFERENCES

1. Gibson, D. T., and Parales, R. E. (2000) "Aromatic hydrocarbon dioxygenases in environmental biotechnology" *Curr. Opin. Biotechnol. 11*, 236-243.
2. Prescott, A. G., and Lloyd, M. D. (2000) "The iron(II) and 2-oxoacid-dependent dioxygenases and their role in metabolism" *Nat. Prod. Rep. 17*, 367-383.

3. Kappock, T. J., and Caradonna, J. P. (1996) "Pterin-Dependent Amino Acid Hydroxylases" *Chem. Rev. 96*, 2659-2756.

4. Rocklin, A. M., Tierney, D. L., Kofman, V., Brunhuber, N. M. W., Hoffman, B. M., Christoffersen, R. E., Reich, N. O., Lipscomb, J. D., and Que, L., Jr. (1999) "Role of the nonheme Fe(II) center in the biosynthesis of the plant hormone ethylene" *Proc. Natl. Acad. Sci. USA 96*, 7905-7909.

5. Fitzpatrick, P. F. (1999) "Tetrahydropterin-dependent amino acid hydroxylases" *Annu. Rev. Biochem. 68*, 355-381.

6. Liu, P., Murakami, K., Seki, T., He, X., Yeung, S. M., Kuzuyama, T., Seto, H., and Liu, H. (2001) "Protein purification and function assignment of the epoxidase catalyzing the formation of fosfomycin" *J. Am. Chem. Soc. 123*, 4619-4620.

7. Liu, P., Liu, A., Yan, F., Wolfe, M. D., Lipscomb, J. D., and Liu, H. W. (2003) "Biochemical and spectroscopic studies on (*S*)-2-hydroxypropylphosphonic acid epoxidase: a novel mononuclear non-heme iron enzyme" *Biochemistry 42*, 11577-11586.

8. Liu, P., Mehn, M. P., Yan, F., Zhao, Z., Que, L., Jr., and Liu, H.-W. (2004) "Oxygenase activity in the self-hydroxylation of (*S*)-2-hydroxypropylphosphonic acid epoxidase involved in fosfomycin biosynthesis" *J. Am. Chem. Soc. 126*, 10306-10312.

9. Aberg, A., Ormèo, M., Nordlund, P., and Sjèoberg, B. M. (1993) "Autocatalytic generation of dopa in the engineered protein R2 F208Y from Escherichia coli ribonucleotide reductase and crystal structure of the dopa-208 protein" *Biochemistry 32*, 9845-9850.

10. Paz, M. A., Fluckiger, R., Boak, A., Kagan, H. M., and Gallop, P. M. (1991) "Specific detection of quinoproteins by redox-cycling staining" *J. Biol. Chem. 266*, 689-692.

11. Lord, R. C., and Yu, N. T. (1970) "Laser-excited Raman spectroscopy of biomolecules. I. Native lysozyme and its constituent amino acids" *J. Mol. Biol. 50*, 509-524.

12. Andersson, K. K., Cox, D. D., Que, L., Jr., Flatmark, T., and Haavik, J. (1988) "Resonance Raman studies on the blue-green-colored bovine adrenal tyrosine 3-monooxygenase (tyrosine hydroxylase). Evidence that the feedback inhibitors adrenaline and noradrenaline are coordinated to iron" *J. Biol. Chem. 263*, 18621-18626.

13. Ormö, M., deMarê, F., Regnström, K., Aberg, A., Sahlin, M., Ling, J., Loehr, T. M., Sanders-Loehr, J., and Sjöberg, B. M. (1992) "Engineering

of the iron site in ribonucleotide reductase to a self-hydroxylating monooxygenase" *J. Biol. Chem. 267*, 8711-8714.

14. Smith, J. J., Thomson, A. J., Proudfoot, A. E., and Wells, T. N. (1997) "Identification of an Fe(III)-dihydroxyphenylalanine site in recombinant phosphomannose isomerase from *Candida albicans*" *Eur. J. Biochem. 244*, 325-333.

15. Que, L., Jr. (1988) *Biological Applications of Raman Spectroscopy*, Vol. 3, Wiley, New York.

16. Pyrz, J. W., Roe, A. L., Stern, L. J., and Que, L., Jr. (1985) "Model studies of iron-tyrosinate proteins" *J. Am. Chem. Soc. 107*, 614-620.

17. Cox, D. D., Benkovic, S. J., Bloom, L. M., Bradley, F. C., Nelson, M. J., Que, L., Jr., and Wallick, D. E. (1988) "Catecholate LMCT bands as probes for the active sites of nonheme iron oxygenases" *J. Am. Chem. Soc. 110*, 2026-2032.

18. Ryle, M. J., Liu, A., Muthukumaran, R. B., Ho, R. Y. N., Koehntop, K. D., McCracken, J., Que, L., Jr., and Hausinger, R. P. (2003) "O_2- and α-ketoglutarate-dependent tyrosyl radical formation in TauD, an α-keto acid-dependent non-heme iron dioxygenase" *Biochemistry 42*, 1854-1862.

19. Michaud-Soret, I., Andersson, K. K., Que, L., Jr., and Haavik, J. (1995) "Resonance Raman studies of catecholate and phenolate complexes of recombinant human tyrosine hydroxylase" *Biochemistry 34*, 5504-5510.

20. Ling, J., Sahlin, M., Sjèoberg, B. M., Loehr, T. M., and Sanders-Loehr, J. (1994) "Dioxygen is the source of the mu-oxo bridge in iron ribonucleotide reductase" *J. Biol. Chem. 269*, 5595-5601.

21. Salama, S., Stong, J. D., Neilands, J. B., and Spiro, T. G. (1978) "Electronic and resonance Raman spectra of iron(III) complexes of enterobactin, catechol, and *N*-methyl-2,3-dihydroxybenzamide" *Biochemistry 17*, 3781-3785.

22. Waite, J. H., Housley, T. J., and Tanzer, M. L. (1985) "Peptide repeats in a mussel glue protein: theme and variations" *Biochemistry 24*, 5010-5014.

23. Waite, J. H., and Rice-Ficht, A. C. (1989) "A histidine-rich protein from the vitellaria of the liver fluke *Fasciola hepatica*" *Biochemistry 28*, 6104-6110.

24. Costas, M., Mehn, M. P., Jensen, M. P., and Que, L., Jr. (2004) "Dioxygen activation at mononuclear nonheme iron active sites: enzymes, models, and intermediates" *Chem. Rev. 104*, 939-986.

25. Hegg, E. L., and Que, L., Jr. (1997) "The 2-His-1-carboxylate facial triad--an emerging structural motif in mononuclear non-heme iron(II) enzymes" *Eur. J. Biochem. 250*, 625-629.

26. Liu, A., Ho, R. Y., Que, L., Jr., Ryle, M. J., Phinney, B. S., and Hausinger, R. P. (2001) "Alternative reactivity of an α-ketoglutarate-dependent iron(II) oxygenase: enzyme self-hydroxylation" *J. Am. Chem. Soc. 123*, 5126-5127.

27. Wolfe, M. D., and Lipscomb, J. D. (2003) "Hydrogen peroxide-coupled cis-diol formation catalyzed by naphthalene 1,2-dioxygenase" *J. Biol. Chem. 278*, 829-835.

28. Karlsson, A., Parales, J. V., Parales, R. E., Gibson, D. T., Eklund, H., and Ramaswamy, S. (2003) "Crystal structure of naphthalene dioxygenase: side-on binding of dioxygen to iron" *Science 299*, 1039-1042.

29. Groves, J. T. (1985) "Key elements of the chemistry of cytochrome P-450. The oxygen rebound mechanism" *J. Chem. Ed. 62*, 928-931.

Chapter 4: Hidden Protein Radical in HppE

4.1 INTRODUCTION

In recent years, there has been rapidly growing appreciation for the catalytic importance of protein-centered radicals in metalloenzymes (*1*). The very first catalytically essential protein-centered radical was identified on a tyrosine residue in ribonucleotide reductase by Dr. Peter Reichard and coworkers in 1977 (*2*). Since then, many stable or transient protein radicals have been discovered, including the tyrosine radicals in photosystem II (*3*) and prostaglandin H synthase (*4*), the glycine radicals in pyruvate formate-lyase (*5*) and anaerobic ribonucleotide reductase (*E. coli*) (*6*), the cysteine radicals in ribonucleotide reductases (*7*), and the tryptophan radicals in cytochrome c peroxidase (*8*). In addition, radicals have also been found on modified tyrosine residues in galactose oxidase (*9*) and amine oxidases (*10*), and modified tryptophan residue in methylamine dehydrogenase (*11, 12*). The formation of an amino acid derived radical is a posttranslational modification event and always involves a metallo-cofactor. For instance, diferric cluster, adenylcobalamine and SAM-bound $[Fe_4S_4]$ cluster are the metallo-cofactors responsible for the generation of protein-centered radicals in Class I, II and III ribonucleotide reductases, respectively (*1*).

HppE is a new type of mononuclear non-heme iron-dependent enzyme (*13*). The as-purified HppE is an apoprotein that needs to be reconstituted with iron *in vitro* to restore its full catalytic activity. As described in Chapter 2, the apo-HppE was reconstituted with $Fe^{II}(NH_4)_2(SO_4)_2$ under aerobic conditions, and

the resulting reconstituted HppE was considered in the form of Fe^{III}-HppE. The reconstituted HppE has been subjected to extensive EPR analyses leading to a preliminary catalytic model for the enzymatic epoxidation reaction (Figure 2-14). Interestingly, it was found that the total spin of the ferric center measured by EPR analyses (Figure 2-4) cannot count for the total iron content determined by iron titration (Chapter 2). Initially, the hidden iron was attributed to the potential occupancy of EPR-silent Fe^{II} occupying in enzyme active site. However, when the reconstituted HppE sample was exposed to excess nitric oxide, no ferrous ion, which should form an EPR-sensitive Fe^{II} nitrosyl complex, was detected (Chapter 2). To account for the discrepancy, we have hypothesized the formation of a spin-coupled [Fe^{III}-R•] complex (R• stands for an organic radical) in the enzyme active site as a result of *in vitro* aerobic reconstitution of HppE. Since Fe^{III} has a d^5 electronic configuration with a net spin of either $S = 1/2$ (low spin) or $S = 5/2$ (high spin), and the organic radical has an unpaired electron with a net spin of $S = 1/2$, the total spin number of the coupled complex is an integer. In regular EPR spectra, the spin adduct and its metal and radical components are all invisible. The unpaired spin is presumably localized to an active site residue that is in close vicinity to the ferric center. The only precedent of such type of metal-coupled protein radical is found in galactose oxidase, in which an unpaired electron on a modified tyrosine residue, which is also an active site metal ligand, is spin-coupled to the enzyme cupric center (*9*).

This Chapter describes our preliminary attempts to verify the presence of the putative Fe^{III}-coupled protein-centered radical. In collaboration with Dr.

Aimin Liu and Dr. John D. Lipscomb at the University of Minnesota, I have combined EPR spectral analysis with a variety of other biochemical methods including the uses of radical scavenger, metal chelating agent, and spin-trapping technique to search for the spin-coupled metal radical complex. Although the study is still in progress, the preliminary data have provided evidence supporting the presence of such a complex. The mechanistic implications of these results on the epoxidation and self-modification reactions catalyzed by HppE are discussed herein.

4.2 MATERIALS AND METHODS

General. HppE was purified using the same procedure as previously reported (*13*). As-purified apo HppE was reconstituted with one equivalent of $Fe^{II}(NH_4)_2(SO_4)_2$ aerobically and the resultant reconstituted HppE is green in color, which is referred as the reconstituted HppE or the oxidized HppE in this Chapter. Purified HppE mutants Y102F, Y103F and Y105F were kindly provided by Dr. Zongbao Zhao. All chemicals including spin trapping agents were purchased from Sigma (St. Louis, MO), unless noted otherwise.

Preparation of HppE Sample with Radical Scavenger. The 330 mM stock solution of radical scavenger, hydroxylurea (HU), was prepared with Tris·HCl buffer (pH 7.5, 50 mM). A typical EPR sample is 150 μL in total volume containing 250 μM reconstituted HppE and 25 mM HU in Tris·HCl buffer (pH 7.5, 50 mM). The sample was left on ice for 2 h before it was frozen in liquid N_2.

Preparation of HppE Sample with Metal Chelator. The 0.5 M stock solution of metal chelator, ethylenediamine tetraacetic acid (EDTA), was prepared in ddH_2O and its pH was adjusted to 8.0 with NaOH. A typical EPR sample of 150 μL in volume contained 250 μM reconstituted HppE and 16 mM EDTA in Tris·HCl buffer (pH 7.5, 50 mM). The sample was mixed for a few seconds at room temperature before it was frozen in liquid N_2.

Preparation of HppE Sample with Spin Trapping Agent. The 1.5 M stock solution of spin trapping agent, 5,5-dimethyl-1-pyrroline-N-oxide (DMPO), was prepared in Tris·HCl buffer (pH 7.5, 50 mM). Prior to mixing, DMPO powder and buffer were both vacuumed and flushed with argon. The solution was prepared, stored, and used in the dark. A typical EPR sample of 150 μL in volume contained 250 μM reconstituted HppE and 500 mM DMPO in Tris·HCl buffer (pH 7.5, 50 mM). The HppE mutants Y102F, Y103F and Y105F were aerobically reconstituted with one equivalent of $Fe^{II}(NH_4)_2(SO_4)_2$. A typical EPR sample of 200 μL in volume contained 500 μM reconstituted mutant and 500 mM DMPO in Tris·HCl buffer (pH 7.5, 50 mM). All samples were mixed for a few seconds at room temperature prior to being frozen in liquid N_2.

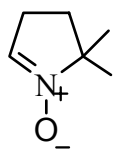

DMPO

Preparation of HppE Sample with Substrate. The 0.2 M stock solution of HppE substrate, (*S*)-HPP, was prepared in Tris·HCl buffer (pH 7.5, 50 mM). The EPR sample contained 250 μM reconstituted HppE and 10-fold excess of (*S*)-HPP in Tris·HCl buffer (pH 7.5, 50 mM). The samples were incubated for 1 min or 1 h at room temperature before being frozen in liquid N_2.

EPR Spectroscopy. EPR first derivative spectra of HppE were collected at X-band microwave frequency with 100-kHz field modulation on a Bruker Elexsys E500 spectrometer. The experimental conditions for EPR are the same as reported in Chapter 2.

4.3 RESULTS

EPR Spectra of Reconstituted HppE with Radical Scavengers. In the first set of experiments, a free radical scavenger, HU, was used to quench the radical spin coupled to the ferric center in the active site of HppE, in hope of visualizing the metal with half-integer spin number (S = 1/2 or 5/2) by EPR spectroscopy. HU was chosen because it is capable of quenching the protein radicals specially without disturbing the iron center, as demonstrated in the study of ribonucleotide reductase (*14*). Figure 4-1 shows the EPR spectra of the reconstituted HppE before and after incubation with HU on ice for two hours. Interestingly, the intensity of EPR signal of the ferric ion increased by almost 30%. This result collaborates well with the existence of the diamagnetic Fe^{III}-radical couple in reconstituted HppE. In addition, it also revealed that the radical species in the enzyme active site is accessible to an external radical scavenger. However, the use of a radical scavenger neither provided direct evidence for the metal-coupled radical, nor can it distinguish the identity of the organic radical.

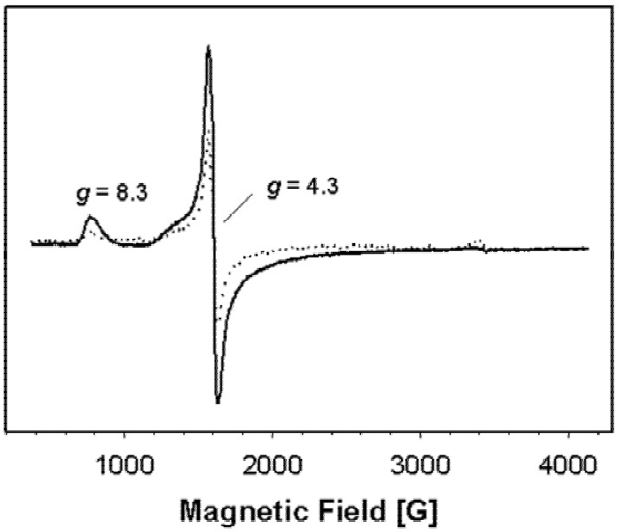

Figure 4-1 EPR spectra of the reconstituted HppE (dotted line) and the reconstituted HppE in the presence of 100× HU (solid line). Instrumental parameters: temperature, 2 K; microwave frequency, 9.6 GHz; microwave power, 0.6 mW; modulation amplitude, 5 G; time constant, 0.02 s; sweep rate, 50 G/s. The important *g* values are given in spectra.

EPR Spectra of Reconstituted HppE with Metal Chelator. The use of metal chelators like EDTA may allow us to directly detect and identify the postulated protein-centered radical. This is based on the assumption that EDTA can tightly bind the active site ferric ion and the iron-EDTA complex can be removed from the enzyme active site. If there exists the proposed Fe^{III}-coupled protein-centered radical in HppE active site, and if the radical is substantially stable for being alone and can be trapped in frozen state, this radical may be discernible by EPR spectroscopy when its spin coupling to the iron is broken. The reconstituted HppE was quickly mixed with the strong iron-chelating agent, EDTA, and frozen by liquid nitrogen, followed by EPR measurement. In

contrast to the EPR spectrum of the reconstituted HppE (Figure 4-2A), two new EPR features appeared after the EDTA treatment (Figure 4-2B). A sharp and isotropic signal that pumps into the low field region (g = 4.3), which is distinct from the enzyme-bound S = 5/2 ferric signal, has been assigned to a ferric EDTA complex (S = 5/2). The total spin content of iron increased nearly 30% as indicated by spin quantitation on the ferric EPR signals. The increase in iron signal intensity again implicated the presence of EPR-silent iron in the reconstituted HppE, which accounts for about 30% of the total iron.

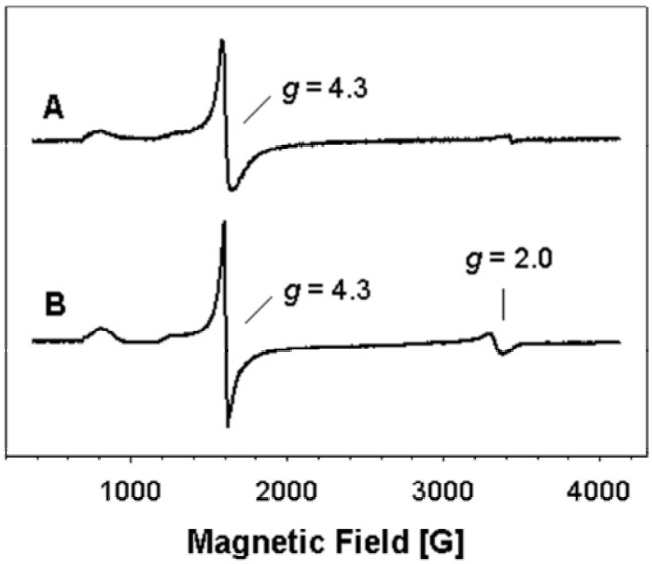

Figure 4-2. EPR spectra of the reconstituted HppE (A) and the reconstituted HppE treated with EDTA (B). Instrumental parameters are the same as in Figure 4-1. The important g values are given in spectra.

The most notable new feature after EDTA treatment is a new signal at g = 2.0 at the high-field region of the EPR spectrum (Figure 4-3). This EPR signal

can be severely saturated by microwave power at temperatures below 20 K. The temperature dependence of the signal intensity obeys the Curie law expected for a free radical. The power saturation analysis shows that the relaxation of this radical species is not strongly influenced by the metal ion (Table 4-1). Its lineshape and partially resolved hyperfine coupling are remarkably similar to those of tyrosine and tryptophan-harbored radicals reported in literature (*15*). Spin quantitation on the free radical signal shows 0.35 spin per HppE monomer. It should be noted that this number is largely dependent on the freezing time since free radicals are usually unstable at room temperature and often decay quickly over time. Since the optimal conditions for trapping this radical have not been fully established, the result is not always reproducible.

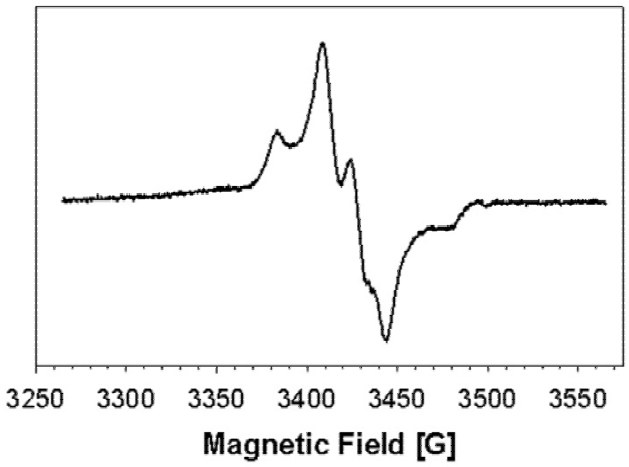

Figure 4-3. EPR spectrum of the reconstituted HppE treated with EDTA (g = 2 region). Instrumental parameters are the same as in Figure 4-1.

EPR Spectra of Reconstituted HppE with Spin Trapping Agents. More evidence for the protein radical was acquired by spin-trapping EPR technique.

Spin traps, such as DMPO, 2-methyl-2-nitrosopropane (MNP) and phenyl-N-tert-butylnitrone (PBN), are a group of relatively inert compounds that, however, can react with transient or unstable free radicals giving rise to longer lived radical adducts. If there exists an Fe^{III}-coupled protein radical like [Fe^{3+}-R•] in HppE, the amino acid residue R that harbors the unpaired electron may react with a spin trap to form a covalent adduct. The unpaired electron typically resides at the spin trap part of the adduct. Consequently, the reduction of the spin coupling between the metal center and the protein radical should make both visible in the EPR spectrum.

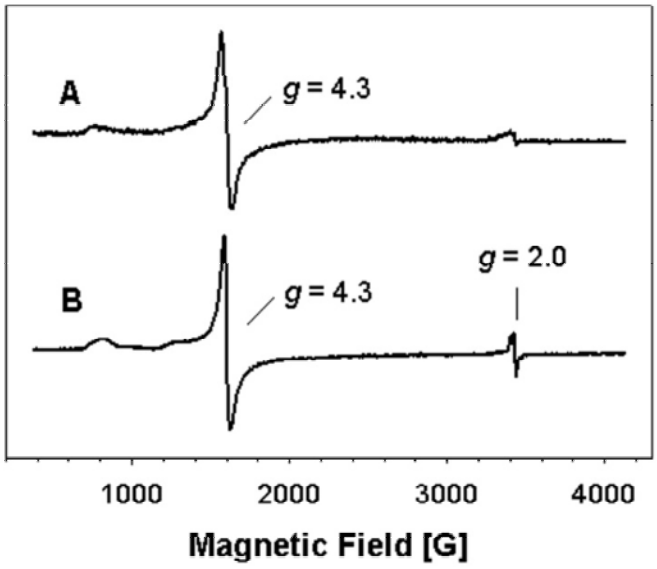

Figure 4-4. EPR spectra of the reconstituted HppE (A) and the reconstituted HppE treated with DMPO (B). Instrumental parameters are the same as in Figure 4-1. The important *g* values are given in spectra.

Several purified spin trapping agents were tested and DMPO was found the most effective among them. The DMPO treatment of the reconstituted HppE led to a new EPR signal around g = 2 region (Figures 4-4B and 4-5). The trapped signal represents ~ 0.3 spin per monomer as indicated by spin quantitation. Since neither the reconstituted HppE nor DMPO exhibits the g = 2 feature in their respective EPR spectrum, this new feature is most likely originated from the spin adduct of DMPO and the protein radical. The DMPO adduct of HppE was examined by EPR spectroscopy at a wide range of temperatures. Its EPR relaxation property as quantified by the $P_{1/2}$ values at various temperatures is comparable to that of the radical signal produced by EDTA treatment depicted above (Table 4-1). It should be noted that the EPR signal of the DMPO-HppE radical adduct closely resembles that of the spin-trapped DMPO radical in metmyoglobin, where a long-lived protein-based tyrosyl radical was initially produced by hydrogen peroxide treatment (*16*).

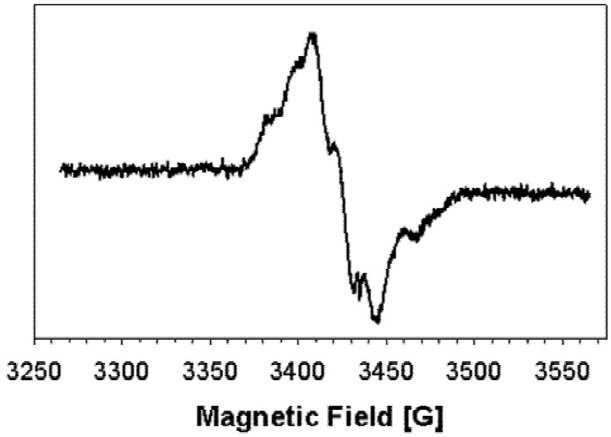

Figure 4-5. EPR spectrum of the reconstituted HppE treated with DMPO (g = 2 region). Instrumental parameters are the same as in Figure 4-1.

Sample	Temperature (K)			
	2	20	50	120
Reconstituted HppE + EDTA	0.007	0.092	0.286	5.50
Reconstituted HppE + DMPO	0.006	0.043	0.063	0.516

Table 4-1 EPR microwave saturation behavior of the radical species in the reconstituted HppE after chemical treatments. The $P_{1/2}$ parameter, as the indicator of the relaxation property of EPR signals, shown in the table were calculated by an earlier reported method (*17*).

At different temperatures, the EPR spectra of the HppE-DMPO adduct changed their line shape (Figures 4-6A and B), suggesting the existence of multiple paramagnetic species in the sample. The dominant radical species reflected in spectrum A (dotted line) is more likely the nitroxide radical from DMPO (*18*) because the intensity if this corresponding EPR signal increases with the rising temperature. In free solution, where the nitroxide group of the DMPO-protein radical adduct can move rapidly and isotropically, its EPR signal usually consists of four narrow lines with a height ratio of 1:2:2:1. This is unique as compared to the EPR spectra of all other spin trap adducts. The 4-line splitting pattern is due to the nuclear spins of neighboring N and H atoms (I_N = 1 and I_H = 1/2) in DMPO, which all have the same coupling constant with the O-centered nitrosyl radical on the spin trap (2×[1+1/2]+1=4) (*19*). However, in the frozen state where molecular tumbling slows down and thus anisotropy becomes much more substantial, the EPR spectrum of DMPO radical is generally less resolved. In Figure 4-6, only the largest hyperfine splitting can be measured (A_{zz} = 34 G) while the other two smaller splittings are obscured in the central

region of the spectra. The hyperfine coupling constant (A_{zz}) of 34 G is similar to the constant observed in the EPR spectrum of tert-butyl nitroxide spin label in crystal form (*18*).

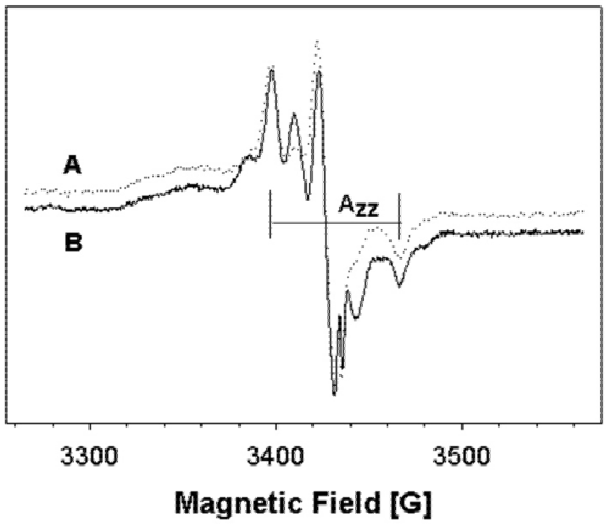

Figure 4-6 EPR spectra of the reconstituted HppE treated with DMPO (g = 2 region) at (A) 200 K; (B) 150 K. Instrumental parameters are the same as in Figure 4-1 except for, microwave power, 1 mW, and scan time: 50.

EPR Spectra of Reconstituted HppE mutants with Spin Trapping Agents. To identify the radical harboring site in HppE, three tyrosine mutants, Y102F, Y103F and Y105F were also aerobically reconstituted with iron *in vitro* and then treated with DMPO. EPR spectral analysis showed that all three mutants formed radical adducts with DMPO (Figure 4-7), whose signals are all similar to that of the DMPO adduct of the wild type HppE. Thus, it is reasonable to conclude that a similar type of radical was also formed in mutant proteins. The only difference

between the EPR signals derived from these mutants is their intensities. It is not clear what is the cause of the variation in EPR signal intensity.

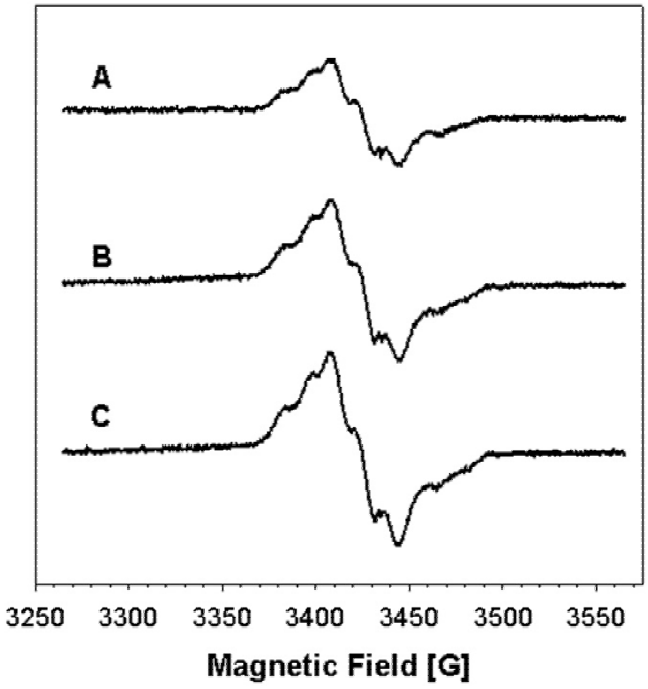

Figure 4-7 EPR spectra of the reconstituted HppE mutants treated with DMPO (g =2 region). (A) Y105F; (B) Y103F; (C) Y102F. Instrumental parameters are the same as in Figure 4-1.

EPR Spectra of Reconstituted HppE with Substrate. The EPR spectrum of the reconstituted HppE incubated with (*S*)-HPP was shown and discussed in Chapter 2. However, it was discovered later that the length of incubation time has significant effects on the spectral properties of the enzyme-substrate complex. In contrast to the spectrum reported in Chapter 2 (Figure 2-4B), which was recorded 1 min after mixing of enzyme and substrate (Figure 4-8B), the new spectrum that was recorded after 1 h of incubation varies considerably (Figure 4-

8A). The long time incubation led to an increase in overall intensity of the enzyme ferric signal (S = 5/2). This intensity enhancement is reminiscent of the EPR spectral change induced by the treatments of HU (Figure 4-1), EDTA (Figure 4-2), and DMPO (Figure 4-3), reflecting the relaxation of the spin coupling between ferric ion and the protein radical. Except for HU treatment, which frees up the ferric ion from diamagnetic coupling by quenching the coupled radical, the addition of EDTA and DMPO to the reconstituted HppE resulted in the appearance of free radical-like signals around g = 2. A g = 2 signal was also observed in the long-time incubated sample of the HppE-substrate complex (Figure 4-8A), in addition to the ferric signal with higher intensity.

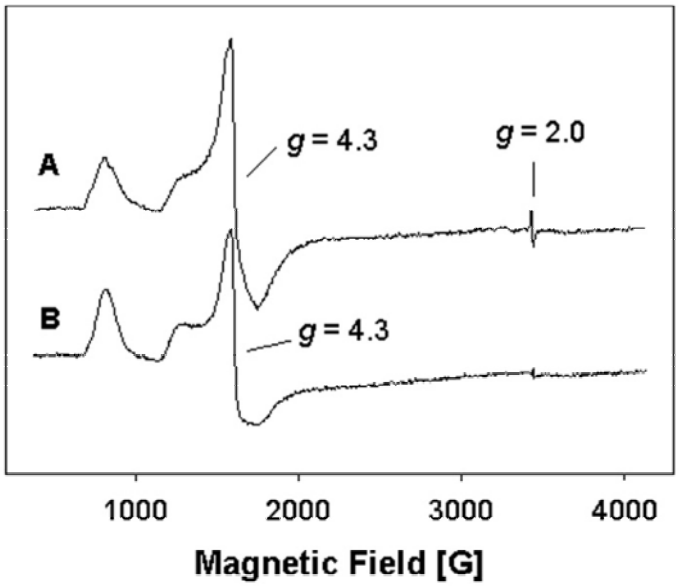

Figure 4-8 EPR spectra of the reconstituted HppE incubated with (*S*)-HPP for 1 h (A) and for 1 min (B). Instrumental parameters are the same as in Figure 4-1. The important g values are given in spectra.

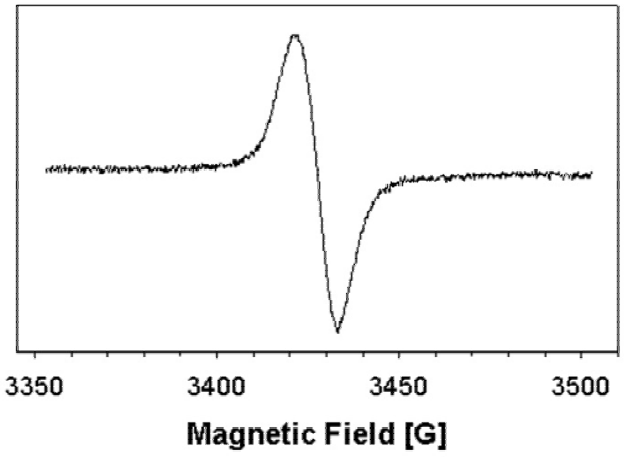

Figure 4-9 EPR spectrum of the reconstituted HppE incubated with (*S*)-HPP for 1 h (g = 2 region). Instrumental parameters are the same as in Figure 4-1.

Figure 4-9 shows an expanded g = 2 region of spectrum A in Figure 4-8. The new radical-like signal has a narrow linewidth, less than 40 G, which is in sharp contrast to the linewidth of more than 120 G of the radical signals observed in the EPR spectra of the reconstituted HppE treated with EDTA (Figure 4-3) and DMPO (Figure 4-5). Given that the broad EPR signals are characteristic for the radicals with low tumbling rate, especially protein radicals, the narrow signal observed at g = 2 more likely represents a free organic radical. Further analysis showed an unusual temperature dependence property of this EPR signal. In response to the increased temperature, its intensity was not increased but actually decreased. In addition, this signal does not show any hyperfine features as most other free radical signals do. All of these make it distinct from normal radicals, including the putative protein radical in HppE revealed by EDTA-treatment and

the radical trapped as a DMPO adduct in HppE. Currently, we can only postulate that this is a substrate radical loosely coupled to the iron center. As a part of metal-substrate complex, its EPR properties resemble those of metal ions more than those of organic radicals. However, the coupling is not strong enough to make it as another EPR-silent Fe^{III}-radical adduct.

4.4 DISCUSSION

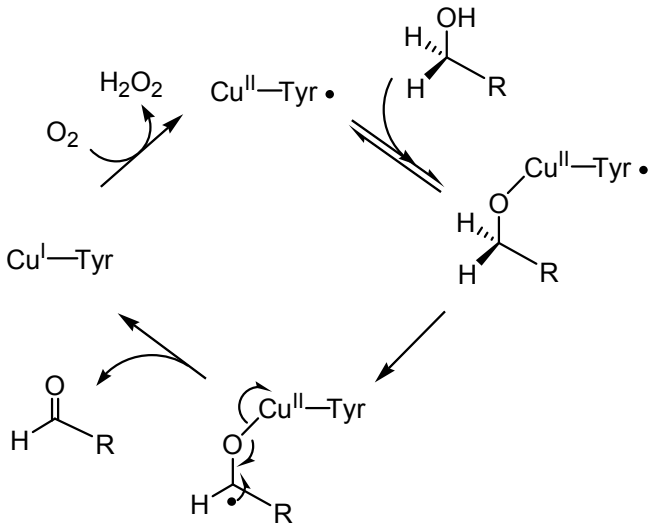

Figure 4-10 Proposed mechanism for galactose oxidase.

EPR is one of the most powerful tools in the study of free radicals. The above results obtained from EPR spectral analysis combined with other techniques, may be attributed to the presence of a high spin ferric center (S = 5/2) is antiferromagnetically coupled with a protein radical (S = 1/2) in the active site of HppE. Formation of such an Fe^{III}-radical couple with a ground state of S = 2 is unprecedented for a metal-radical complex, in which either metal ion or radical is EPR-silent. The only close example is the complex of a cupric ion coupled

with a modified tyrosine radical in the active site of galactose oxidase (*9*) and its analogues (*20*). In those enzymes, the active site tyrosine harboring the unpaired electron is one of the copper ligands. When the substrate binds to the cupric center, it should also be close proximity to the tyrosyl radical, which can abstract hydrogen from the substrate forming a radical intermediate (Figure 4-10).

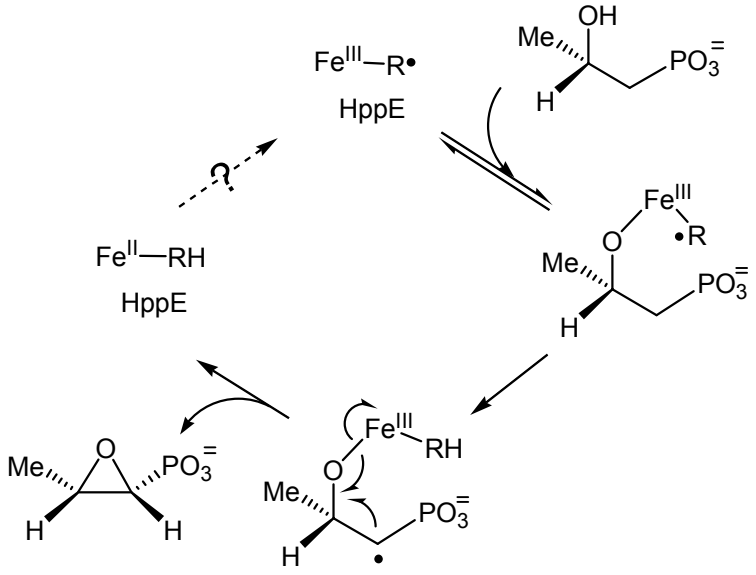

Figure 4-11 Proposed mechanism for HppE-catalyzed epoxidation involving the Fe^{III}-coupled tyrosine radical.

A catalytic role analogous to that of the Cu^{II}-coupled tyrosyl radical in galactose oxidase was once proposed for the Fe^{III}-coupled protein radical in HppE (Figure 4-11). Since the Fe^{III}-radical pair is a redox equivalent of Fe^{IV} reactive species, it is plausible in principle that it can mediates radical formation at C_1 of (*S*)-HPP via hydrogen abstraction. The subsequent steps simply replicate the mechanism proposed in Figure 2-14 including the radical-induced Fe-O bond cleavage and epoxide ring closure (Figure 2-14). However, this mechanism

cannot explain how the Fe^{IV} equivalent is generated in the absence of exogenous electrons from NAD(P)H, which has been known as an indispensable electron donor for HppE to catalyze its epoxidation reaction *in vitro*. In fact, the copper dependent galactose oxidase catalyzes a two-electron redox cycle, in which dioxygen is reduced to hydrogen peroxide, whereas the non-heme iron dependent HppE catalyzes a four-electron redox cycle, in which dioxygen is fully reduced to water. Therefore, the strategy to regenerate Cu^{II}-tyrosyl radical complex in galactose oxidase, which only requires two oxidative equivalents produced in the conversion of dioxygen to hydrogen peroxide (Figure 4-10), is not applicable to the epoxidation reaction catalyzed by HppE. Besides, the mechanism shown in Figure 4-11 predicts a single turnover epoxidation, which has never been observed even in the incubation when hundred milligrams of enzyme was used.

In addition to its epoxidase activity, HppE has recently been shown to have oxygenase activity as well, capable of self-hydroxylating an active site tyrosine residue, Tyr105, to DOPA (*21*). Although the exact mode of the self-hydroxylation reaction remains to be determined, several radical-based mechanisms involving a tyrosyl radical intermediate have been proposed for the analogous reactions occurring in TauD (*22*), the R2 protein mutant F208Y of Class I ribonucleotide reductase (*23*), and the conversion of phenol to catechol catalyzed by horseradish peroxidase (*24*). A similar radical mechanism for self-hydroxylation of HppE has also been discussed in Chapter 3 (Figure 3-13), in which the oxoferryl species, a product of the activation of the enzyme ferrous center by dioxygen and ascorbate, is responsible for the formation of the tyrosyl

radical intermediate. The possible presence of the Fe^{III}-coupled radical complex as implicated by the current experimental results, allows one to propose an alternative way to generate the tyrosyl radical, and to insert an oxygen atom into the phenol ring. As shown in Figure 4-12, the tyrosyl radical and its coupled ferric center are produced together after two consecutive reversible reactions. In the absence of exogenous electrons that are necessary for the in vitro self-hydroxylation, the metal-radical adduct may exit the pathway by releasing the bound hydrogen peroxide. Before the radical is eventually quenched, it may be stabilized by spin coupling to the ferric ion. It is believed that the spin adduct being trapped by EDTA and DMPO treatments exists in this state. Alternatively, the addition of electron donors such as ascorbate would push the reaction forward having the tyrosine residue converted to DOPA.

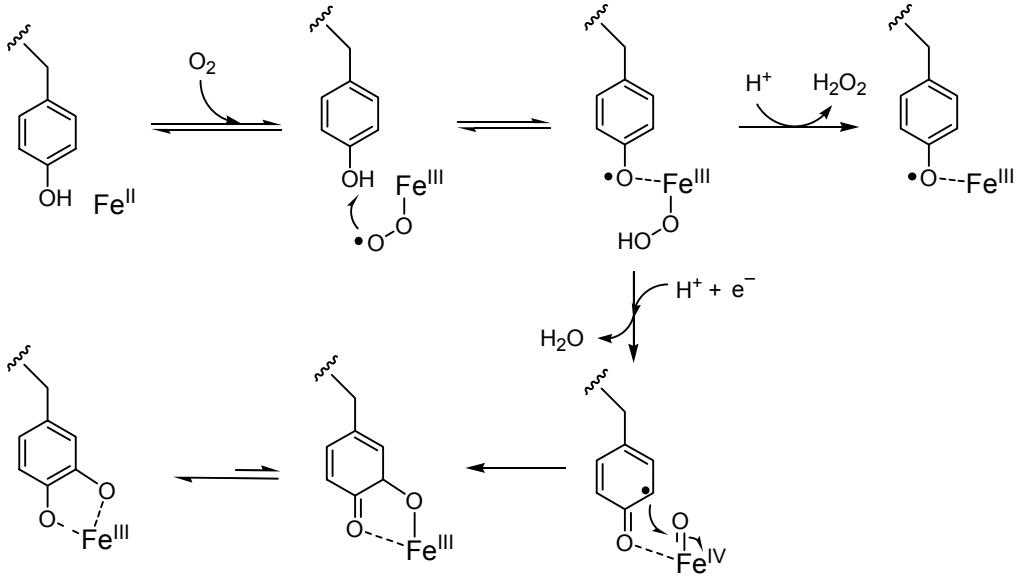

Figure 4-12 Proposed mechanism for self-hydroxylation of HppE involving the Fe^{III}-coupled tyrosine radical.

If the Fe^{III}-coupled protein radical indeed plays a part in the self-hydroxylation as illustrated in Figure 4-12, Tyr105, as the residue to be modified, should also be the docking site of the protein radical as well. Unfortunately, mutation of the particular residue did not prevent the formation of protein radical, since radical intermediate could still be trapped by DMPO treatment (Figure 4-7). As we have already observed in the *in vitro* self-hydroxylation of HppE mutants, when Tyr105 is not available, Tyr103 becomes the primary modification site. Therefore, it is conceivable that Tyr103 harbors the unpaired electron in the Y105F mutant, which, upon DMPO treatment, gives the observed spin-trapping adduct. To test the possibility, the double mutant Y103F/Y105F was prepared for the future study.

The above discussion focuses on the possible role of the Fe^{III}-coupled protein radical in the self-hydroxylation of HppE and its potential relevance to the epoxidase activity of HppE. However, it is also important to pay attention to the odd signal at $g = 2$ in the EPR spectrum of the reconstituted HppE which was incubated with substrate for longer than 1 h. As previously rationalized, this signal is more likely derived from a free organic radical than from a protein-centered radical. According to the mechanism shown in Figure 4-12, it may be assigned to a metal-bound substrate radical intermediate (Figure 4-13), which may explain its unusual spectral properties. The equilibrium between two key intermediates A and B should lean toward the retention, instead of the fission, of the C-H bond in substrate intermediate A, because the C-H bond is believed to be a stronger bond than the O-H bond. The following steps involving the

exogenous electron transfer and the formation of the Fe^{IV}-oxo species provide the driving forces to move the reaction forward. The cycle ends up with the radical-induced epoxide formation and iron reduction. This mechanism is very close to the one discussed in Chapter 2 (Figure 2-13), in which Fe^{III}-superoxide is proposed to be responsible for hydrogen abstraction. More experiments are in progress to elucidate the identity of the unusual EPR signal at $g = 2$.

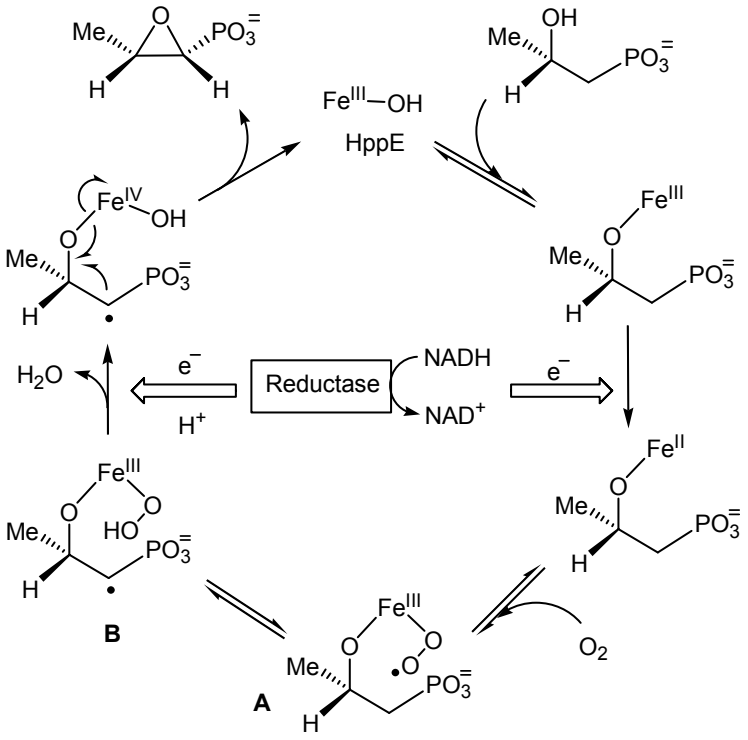

Figure 4-13 Proposed mechanism for HppE-catalyzed epoxidation involving the Fe^{III}-bound substrate radical.

It is worth noting that the above equilibrium hypothesis is consistent with the competitive relationship between the epoxidase and the oxygenase activities of HppE. As we have demonstrated in Chapter 3, the self-modification of HppE

prevails the in the absence of substrate, and the addition of substrate switches on its epoxidase activity resulting in the conversion of substrate to fosfomycin. The determining factor is substrate binding, which also facilitates the conversion of the EPR-silent protein radical to the EPR-visible substrate radical (Figure 4-8). It appears that substrate binds to the active site of HppE and shifts the equilibrium from Fe^{III}-coupled protein radical to Fe^{III}-bound substrate radical.

4.5 REFERENCE

1. Stubbe, J., and van der Donk, W. A. (1998) "Protein radicals in enzyme catalysis" *Chem. Rev. 98*, 705-762.
2. Sjöberg, B. M., Reichard, P., Gräslund, A., and Ehrenberg, A. (1977) "Nature of the free radical in ribonucleotide reductase from *Escherichia coli*" *J. Biol. Chem. 252*, 536-541.
3. Barry, B. A., El-Deeb, M. K., Sandusky, P. O., and Babcock, G. T. (1990) "Tyrosine radicals in photosystem II and related model compounds. Characterization by isotopic labeling and EPR spectroscopy" *J. Biol. Chem. 265*, 20139-20143.
4. Karthein, R., Dietz, R., Nastainczyk, W., and Ruf, H. H. (1988) "Higher oxidation states of prostaglandin H synthase. EPR study of a transient tyrosyl radical in the enzyme during the peroxidase reaction" *Eur. J. Biochem. 171*, 313-320.
5. Unkrig, V., Neugebauer, F. A., and Knappe, J. (1989) "The free radical of pyruvate formate-lyase. Characterization by EPR spectroscopy and involvement in catalysis as studied with the substrate-analogue hypophosphite" *Eur. J. Biochem. 184*, 723-728.
6. Mulliez, E., Fontecave, M., Gaillard, J., and Reichard, P. (1993) "An iron-sulfur center and a free radical in the active anaerobic ribonucleotide reductase of *Escherichia coli*" *J. Biol. Chem. 268*, 2296-2299.
7. Licht, S., Gerfen, G. J., and Stubbe, J. (1996) "Thiyl radicals in ribonucleotide reductases" *Science 271*, 477-481.
8. Huyett, J. E., Doan, P. E., Gurbiel, R., Houseman, A. L. P., Sivaraja, M., Goodin, D. B., and Hoffman, B. M. (1995) "Compound ES of cytochrome c peroxidase contains a Trp π-cation radical: characterization by

continuous wave and pulsed Q-band external nuclear double resonance spectroscopy" *J. Am. Chem. Soc. 117*, 9033-9041.

9. Whittaker, M. M., and Whittaker, J. W. (1990) "A tyrosine-derived free radical in apogalactose oxidase" *J. Biol. Chem. 265*, 9610-9613.

10. Dooley, D. M., McGuirl, M. A., Brown, D. E., Turowski, P. N., McIntire, W. S., and Knowles, P. F. (1991) "A Cu(I)-semiquinone state in substrate-reduced amine oxidases" *Nature 349*, 262-264.

11. Chen, L. Y., Mathews, F. S., Davidson, V. L., Huizinga, E. G., Vellieux, F. M., Duine, J. A., and Hol, W. G. (1991) "Crystallographic investigations of the tryptophan-derived cofactor in the quinoprotein methylamine dehydrogenase" *FEBS Lett. 287*, 163-166.

12. McIntire, W. S., Wemmer, D. E., Chistoserdov, A., and Lidstrom, M. E. (1991) "A new cofactor in a prokaryotic enzyme: tryptophan tryptophylquinone as the redox prosthetic group in methylamine dehydrogenase" *Science 252*, 817-824.

13. Liu, P., Liu, A., Yan, F., Wolfe, M. D., Lipscomb, J. D., and Liu, H. W. (2003) "Biochemical and spectroscopic studies on (S)-2-hydroxypropylphosphonic acid epoxidase: a novel mononuclear non-heme iron enzyme" *Biochemistry 42*, 11577-11586.

14. Barlow, T., Eliasson, R., Platz, A., Reichard, P., and Sjöberg, B. M. (1983) "Enzymic modification of a tyrosine residue to a stable free radical in ribonucleotide reductase" *Proc. Nat. Acad. Sci. USA 80*, 1492-1495.

15. Gräslund, A., and Sahlin, M. (1996) "Electron paramagnetic resonance and nuclear magnetic resonance studies of class I ribonucleotide reductase" *Annu. Rev. Biophys. Biomol. Struct. 25*, 259-286.

16. Gunther, M. R., Tschirret-Guth, R. A., Witkowska, H. E., Fann, Y. C., Barr, D. P., Ortiz De Montellano, P. R., and Mason, R. P. (1998) "Site-specific spin trapping of tyrosine radicals in the oxidation of metmyoglobin by hydrogen peroxide" *Biochem. J. 330*, 1293-1299.

17. Sahlin, M., Gräslund, A., and Ehrenberg, A. (1986) "Determination of relaxation time for a free radical from microwave saturation studies." *J. Magn. Reson. 67*, 135-137.

18. Knowles, P. F., Marsh, D., and Rattle, H. W. E. (1976) *Magnetic Resonance of Biomolecule: an introduction to the theory and practice of NMR and ESR in biological systems*, John Wiley & Sons, Ltd., New York.

19. Tomasi, A., and Iannone, A. (1993) in *Biological Magnetic Resonance* (Berliner, L. J., and Reuben, J., Eds.) pp 353-384, Plenum Press, New York.

20. Whittaker, M. M., Kersten, P. J., Nakamura, N., Sanders-Loehr, J., Schweizer, E. S., and Whittaker, J. W. (1996) "Glyoxal oxidase from *Phanerochaete chrysosporium* is a new radical-copper oxidase" *J. Biol. Chem. 271*, 681-687.

21. Liu, P., Mehn, M. P., Yan, F., Zhao, Z., Que, L., Jr., and Liu, H.-W. (2004) "Oxygenase activity in the self-hydroxylation of (*S*)-2-hydroxypropylphosphonic acid epoxidase involved in fosfomycin biosynthesis" *J. Am. Chem. Soc. 126*, 10306-10312.

22. Ryle, M. J., Liu, A., Muthukumaran, R. B., Ho, R. Y., Koehntop, K. D., McCracken, J., Que, L., Jr., and Hausinger, R. P. (2003) "O_2- and α-ketoglutarate-dependent tyrosyl radical formation in TauD, an α-keto acid-dependent non-heme iron dioxygenase" *Biochemistry 42*, 1854-1862.

23. Ling, J., Sahlin, M., Sjöberg, B. M., Loehr, T. M., and Sanders-Loehr, J. (1994) "Dioxygen is the source of the mu-oxo bridge in iron ribonucleotide reductase" *J. Biol. Chem. 269*, 5595-5601.

24. Dordick, J. S., Klibanov, A. M., and Marletta, M. A. (1986) "Horseradish peroxidase catalyzed hydroxylations: mechanistic studies" *Biochemistry 25*, 2946-2951.

Chapter 5: Active Site Structure of HppE

5.1 INTRODUCTION

To gain more insights into the catalytic mechanism of HppE, it is important to characterize the metal center, to determine its involvement in substrate binding, and to study its role in catalysis. A recently reported multiple protein sequence alignment predicted a β-barrel fold in the tertiary structure of HppE, and thus categorized HppE as a member of the cupin superfamily (*1*). This structural family was named after the Latin word '*cupa*', which means small barrel, because the β-barrel fold is the basic structural element in all cupin proteins. In addition to the resemblance of their tertiary structures, two or three histidine residues and one glutamate residue that are associated with active site metal binding are conserved among most of the family members. For HppE from *Streptomyces wedmonresis*, His138, Glu142 and His180 are the conserved amino acid residues that may serve as ligands for the iron center (*2*). This potential metal binding triad is also preserved in HppE from *Pseudomonas syringae* PB-5123 (*3*) (Figure 5-1). This chapter describes a combined study on the iron-binding site in HppE by site-directed mutagenesis and spectroscopic analyses. The effects of mutation of several conserved active site residues on iron binding, substrate binding, self-hydroxylation and enzymatic epoxidation are reported. Our studies show that the iron coordination in HppE involves a 2-His-1-carboxylate core. The spectral analyses also shed light on the mechanism of enzyme catalysis.

```
S. wendomorensis      MSNTKTASTG FAELLKDRRE QVKMDHAALA SLLGETPETV AAWENGEGGE  50
P. syringae           M–DVRTLAVG KAH-LEALLA TRKM---TLE HLQDVRHDAT QVYFDGLEHL  45
Consensus             M....T...G .A..L..... ..KM....L. .L........ .....G....  50

S. wendomorensis      LTLTQLGRIA HVLGTSIGAL TPPAGNDLDD GVIIQMPDER PILKGVRDNV 100
P. syringae           QNVAQY--LA IPLSEFFVGQ TQ---SDLDD GVKIARRNGG FKREEIRGGV  90
Consensus             ....Q....A ..L..... T.....DLDD GV.I...... ......R..V 100

S. wendomorensis      DYYVYNCLVR TKRAPSLVPL VVDVLTDNPD DAKFNSGHAG NEFLFVLEGE 150
P. syringae           HYYTYEHLVT TNQDPGLMAL RLDLHSDDEQ PLRLNGGHGS REIVYVTRGA 140
Consensus             .YY.Y..LV. T...P.L..L ..D...D... ....N.GH.. .E...V..G. 150

S. wendomorensis      IHMKW-GDKE NPKEALLPTG ASMFVEEHVP HAFTAAKGTG SAKLIAVNF- 198
P. syringae           VRVRWVGDND ELKEDVLNEG DSIFILPNVP HSFTNHVGGA KSEIIAINYG 190
Consensus             ....W.GD.. ..KE..L..G .S.F....VP H.FT...G.. ....IA.N.. 200
```

Figure 5-1. Sequence alignment of HppE isolated from *Streptomyces wedmorensis* and *Pseudomonas syringae*. The conserved residues likely to constitute the proposed 2-His-1-carboxylate facial triad are boxed.

5.2 MATERIALS AND METHODS

Site-directed Mutagenesis. Mutagenesis of the HppE gene (*fom4*) was carried out using QuickChange™ site-directed mutagenesis kit from Strategene (La Jolla, CA). The oligonucleotides used for mutagenesis were customarily synthesized by Integrated DNA Technology (Coralville, IA) (Table 5-1). The PCR conditions are the same as previously reported in Chapter 3. The constructed mutant plasmids were amplified in *E. coli* strain DH5α and purified with Qiaprep® spin miniprep kit (Qiagen, Valencia, CA). Once the mutation was verified by DNA sequencing performed by the core facility of the Institute for Cellular and Molecular Biology, the University of Texas at Austin, the mutant plasmids were used to transform *E. coli* cell BL21(DE3) (Novagen, Madison, WI)

for overexpression. The mutant Y105F was previously constructed by Dr. Zongbao Zhao (*4*).

Mutant	*Oligonucleotide sequence*
H138A	5'-GAAGTTCAACTCGGGCGCCGCCGGCAACGAG-3'
E142A	5'-GCCACGCCGGCAACGCGTTCCTCTTCGTGCTCG-3'
H180A	5'-GGAGGAGCACGTGCCGGCCGCCTTCACGGCGGC-3'

Table 5-1. Oligonucleotide primers used for site-directed mutagenesis. (Note: the sites of mutation are underlined).

Expression and Purification. The wild-type HppE and its mutants were overproduced by growing the corresponding recombinant strains in LB medium and then purified according to previously reported procedures (*5*). SDS-PAGE was used to monitor the elution processes during purification. The purified enzymes were desalted, concentrated, and stored at – 80 °C.

NBT Quinone Staining. Proteins were first subjected to SDS-PAGE with pre-stained broad-range protein marker (New England Biolabs, Beverly, MA) and then transferred onto a nitro-cellulose membrane using the Mini Trans-Blot Cell Assembly (Bio-Rad, Hercules, CA). The transblotting was conducted in the transfer buffer (25 mM Tris·HCl, 192 mM glycine, 20% methanol) at 100 V for 1 h. The DOPA-containing proteins were visualized with a temporary staining solution (0.1% (w/v) ponceau S, 5% (v/v) acetic acid). After the temporary stains were removed by washing with ddH_2O, the protein-containing nitro-cellulose membrane was immersed in a solution of 0.24 mM nitroblue tetrazolium (NBT) and 2 M potassium glycinate, pH 10, in the dark for 45 min to visualize the DOPA-containing protein band (*6*).

Preparation of Ferric Enzyme Samples. The apo-proteins of the wild-type and mutant enzymes were made anaerobic by repeated cycles of vacuum and flushing with argon. A molar equivalent of $Fe^{II}(NH_4)_2(SO_4)_2$ from an anaerobic stock solution was added to the apo-proteins under anaerobic conditions. The Fe^{II}-loaded proteins were subsequently exposed to air until all of the iron was oxidized to the ferric state.

Preparation of Cupric Enzyme Samples. One molar equivalent of cupric ion from a $CuCl_2$ stock solution (20 mM) was slowly added to the apo-proteins of the wild-type and mutant enzymes. Rapid addition of the buffered cupric solution often led to protein precipitation. To prepare substrate-containing samples, the Cu^{II}-reconstituted proteins were further incubated with ten molar equivalents of (*S*)-HPP.

Preparation of Ferrous Enzyme Nitrosyl Samples. The Fe^{II}-loaded proteins were prepared as described above. Subsequent incubation of each sample with ten molar equivalents of (*S*)-HPP was carried out anaerobically in the EPR tubes. Nitric oxide gas was introduced to the substrate-bound enzyme samples through a gas-tight Hamilton syringe under argon. The samples were frozen by slow immersion in liquid nitrogen for later EPR analysis.

Epoxidase Activity Assay. A new assay was developed which contains 70 μM enzyme, 70 μM $Fe^{II}(NH_4)_2(SO_4)_2$, 15 mM (*S*)-HPP, 60 μM FMN, 22.5 mM NADH in 20 mM Tris·HCl buffer, pH 7.5 (totally 200 μL). The reaction was carried out at room temperature with vigorous shaking and then quenched by the addition of 40 μL of EDTA (0.5 M). The reaction mixture was kept on ice for

immediate NMR analysis or frozen at –80 °C and thawed shortly before analysis. The enzyme activity was calculated based on the integration of the ^{31}P NMR peaks assigned to product (δ 10.9) and substrate (δ 19.9). A sample of wild-type HppE was run in parallel as the standard in comparing enzyme activity of different mutants.

In vitro Self-hydroxylation. As-purified apo-proteins were diluted with ddH_2O to 1 mg/mL and were aerobically incubated with an equivalent of $Fe^{II}(NH_4)_2(SO_4)_2$ and ten equivalents of ascorbate at 4 °C for 1 h. The mixtures were concentrated by Amicon concentrator with a membrane pore size of 10 kDa (Millipore, Bedford, MA). The final protein concentrations were between 10-20 mg/mL. The extent of self-hydroxylation of each HppE mutant was analyzed by NBT quinone staining and UV-vis absorption spectroscopy.

EPR Spectroscopy. EPR first derivative spectra of HppE were collected at X-band microwave frequency with 100-kHz field modulation using either a Bruker Elexsys E500 in Dr. John D. Lipscomb's lab at the University of Minnesota or an EMX spectrometer in Dr. Aimin Liu's lab at the University of Mississippi Medical Center, both of which were equipped with a 10-kilogauss magnet and with an Oxford Instruments ESR900 cryostat. A calibrated frequency meter and a Bruker ER035M NMR Gauss meter were used for the *g*-value determinations. Spin quantification on the EPR spectra of the mutant enzymes was performed by comparing the double integration using wild-type enzyme as a standard

Preparation of Selenomethionine-labeled HppE. To prepare selenomethionine-labeled HppE (SeMet-HppE), the plasmid pPL001 that contains *fom4*, the gene coding for HppE, was used to transform methionine-auxotrophic *E. coli* strain B834(DE3) (Novagen, Madison, WI). The transformed cells were grown in LeMaster medium supplemented with 25 mg L-selenomethionine (SeMet) (*7*). The LeMaster medium consisted of two parts, the autoclavable and non-autoclavable portions. The recipe for the autoclavable portion (2 L): alanine: 1.00 g; arginine HCl: 1.16 g; aspartic acid: 0.8 g; cysteine: 0.06 g; glutamic acid: 1.34 g; glutamine: 0.66 g; glycine: 1.08 g; histidine: 0.12 g; isoleucine: 0.46 g; leucine: 0.46 g; lysine HCl: 0.84 g; phenylalanine: 0.26 g; proline: 0.2 g; serine: 4.16 g; threonine: 0.46 g; tyrosine: 0.34 g; valine: 0.46 g; adenine: 1.00 g; guanosine: 1.34 g; thymine: 0.34 g; uracil: 1.00 g; sodium acetate: 3.00 g; succinic acid: 3.00 g; ammonium chloride 1.5 g; sodium hydroxide: 2.16 g; K_2HPO_4: 21.00 g. After measurement, the autoclavable portion of the LeMaster medium was stored dry in a freezer. The recipe for the nonautoclavable portion (200 mL dd H_2O): 20 g of glucose; 0.5 g of $MgSO_4 \cdot 7H_2O$; and 6.6 μL of concentrated H_2SO_4. The nonautoclavable portion was mixed and sterilized by filtering through a 0.22 μm filter system.

When LeMaster medium was needed, 2 L of dd H_2O was used to prepare a suspension of the above solid mixture. This "pre-medium" was autoclave and cooled to room temperature. The suspension was removed by filtration if there was any. The pH of the solution was adjusted to 7.5 as necessary. The above mentioned autoclavable portion (1 L) was mixed with 100 mL of filter sterilized

non-autoclavable portion. Prior to inoculation, 25 mg of DL-SeMet were added to complete the LeMaster medium. When the LeMaster medium was warmed to 37 °C, it was then inoculated by the overnight pre-culture (LB medium). It is important to note that during the purification process, all of the buffers contained 1 mM of DTT to prevent the oxidation of incorporated SeMet.

5.3 RESULTS

Preparation of HppE Mutants. Using plasmid pPL1001, which contains HppE-encoding gene (*fom4*), as the template, the H138A, E142A, and H180A mutant plasmids were constructed. The mutations were confirmed by DNA sequencing, and the mutant enzymes were expressed and purified by protocols previously developed for the wild-type HppE (*5*). EDTA and DTT were used throughout purification, making the isolated proteins essentially iron-free. The Y105F mutant that was prepared in an early study was also used (*4*).

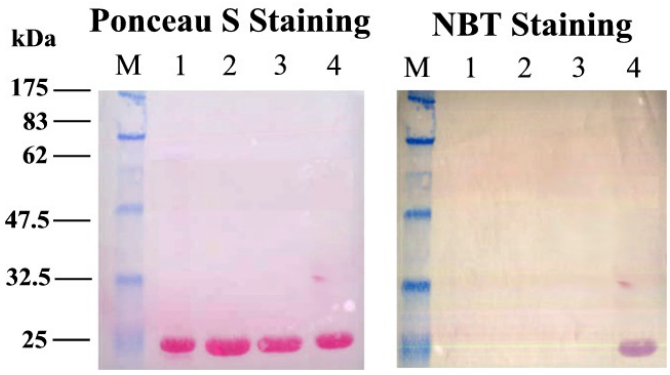

Figure 5-2. Ponceau S (left) and NBT (right) staining of purified HppE and its mutants. M). protein marker; 1). H138A; 2). E142A; 3). H180A; 4). Wild type (Note: Ponceau S staining shows all proteins while NBT staining only shows modified proteins).

These purified mutants proteins, along with the wild-type HppE, were subjected to SDS-PAGE followed by transblotting onto a nitro-cellulose membrane. The protein bands on the membrane were visualized by a reversible red dye, ponceau S, and all proteins were shown to have been purified to near homogeneity (Figure 5-2). After a thorough rinse to remove the red dye, the membrane was subjected to the NBT quinone staining (*6*). This quinone staining method was designed to identify quinonoid compounds, such as 1,2,4-trihydroxybenzene, menadione, and DOPA. It is also a convenient assay for quinonoid proteins, and has been applied to detect DOPA formation in HppE as a result of self-hydroxylation (*4*). Here, the H138A, E142A, and H180A mutants were found to be insensitive to the NBT staining (Figure 5-2). Evidently, mutation at H138, E142, or H180 significantly impairs the oxygenase activity of HppE, resulting in no or little *in vivo* self-hydroxylation of these three mutants.

Electronic Absorption of Reconstituted HppE Mutants. The low aqueous solubility of ferric ion at neutral pH precludes the reconstitution of apo-HppE by mixing with ferric ion directly to generate Fe^{III}-HppE. To prepare Fe^{III}-reconstituted HppE, the apo-enzyme was incubated with a stoichiometric amount of $Fe^{II}(NH_4)_2(SO_4)_2$ and then oxidized by air. As we have shown in Chapter 4, a portion of the iron possibly exists in the complex with a hidden protein radical in the reconstituted HppE. Thus, the oxidized HppE does not completely equal to Fe^{III}-HppE. However, the small amount of spectroscopically invisible iron will have little effects on the biophysical results obtained in this study. Thus, the reconstituted HppE will be considered as Fe^{III}-enzyme in this chapter.

As shown in Figure 5-3, the optical spectrum of Fe^{III}-reconstituted wild-type HppE displays a broad peak centered around 680 nm ($\varepsilon \approx 450\ M^{-1}cm^{-1}$) that has been identified as the ligand-to-metal charge transfer (LMCT) band of the Fe^{III}-catecholate complex (*4*). When the H138A, E142A, and H180A mutants were aerobically reconstituted with an equivalent of $Fe^{II}(NH_4)_2(SO_4)_2$, a bright yellow color appeared in all protein solutions. After one-hour aerobic incubation to give Fe^{III}-HppE, when the yellow color reached its maximal intensity, the electronic absorption spectra of these reconstituted enzymes were recorded. As shown in Figure 5-3, the spectra of these mutants are clearly different from that of the wild-type HppE, lacking the characteristic absorption band of the Fe^{III}-catecholate complex at 680 nm. These data are in accord with the results obtained from the NBT staining experiments, confirming the absence of *in vivo* self-hydroxylation in these mutant enzymes.

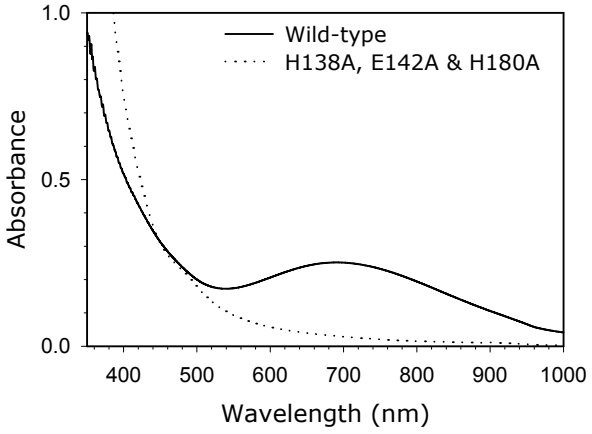

Figure 5-3 Electronic absorption spectra of Fe^{III}-HppE and its mutants (protein concentrations, 0.5 mM).

Spectral Properties of Cu^{II}-Substituted HppE and its Mutants. The lack of an EPR signal and the facile oxidation of the enzyme bound ferrous center have made direct spectroscopic studies a challenging task. To circumvent these problems, the Fe^{II} in enzymes is often replaced by other divalent metal ions that are aerobically stable and spectroscopically accessible. One of the most commonly used metal ion substitutes chosen as EPR spectroscopic probe is Cu^{II} because of its well-documented EPR properties and well-understood coordination chemistry. Furthermore, Cu^{II} was found inhibitory to the epoxidase activity of HppE, implying that it is a competitor for the iron-binding enzyme active site. In the study, the wild-type apo-HppE was reconstituted with Cu^{II} at 1:1 ratio. The electronic and EPR spectra of the resulting Cu^{II}-HppE exhibit typical spectral properties of a type II copper center. These include an absorption maximum at 690 nm (ε = 84 $M^{-1}cm^{-1}$) which is characteristic for the low-intensity d→d transitions in type II Cu^{II} (Figure 5-4), and the EPR spectrum with a $g_{//}$ value of 2.276 and an $A_{//}$ value of 172×10^{-4} cm^{-1}, that are indicative of a type II Cu center with a tetrahedral coordination geometry (Figure 5). In the presence of (*S*)-HPP the absorption maximum shifts to 860 nm (ε = 92 $M^{-1}cm^{-1}$) (Figure 5-4). The Cu^{II} EPR signal also changes, exhibiting a smaller $A_{//}$ value of 135×10^{-4} cm^{-1} and an increased $g_{//}$ value of 2.366 (Figure 5-5), both of which are consistent with a more oxyanion-rich environment (*8*). Such a large increase in $g_{//}$ value accompanying the addition of substrate strongly suggests that Cu^{II} binds in enzymatic active site and the substrate directly coordinates to it.

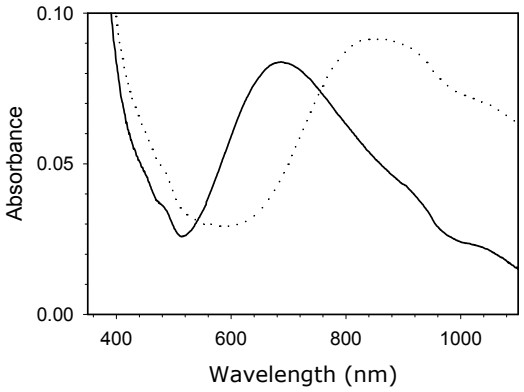

Figure 5-4 Electronic absorption spectra of Cu^{II}-substituted HppE (solid line) and its substrate-bound complex (dotted line) (protein concentration, 0.8 mM, in dd H_2O).

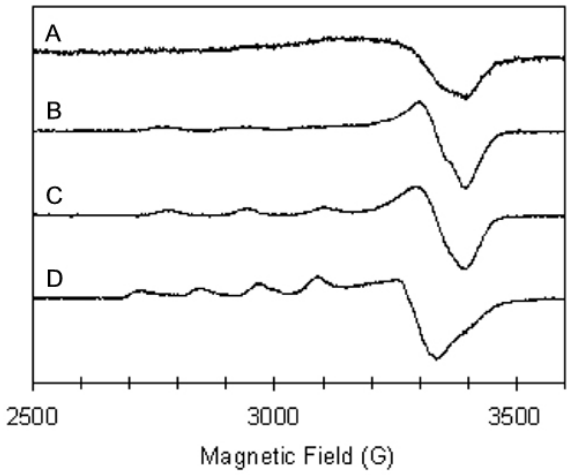

Figure 5-5 EPR spectra of the Cu^{II}-substituted HppE. (A) $CuSO_4$ in the Tris·HCl buffer; (B) Complex of (*S*)-HPP and $CuSO_4$; (C) Cu^{II}-substituted HppE; and (D) Cu^{II}-substituted HppE in the presence of excess amount of substrate. Samples contained 625 μM Cu^{II} and/or 625 μM HppE. Instrumental parameters: temperature, 20 K; microwave power, 0.6 mW; modulation amplitude, 0.3 mT, and sweep speed, 1.3 mT/s.

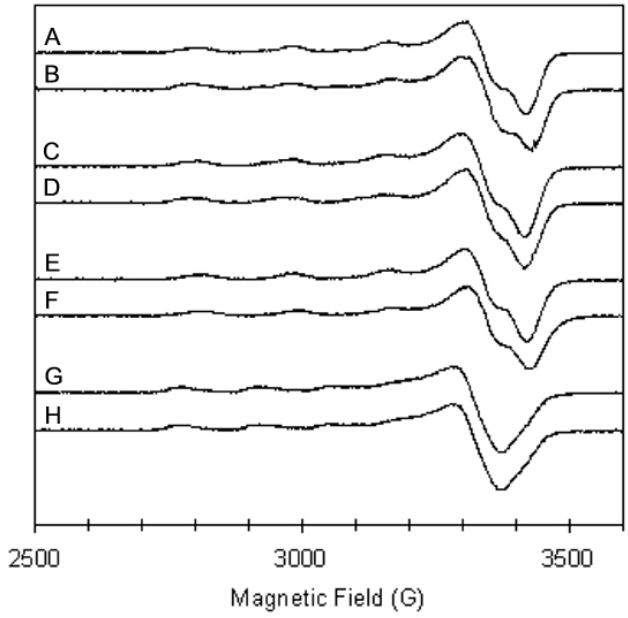

Figure 5-6. EPR spectra of Cu^{II}-substituted HppE mutants. (A) E142A; (B) E142A in the presence of substrate; (C) H138A; (D) H138A in the presence of substrate; (E) H180A; (F) H180A in the presence of substrate; and (G) Y105F; (H) Y105F in the presence of substrate. Protein concentration of each mutants was 500 μM (polypeptide). Instrumental parameters are the same as Figure 5-5 with the exception microwave power is 0.1 mW and each spectrum is average of two scans.

The HppE mutants were also reconstituted with Cu^{II} and characterized by electronic absorption and EPR spectroscopies. The observed spectral parameters are listed in Table 5-2. Overall, the spectra of the H138A, E142A and H180A mutants are similar to each other but significantly different from that of the wild-type enzyme. In particular, they do not respond to the addition of substrate HPP in the same way as the Cu^{II}-substituted wild-type enzyme does (Figure 5-6). For example, the spectra of the Cu^{II}-HppE mutants, without bound substrate, differ

from the wild-type enzyme by a blue-shift of the weak cupric d→d transition from 690 nm to 610-615 nm and the less rhombic EPR signals with smaller $g_{//}$ and larger $A_{//}$ values. When (*S*)-HPP is added, dramatic changes were made to the spectra of Cu^{II}-HppE ($\Delta\lambda_{max} \approx 170$ nm for UV-vis and $\Delta g_{//} = 0.09$ and $\Delta A_{//} = 37\times10^{-4}$ cm^{-1} in EPR), while those of Cu^{II}-reconstituted H138A, E142A, and H180A mutants were practically unchanged (Table 5-2). These results clearly indicate that alterations at these positions have great impacts on the metal coordination properties of HppE.

Cu^{II}-substituted protein	(*S*)-HPP	Optical Features		EPR Parameters		
		λ_{max} (nm)	ε ($M^{-1}cm^{-1}$/Cu)	$g_{//}$	$A_{//}$[a]	$g_{\perp}$
Wild type	-	690	84	2.276	172	2.063
	+	860	92	2.366	135	2.099
H138A	-	611	107	2.233	187	2.054
	+	611	111	2.234	195	2.054
E142A	-	615	75	2.234	185	2.055
	+	618	76	2.238	187	2.054
H180A	-	610	142	2.233	183	2.053
	+	608	130	2.230	180	2.052
Y105F	-	648	115	2.299	152	2.067
	+	635 736	104 102	2.298	155	2.067
Cu^{II} (Tris·HCl buffer)	-	648	50	NR[b]	NR	2.076
	+	640	55	2.279	172	2.061

Table 5-2. Spectral parameters of copper-substituted HppE mutants. (Note: [a]EPR hyperfine coupling parameter A is given in 10^{-4} cm^{-1}; [b]NR, the spectrum has no resolved features to record the corresponding parameters.)

In contrast, the spectroscopic properties of mutant Y105F seems to stand in between those of wild-type and other mutants (Table 5-2). For example, the

addition of (*S*)-HPP to Cu^{II}-Y105F led to the emergence of a new peak around 740 nm in the UV-vis absorption spectrum, nearly 100 nm apart from the original 648 nm. The significant change in maximum absorption has also been observed with the wild-type HppE upon substrate binding, and thus presumably an indication of coordination of (*S*)-HPP to Y105F-bound Cu^{II}. However, such a large spectroscopic change is not reflected in the EPR spectra of Cu^{II}-Y105F. Probably, the signal for (*S*)-HPP-bound Cu^{II} as a minor species is buried in the background of unbound Cu^{II}. Clearly, the mutation of Tyr105 has considerable impacts on the metal coordination environment in HppE active site, though its effects are different from those induced by the mutations of iron ligands.

Fe^{II}·(S)-HPP Nitrosyl Complexes of HppE Mutants. An Fe^{II}-HppE·(*S*)-HPP nitrosyl ternary intermediate, which presents a nearly homogenous EPR signal with principal *g* values of 1.97, 3.63, and 4.2 (*S* = 3/2) and E/D of 0.066 (Figure 5-7A), had been characterized in our earlier studies (*1*). The EPR spectrum of this intermediate is reminiscent of those of the Fe^{II}-enzyme-substrate nitrosyl complexes observed in IPNS and ACCO (*9, 10*). This ternary complex is believed to be the catalytically active form of enzyme-substrate-O_2 intermediate. Mutation of the iron ligands is expected to change the above spectroscopic fingerprint of the ternary complex because the EPR lineshape has been shown to be very sensitive to changes in the iron ligation and environment for many other enzymes. To assess the roles of H138, E142, and H180 on iron coordination in HppE, the H138A, E142A, and H180A mutants were

anaerobically reconstituted with ferrous ion, (*S*)-HPP, exposed to NO and then analyzed by EPR spectroscopy.

As shown in Figure 5-7, in the presence of substrate and NO under anaerobic conditions, these mutants exhibit an EPR signal with *g* values of 2.013 and 2.039 in addition to an anomalous signal from unbound NO at about *g* = 1.96 (spectra B-D). The signals appeared slightly above *g* = 2 are absent in the EPR spectrum of the wild-type enzyme (Figure 5-7A). We assign them to nonspecifically bound Fe^{II} nitrosyl species that have previously been noted with many non-heme iron-nitrosyl complexes in proteins and model systems (*11-16*). In the *g* = 4 region, signals from an *S* = 3/2 species with different E/D values than that exhibited by the wild-type enzyme were observed in Figures 5-7B-D of the mutant enzymes. The *S* = 3/2 species in each EPR spectrum were quantitated by double integration and compared with that of the wild type enzyme at the same concentration (Table 5-3). It is clear that point mutation of His138, Glu142, and His180 significantly reduces the iron binding affinity, suggesting these residues as the metal binding ligands in the wild type HppE. The roles of E142 and H180 are especially critical for the metal coordination at the active site.

The EPR spectrum of the Y105F mutant protein-substrate-NO complex was also recorded, and showed characteristics for an *S* = 3/2 species with *g* values of 1.99, 3.94, and 4.11 (E/D = 0.024) (Figure 5-7E). Despite the fact that the total content of protein-bound iron in this mutant is lower than that of the wild-type enzyme, there is no iron nonspecifically bound to protein indicated by the EPR data, which is in contrast to the H138A, E142A, and H180A mutants. The

results suggested that the majority of the iron present in the EPR spectrum of Y105F is still bound to the active site. Unlike the above three residues that have been implicated as metal binding ligands, Tyr105 is unlikely to be a ligand of the metal center in HppE, which is consistent with the lack of the characteristic Fe^{III}-tyrosine LMCT band in the UV-vis absorption spectrum of Fe^{III}-reconstituted wild type HppE.

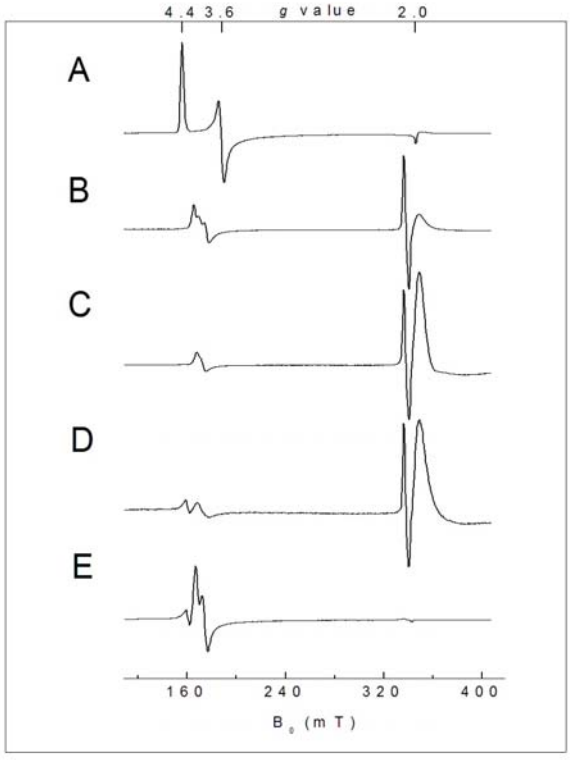

Figure 5-7 EPR spectra of the Fe^{II}·substrate·NO complexes obtained with HppE and its mutants. (A)Wild type, (B) H38A, (C) E142A, (D) H180A, and (E) Y105F. Instrumental parameters: temperature 2 K, microwave frequency 9.6 GHz, modulation frequency 100 KHz, power, 0.6 mW, sweep time 162 s. Samples C and D possess large excess NO (as shown at g = 1.96) in order to detect the full amount of Fe^{II} at the active site.

Epoxidase Activity of Mutant Enzymes. In our previous studies, holo-HppE was generated by reconstitution of the apoenzyme with Fe^{II} under aerobic conditions (*5*). The resultant Fe^{III}-enzyme was passed through a gel-filtration column to remove the unbound iron prior to the activity assay. However, we encountered problems in applying this protein preparation method to determine the activity of HppE mutants. This is due to their reduced iron binding affinities, so a larger amount of iron was depleted from the HppE mutants during the gel-filtration step, making comparison of enzyme activity between the wild-type and the mutant enzymes invalid. In order to ensure equal conditions for all the enzymes, a stoichiometric amount of $Fe^{II}(NH_4)_2(SO_4)_2$ was added directly to the apo-enzyme (1:1 ratio) in the assay solution to reconstitute the enzyme *in situ*. The epoxidase activities determined under the new assay conditions are given in Table 5-3. The E142A and H180A mutants are catalytically inactive. Because the substitution of Glu142 or His180 by alanine leads to low iron content and totally abolishes the epoxidase activity of HppE, these two residues are likely part of the metal binding core as deduced by sequence alignment. However, mutation of another putative iron-binding ligand, His138, did not completely inactivate the enzyme. Instead, the H138A mutant retained 20% of the wild-type activity. Table 5-3 shows that the level of residual activity of the H138A mutant correlates well to its iron-binding affinity, which is much higher than those found for the E142A and H180A mutants. Thus, while His138 may still be an important ligand for metal binding, it is not an essential residue for HppE activity. It is worth mentioning that site-directed mutagenesis has been performed on many

mononuclear non-heme iron enzymes to define their metal binding sites (*17-25*). Among which, the H138A mutant of HppE is unusual since it retains more than an average of the residual enzyme activity than all known examples prepared thus far.

Enzymes	H138A	E142A	H180A	Y105F	Wild-type
Active site iron[a] (%)	26.6	3.1	4.4	16.1	100
Self-hydroxylation (ε_{680}, $M^{-1}cm^{-1}$)	200	0	0	250	450
Epoxidase Activity (%)[b]	19.9	0	0	33.4	100

Table 5-3 Properties of iron-reconstituted HppE mutants. (Note: [a]The iron content is calculated from the EPR spectra of Fe^{II}-enzyme·(*S*)-HPP nitrosyl complexes; [b]The activity was obtained under new assay conditions.)

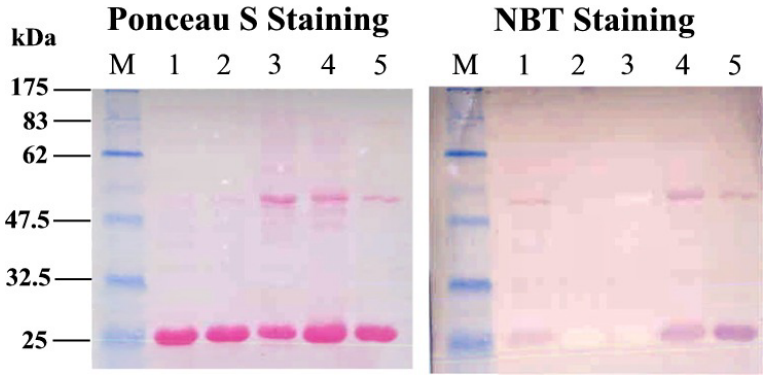

Figure 5-8 Ponceau S (left) and NBT (right) staining of *in vitro* modified HppE and its mutants. M. protein marker; 1. H138A; 2. E142A; 3. H180A; 4. Y105F; 5. Wild type (Note: Ponceau S staining shows all proteins while NBT staining only shows modified proteins).

Self-hydroxylation Activity of Mutant Enzymes. On the basis of the NBT staining and the UV-vis spectral analyses of purified proteins, mutations of

His138, Glu142 and His180 have clearly eliminated the post-translational modification that would otherwise have occurred to HppE *in vivo*. The loss of self-hydroxylation capability of these mutants is directly associated with the decrease in their iron-binding affinity (Table 5-3), since the self-inflicted hydroxylation in HppE has been established to be iron-dependent. To avoid dealing with the control of iron concentration *in vivo* (as in the experiments reported in Figures 5-2), the HppE mutants were tested *in vitr*o for their self-hydroxylation activity. The proteins were reconstituted with $Fe^{II}(NH_4)_2(SO_4)_2$ and ascorbate under aerobic conditions (*4*) and the extend of self-hydroxylation was visualized by NBT staining (Figure 5-8) and analyzed by UV-vis absorption spectroscopy (Figure 5-9).

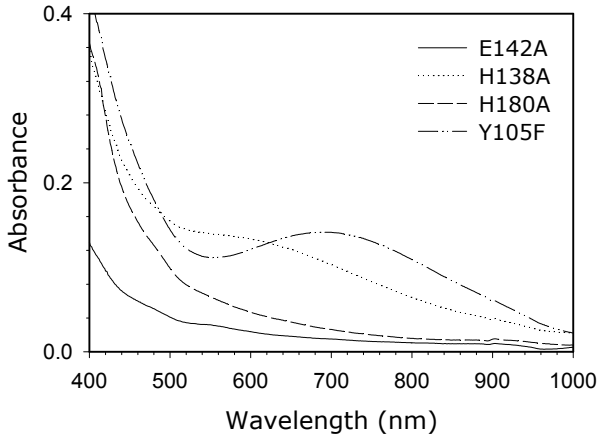

Figure 5-9 Electronic absorption spectra of HppE mutants aerobically reconstituted with iron in the presence of ascorbate (Protein concentration, 0.6 mM).

As summarized in Table 5-3, the self-hydroxylation activities of these HppE mutants show similar trends as their epoxidase activities, and are related to

their iron contents. While the E142A and H180A mutants are clearly inactive, the H138A mutant demonstrates a moderate activity. The evidence includes the weak purple stain upon treatment with NBT (Figure 5-8, lane 2), and the development of a green chromophore during the *in vitro* incubation (Figure 5-9). This green chromophore is presumably an Fe^{III}-catecholate (DOPA) charge transfer complex, similar to that forms in the wild-type HppE (*4*). The observed blue-shift of the absorption maximum, from 680 nm for the wild type enzyme to 600 nm for the H138A mutant, may simply reflect the alteration of the iron environment in the active site of this mutant. As previously reported, self-hydroxylation can also occur in the Y105F mutant, and the site of modification has been proposed to be at Tyr103 (*4*). Since the UV-vis spectrum of the self-modified Y105F mutant and that of the wild-type enzyme are nearly superimposable, showing maximal absorption at 680 nm, the iron coordination environment of the Y105F mutant and that of the wild-type enzyme are likely to be alike. Again, the mutation of Tyr105 seems to have little effect on the iron active site as compared to the mutations of these putative amino acid ligands, His138, Glu142 and His180.

X-ray Crystal Structure of HppE. The three-dimensional structure of HppE confirms its identity as a member of the cupin superfamily, possessing the characteristic β-barrel fold in which antiparallel β-stands are wrapped around a barrel core in a jelly-roll variant of a Greek Key or β-sandwich motif (Figure 5-10). As expected, the epoxidase is a physiological homotetramer with one iron per monomer, and the metal is bound to one end of each β-barrel via direct

coordination with facial triad ligands, 2-His-1-Glu. The monomer consists of two domains: an α-domain, which is all α-helical, and a β-domain, which consists of all anti-parallel β-strands in a jelly-roll β-barrel motif. In consistence with the results from the above site-directed mutagenetic study, the facial triad, His138, His180, and Glu142, is housed within the β-barrel, defining the HppE active site (Figure 5-11). The facial triad ligands in all cupin enzymes occupy one end of the β-barrel, and the opposite end is responsible for the vast catalytic diversity of reactivity and substrate specificity, regioselectivity, and stereoselectivity in this protein family (*26*). Based upon the overall HppE structure, residues on the "tunable" face of the β-domain that are potentially significant for catalysis include: Tyr105, Tyr103, Tyr102, and Arg97 (Figure 5-11). The α-domain also contributes one residue to the active site, Lys23, positioned between helix 1 and helix 2.

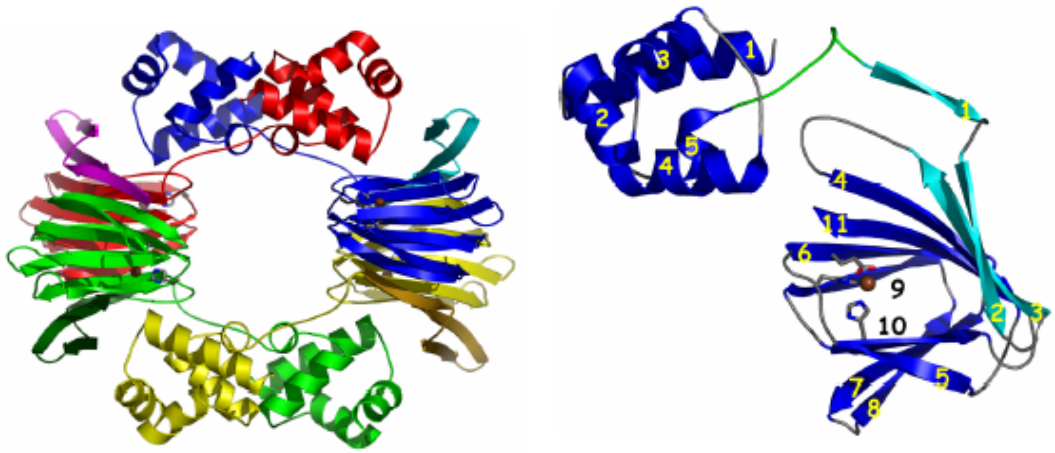

Figure 5-10 The overall structure of HppE. (Left) The HppE tetramer; (Right) a HppE monomer consisting of an α-domain, an interdomain linker to a single β-strand 1, and a β-domain.

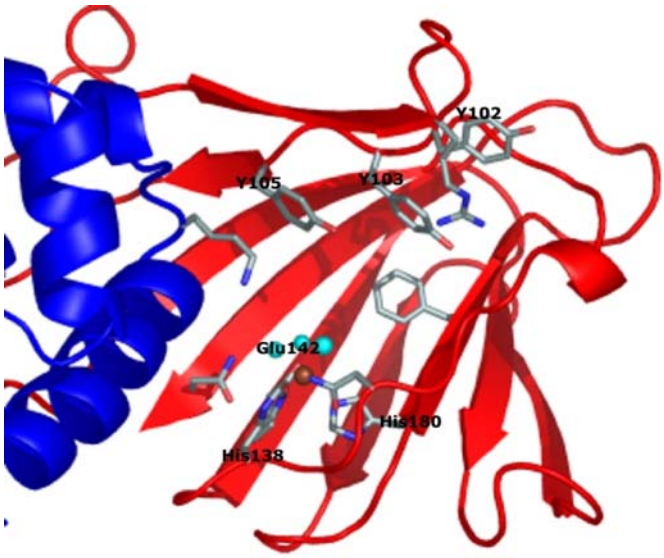

Figure 5-11 The active site of HppE. (Note: the important residues are labeled.)

5.4 DISCUSSION

As mentioned early, sequence analysis has suggested HppE as a member of the cupin superfamily (*1*). The crystal structures of several cupin metalloproteins have recently been solved, such as Mn^{II}-bound barley germin, Zn^{II}-bound phosphomannose isomerase, Fe^{II}-bound α-KG-dependent dioxygenases and Fe^{II}-bound aromatic ring cleaving dioxygenases (*27*). In all these structures, the divalent metal centers have a similar coordination environment, having two or three histidines and one carboxylate as metal binding ligands. Such a 2-His-1-carboxylate facial triad has been found in many mononuclear non-heme iron-dependent enzymes (*28*), including BphC (*29, 30*), IPNS (*31*), the Rieske-type dioxygenase NDO (*32*), the pterin-dependent PheH

(*33*), TyrH (*34*) and TrpH (*35*), and the α-KG-dependent DAOCS (*36*), CAS (*37*) and TauD (*38*).

A similar 2-His-1-carboxylate Fe^{II}-binding triad, His138, Glu142 and His180, can also be located in HppE (*1*). In this study, we combined site-directed mutagenesis with EPR spectral analyses to confirm the involvement of these conserved residues as the metal-binding ligands. In the EPR spectra of the Cu^{II}-reconstituted HppE, the large increase of the $g_{//}$ value due to the addition of (*S*)-HPP suggests a direct coordination of substrate to the metal active site. In addition, study of the EPR-homogeneous Fe^{II}-HppE·(*S*)-HPP·NO ternary complex (*5*) clearly showed that single mutation at His138, Glu142, or His180 greatly affected the formation of this ternary complex. These results are particularly revealing, since this ternary complex represents the catalytically competent form of HppE. Thus, the metal binding ability of each mutant, deduced from the iron content of the respective ternary complex, is truly catalytically relevant. In fact, the iron contents determined in this study exhibit good correlation with the epoxidase and self-hydroxylation activity of the HppE mutants (Table 5-3), confirming the iron-dependence of the catalytic activities of HppE. Through our study, the putative amino acid ligands can be categorized into two groups. Glu142 and His180 are the metal ligands since replacement of either of these two residues with alanine led to significant metal ion loss from the enzyme active site. As a result, no enzyme activity on epoxidation and self-hydroxylation can be detected in mutants E142A and H180A. On the other hand, mutant H138A also endures significant reduction in its active site iron content and its catalytic

competency in epoxidation and self-hydroxylation reactions. However, the mutation of His138 does not completely knock out the ability of HppE to bind iron nor its catalytic activities. In proportion to the residual 27% iron content, the mutant H138A retains 20% of the wild type epoxidase activity, which is in sharp contrast to the mutants of other two metal binding residues. While the properties of the H138A and Y105F mutants are similar (Table 5-3), the H138A mutant is distinct from the Y105F mutant by forming a chromophore with a maximum absorption at 600 nm, rather than 680 nm, as a result of the *in vitro* self-hydroxylation (Figure 5-9 and Table 5-3). The apparent disparity on optical absorption suggests a major alteration in iron coordination environment induced by the mutation of His138 to alanine. Thus, His138, as an iron ligand, bears unusual characteristics. The X-ray crystal structure of HppE resolved very recently has confirmed the above conclusion and also proved that the epoxidase belongs to the cupin structural superfamily.

It is worth noting that the retention of ~20% of the wild-type activity of the HppE H138A mutant is highly unusual, because the mutation of an amino acid residue that serves as iron ligand in other enzymes generally led to more drastic reduction of enzyme activities. In most cases, including PheH (*17*), TyrH (*20, 24*), IPNS (*18*), toluene dioxygenase (*22*), ACCO (*25*), TfdA (*21*) and CAS (*19, 23*), the catalytic activity was completely abolished because of the mutations. Few exceptions are known, such as the CAS H145Q and H280Q mutants (*23*) and the TyrH H336E and H336Q mutants (*20*), where residual catalytic activities ranging from < 3% for the CAS mutants (*23*) to about 4~12% for the TyrH

mutants were reported (*20*). The residual activities found in these H → Q mutants may be attributed to the competence of glutamine to replace histidine in binding of iron. However, the same reasoning is not applicable to HppE since the histidine at position 138 is replaced by an alanine that cannot serve as a metal ligand like glutamine. In view of the good correlation between the iron content and the residual enzyme activities of H138A, it is likely that another amino acid residue in the active site may be a substitute of His138 to bind the iron and attenuate the effects of mutation on iron binding and catalytic activity. As suggested by the crystal structure of HppE, the residues Asn135 and Asn198 may play the role as the backup ligands.

Besides His138, Glu142 and His180, Tyr105 is another active site residue that has been identified in our earlier studies as the site of self-hydroxylation to give DOPA in HppE (*4*). As the precursor of DOPA, Tyr105 must be in close proximity to the iron center in HppE. However, UV-vis and EPR spectral analyses showed no evidence of direct ligation of Tyr105 to iron in the active site of HppE. In contrast, DOPA105, being a bidentate ligand, forms a complex with Fe^{III} in the active site of HppE to give its green color. Since only a small portion (~25%) of HppE is estimated to be post-translationally modified at Tyr105 on the basis of the low extinction coefficient of Fe^{III}-HppE at 680 nm (ε_{680} = 450 $M^{-1}cm^{-1}$), there must exist two iron coordination environments corresponding to the modified and unmodified forms of HppE. Interestingly, such a coordination heterogeneity around the iron binding site becomes indiscernible in the ternary complex of Fe^{II}-HppE, (*S*)-HPP and nitric oxide. The fact that this ternary

complex displayed a homogeneous EPR signal, accountable for >95% iron bound in the active site (*5*), ruled out the possibility of direct ligation of DOPA to the ferrous center in the HppE-substrate complex. The conclusion has been substantiated by the newly resolved crystal structure. As a part of the secondary iron coordination sphere, Tyr105 has shown its catalytic importance by the significant impact of its mutation on the iron binding affinity and catalytic activity. In the catalytic mechanism of HppE, Tyr105 may serve as a general acid/base or be part of the electron transfer conduit.

Enzymes carrying a 2-His-1-carboxylate triad motif to bind a mononuclear iron catalyze a great variety of reactions. Despite the diverse reaction types catalyzed by these enzymes, there is a common mechanistic theme shared among these catalysts. The 2-His-1-carboxylate motif provides an iron-coordination platform in these enzymes, on which Fe^{II}-dependent dioxygen activation takes place in the presence of substrate or cofactor (*28*). Our proposed enzyme mechanisms in previous chapters for HppE, which all rely on a ferrous center to activate dioxygen, fit well with this general mechanistic model.

In summary, a 2-His-1-carboxlyate iron-binding motif has been experimentally identified in HppE. Its presence is consistent with our previously proposed catalytic model, especially the dependence of its catalysis on dioxygen activation by ferrous center. Site-specific mutation of two of these iron-binding residues, Glu142 and His180, resulted in complete loss in enzyme activities. In contrast, the H138A mutant retains 20% of the wild type activity, suggesting the presence of a nearby residue capable of serving as a metal binding ligand. The

site of self-hydroxylation, Tyr105, is not directly ligated to the iron center, although the resulting product, DOPA, does bind iron in the modified HppE.

5.5 REFERENCE

1. Dunwell, J. M., Culham, A., Carter, C. E., Sosa-Aguirre, C. R., and Goodenough, P. W. (2001) "Evolution of functional diversity in the cupin superfamily" *Trends. Biochem. Sci. 26*, 740-746.
2. Hidaka, T., Goda, M., Kuzuyama, T., Takei, N., Hidaka, M., and Seto, H. (1995) "Cloning and nucleotide sequence of fosfomycin biosynthetic genes of *Streptomyces wedmorensis*" *Mol. Gen. Genet. 249*, 274-280.
3. Kuzuyama, T., Seki, T., Kobayashi, S., Hidaka, T., and Seto, H. (1999) "Cloning and expression in *Escherichia coli* of 2-hydroxypropylphosphonic acid epoxidase from the fosfomycin-producing organism, *Pseudomonas syringae* PB-5123" *Biosci Biote.chnol. Biochem. 63*, 2222-2224.
4. Liu, P., Mehn, M. P., Yan, F., Zhao, Z., Que, L., Jr., and Liu, H.-W. (2004) "Oxygenase activity in the self-hydroxylation of (*S*)-2-hydroxypropylphosphonic acid epoxidase involved in fosfomycin biosynthesis" *J. Am. Chem. Soc. 126*, 10306-10312.
5. Liu, P., Liu, A., Yan, F., Wolfe, M. D., Lipscomb, J. D., and Liu, H. W. (2003) "Biochemical and spectroscopic studies on (*S*)-2-hydroxypropylphosphonic acid epoxidase: a novel mononuclear non-heme iron enzyme" *Biochemistry 42*, 11577-11586.
6. Paz, M. A., Fluckiger, R., Boak, A., Kagan, H. M., and Gallop, P. M. (1991) "Specific detection of quinoproteins by redox-cycling staining" *J. Biol. Chem. 266*, 689-692.
7. LeMaster, D. M., and Richards, F. M. (1985) "^{1}H-^{15}N heteronuclear NMR studies of *Escherichia coli* thioredoxin in samples isotopically labeled by residue type" *Biochemistry 24*, 7263-7268.
8. Peisach, J., and Blumberg, W. E. (1974) "Structural implications derived from the analysis of electron paramagnetic resonance spectra of natural and artificial copper proteins" *Arch. Biochem. Biophys. 165*, 691-708.
9. Rocklin, A. M., Tierney, D. L., Kofman, V., Brunhuber, N. M. W., Hoffman, B. M., Christoffersen, R. E., Reich, N. O., Lipscomb, J. D., and Que, L., Jr. (1999) "Role of the nonheme Fe(II) center in the biosynthesis of the plant hormone ethylene" *Proc. Natl. Acad. Sci. USA 96*, 7905-7909.

10. Orville, A. M., Chen, V. J., Kriauciunas, A., Harpel, M. R., Fox, B. G., Mèunck, E., and Lipscomb, J. D. (1992) "Thiolate ligation of the active site Fe^{2+} of isopenicillin N synthase derives from substrate rather than endogenous cysteine: spectroscopic studies of site-specific Cys → Ser mutated enzymes" *Biochemistry 31*, 4602-4612.

11. D'Autreaux, B., Horner, O., Oddou, J.-L., Jeandey, C., Gambarelli, S., Berthomieu, C., Latour, J.-M., and Michaud-Soret, I. (2004) "Spectroscopic description of the two nitrosyl-iron complexes responsible for inhibition by nitric oxide" *J. Am. Chem. Soc. 126*, 6005-6016.

12. Foster, M. W., and Cowan, J. A. (1999) "Chemistry of nitric oxide with protein-bound Iron sulfur centers. insights on physiological reactivity" *J. Am. Chem. Soc. 121*, 4093-4100.

13. Kennedy, M. C., Gan, T., Antholine, W. E., and Petering, D. H. (1993) "Metallothionein reacts with Fe^{2+} and NO to form products with A g = 2.039 ESR signal" *Biochem. Biophys. Res. Commun. 196*, 632-635.

14. Lancaster, J. R., Jr., and Hibbs, J. B., Jr. (1990) "EPR demonstration of iron-nitrosyl complex formation by cytotoxic activated macrophages" *Proc. Natl. Acad. Sci. USA 87*, 1223-1227.

15. Drapier, J. C., Pellat, C., and Henry, Y. (1991) "Generation of EPR-detectable nitrosyl-iron complexes in tumor target cells cocultured with activated macrophages" *J. Biol. Chem. 266*, 10162-10167.

16. Reginato, N., McCrory, C. T. C., Pervitsky, D., and Li, L. (1999) "Synthesis, X-ray crystal structure, and solution behavior of $Fe(NO)_2(1\text{-MeIm})_2$: implications for nitrosyl non-heme-iron complexes with g = 2.03" *J. Am. Chem. Soc. 121*, 10217-10218.

17. Balasubramanian, S., Carr, R. T., Bender, C. J., Peisach, J., and Benkovic, S. J. (1994) "Identification of metal ligands in Cu(II)-inhibited Chromobacterium violaceum phenylalanine hydroxylase by electron spin echo envelope modulation analysis of histidine to serine mutations" *Biochemistry 33*, 8532-8537.

18. Borovok, I., Landman, O., Kreisberg-Zakarin, R., Aharonowitz, Y., and Cohen, G. (1996) "Ferrous active site of isopenicillin N synthase: genetic and sequence analysis of the endogenous ligands" *Biochemistry 35*, 1981-1987.

19. Doan, L. X., Hassan, A., Lipscomb, S. J., Dhanda, A., Zhang, Z., and Schofield, C. J. (2000) "Mutagenesis studies on the iron binding ligands of clavaminic acid synthase" *Biochem. Biophys. Res. Commun. 279*, 240-244.

20. Fitzpatrick, P. F., Ralph, E. C., Ellis, H. R., Willmon, O. J., and Daubner, S. C. (2003) "Characterization of metal ligand mutants of tyrosine hydroxylase: insights into the plasticity of a 2-histidine-1-carboxylate triad" *Biochemistry 42*, 2081-2088.

21. Hogan, D. A., Smith, S. R., Saari, E. A., McCracken, J., and Hausinger, R. P. (2000) "Site-directed mutagenesis of 2,4-dichlorophenoxyacetic acid/α-ketoglutarate dioxygenase. Identification of residues involved in metallocenter formation and substrate binding" *J. Biol. Chem. 275*, 12400-12409.

22. Jiang, H., Parales, R. E., Lynch, N. A., and Gibson, D. T. (1996) "Site-directed mutagenesis of conserved amino acids in the alpha subunit of toluene dioxygenase: potential mononuclear non-heme iron coordination sites" *J. Bacteriol. 178*, 3133-3139.

23. Khaleeli, N., Busby, R. W., and Townsend, C. A. (2000) "Site-directed mutagenesis and biochemical analysis of the endogenous ligands in the ferrous active site of clavaminate synthase. The His-3 variant of the 2-His-1-carboxylate model" *Biochemistry 39*, 8666-8673.

24. Ramsey, A. J., Daubner, S. C., Ehrlich, J. I., and Fitzpatrick, P. F. (1995) "Identification of iron ligands in tyrosine hydroxylase by mutagenesis of conserved histidinyl residues" *Protein. Sci. 4*, 2082-2086.

25. Zhang, Z., Barlow, J. N., Baldwin, J. E., and Schofield, C. J. (1997) "Metal-catalyzed oxidation and mutagenesis studies on the iron(II) binding site of 1-aminocyclopropane-1-carboxylate oxidase" *Biochemistry 36*, 15999-16007.

26. Hausinger, R. P. (2004) "FeII/α-ketoglutarate-dependent hydroxylases and related enzymes." *Crit. Rev. Biochem. Mol. Biol. 39*, 21-68.

27. Dunwell, J. M., Purvis, A., and Khuri, S. (2004) "Cupins: the most functionally diverse protein superfamily?" *Phytochemistry 65*, 7-17.

28. Que, L., Jr. (2000) "One motif--many different reactions" *Nat. Struct. Biol. 7*, 182-184.

29. Senda, T., Sugiyama, K., Narita, H., Yamamoto, T., Kimbara, K., Fukuda, M., Sato, M., Yano, K., and Mitsui, Y. (1996) "Three-dimensional structures of free form and two substrate complexes of an extradiol ring-cleavage type dioxygenase, the BphC enzyme from *Pseudomonas sp*. strain KKS102" *J. Mol. Biol. 255*, 735-752.

30. Han, S., Eltis, L. D., Timmis, K. N., Muchmore, S. W., and Bolin, J. T. (1995) "Crystal structure of the biphenyl-cleaving extradiol dioxygenase from a PCB-degrading *pseudomonas*" *Science 270*, 976-980.

31. Roach, P. L., Clifton, I. J., Hensgens, C. M., Shibata, N., Schofield, C. J., Hajdu, J., and Baldwin, J. E. (1997) "Structure of isopenicillin N synthase complexed with substrate and the mechanism of penicillin formation" *Nature 387*, 827-830.

32. Karlsson, A., Parales, J. V., Parales, R. E., Gibson, D. T., Eklund, H., and Ramaswamy, S. (2003) "Crystal structure of naphthalene dioxygenase: side-on binding of dioxygen to iron" *Science 299*, 1039-1042.

33. Erlandsen, H., Fusetti, F., Martinez, A., Hough, E., Flatmark, T., and Stevens, R. C. (1997) "Crystal structure of the catalytic domain of human phenylalanine hydroxylase reveals the structural basis for phenylketonuria" *Nat. Struct. Biol. 4*, 995-1000.

34. Goodwill, K. E., Sabatier, C., Marks, C., Raag, R., Fitzpatrick, P. F., and Stevens, R. C. (1997) "Crystal structure of tyrosine hydroxylase at 2.3 A and its implications for inherited neurodegenerative diseases" *Nat. Struct. Biol. 4*, 578-585.

35. Wang, L., Erlandsen, H., Haavik, J., Knappskog, P. M., and Stevens, R. C. (2002) "Three-dimensional structure of human tryptophan hydroxylase and its implications for the biosynthesis of the neurotransmitters serotonin and melatonin" *Biochemistry 41*, 12569-12574.

36. Valegård, K., van Scheltinga, A. C., Lloyd, M. D., Hara, T., Ramaswamy, S., Perrakis, A., Thompson, A., Lee, H. J., Baldwin, J. E., Schofield, C. J., Hajdu, J., and Andersson, I. (1998) "Structure of a cephalosporin synthase" *Nature 394*, 805-809.

37. Zhang, Z., Ren, J., Stammers, D. K., Baldwin, J. E., Harlos, K., and Schofield, C. J. (2000) "Structural origins of the selectivity of the trifunctional oxygenase clavaminic acid synthase" *Nat. Struct. Biol. 7*, 127-133.

38. Elkins, J. M., Ryle, M. J., Clifton, I. J., Dunning Hotopp, J. C., Lloyd, J. S., Burzlaff, N. I., Baldwin, J. E., Hausinger, R. P., and Roach, P. L. (2002) "X-ray crystal structure of Escherichia coli taurine/α-ketoglutarate dioxygenase complexed to ferrous iron and substrates" *Biochemistry 41*, 5185-5192.

Chapter 6: Substrate Binding Mode

6.1 INTRODUCTION

Like many other mononuclear non-heme iron enzymes, HppE conserves both high regiospecificity and stereospecificity in its catalysis. When the racemic substrate (*R*,*S*)-HPP was used in the in vitro epoxidation system of HppE, two different products were isolated (*1*). Besides the natural product fosfomycin (**6-1**), the other product was identified as a ketone compound, 2-oxopropyl-phosphonic acid (**6-3**). Dr. Zongbao Zhao of our group chemically synthesized both enantiomers of HPP, and demonstrated that (*S*)-HPP (**6-2**), the natural substrate of HppE, is the precursor of fosfomycin (**6-1**), while (*R*)-HPP (**6-4**) is the precursor of the ketone product (**6-3**). Such distinct outcome from a pair of enantiomers catalyzed by a single enzyme is rare in nature, not to mention that the conversion of (*S*)-HPP and (*R*)-HPP by HppE into their respective products is actually exclusive. To explain the unusual results, a radical mechanism involving different regiospecific hydrogen abstraction has been proposed (Figure 6-1). The initial evidence to support the regiospecificity in HppE catalysis was obtained from the study using difluoro-substituted compounds (**6-7** and **6-8**). The replacement of both C_1 hydrogens in (*S*)-HPP (**6-2**) with fluorine prevented the formation of the putative radical intermediate (**6-5**) and thus inhibited the epoxidation reaction as expected (Figure 6-2). In contrast, the H $\rightarrow$ F substitution at C_1 atom of (*R*)-HPP (**6-4**) did not affect the radical generation at C_2 atom, thus the conversion of **6-8** to **6-9** would still occur.

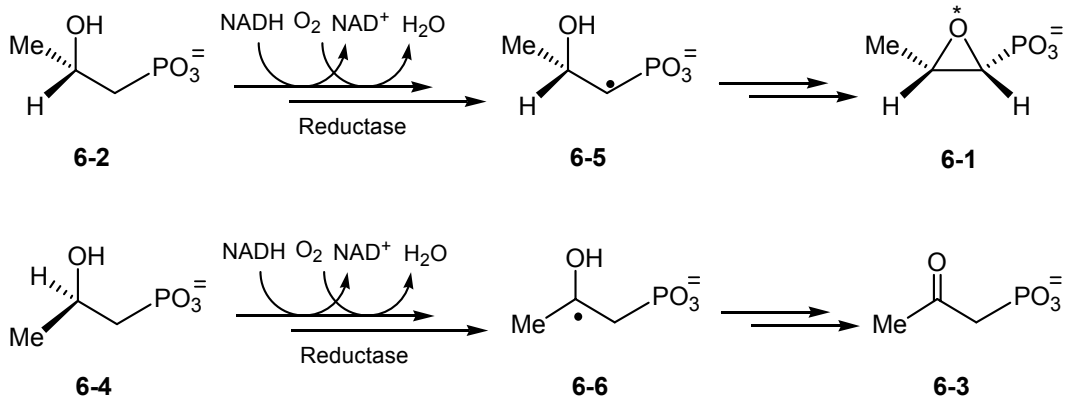

Figure 6-1 The distinct outcomes of the oxidation of (*S*)-HPP and (*R*)-HPP by HppE.

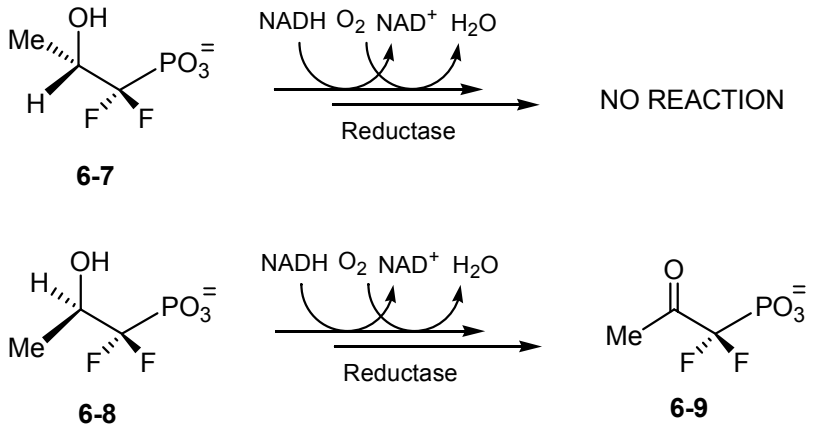

Figure 6-2 The distinct outcomes of the oxidation of (*S*)-FHPP and (*R*)-FHPP by HppE.

In an earlier study to determine the stereochemical course at C-1 position during the epoxidation process, Hammerschmidt *et al.* synthesized both (*S*)-[1-$^2H_1$]-2-hydroxyethylphosphonic acid (**6-10**) and (*R*)-[1-$^2H_1$]-2-hydroxyethyl-phosphonic acid (**6-11**) and fed them to fosfomycin producing strain *S. fradiae*

(*2*). The resulting fosfomycin (**6-1**) in the cell extract was transformed to (1*R*,2*R*)-2-amino-1-hydroxypropylphosphonic acid (**6-12** and **6-13**) to ease the isolation and characterization process. Their final results showed that the deuterium of **6-11** was lost in **6-13**, while the deuterium of **6-10** was retained in **6-12**. The observation can be interpreted as a result of the stereospecific hydrogen abstraction in HppE catalysis. Evidently, the putative iron-oxygen reactive species can precisely recognize and specifically remove the pro-*R* hydrogen in (*S*)-HPP (**6-2**).

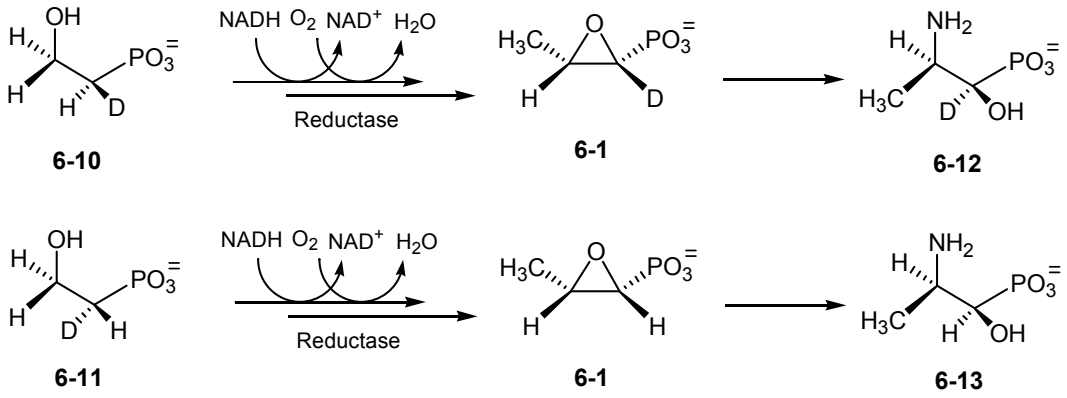

Figure 6-3 Study of the stereochemical course of HppE catalysis at C_1 position using deuterated 2-hydroxyethylphosphonic acids.

The strict regiospecificity and stereospecificity in HppE catalysis, deduced from the results shown in Figures 6-2 and 6-3, require the formation of such an enzyme-substrate complex that the hydroxyl and the phosphonate groups of HPP are anchored in the active site in a rigid manner. Such a rigid substrate binding mode would allow only the pro-*R* α-H in (*S*)-HPP (**6-2**) or the β-H in (*R*)-HPP (**6-4**) to be productively poised for abstraction, then leading to the corresponding

products. Therefore, the regiospecific and stereospecific hydrogen abstraction is not only determined by the chemical reactivity of the hydrogen atoms involved but also their relative positions in the active site of HppE.

The above observations prompted us to study substrate binding modes in the enzyme active site of HppE, which must be a critical factor in determining the catalytic mechanism and product formation. In this chapter, we report the spectroscopic study on the enzyme-substrate interactions of HppE at its reduced state in collaboration with Dr. Aimin Liu at University of Mississippi Medical Center. Using nitric oxide as an O_2 analogue, we were able to detect and characterize the Fe^{II}-loaded enzyme and its complexes with substrates and substrate analogues. In consistence with the recently resolved crystal structure of HppE, the EPR data showed that the active site Fe of HppE is well suited for direct binding with substrates and substrate analogues. The results have also enhanced our understanding of ring closure in all antibiotic biosyntheses and multiple catalytic functions that commonly observed with nonheme iron enzymes.

6.2 MATERIALS AND METHODS

General. HppE from *S. wedmorensis* was expressed using *E. coli* BL21(DE3)/pPL1001 and purified to its homogeneity as previously described (*3*). The purified protein was stored in Tris·HCl buffer (20 mM, pH 7.5) at -80 °C for the biochemical and biophysical studies. The as-isolated HppE was essentially an apoprotein (metal-free). All reagents and solvents were purchased from commercial sources and were used without further purification unless otherwise noted. Biochemicals were purchased from Sigma (St. Louis, MO). Labeled

water (36.8% ^{17}O and 48.8% ^{18}O) were obtained from Isotec Inc. (Miamisburg, OH).

Preparation of ^{17}O-Labeled HPP. (*S*)- and (*R*)-HPP labeled with ^{17}O in their hydroxyl groups are synthesized by Dr. Sung-Ju Moon, following the established procedure in Chapter 2 except for the replacement of THF with pTSA and $H_2{}^{17}O$ in the first step (Figure 6-4).

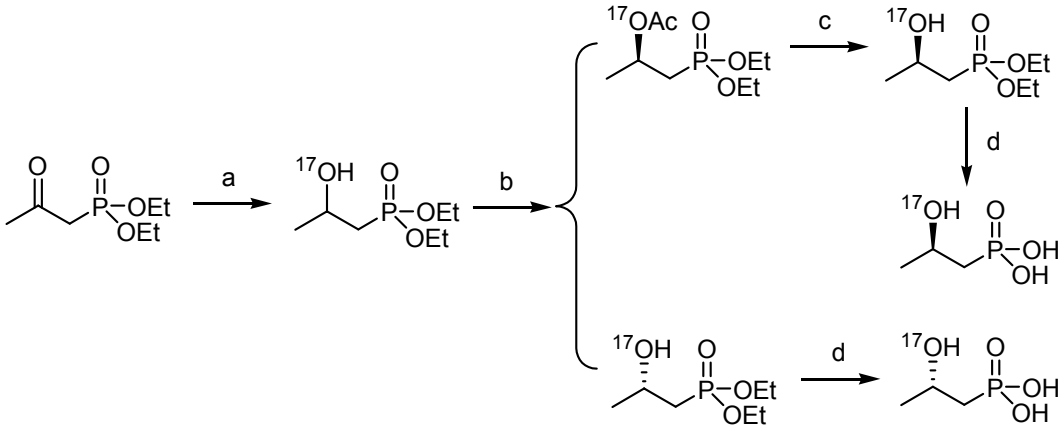

Figure 6-4 Synthetic scheme for (*S*)-2-[^{17}O]hydroxypropyl phosphonic acid and (*R*)-2-[^{17}O]hydroxypropyl phosphonic acid. Reagents and conditions: a) $NaBH_4$/pTSA/$H_2{}^{17}O$; b) lipase/vinyl acetate/isopropyl ether; c) NH_3/MeOH; d) TMSBr/CH_2Cl_2.

(*S*)-HPP labeled with ^{17}O in its phosphonate group was prepared by dissolving 0.04 mmol chemically synthesized and lyophilized unlabeled (*S*)-HPP in 0.2 mL of $H_2{}^{17}O$. The mixture was allowed to undergo isotope exchange for 1-2 weeks. ^{17}O isotope enrichment in all labeled compounds was determined by the Mass Spectrometry Laboratory of Department of Chemistry and Biochemistry at University of Texas at Austin.

Preparation of Substrate Analogues. Fosfomycin (**6-1**) and (*S*)-3-hydroxybutyric acid (HBA, **6-14**) were purchased from Aldrich (Milwaukee, WI) and Sigma (St. Louis, MO), respectively. 2-Methylpropylphosphonic acid (MPP, **6-15**) was chemically synthesized as shown in Figure 6-5. Briefly, 1.1 mL of isobutyl bromide (**6-16**) and 3.4 mL of triethylphosphite were mixed together and incubated with tetrabutylammonium iodide at 150 °C for 3 h. The product diethyl isobutylphosphonate (**6-17**) was purified by silica gel column chromatography. Compound **6-17** (0.5 g, 2.6 mmol) was then incubated with 0.5 mL of TMSBr and 0.25 mL allyltrimethylsilane for 24 h at room temperature. The final product MPP (**6-15**) was neutralized with NH_4HCO_3, extracted with water, and lyophilized into powder form.

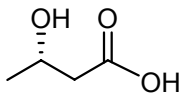

6-14

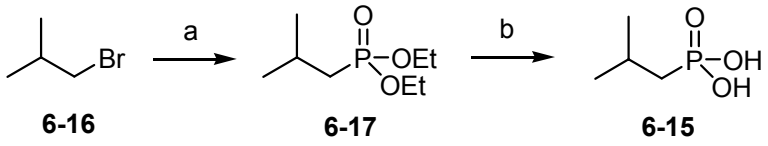

6-16 **6-17** **6-15**

Figure 6-5 Synthetic scheme for 2-methylpropylphosphonic acid (MPP, **6-15**). Reagents and conditions: a) $P(OEt)_3$/tetrabutylammonium iodide, 150 °C, 2h; b) TMSBr/allyltrimethylsilane/CH_2Cl_2, 24 h.

Preparation of NO Samples of Fe^{II}-HppE with Substrate and Substrate Analogues. Samples were made anaerobic by repeated cycles of vacuuming and flushing with argon that had been passed over a column of copper catalyst (BASF inc.) heated at 150 ºC. Approximately 3 h of argon bubbling was required to prepare 5 mL of double distilled H_2O or Tris·HCl (20 mM, pH 7.5) buffer with

reasonably good anaerobicity. The Fe^{II} stock solution was prepared by adding 1 mL of anaerobic H_2O through a gas-tight syringe into a serum vial containing pre-weighted $Fe^{II}(NH_4)_2(SO_4)_2 \cdot 6H_2O$ (99.997%, Aldrich) under anaerobic conditions. Anaerobic protein samples were prepared in a reaction vial and then transferred to the EPR sample tubes under the protection of argon. Samples were frozen by slow immersion in liquid N_2. Nitric oxide was introduced through a gas-tight syringe to the headspace of the quartz EPR tubes or UV-vis cuvettes containing the anaerobic ferrous enzymes. An argon flush was maintained above the sample to protect the sample from O_2 and to minimize an anomalous EPR signal near $g = 2$ which derives from NO itself rather than the enzyme-nitrosyl complex.

The ternary enzyme·substrate (or substrate analogues)·nitrosyl complexes were made by initially adding either substrate (or substrate analogues)·or NO to the enzyme at its reduced state, followed by the addition of the third component. For the isotope-labeling experiments, ^{17}OH-labeled substrates were first added to the enzyme, followed by NO gas. Control samples were prepared in parallel using natural-abundant substrate.

EPR Spectroscopy. EPR spectra were recorded at X-band with a Bruker E500 spectrometer equipped with an Oxford Instruments ESR-10 liquid helium cryostat. Temperature was controlled by a digitalized Oxford temperature controller. A Bruker ER035M Gauss Meter was used during measurements for the *g*-value determination. EPR spectra of the $S = 3/2$ complexes were analyzed according to the spin Hamiltonian:

$$\hat{\mathcal{H}} = g\beta_e B_0 S + D[\hat{S}_z^2 - 5/4 + E/D(S_x^2 - S_y^2)]$$

where B_0 is the magnetic field, D is the axial zero-field splitting parameter and E/D indicates the degree of rhombic distortion in the electronic environment. Changes in the E/D are diagnostic of changes in the environment of the iron. E/D values were determined by program RHOMBO (from Dr. W. R. Hagen, calculating all effective g values for high-spin Kramers systems) and verified by computer simulation of the observed EPR data using programs of W95EPR (from Dr. F. Neese) (*4*) and SimFonia (Bruker). Energy level calculations were conducted by Dr. Aimin Liu with the program EPR-NMR version 6.3 developed by Drs. J. A. Weil and M. J. Mombourquette.

6.3 RESULTS

NO Binding to the Ferrous Center in the Absence of Substrate. Since the as-isolated HppE is essentially metal-free, it was reconstituted with a stoichiometric amount of $Fe^{II}(NH_4)_2(SO_4)_2$ under anaerobic conditions (*3*). The resultant Fe^{II}-HppE was a colorless protein with an identical optical spectrum as that of apo-enzyme, in which there is no apparent optical features above 300 nm (Figure 6-6A and B). Likewise, this sample exhibits no detectable EPR signals at cryogenic temperatures. However, addition of NO to the reduced enzyme yielded a pale yellow complex with two absorption bands at 445 nm ($\varepsilon \approx 750$ $M^{-1}cm^{-1}$ per iron) and 640 nm ($\varepsilon \approx 250$ $M^{-1}cm^{-1}$ per iron) (Figure 6-6C). These bands are characteristic for the charge transfer transitions previously observed in ferrous-nitrosyl complexes of enzymes and model compounds (Table 6-1). A shoulder at 340 nm ($\varepsilon \approx 1000$ $M^{-1}cm^{-1}$ per iron) was also noted in the spectrum. This feature was observed in an earlier study of IPNS and was assigned to

nonspecific interactions of NO with proteins because of the dependence of its intensity on the NO concentration (*5*). When the Fe^{II}-HppE·nitrosyl binary complex was allowed to undergo repeated cycles of evacuation and flushing with argon, it returned to the colorless form. A green chromophore slowly developed during O_2 exposure. The resulting spectrum (Figure 6-6D) is identical to the oxidized Fe^{III}-HppE obtained from the reconstitution of apo-HppE with $Fe^{II}(NH_4)_2(SO_4)_2$ in the presence of O_2 (*6*). These results strongly suggest that the ferrous center of HppE is accessible by external small molecules such as NO and O_2, and the binding of NO is facile and reversible under appropriate conditions.

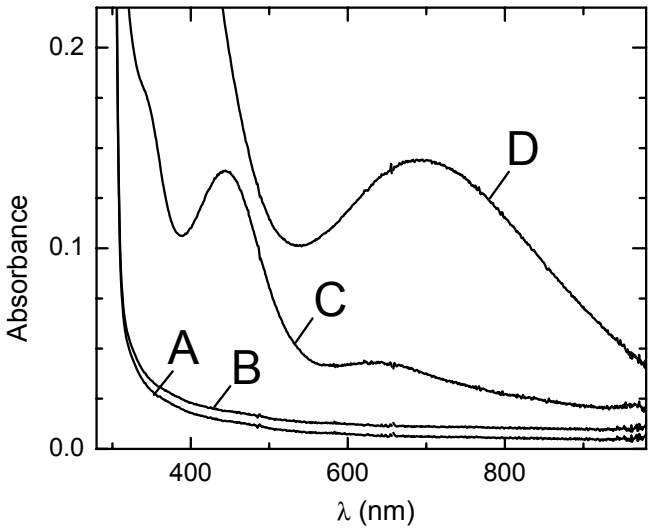

Figure 6-6 Electronic absorption spectra of Fe^{II}-HppE. (A) As-isolated HppE (metal-free, 200 μM); (B) Fe^{II}-HppE (180 μM); (C) sample B exposed to NO; and (D) sample *C* treated with repeated cycles of evacuation and flushing with argon, followed by O_2 exposure.

The corresponding EPR spectrum of the Fe^{II}-HppE·nitrosyl binary complex was previously reported (Chapter 2) (*3*). Two types of high-spin (S = 3/2) centers of Fe^{II}-nitrosyl complexes were identified by spectral simulation.

NO Binding to the Ferrous Center in the Presence of Substrate. The EPR spectrum of the nitrosyl adduct of the reduced HppE is composed of two superimposed S = 3/2 species with different relaxation properties. These resonances disappeared in the EPR spectrum of the ternary complex of reduced HppE, (*S*)-HPP (**6-2**), and NO as previously reported (Chapter 2) (*3*). Interestingly, when (*S*)-HPP (**6-2**) in the Fe^{II}-HppE·substrate·NO complex was replaced with (*R*)-HPP (**6-4**), the same type of EPR signal was observed (Figure 6-7 solid line). This EPR signal (S = 3/2) is comprised of the same principal g-values of 2.00, 3.63, and 4.41 with E/D = 0.077 (Table 6-1).

The above result strongly indicated that both (*S*)- and (*R*)-HPP bind to the metal center of HppE in nearly the same patterns. However, a small but reproducible difference in spectral width was discernible between the spectra of the two substrates (≈ 5 G) (Figure 6-7 solid and dotted lines). Although the exact cause for the small spectral difference is not known, it is presumably due to the chiral inequality between the two enantiomers. Because of the distinct chiralities at C_2 position of (*S*)- and (*R*)-HPP, the average distances from the hydrogen atoms at C_1 and C_2 to the iron center should also be different between these two enzyme-substrate complexes. The total paramagnetic effects of these hydrogen atoms on the iron-nitrosyl complex are also expected to be different in these two different samples. These observation lead to the proposed mechanistic

model to account for the different turnover products obtained with (*S*)- and (*R*)-HPP (Figure 6-18).

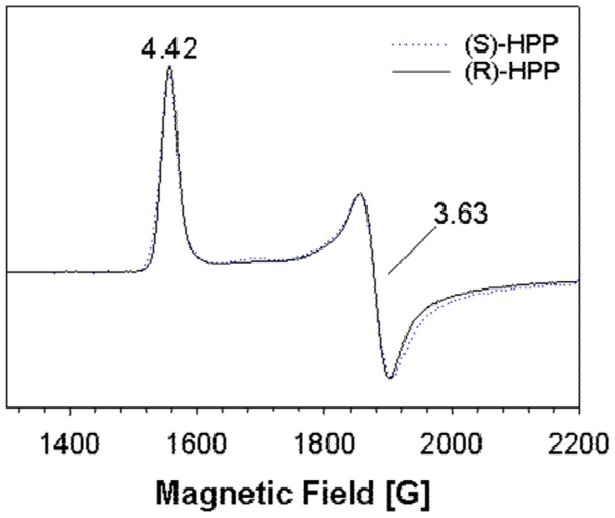

Figure 6-7 EPR Spectra of the ternary complex of Fe^{II}-HppE·substrate·NO. For better comparison, the spectra of (*R*)-HPP (solid line) and (*S*)-HPP (dotted line) are overlaid. Instrumental parameters: temperature 2 K, microwave frequency 9.6 GHz, microwave power 0.6 mW, modulation amplitude 5 G, time constant 0.02 s, and a sweep rate of 50 G/s. The important g values are given in spectra.

The energy level separations for the EPR signal of ternary complex of reduced HppE, substrate and NO are depicted by the pattern of splitting shown in Figure 6-8. The zero-field splitting is a result of interelectronic interactions and ligand fields of low symmetry and is quantified as a correction to the energies of the individual states arising from spin-orbit coupling (*7*). Figure 6-8 illustrates the presence of a zero-filed splitting phenomenon for this species with the axial parameter $D \neq 0$ (*8, 9*). In fact, the energy level splitting experiences an asymmetry in its environment that is consistent with our observed *E/D* value.

Studies of ferrous enzymes and inorganic model complexes have shown that binding of NO to ferrous ion generates species exhibiting such S = 3/2 EPR resonances (*5, 10-17*). The crystal structures of some of these complexes, for example, IPNS (*18*), have shown that the nitrogen of NO is coordinated directly to the iron. Together, the appearance of the characteristic S = 3/2 EPR resonances, and the facile reversibility of the binding process, are compelling evidence indicating the direct ligation of NO to the ferrous center, either in the absence or in the presence of substrate.

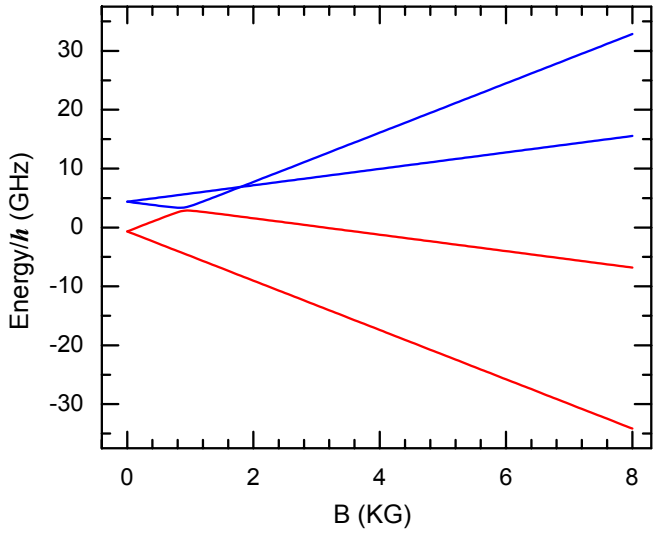

Figure 6-8 Energy levels for the S = 3/2 EPR signal of the ternary complex Fe^{II}-HppE·substrate·NO.

The increased rhombicity, upon substrate addition, makes all three axes of the ligand field distinct from each other. This has been a common feature for many of the metalloproteins-substrate complexes. However, the $\Delta(g_z\text{-}g_y)$ derivation of 0.78 (4.41 – 3.63 = 0.78) for the ternary complex of HppE is the

largest so far among characterized Fe^{II}-substrate nitrosyl complexes (Table 6-1). For example, in the cases of IPNS-ACV-NO and ACCO-ACC-NO complexes, the $\Delta(g_z\text{-}g_y)$ is 0.41 (*5, 15*). The Fe-NO distance of IPNS ternary complex has been estimated to be 2.13 Å based on the crystal structure (*18*). In another example, the g_y to g_z peak-to-peak width of the ternary complex of the α-KG-dependent enzyme TfdA is 8.9 millitesla (6.4 mT in the absence of substrate) (*13*), whereas this deviation is about four times greater (36.4 mT) for the EPR signals of the HppE ternary complex. The remarkable large splitting of the g_y and g_z components suggests a dramatic redistribution of the electron density upon NO coordination. This redistribution allows the enzyme ferrous center to exhibit like a ferric ion with $S = 5/2$ spin state, which is antiferromagnetically coupled to NO^- ($S = 1$) through direct orbital overlap. This proposal is consistent with the conclusion from previous studies on the $\{FeNO\}^7$ complexes using magnetic circular dichroism and X-ray absorption edge spectroscopic studies as well as X_α calculations (*12, 17*).

Species	*g*	λ (nm)	Refs
Fe^{II}-HppE·NO	1.99, 3.57, 3.91, 4.36 1.99, 3.65, 3.94, 4.16	340, 445, 640	(*3*)
Fe^{II}-HppE ·(*S*)-HPP·NO	1.99, 3.63, 4.42	N/D	(*3*)
Fe^{II}-IPNS·NO Fe^{II}-IPNS·ACV·NO	2.00, 3.95, 4.09 1.99, 3.81, 4.22	430, 600 508, 720	(*5*)
Fe^{II}-TfdA·α-KG·2,4D·NO	2.02, 3.99, 4.04	449, 657	(*13*)
Fe^{II}-TauD·α-KG·Taurine·NO	2.01, 4.02, 4.05	456, 662	(*16*)
Gentisate 1,2-dioxygenase·NO (two different sources)	1.99, 3.85, 4.19 2.0, 3.98, 4.06	N/D	(*19*)

ACCO·ACC·NO	3.81, 4.22		(*15*)
Reduced 3,4-PCD·NO	1.987, 3.679, 4.330		(*14*)
Reduced 3,4-PCD·PCA·NO	1.85, 2.99, 4.92		
Reduced 4,5-PCD·PCA·NO	3.91, 4.09		(*10, 11*)
	3.82, 3.87, 4.12, 4.17		
Reduced SOR·NO	2.00, 3.76, 4.34	475	(*12*)
	2.00, 4.00		
Fe^{II}(EDTA)-NO	2.00, 3.95, 4.11	340, 430, 640	(*17*)

Table 6-1 Spectral properties of Fe^{II}-nitrosyl complexes.

NO Binding to the Ferrous Center in the Presence of Substrate Analogues. To determine the role of each functional group of HPP in iron binding, substrate analogues were designed to selectively replace the hydroxyl and the phosphonate groups with methyl group in MPP (**6-15**) and carboxylate group in HBA (**6-14**), respectively. The EPR spectra of the ternary complexes formed with reduced HppE, nitric acid and these substrate analogues were shown in Figure 6-9 (B and C). In comparison with the spectrum of (*S*)-HPP (**6-2**) (Figure 6-9A), the EPR signal of HBA (**6-14**) is narrower and less heterogeneous. Two species were identified by spectral simulation (Figure 6-10), characterized by *g* values of 4.256, 3.804 and 1.993 (E/D = 0.038, Figure 6-10B), and 4.05, 3.98, and 1.999 (E/D = 0.006, Figure 6-10C), respectively. Similarly, the EPR spectrum of MPP becomes even more heterogeneous, which comprises three distinct species with *g* values of 4.448, 3.613, and 1.975 (E/D = 0.070, Figure 6-11B), 4.173, 3.886, and 1.999 (E/D = 0.024, Figure 6-11C) and 4.02 and 2.0 (E/D = 0, Figure 6-11D). It is clear that binding of the phosphonate group to Fe^{II} has a greater effect to the

unusually broad EPR signal of the ternary complex of Fe^{II}-HppE·(*S*)-HPP·NO. Given that the phosphonate is highly negatively charged at neutral pH, a direct interaction between (*S*)-HPP (**6-2**) and the ferrous center via the phosphonate group can be established. On the other hand, the hydroxyl group of (*S*)-HPP (**6-2**) also plays an important role in positioning the substrate in the active site, since multiple binding modes appeared when it was replaced with a methyl group (Figure 6-9C).

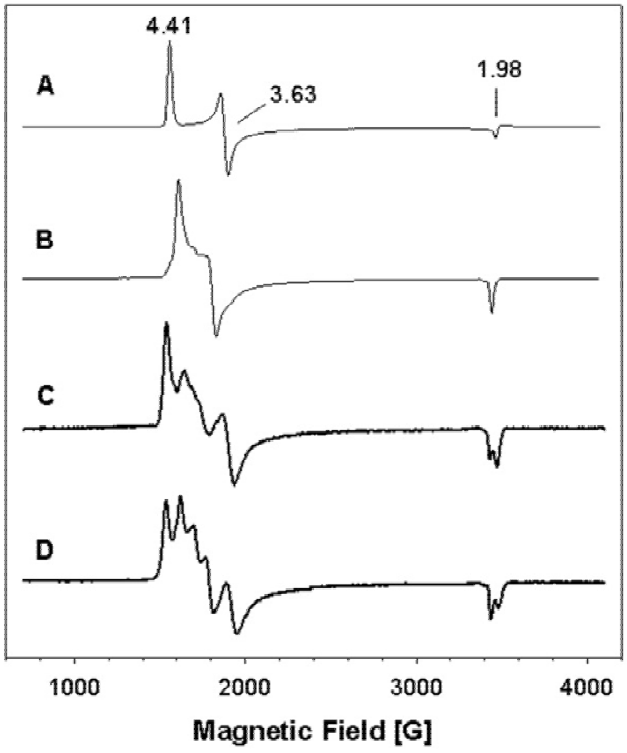

Figure 6-9 EPR spectra of reduced HppE nitrosyl complexes with substrate or substrate analogues. The ternary complex is comprised of 250 mM Fe^{II}-HppE, NO, and 2.5 mM (*S*)-HPP (A), or HBP (B), or MPP (C) or fosfomycin (D). Instrumental parameters are the same as shown in Figure 6-7. The important g values are given in spectra

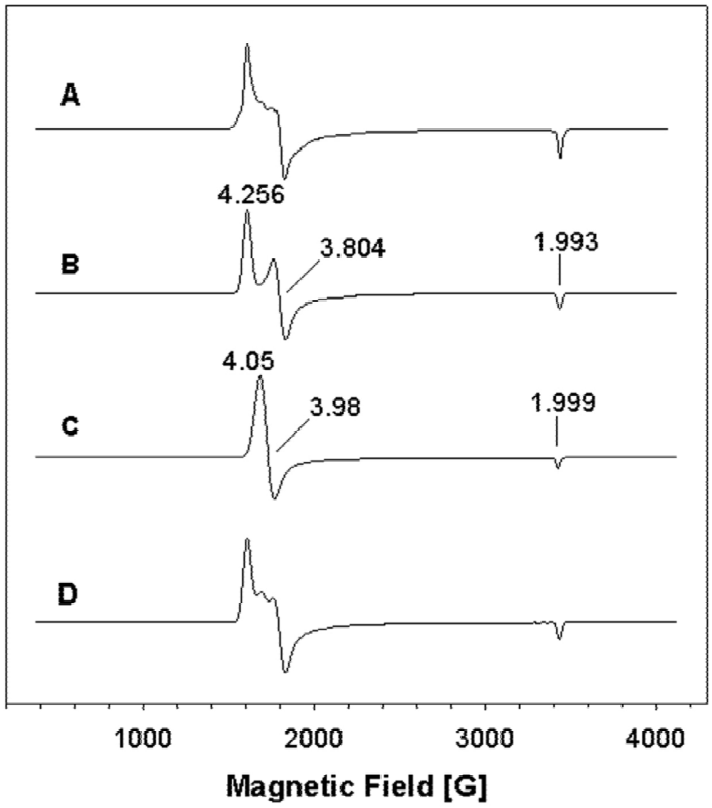

Figure 6-10 Simulations of the experimental EPR spectra of the ternary complex Fe^{II}-HppE·HBC·NO. (A) Experimental spectrum; (B) Simulated spectrum of E/D = 0.038 species (C) Simulated spectrum of E/D = 0.006 species (D) Simulated spectrum consisting of 75% (B) and 25% (C). The important g values are given in spectra

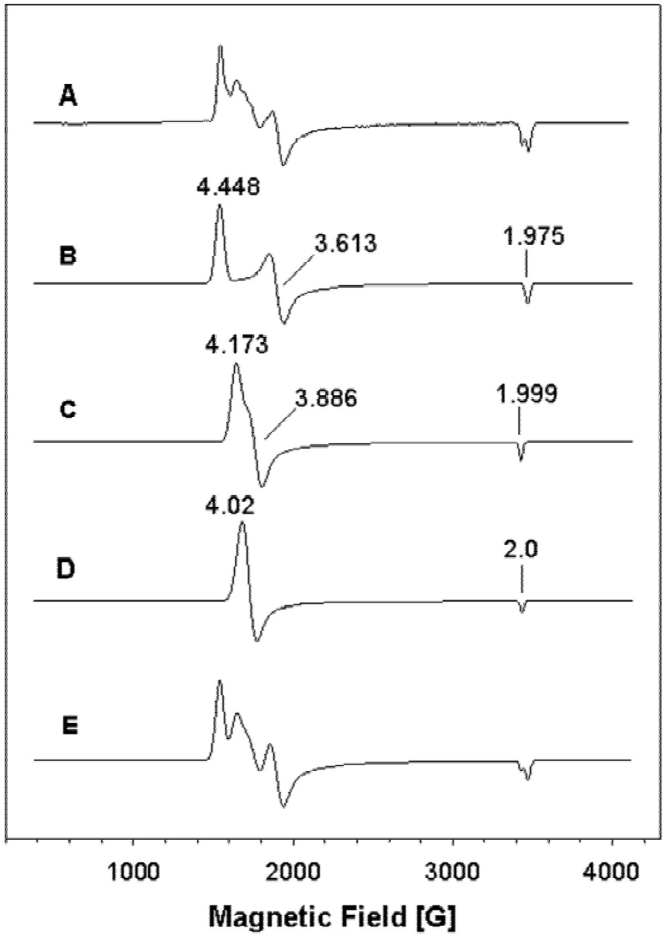

Figure 6-11 Simulations of the experimental EPR spectra of the ternary complex Fe^{II}-HppE·MPP·NO. (A) Experimental spectrum; (B) Simulated spectrum of E/D = 0.07 species; (C) Simulated spectrum of E/D = 0.024 species; (D) Simulated spectrum of E/D = 0 species; (E) Simulated spectrum consisting of 60% (B) 30% (C) and 10% (D). The important g values are given in spectra

Interestingly, when fosfomycin (**6-1**) was tested as a substrate analogue, its binding exhibited similar effects on the EPR spectrum of the Fe^{II}-HppE nitrosyl adduct as observed with MPP (**6-15**) (Figure 6-9C and D). The

simulation analysis of its spectrum revealed the presence of a nearly identical set of EPR-sensitive species with *g* values of 4.47, 3.60, and 1.97 (E/D = 0.073, Figure 6-12B), 4.233, 3.835 and 1.998 (E/D = 0.033, Figure 6-12C), and 4.03 and 2.0 (E/D = 0, Figure 6-12D). The only difference between these two spectra is the contribution percentage of each species to the whole spectrum. The resemblance in binding patterns between MPP and fosfomycin suggested that the epoxide oxygen play little role to bind metal. Since the fosfomycin is the product and needs to be released, it is not surprising that (*S*)-HPP (**6-2**) binds more tightly to HppE active site than fosfomycin does (**6-1**).

NO Binding to the Ferrous Center in the Presence of Isotope-labeled Substrates. Since the $S = 3/2$ EPR signal is derived from the ferrous nitrosyl complex bound with (*S*)-HPP (**6-2**) in HppE, the presence of any paramagnetic isotope as part of any of the component forming the complex would in principle affect the EPR signal. The extent of effects is determined by the type of interaction and the distance between interacting species. For example, when $^{57}Fe^{II}$ was used to prepare the ternary complex of Fe^{II}-HppE·(*S*)-HPP·NO, the hyperfine interaction between the electronic spin of ferrous ion and its $I = 1/2$ nuclear ground state (^{57}Fe) resulted in approximately 36 Gauss broadening of the spectral feature around $g = 4.41$ in the EPR spectra when compared to that of ^{56}Fe ($I = 0$) sample (Figure 6-13A and C).

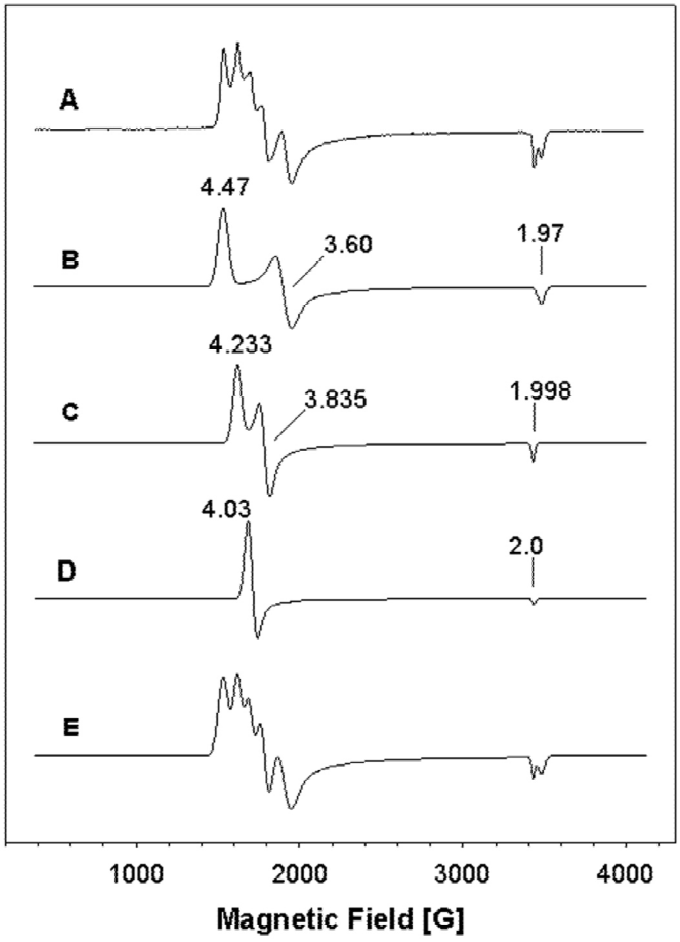

Figure 6-12 Simulations of experimental EPR spectra of ternary complex Fe^{II}-HppE·MPP·NO. (A) Experimental spectrum; (B) Simulated spectrum of E/D = 0.073 species; (C) Simulated spectrum of E/D = 0.033 species; (D) Simulated spectrum of E/D = 0 species; (E) Simulated spectrum consisting of 40% (B) 40% (C) and 20% (D). The important g values are given in spectra

Similarly, ^{17}O-enriched HPP was prepared in order to evaluate whether the substrate binds directly to the iron center in the reduced HppE and, more importantly, to identify the binding group(s) of the substrate (i.e. –OH vs. $–PO_3$).

In the EPR spectrum of Fe^{II}-HppE nitrosyl complex bound with chemically synthesized ^{17}OH-enriched (*S*)-HPP, broadening effect is apparent. Considering the low ^{17}O enrichment in HPP, the 20 G increase in the linewidth of the resonance at 4.41 is significant and strongly supports the direct coordination of the hydroxyl oxygen of (*S*)-HPP to the ferrous center (Figure 6-14B and C).

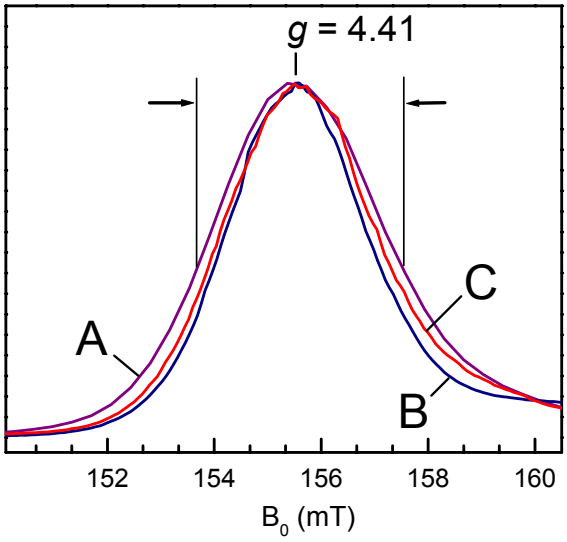

Figure 6-13 The $g = 4.41$ component of the EPR signal of isotope-labeled ternary complexes of Fe^{II}-HppE·(*S*)-HPP·NO. (A) ^{57}Fe-HppE + ^{16}OH-(*S*)-HPP; (B) ^{16}OH-(*S*)-HPP; (C) ^{56}Fe-HppE +^{17}OH-(*S*)-HPP. Instrumental parameters are the same as shown in Figure 6-7.

Unfortunately, no isotope broadening was observed for the g_y (3.63) component in each of the above cases. While the isotope effect is also expected for the g_z component (2.00), this component is often overlapped with an anomalous resonance arising from NO itself in the samples (not shown). This NO-derived signal was particularly prevalent in samples prepared with excess

NO. Thus, unlike the $g_x = 4.41$ resonance, the g_z component is masked here and uninformative.

HPP with ^{17}O enriched in the phosphonate group was prepared by incubating unlabeled HPP in $H_2{}^{17}O$ for weeks. When this $P^{17}O_3$-HPP was bound in the Fe^{II}-HppE nitrosyl complex, it drastically broadened both g_x and g_y components of the EPR signal of the complex (Figure 6-14). Such a significant isotope effect strongly supports the direct coordination between the phosphonate oxygen and the ferrous center. Together with the coordination between the hydroxyl oxygen of HPP and the enzyme metal center, a bidentate binding pattern of HPP to the active site iron in HppE can now be established.

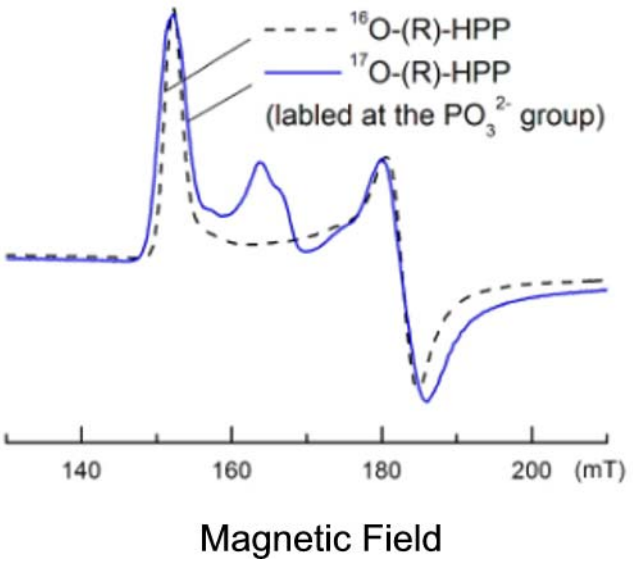

Figure 6-14 EPR Spectra of ternary complexes of Fe^{II}-HppE·$P^{17}O_3$-(*R*)-HPP·NO. Instrumental parameters are the same as shown in Figure 6-7.

Crystal Structure of Co^{II}-reconstituted HppE bound with (S)-HPP. To investigate substrate binding without turnover, Co^{II}-HppE, which has been shown to be catalytically inactive (*20*), was used to prepare an inert enzyme-substrate model system. The presence of a moderately heavy atom in the substrate, such as phosphorous, gave rise to a high electron density peak showing the position of the phosphonic acid moiety and the orientation of the substrate (Figure 6-15). Surprisingly, the structure of Co^{II}-HppE in complex with substrate reveals two modes of substrate binding. In one of the two molecules of HppE present in the asymmetric unit, substrate binds in a monodentate fashion with one of the oxygen atoms of the phosphonate moiety coordinating the metal and displacing one bound water (Figure 6-16A). In the other molecule, (*S*)-HPP (**6-2**) forms a bidentate interaction with the metal center via the 2-hydroxyl oxygen as well as an oxygen atom from the phosphonate group, and leaving a coordination site open for subsequent dioxygen binding (Figure 6-16B).

The bidentate binding of (*S*)-HPP (**6-2**) induces a conformational change in the β-barrel, while substrate bound in a monodentate fashion physically precludes this conformational change from occurring. The conformational change involves β-strands 2 and 3 (Figure 6-16C, colored in green and yellow), which form a β-hairpin substructure and act as a cantilever responding to the positioning of substrate in the bidentate orientation by moving in and sealing off the active site. Movements near the hinge or fulcrum of the hairpin are subtle while those near the end are more appreciable (Figure 6-16C). Specifically, Tyr105 moves toward the metal center by 1.5 Å, positioning its hydroxyl group

within hydrogen bonding distance to a phosphonate oxygen of (*S*)-HPP (**6-2**) (2.7 Å), while Tyr102 moves 8.0 Å toward the metal. Alignment of the two substrate binding modes reveals that the monodentate binding position of (*S*)-HPP sterically precludes strand 3 motion toward the metal center.

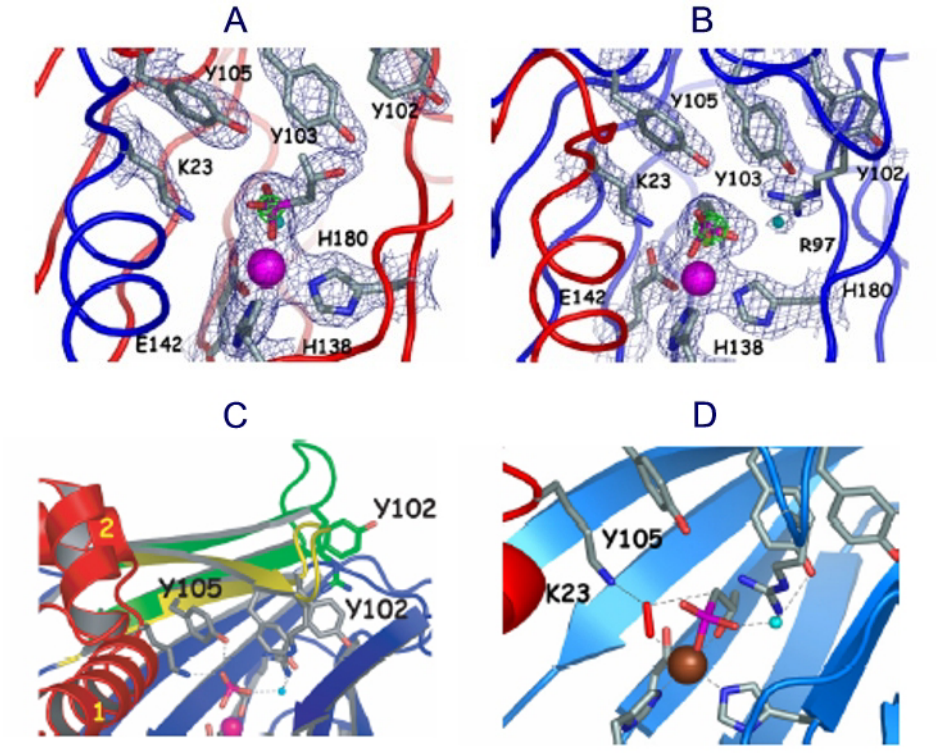

Figure 6-15 Crystal structure of HppE bound with substrate. (A) The Co^{II}-HppE·(*S*)-HPP active site illustrating monodentate substrate binding. (B) The active site illustrating bidentate substrate binding. (C) Conformational changes of enzyme upon substrate binding. Comparison between structures of Fe^{II}-HppE and Co^{II}-HppE·(*S*)-HPP shows that a cantilever hairpin changes conformation between a substrate-free state (green) and a substrate-bound state (yellow). (D) A structural model of the ternary complex of HppE. The open coordination site in Co^{II}-HppE·(*S*)-HPP is occupied by dioxygen in this model.

With the substrate in the bidentate position and the cantilever closed, the methyl group of (*S*)-HPP (**6-2**) lies within a small hydrophobic cavity consisting of Phe182, Val122, Leu193, Leu144, and Ala195. Tyr105, Lys23, and Asn135 are within hydrogen bonding distance to the phosphonic acid oxygens of (*S*)-HPP (**6-2**), while Tyr103 hydrogen bonds to substrate through a bridging water molecule (Figure 6-16).

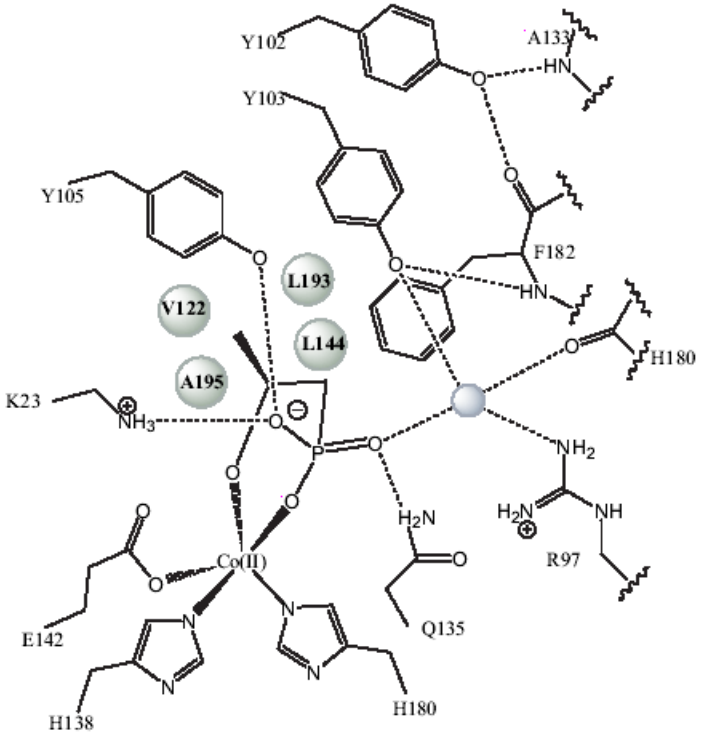

Figure 6-16 Schematic illustration of interactions of bidentate bound (*S*)-HPP with protein and metal.

6.4 DISCUSSION

Nitric oxide was chosen as an O_2 surrogate in this study because of its preference to bind to ferrous ions and to form EPR-visible $S = 1/2$ (*21-24*) or $S = 3/2$ (*10, 11, 14, 17, 25-29*) fingerprinting signals of $\{FeNO\}^7$ according to the Enemark-Feltham formalism (*30*). It has been used extensively as a probe to study oxygen binding site in other nonheme iron enzymes such as IPNS, LPO, PCD dioxygenases, and a few α-KG-dependent dioxygenases (*10, 11, 14, 17, 19, 27, 29*). Using this probe, we have conducted the EPR and optical absorption studies on the reduced HppE. The results presented here unambiguously demonstrated that the reduced iron center of HppE is fairly accessible to its substrates and NO. If NO is an effective analog of O_2 in this system, O_2 would occupy the same site and be activated. The substrate ligation to iron was deduced from the isotope effects brought by the ^{17}O-enrichment in the hydroxyl groups of both (*S*)- and (*R*)-HPP on the linewidth of the EPR signal of the enzyme ternary complex. The EPR resonances were broadened by the hyperfine interactions between the iron-nitrosyl center and the ^{17}O nucleus ($I = 5/2$) in substrate, which constituted a strong line of evidence for direct coordination of the hydroxyl and the phosphonate groups of (*S*)- and (*R*)-HPP to the active site iron in the reduced enzyme nitrosyl complex. Such evident broadening effects usually require the strong hyperfine interactions between the coupled nuclei connected by chemical bond since the interactions through space are generally too weak to affect the EPR spectrum. The σ-bond connecting iron center and hydroxyl oxygen of (*S*)-HPP is believed to provide a convenient path for fast

electron transfer from the substrate radical to iron and thus may greatly facilitate the formation of the final product. Although the isotope-labeling technique has not been applied to study the coordination pattern of the product, fosfomycin (**6-1**), to the enzyme active site, the preliminary results from EPR study strongly argued against the coordination between the epoxide oxygen and the iron center (Figure 6-9).

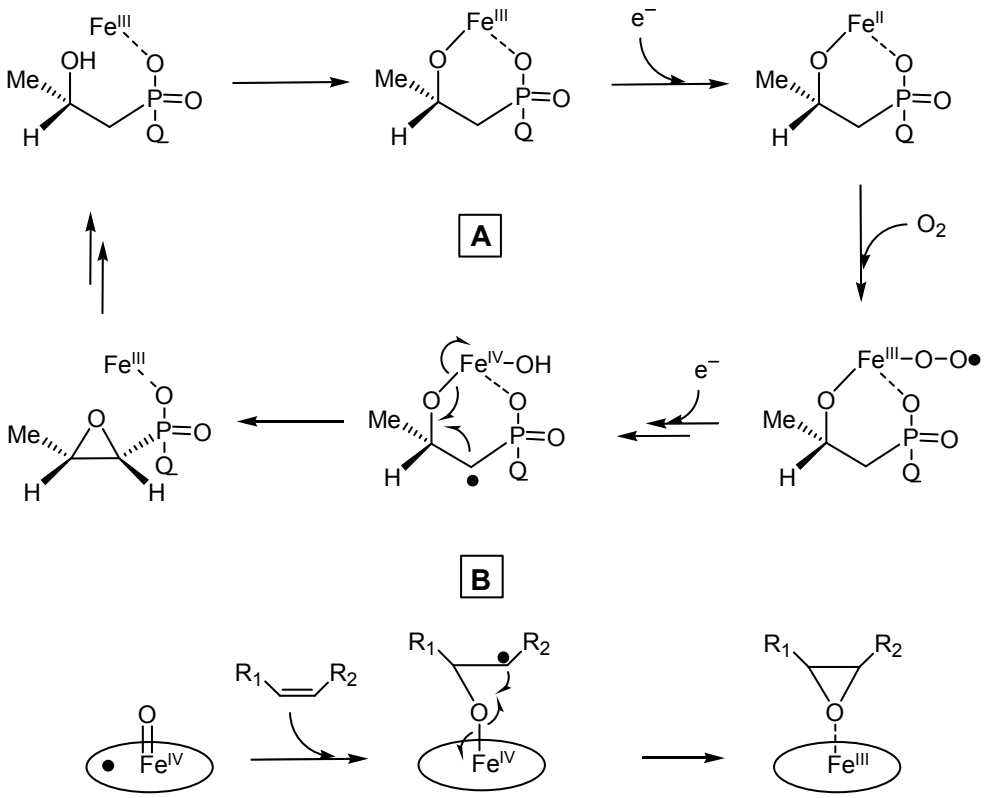

Figure 6-17 Comparison of the mechanisms proposed for the epoxidation reactions catalyzed by (a) HppE and (b) P-450.

Figure 6-17A shows a revised mechanistic model highlighting the coordination patterns of the ferrous center of HppE in the catalytic cycle. The

direct ligation of substrate to iron is now integrated into the proposed mechanism of HppE, in which the generation of an enzyme-bound substrate radical via hydrogen abstraction by an iron-oxygen species is followed by an intramolecular rearrangement of the substrate radical leading to epoxide formation. The two binding modes (mono- and bidentate) of substrate to the iron center revealed by X-ray crystallographic study suggest a two-step substrate binding process, which is also incorporated into the revised mechanism. Since the iron in the $\{Fe\text{-}NO\}^7$ complex exhibits strong properties of ferric ion, the binding pattern and dynamics of HPP established in the reduced HppE can now be extended to the oxidized form of the enzyme. The most important aspect of this model is that both substrate and O_2 bind directly to the iron, resulting in the formation of an activated iron-oxygen species, which is proximal to the pro-*R* α-H atom to be abstracted in (*S*)-HPP (**6-2**).

The formation of enzyme-bound substrate radical and the subsequent intramolecular rearrangement of the radical intermediate have been proposed for many other oxidative cyclization reactions. In the epoxidation reaction catalyzed by cytochrome P450, the high-valent iron-oxo species (Compound I) is believe to be the oxidizing agent responsible for the insertion of oxygen to the olefin substrates (*31*). However, the detailed mechanism for oxygen incorporation by P450 has been a controversial topic. More recent experimental results obtained with model compounds (*32*), seem to favor a step-wise mechanism (Figure 6-17B). Briefly, the C-O bonds are formed in two consecutive steps, the first one resulting in radical intermediate formation and the

second step leading to epoxide ring closure via intramolecular rearrangement (Figure 6-17B). Apparently, the epoxidation reactions catalyzed by HppE and P450 follow a similar path for the ring closure step. However, the first C-O bond formation reaction is not necessary for HppE. A similar mechanistic model has been proposed in other non-heme iron enzyme catalyzed reactions. For example, IPNS catalyzes a two-staged bicyclization reaction, in which the substrate binds directly to the active site iron via its thiol group throughout the reaction course (*5*). The second stage of the reaction is the abstraction of the valinyl β-hydrogen initiated by the thiol sulfur-coordinated iron-oxo species. The resulting radical intermediate then undergoes a rearrangement, giving rise to the thiazolidine ring product. The two-step mechanism resembles those of aforementioned epoxidation reactions, except that an Fe-S bond replaces the Fe-O bond, and the product is a five-member ring instead of an epoxide ring, in the case of IPNS. Interestingly, such direct ligation of substrate to iron center seems not to be the case in the cyclization reaction catalyzed by CAS, as indicated by the recently solved crystal structure of CAS bound with substrate and cosubstrate α-KG (*33*). Only α-KG is bonded to the active site iron in a bidentate mode. However, it is still possible that the hydroxyl group of substrate can bind to the iron soon after the first oxidative half-reaction is over, in which α-KG is cleaved into succinate and CO_2.

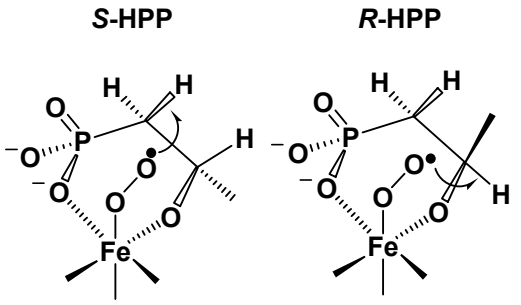

Figure 6-18 Proposed model to account for the stereochemistry in HppE catalysis. (Note: the iron-superoxide used here as an iron-oxygen reaction species is only for illustrative purpose.)

In this study, (*R*)-HPP has been shown to bind to HppE in a very similar manner as (*S*)-HPP. The EPR spectra of their enzyme-substrate nitrosyl ternary complexes are nearly identical except for a minor difference in linewidth. As previously mentioned, (*S*)- and (*R*)-HPP are converted exclusively to their respective epoxide and ketone products, which preludes the possibility of radical rearrangement between C_1 and C_2. Because of the similar binding modes and the distinct outcomes of product formation of (*S*)- and (*R*)-HPP, the hydrogen atom presented closest to the iron center must be the pro-*R* α-H in the case of (*S*)-HPP and the β-H in the case of (*R*)-HPP, respectively. The formation of such enzyme-substrate complexes allows the reactive iron-oxygen species specifically abstract the nearest hydrogen atom in each substrate, giving rise to distinct substrate radical intermediates and the final products. In a good agreement with this model, (*S*)-FHPP (**6-7**), as both its α-H atoms are replaced by fluorine while its β-H is too far from the reactive center, cannot be turned over by HppE. However, it still can bind to HppE, so it serves as a competitive inhibitor of HppE

(*1*). Indeed, the earlier EPR experimental results have shown that α-difluorinated substrate analogues bind to the enzyme in almost the same way as (*S*)- and (*R*)-HPP.

In summary, this study has provided a clear picture for the binding of substrates and substrate analogues to HppE in the presence of dioxygen analogue, nitric oxide. By using isotope-labeled substrate, a bidentate mode of substrate binding to the active site iron has been established. The crystallographic results led to further details revealing multiple binding modes, and thus implicated a likely two-step substrate binding process. The EPR spectral data offered many mechanistic insights that are consistent with the previously determined stereochemistry of enzyme catalysis. Comparable to other epoxidation and cyclization, HppE-catalyzed epoxidation also involves the generation of an enzyme-bound substrate radical intermediate. Continued mechanistic studies are in progress for a better understanding of the catalytic mechanism of HppE.

6.5 REFERENCE

1. Zhao, Z., Liu, P., Murakami, K., Kuzuyama, T., Seto, H., and Liu, H.-w. (2002) "Mechanistic studies of HPP epoxidase: configuration of the substrate governs its enzymatic fate" *Angew. Chem. Int. Ed. 41*, 4529-4532.
2. Hammerschmidt, F., and Kaehlig, H. (1991) "Biosynthesis of natural products with a phosphorus-carbon bond. 7. Synthesis of 1,1-$^{2}H_{2}$-, 2,2-$^{2}H_{2}$-, (*R*)- and (*S*)-1-$^{2}H_{1}$(2-hydroxyethyl)phosphonic acid and (*R*,*S*)-1-$^{2}H_{1}$(1,2-dihydroxyethyl)phosphonic acid and incorporation studies into fosfomycin in *Streptomyces fradiae*" *J. Org. Chem. 56*, 2364-2370.
3. Liu, P., Liu, A., Yan, F., Wolfe, M. D., Lipscomb, J. D., and Liu, H. W. (2003) "Biochemical and spectroscopic studies on (*S*)-2-hydroxypropylphosphonic acid epoxidase: a novel mononuclear non-heme iron enzyme" *Biochemistry 42*, 11577-11586.

4. Neese, F., Zumft, W. G., Antholine, W. E., and Kroneck, P. M. H. (1996) "The Purple Mixed-Valence CuA Center in Nitrous-oxide Reductase: EPR of the Copper-63-, Copper-65-, and Both Copper-65- and ^{15}N Histidine-Enriched Enzyme and a Molecular Orbital Interpretation" *J. Am. Chem. Soc. 118*, 8692-8699.

5. Chen, V. J., Orville, A. M., Harpel, M. R., Frolik, C. A., Surerus, K. K., Münck, E., and Lipscomb, J. D. (1989) "Spectroscopic studies of isopenicillin N synthase. A mononuclear nonheme iron(II) oxidase with metal coordination sites for small molecules and substrate" *J. of Biol. Chem. 264*, 21677-21681.

6. Liu, P., Mehn, M. P., Yan, F., Zhao, Z., Que, L., Jr., and Liu, H.-W. (2004) "Oxygenase activity in the self-hydroxylation of (*S*)-2-hydroxypropylphosphonic acid epoxidase involved in fosfomycin biosynthesis" *J. Am. Chem. Soc. 126*, 10306-10312.

7. Palmer, G. (1979) in *The Porphyrins* (Dolphin, D. E., Ed.), Academic Press, New York.

8. Palmer, G. (2000) in *Physical methods in bioinorganic chemistry: spectroscopy and magnetism* (Que, L., Jr., Ed.), University Science Books, Sausalito, Calif. USA.

9. Blumberg, W. E., and Peisach, J. (1973) "Measurement of zero field splitting and the determination of ligand composition in mononuclear nonheme iron proteins" *Ann. N. Y. Acad. Sci. 222*, 539-560.

10. Arciero, D. M., Lipscomb, J. D., Huynh, B. H., Kent, T. A., and Münck, E. (1983) "EPR and Mössbauer studies of protocatechuate 4,5-dioxygenase. Characterization of a new Fe^{2+} environment" *J. Biol. Chem. 258*, 14981-14991.

11. Arciero, D. M., Orville, A. M., and Lipscomb, J. D. (1985) "[^{17}O]Water and nitric oxide binding by protocatechuate 4,5-dioxygenase and catechol 2,3-dioxygenase. Evidence for binding of exogenous ligands to the active site Fe^{2+} of extradiol dioxygenases" *J. Biol. Chem. 260*, 14035-14044.

12. Clay, M. D., Cosper, C. A., Jenney, F. E., Jr., Adams, M. W. W., and Johnson, M. K. (2003) "Nitric oxide binding at the mononuclear active site of reduced pyrococcus furiosus superoxide reductase" *Proc. Natl. Acad. of Sci. USA 100*, 3796-3801.

13. Hegg, E. L., Whiting, A. K., Saari, R. E., McCracken, J., Hausinger, R. P., and Que, L., Jr. (1999) "Herbicide-degrading α-keto acid-dependent enzyme TfdA: metal coordination environment and mechanistic insights" *Biochemistry 38*, 16714-16726.

14. Orville, A. M., and Lipscomb, J. D. (1993) "Simultaneous binding of nitric oxide and isotopically labeled substrates or inhibitors by reduced protocatechuate 3,4-dioxygenase" *J. Biol. Chem. 268*, 8596-8607.

15. Rocklin, A. M., Tierney, D. L., Kofman, V., Brunhuber, N. M. W., Hoffman, B. M., Christoffersen, R. E., Reich, N. O., Lipscomb, J. D., and Que, L., Jr. (1999) "Role of the nonheme Fe(II) center in the biosynthesis of the plant hormone ethylene" *Proc. Natl. Acad. Sci. USA 96*, 7905-7909.

16. Ryle, M. J., Padmakumar, R., and Hausinger, R. P. (1999) "Stopped-flow kinetic analysis of Escherichia coli taurine/α-ketoglutarate dioxygenase: interactions with α-ketoglutarate, taurine, and oxygen" *Biochemistry 38*, 15278-15286.

17. Zhang, Y., Pavlosky, M. A., Brown, C. A., Westre, T. E., Hedman, B., Hodgson, K. O., and Solomon, E. I. (1992) "Spectroscopic and theoretical description of the electronic structure of the $S = 3/2$ nitrosyl complex of non-heme iron enzymes" *J. Am. Chem. Soc. 114*, 9189-9191.

18. Roach, P. L., Clifton, I. J., Hensgens, C. M., Shibata, N., Schofield, C. J., Hajdu, J., and Baldwin, J. E. (1997) "Structure of isopenicillin N synthase complexed with substrate and the mechanism of penicillin formation" *Nature 387*, 827-830.

19. Harpel, M. R., and Lipscomb, J. D. (1990) "Gentisate 1,2-dioxygenase from *Pseudomonas acidovorans*" *Methods Enzymol. 188*, 101-107.

20. Liu, P., Liu, A., Yan, F., Wolfe, M. D., Lipscomb, J. D., and Liu, H. W. (2003) "Biochemical and spectroscopic studies on (S)-2-hydroxypropylphosphonic acid epoxidase: a novel mononuclear non-heme iron enzyme" *Biochemistry 42*, 11577-86.

21. Drapier, J. C., Pellat, C., and Henry, Y. (1991) "Generation of EPR-detectable nitrosyl-iron complexes in tumor target cells cocultured with activated macrophages" *J. Biol. Chem. 266*, 10162-10167.

22. Le Brun, N. E., Andrews, S. C., Moore, G. R., and Thomson, A. J. (1997) "Interaction of nitric oxide with non-haem iron sites of *Escherichia coli* bacterioferritin: reduction of nitric oxide to nitrous oxide and oxidation of iron(II) to iron(III)" *Biochem. J. 326*, 173-179.

23. Woolum, J. C., Tiezzi, E., and Commoner, B. (1968) "Electron spin resonane of iron-nitric oxide complexes with amino acids, peptides and proteins" *Biochim. Biophys. Acta. 160*, 311-320.

24. Boese, M., Mordvintcev, P. I., Vanin, A. F., Busse, R., and Mèulsch, A. (1995) "*S*-nitrosation of serum albumin by dinitrosyl-iron complex" *J. Biol. Chem. 270*, 29244-29249.

25. Arciero, D. M., and Lipscomb, J. D. (1986) "Binding of ^{17}O-labeled substrate and inhibitors to protocatechuate 4,5-dioxygenase-nitrosyl complex. Evidence for direct substrate binding to the active site Fe^{2+} of extradiol dioxygenases" *J. Biol. Chem. 261*, 2170-2178.

26. Harpel, M. R., and Lipscomb, J. D. (1990) "Gentisate 1,2-dioxygenase from *Pseudomonas*. Substrate coordination to active site Fe^{2+} and mechanism of turnover" *J. Biol. Chem. 265*, 22187-22196.

27. Orville, A. M., and Lipscomb, J. D. (1997) "Cyanide and nitric oxide binding to reduced protocatechuate 3,4-dioxygenase: insight into the basis for order-dependent ligand binding by intradiol catecholic dioxygenases" *Biochemistry 36*, 14044-10455.

28. Wolgel, S. A., Dege, J. E., Perkins-Olson, P. E., Jaurez-Garcia, C. H., Crawford, R. L., Münck, E., and Lipscomb, J. D. (1993) "Purification and characterization of protocatechuate 2,3-dioxygenase from *Bacillus macerans*: a new extradiol catecholic dioxygenase" *J. Bacteriol. 175*, 4414-4426.

29. Nelson, M. J. (1987) "The nitric oxide complex of ferrous soybean lipoxygenase-1. Substrate, pH, and ethanol effects on the active-site iron" *J. Biol. Chem. 262*, 12137-12142.

30. Enemark, J. H., and Feltham, R. D. (1974) "Principles of structure, bonding, and reactivity for metal nitrosyl complexes" *Coord. Chem. Rev. 13*, 339-406.

31. Ortiz de Montellano, P. R., and De Voss, J. J. (2002) "Oxidizing species in the mechanism of cytochrome P450" *Nat. Prod. Rep. 19*, 477-493.

32. Gross, Z., Nimri, S., Barzilay, C. M., and Simkhovich, L. (1997) "Reaction profile of the last step in cytochrome P-450 catalysis revealed by studies of model complexes" *J. Biol. Inorg. Chem. 2*, 492-506.

33. Zhang, Z., Ren, J., Stammers, D. K., Baldwin, J. E., Harlos, K., and Schofield, C. J. (2000) "Structural origins of the selectivity of the trifunctional oxygenase clavaminic acid synthase" *Nat. Struct. Biol. 7*, 127-133.

Appendix

LIST OF ABBREVIATIONS

ACC	1-aminocyclo-propane-1-carboxylic acid
ACCO	1-aminocyclopropane-1-carboxylate oxidase
ACV	δ-(L-α-aminoadipoyl)-L-cysteinyl-D-valine
AEP	2-aminoethylphosphonic acid
BphC	2,3-dihydroxybiphenyl 1,2-dioxygenase
BSA	bovine serum albumin
CAS	clavaminic acid synthase
DAOCS	deacetoxycephalosporin C synthase
DEAE	diethylaminoethyl
DOPA	L-3,4-dioxyphenylalanine
DTT	dithiothreitol
E_3	CDP-4-keto-6-deoxy-$\Delta^{3,4}$-glucoseen reductase
EDTA	ethylenediaminetetraacetic acid
EPR	electron paramagnetic resonance
ESEEM	electron spin echo envelope modulation
FAD	flavin adenine dinucleotide
FMN	flavin mononucleotide
FPLC	fast protein liquid chromatography
H6H	hyoscyamine 6β-hydroxylase
HPP	2-hydroxypropyl phosphonic acid

HppE	(*S*)-2-hydroxypropylphosphonic acid epoxidase
ID medium	Iron-depletion medium
IPNS	isopenicillin N synthase
IPTG	isopropylthio-β-galactoside
LB medium	Luria-Bertani medium
LI medium	Low-iron medium
LMCT	ligand-to-metal charge transfer
MLCT	metal-to-ligand charge transfer
MMO	methane monooxygenase
MMOH	methane monooxygenase hydroxylase component
MMOR	methane monooxygenase B component
NAD^+	nicotinamide adenine dinucleotide, reduced form
NADH	nicotinamide adenine dinucleotide, oxidized form
NBT	nitroblue tetrazolium
NDO	naphthalene 1,2-dioxygenase;
NO	nitric oxide;
$P450_{CAM}$	camphor inducible bacterial P450 monooxygenase
PCR	polymerase chain reaction
PEP	phosphoenolpyruvate
PMI	phosphomannose isomerase
PnAA	phosphonoacetaldehyde
PnPy	phosphonopyruvate
PPOH	*cis*-propenylphosphonic acid

PQQ	pyrroloquinoline quinone
RNR	ribonucleotide reductase
rR	resonance Raman
SDS	sodium dodecyl sulfate
PAGE	polyacrylamide gel electrophoresis
SeMet	seleno-DL-methionine
SLO	soybean lipoxygenase
TauD	taurine dioxygenase;
TfdA	2,4-dichlorophenoxyacetic acid dioxygenase;
TLC	thin layer chromatography
Tris	tris(hydroxymethyl)aminomethane
TyrH	tyrosine hydroxylase
UDP-GlcNAc	UDP-*N*-acetylglucosamine
UDP-MurNAc-pentapeptide	UDP-acetylmuramyl-pentapeptide
WT	wild-type

Bibliography

Aberg, A., Ormö, M., Nordlund, P., and Sjöberg, B. M. (1993) "Autocatalytic generation of dopa in the engineered protein R2 F208Y from Escherichia coli ribonucleotide reductase and crystal structure of the dopa-208 protein" *Biochemistry 32*, 9845-9850.

Andersen, O. A., Flatmark, T., and Hough, E. (2002) "Crystal structure of the ternary complex of the catalytic domain of human phenylalanine hydroxylase with tetrahydrobiopterin and 3-(2-thienyl)-L-alanine, and its implications for the mechanism of catalysis and substrate activation" *J. Mol. Biol. 320*, 1095-1108.

Andersson, K. K., Cox, D. D., Que, L., Jr., Flatmark, T., and Haavik, J. (1988) "Resonance Raman studies on the blue-green-colored bovine adrenal tyrosine 3-monooxygenase (tyrosine hydroxylase). Evidence that the feedback inhibitors adrenaline and noradrenaline are coordinated to iron" *J. Biol. Chem. 263*, 18621-18626.

Arciero, D. M., and Lipscomb, J. D. (1986) "Binding of ^{17}O-labeled substrate and inhibitors to protocatechuate 4,5-dioxygenase-nitrosyl complex. Evidence for direct substrate binding to the active site Fe^{2+} of extradiol dioxygenases" *J. Biol. Chem. 261*, 2170-2178.

Arciero, D. M., Lipscomb, J. D., Huynh, B. H., Kent, T. A., and Münck, E. (1983) "EPR and Mössbauer studies of protocatechuate 4,5-dioxygenase. Characterization of a new Fe^{2+} environment" *J. Biol. Chem. 258*, 14981-14991.

Arciero, D. M., Orville, A. M., and Lipscomb, J. D. (1985) "[^{17}O]Water and nitric oxide binding by protocatechuate 4,5-dioxygenase and catechol 2,3-dioxygenase. Evidence for binding of exogenous ligands to the active site Fe^{2+} of extradiol dioxygenases" *J. Biol. Chem. 260*, 14035-14044.

Balasubramanian, S., Carr, R. T., Bender, C. J., Peisach, J., and Benkovic, S. J. (1994) "Identification of metal ligands in Cu(II)-inhibited Chromobacterium violaceum phenylalanine hydroxylase by electron spin echo envelope modulation analysis of histidine to serine mutations" *Biochemistry 33*, 8532-8537.

Barlow, T., Eliasson, R., Platz, A., Reichard, P., and Sjöberg, B. M. (1983) "Enzymic modification of a tyrosine residue to a stable free radical in ribonucleotide reductase" *Proceedings of the National Academy of Sciences of the United States of America 80*, 1492-1495.

Barry, B. A., El-Deeb, M. K., Sandusky, P. O., and Babcock, G. T. (1990) "Tyrosine radicals in photosystem II and related model compounds. Characterization by isotopic labeling and EPR spectroscopy" *J. Biol. Chem. 265*, 20139-20143.

Blumberg, W. E., and Peisach, J. (1973) "Measurement of zero field splitting and the determination of ligand composition in mononuclear nonheme iron proteins" *Ann. N. Y. Acad. Sci. 222*, 539-560.

Boese, M., Mordvintcev, P. I., Vanin, A. F., Busse, R., and Mèulsch, A. (1995) "*S*-nitrosation of serum albumin by dinitrosyl-iron complex" *J. Biol. Chem. 270*, 29244-29249.

Borovok, I., Landman, O., Kreisberg-Zakarin, R., Aharonowitz, Y., and Cohen, G. (1996) "Ferrous active site of isopenicillin N synthase: genetic and sequence analysis of the endogenous ligands" *Biochemistry 35*, 1981-1987.

Boyington, J. C., Gaffney, B. J., and Amzel, L. M. (1993) "The three-dimensional structure of an arachidonic acid 15-lipoxygenase" *Science 260*, 1482-1486.

Bradford, M. M. (1976) "A rapid and sensitive method for the quantitation of microgram quantities of protein utilizing the principle of protein-dye binding" *Anal. Biochem. 72*, 248-254.

Brown, E. D., Vivas, E. I., Walsh, C. T., and Kolter, R. (1995) "MurA (MurZ), the enzyme that catalyzes the first committed step in peptidoglycan biosynthesis, is essential in *Escherichia coli*" *J. Bacteriol. 177*, 4194-4197.

Bugg, T. D. H., and Winfield, C. J. (1998) "Enzymic cleavage of aromatic rings: mechanistic aspects of the catechol dioxygenases and later enzymes of bacterial oxidative cleavage pathways" *Nat. Prod. Rep. 15*, 513-530.

Burzlaff, N. I., Rutledge, P. J., Clifton, I. J., Hensgens, C. M., Pickford, M., Adlington, R. M., Roach, P. L., and Baldwin, J. E. (1999) "The reaction

cycle of isopenicillin N synthase observed by X-ray diffraction" *Nature 401*, 721-724.

Carredano, E., Karlsson, A., Kauppi, B., Choudhury, D., Parales, R. E., Parales, J. V., Lee, K., Gibson, D. T., Eklund, H., and Ramaswamy, S. (2000) "Substrate binding site of naphthalene 1,2-dioxygenase: functional implications of indole binding" *J. Mol. Biol. 296*, 701-712.

Chen, L. Y., Mathews, F. S., Davidson, V. L., Huizinga, E. G., Vellieux, F. M., Duine, J. A., and Hol, W. G. (1991) "Crystallographic investigations of the tryptophan-derived cofactor in the quinoprotein methylamine dehydrogenase" *FEBS Lett. 287*, 163-166.

Chen, V. J., Orville, A. M., Harpel, M. R., Frolik, C. A., Surerus, K. K., Münck, E., and Lipscomb, J. D. (1989) "Spectroscopic studies of isopenicillin N synthase. A mononuclear nonheme iron(II) oxidase with metal coordination sites for small molecules and substrate" *J. of Biol. Chem. 264*, 21677-21681.

Christensen, B. G., Leanza, W. J., Beattie, T. R., Patchett, A. A., Arison, B. H., Ormond, R. E., Kuehl, F. A., Jr., Albers-Schonberg, G., and Jardetzky, O. (1969) "Phosphonomycin: structure and synthesis" *Science 166*, 123-125.

Clay, M. D., Cosper, C. A., Jenney, F. E., Jr., Adams, M. W. W., and Johnson, M. K. (2003) "Nitric oxide binding at the mononuclear active site of reduced pyrococcus furiosus superoxide reductase" *Proc. Natl. Acad. of Sci. USA 100*, 3796-3801.

Colby, J., Stirling, D. I., and Dalton, H. (1977) "The soluble methane mono-oxygenase of *Methylococcus capsulatus* (Bath). Its ability to oxygenate *N*-alkanes, *N*-alkenes, ethers, and alicyclic, aromatic and heterocyclic compounds" *Biochem. J. 165*, 395-402.

Costas, M., Mehn, M. P., Jensen, M. P., and Que, L., Jr. (2004) "Dioxygen activation at mononuclear nonheme iron active sites: enzymes, models, and intermediates" *Chem. Rev. 104*, 939-986.

Cox, D. D., Benkovic, S. J., Bloom, L. M., Bradley, F. C., Nelson, M. J., Que, L., Jr., and Wallick, D. E. (1988) "Catecholate LMCT bands as probes for the active sites of nonheme iron oxygenases" *J. Am. Chem. Soc. 110*, 2026-2032.

D'Autreaux, B., Horner, O., Oddou, J.-L., Jeandey, C., Gambarelli, S., Berthomieu, C., Latour, J.-M., and Michaud-Soret, I. (2004) "Spectroscopic description of the two nitrosyl-iron complexes responsible for inhibition by nitric oxide" *J. Am. Chem. Soc. 126*, 6005-6016.

Davis, M. I., Orville, A. M., Neese, F., Zaleski, J. M., Lipscomb, J. D., and Solomon, E. I. (2002) "Spectroscopic and electronic structure studies of protocatechuate 3,4-dioxygenase: nature of tyrosinate-Fe(III) bonds and their contribution to reactivity" *J. Am. Chem. Soc. 124*, 602-614.

Dette, G. A., Knothe, H., Schèonenbach, B., and Plage, G. (1983) "Comparative study of fosfomycin activity in Mueller-Hinton media and in tissues" *J. Antimicrob. Chemother. 11*, 517-524.

Dix, T. A., Bollag, G. E., Domanico, P. L., and Benkovic, S. J. (1985) "Phenylalanine hydroxylase: absolute configuration and source of oxygen of the 4a-hydroxytetrahydropterin species" *Biochemistry 24*, 2955-2958.

Doan, L. X., Hassan, A., Lipscomb, S. J., Dhanda, A., Zhang, Z., and Schofield, C. J. (2000) "Mutagenesis studies on the iron binding ligands of clavaminic acid synthase" *Biochem. Biophys. Res. Commun. 279*, 240-244.

Dooley, D. M., McGuirl, M. A., Brown, D. E., Turowski, P. N., McIntire, W. S., and Knowles, P. F. (1991) "A Cu(I)-semiquinone state in substrate-reduced amine oxidases" *Nature 349*, 262-264.

Dordick, J. S., Klibanov, A. M., and Marletta, M. A. (1986) "Horseradish peroxidase catalyzed hydroxylations: mechanistic studies" *Biochemistry 25*, 2946-2951.

Drapier, J. C., Pellat, C., and Henry, Y. (1991) "Generation of EPR-detectable nitrosyl-iron complexes in tumor target cells cocultured with activated macrophages" *J. Biol. Chem. 266*, 10162-10167.

Dunwell, J. M., Culham, A., Carter, C. E., Sosa-Aguirre, C. R., and Goodenough, P. W. (2001) "Evolution of functional diversity in the cupin superfamily" *Trends. Biochem. Sci. 26*, 740-746.

Dunwell, J. M., Purvis, A., and Khuri, S. (2004) "Cupins: the most functionally diverse protein superfamily?" *Phytochemistry 65*, 7-17.

Elgren, T. E., Orville, A. M., Kelly, K. A., Lipscomb, J. D., Ohlendorf, D. H., and Que, L., Jr. (1997) "Crystal structure and resonance Raman studies of protocatechuate 3,4-dioxygenase complexed with 3,4-dihydroxyphenylacetate" *Biochemistry 36*, 11504-11513.

Elkins, J. M., Ryle, M. J., Clifton, I. J., Dunning Hotopp, J. C., Lloyd, J. S., Burzlaff, N. I., Baldwin, J. E., Hausinger, R. P., and Roach, P. L. (2002) "X-ray crystal structure of Escherichia coli taurine/α-ketoglutarate dioxygenase complexed to ferrous iron and substrates" *Biochemistry 41*, 5185-5192.

Enemark, J. H., and Feltham, R. D. (1974) "Principles of structure, bonding, and reactivity for metal nitrosyl complexes" *Coord. Chem. Rev. 13*, 339-406.

Erlandsen, H., Fusetti, F., Martinez, A., Hough, E., Flatmark, T., and Stevens, R. C. (1997) "Crystal structure of the catalytic domain of human phenylalanine hydroxylase reveals the structural basis for phenylketonuria" *Nat. Struct. Biol. 4*, 995-1000.

Fitzpatrick, P. F. (1999) "Tetrahydropterin-dependent amino acid hydroxylases" *Annu. Rev. Biochem. 68*, 355-381.

Fitzpatrick, P. F., Ralph, E. C., Ellis, H. R., Willmon, O. J., and Daubner, S. C. (2003) "Characterization of metal ligand mutants of tyrosine hydroxylase: insights into the plasticity of a 2-histidine-1-carboxylate triad" *Biochemistry 42*, 2081-2088.

Flatmark, T., and Stevens, R. C. (1999) "Structural insight into the aromatic amino acid hydroxylases and their disease-related mutant forms" *Chem. Rev. 99*, 2137-2160.

Ford-Hutchinson, A. W., Gresser, M., and Young, R. N. (1994) "5-Lipoxygenase" *Annu. Rev. Biochem. 63*, 383-417.

Foster, M. W., and Cowan, J. A. (1999) "Chemistry of nitric oxide with protein-bound Iron sulfur centers. insights on physiological reactivity" *J. Am. Chem. Soc. 121*, 4093-4100.

García, P., Arca, P., and Evaristo Suárez, J. (1995) "Product of fosC, a gene from *Pseudomonas syringae*, mediates fosfomycin resistance by using ATP as cosubstrate" *Antimicrob. Agents. Chemother. 39*, 1569-1573.

Gardner, H. W. (1991) "Recent investigations into the lipoxygenase pathway of plants" *Biochim. Biophys. Acta. 1084*, 221-239.

Garssen, G. J., Vliegenthart, J. F., and Boldingh, J. (1972) "The origin and structures of dimeric fatty acids from the anaerobic reaction between soya-bean lipoxygenase, linoleic acid and its hydroperoxide" *Biochem. J. 130*, 435-442.

Gibson, D. T., and Parales, R. E. (2000) "Aromatic hydrocarbon dioxygenases in environmental biotechnology" *Curr. Opin. Biotechnol. 11*, 236-243.

Goodwill, K. E., Sabatier, C., Marks, C., Raag, R., Fitzpatrick, P. F., and Stevens, R. C. (1997) "Crystal structure of tyrosine hydroxylase at 2.3 A and its implications for inherited neurodegenerative diseases" *Nat. Struct. Biol. 4*, 578-585.

Gräslund, A., and Sahlin, M. (1996) "Electron paramagnetic resonance and nuclear magnetic resonance studies of class I ribonucleotide reductase" *Annu. Rev. Biophys. Biomol. Struct. 25*, 259-286.

Gross, Z., Nimri, S., Barzilay, C. M., and Simkhovich, L. (1997) "Reaction profile of the last step in cytochrome P-450 catalysis revealed by studies of model complexes" *J. Biol. Inorg. Chem. 2*, 492-506.

Groves, J. T. (1985) "Key elements of the chemistry of cytochrome P-450. The oxygen rebound mechanism" *J. Chem. Ed. 62*, 928-931.

Gunther, M. R., Tschirret-Guth, R. A., Witkowska, H. E., Fann, Y. C., Barr, D. P., Ortiz De Montellano, P. R., and Mason, R. P. (1998) "Site-specific spin trapping of tyrosine radicals in the oxidation of metmyoglobin by hydrogen peroxide" *Biochem. J. 330*, 1293-1299.

Hammerschmidt, F. (1991) "Biosynthesis of natural products with a phosphorus-carbon bond. Part 8. On the origin of the oxirane oxygen atom of fosformycin in *Streptomyces fradiae*" *J. Chem. Soc., Perkin Trans. 1*, 1993-1996.

Hammerschmidt, F. (1991) "Markierte vertreter eines möglichen zwischen-produkts der biosynthese von fosfomycin in *Streptomyces fradiae*: darstellung von (*R*,*S*)-(2-hydroxypropyl)-, (*R*,*S*)-, (*R*)-, (*S*)-(2-hydroxy-[1,1-$^{2}H_{2}$]propyl)- und (*R*,*S*)-(2-[^{18}O]hydroxypropyl)phosphonsäure." *Monatsh. Chem.*, 389-393.

Hammerschmidt, F., and Kaehlig, H. (1991) "Biosynthesis of natural products with a phosphorus-carbon bond. 7. Synthesis of 1,1-$^{2}H_2$-, 2,2-$^{2}H_2$-, (*R*)- and (*S*)-1-$^{2}H_1$(2-hydroxyethyl)phosphonic acid and (*R*,*S*)-1-$^{2}H_1$(1,2-dihydroxyethyl)phosphonic acid and incorporation studies into fosfomycin in *Streptomyces fradiae*" *J. Org. Chem. 56*, 2364-2370.

Han, S., Eltis, L. D., Timmis, K. N., Muchmore, S. W., and Bolin, J. T. (1995) "Crystal structure of the biphenyl-cleaving extradiol dioxygenase from a PCB-degrading *pseudomonas*" *Science 270*, 976-980.

Harpel, M. R., and Lipscomb, J. D. (1990) "Gentisate 1,2-dioxygenase from *Pseudomonas*. Substrate coordination to active site Fe^{2+} and mechanism of turnover" *J. Biol. Chem. 265*, 22187-22196.

Hashimoto, T., Matsuda, J., and Yamada, Y. (1993) "Two-step epoxidation of hyoscyamine to scopolamine is catalyzed by bifunctional hyoscyamine 6β-hydroxylase" *FEBS Lett. 329*, 35-39.

Hashimoto, T., and Yamada, Y. (1987) "Purification and characterization of hyoscyamine 6 β-hydroxylase from root cultures of *Hyoscyamus niger* L. Hydroxylase and epoxidase activities in the enzyme preparation" *Eur. J. Biochem. 164*, 277-285.

Hausinger, R. P. (2004) "Fe^{II}/α-ketoglutarate-dependent hydroxylases and related enzymes." *Crit. Rev. Biochem. Mol. Biol. 39*, 21-68.

Hegg, E. L., and Que, L., Jr. (1997) "The 2-His-1-carboxylate facial triad--an emerging structural motif in mononuclear non-heme iron(II) enzymes" *Eur. J. Biochem. 250*, 625-629.

Hegg, E. L., Whiting, A. K., Saari, R. E., McCracken, J., Hausinger, R. P., and Que, L., Jr. (1999) "Herbicide-degrading α-keto acid-dependent enzyme TfdA: metal coordination environment and mechanistic insights" *Biochemistry 38*, 16714-16726.

Hendlin, D., Stapley, E. O., Jackson, M., Wallick, H., Miller, A. K., Wolf, F. J., Miller, T. W., Chaiet, L., Kahan, F. M., Foltz, E. L., Woodruff, H. B., Mata, J. M., Hernandez, S., and Mochales, S. (1969) "Phosphonomycin, a new antibiotic produced by strains of *streptomyces*" *Science 166*, 122-123.

Hidaka, T., Goda, M., Kuzuyama, T., Takei, N., Hidaka, M., and Seto, H. (1995) "Cloning and nucleotide sequence of fosfomycin biosynthetic genes of *Streptomyces wedmorensis*" *Mol. Gen. Genet. 249*, 274-280.

Hogan, D. A., Smith, S. R., Saari, E. A., McCracken, J., and Hausinger, R. P. (2000) "Site-directed mutagenesis of 2,4-dichlorophenoxyacetic acid/α-ketoglutarate dioxygenase. Identification of residues involved in metallocenter formation and substrate binding" *J. Biol. Chem. 275*, 12400-12409.

Horii, T., Kimura, T., Sato, K., Shibayama, K., and Ohta, M. (1999) "Emergence of fosfomycin-resistant isolates of Shiga-like toxin-producing *Escherichia coli* O26" *Antimicrob. Agents. Chemother. 43*, 789-793.

Huyett, J. E., Doan, P. E., Gurbiel, R., Houseman, A. L. P., Sivaraja, M., Goodin, D. B., and Hoffman, B. M. (1995) "Compound ES of cytochrome c peroxidase contains a Trp π-cation radical: characterization by continuous wave and pulsed Q-band external nuclear double resonance spectroscopy" *J. Am. Chem. Soc. 117*, 9033-9041.

Imai, S., Seto, H., Sasaki, T., Tsuruoka, T., Ogawa, H., Satoh, A., Inouye, S., Niida, T., and Otake, N. (1985) "Studies on the biosynthesis of bialaphos (SF-1293). 6. Production of *N*-acetyl-demethylphosphinothricin and *N*-acetylbialaphos by blocked mutants of *Streptomyces hygroscopicus* SF-1293 and their roles in the biosynthesis of bialaphos" *J. Antibiot. 38*, 687-690.

Jiang, H., Parales, R. E., Lynch, N. A., and Gibson, D. T. (1996) "Site-directed mutagenesis of conserved amino acids in the alpha subunit of toluene dioxygenase: potential mononuclear non-heme iron coordination sites" *J. Bacteriol. 178*, 3133-3139.

Kahan, F. M., Kahan, J. S., Cassidy, P. J., and Kropp, H. (1974) "The mechanism of action of fosfomycin (phosphonomycin)" *Ann. N. Y. Acad. Sci. 235*, 364-386.

Kamigiri, K., Hidaka, T., Imai, S., Murakami, T., and Seto, H. (1992) "Studies on the biosynthesis of bialaphos (SF-1293) 12. C-P bond formation mechanism of bialaphos: discovery of a P-methylation enzyme" *J. Antibiot. (Tokyo) 45*, 781-787.

Kappock, T. J., and Caradonna, J. P. (1996) "Pterin-dependent amino acid hydroxylases" *Chem. Rev. 96*, 2659-2756.

Karlsson, A., Parales, J. V., Parales, R. E., Gibson, D. T., Eklund, H., and Ramaswamy, S. (2003) "Crystal structure of naphthalene dioxygenase: side-on binding of dioxygen to iron" *Science 299*, 1039-1042.

Karthein, R., Dietz, R., Nastainczyk, W., and Ruf, H. H. (1988) "Higher oxidation states of prostaglandin H synthase. EPR study of a transient tyrosyl radical in the enzyme during the peroxidase reaction" *Eur. J. Biochem. 171*, 313-320.

Kauppi, B., Lee, K., Carredano, E., Parales, R. E., Gibson, D. T., Eklund, H., and Ramaswamy, S. (1998) "Structure of an aromatic-ring-hydroxylating dioxygenase-naphthalene 1,2-dioxygenase" *Structure 6*, 571-586.

Kennedy, M. C., Gan, T., Antholine, W. E., and Petering, D. H. (1993) "Metallothionein reacts with Fe^{2+} and NO to form products with A g = 2.039 ESR signal" *Biochem. Biophys. Res. Commun. 196*, 632-635.

Khaleeli, N., Busby, R. W., and Townsend, C. A. (2000) "Site-directed mutagenesis and biochemical analysis of the endogenous ligands in the ferrous active site of clavaminate synthase. The His-3 variant of the 2-His-1-carboxylate model" *Biochemistry 39*, 8666-8673.

Kim, D. H., Lees, W. J., Kempsell, K. E., Lane, W. S., Duncan, K., and Walsh, C. T. (1996) "Characterization of a Cys115 to Asp substitution in the *Escherichia coli* cell wall biosynthetic enzyme UDP-GlcNAc enolpyruvyl transferase (MurA) that confers resistance to inactivation by the antibiotic fosfomycin" *Biochemistry 35*, 4923-4928.

Kim, D. H., Tucker-Kellogg, G. W., Lees, W. J., and Walsh, C. T. (1996) "Analysis of fluoromethyl group chirality establishes a common stereochemical course for the enolpyruvyl transfers catalyzed by EPSP synthase and UDP-GlcNAc enolpyruvyl transferase" *Biochemistry 35*, 5435-5440.

Knowles, P. F., Marsh, D., and Rattle, H. W. E. (1976) *Magnetic Resonance of Biomolecule: an introduction to the theory and practice of NMR and ESR in biological systems*, John Wiley & Sons, Ltd., New York.

Kojo, H., Shigi, Y., and Nishida, M. (1980) "FR-31564, a new phosphonic acid antibiotic: bacterial resistance and membrane permeability" *J. Antibiot. 33*, 44-48.

Kuzuyama, T., Hidaka, T., Kamigiri, K., Imai, S., and Seto, H. (1992) "Studies on the biosynthesis of fosfomycin. 4. The biosynthetic origin of the methyl group of fosfomycin" *J. Antibiot. (Tokyo) 45*, 1812-1814.

Kuzuyama, T., Kobayashi, S., O'Hara, K., Hidaka, T., and Seto, H. (1996) "Fosfomycin monophosphate and fosfomycin diphosphate, two inactivated fosfomycin derivatives formed by gene products of fomA and fomB from a fosfomycin producing organism *Streptomyces wedmorensis*" *J. Antibiot. (Tokyo) 49*, 502-504.

Kuzuyama, T., Seki, T., Dairi, T., Hidaka, T., and Seto, H. (1995) "Nucleotide sequence of fortimicin KL1 methyltransferase gene isolated from *Micromonospora olivasterospora*, and comparison of its deduced amino acid sequence with those of methyltransferases involved in the biosynthesis of bialaphos and fosfomycin" *J. Antibiot. (Tokyo) 48*, 1191-1193.

Kuzuyama, T., Seki, T., Kobayashi, S., Hidaka, T., and Seto, H. (1999) "Cloning and expression in *Escherichia coli* of 2-hydroxypropylphosphonic acid epoxidase from the fosfomycin-producing organism, *Pseudomonas syringae* PB-5123" *Biosci. Biotechnol. Biochem. 63*, 2222-2224.

Lancaster, J. R., Jr., and Hibbs, J. B., Jr. (1990) "EPR demonstration of iron-nitrosyl complex formation by cytotoxic activated macrophages" *Proc. Natl. Acad. Sci. USA 87*, 1223-1227.

Lange, S. J., and Que, L., Jr. (1998) "Oxygen activating nonheme iron enzymes" *Curr. Opin. Chem. Biol. 2*, 159-172.

Le Brun, N. E., Andrews, S. C., Moore, G. R., and Thomson, A. J. (1997) "Interaction of nitric oxide with non-haem iron sites of *Escherichia coli* bacterioferritin: reduction of nitric oxide to nitrous oxide and oxidation of iron(II) to iron(III)" *Biochem. J. 326*, 173-179.

LeMaster, D. M., and Richards, F. M. (1985) "^{1}H-^{15}N heteronuclear NMR studies of *Escherichia coli* thioredoxin in samples isotopically labeled by residue type" *Biochemistry 24*, 7263-7268.

Licht, S., Gerfen, G. J., and Stubbe, J. (1996) "Thiyl radicals in ribonucleotide reductases" *Science 271*, 477-481.

Ling, J., Sahlin, M., Sjèoberg, B. M., Loehr, T. M., and Sanders-Loehr, J. (1994) "Dioxygen is the source of the mu-oxo bridge in iron ribonucleotide reductase" *J. Biol. Chem. 269*, 5595-5601.

Lipscomb, J. D. (1994) "Biochemistry of the soluble methane monooxygenase" *Annu. Rev. Microbiol. 48*, 371-399.

Liu, A., Ho, R. Y., Que, L., Jr., Ryle, M. J., Phinney, B. S., and Hausinger, R. P. (2001) "Alternative reactivity of an α-ketoglutarate-dependent iron(II) oxygenase: enzyme self-hydroxylation" *J. Am. Chem. Soc. 123*, 5126-5127.

Liu, P. (2001) Ph.D. dissertation, "Insights into the enzymes in fosfomycin biosynthesis: mechanistic studies of HPP epoxidase" *Department of Chemsitry*, *The University of Minnesota*, *Minneapolis*, 77.

Liu, P., Liu, A., Yan, F., Wolfe, M. D., Lipscomb, J. D., and Liu, H.-w. (2003) "Biochemical and spectroscopic studies on (*S*)-2-hydroxypropylphosphonic acid epoxidase: a novel mononuclear non-heme iron enzyme" *Biochemistry 42*, 11577-11586.

Liu, P., Mehn, M. P., Yan, F., Zhao, Z., Que, L., Jr., and Liu, H.-W. (2004) "Oxygenase activity in the self-hydroxylation of (*S*)-2-hydroxypropylphosphonic acid epoxidase involved in fosfomycin biosynthesis" *J. Am. Chem. Soc. 126*, 10306-10312.

Liu, P., Murakami, K., Seki, T., He, X., Yeung, S. M., Kuzuyama, T., Seto, H., and Liu, H. (2001) "Protein purification and function assignment of the epoxidase catalyzing the formation of fosfomycin" *J. Am. Chem. Soc. 123*, 4619-4620.

Liu, S., Lu, Z., Jia, Y., Dunaway-Mariano, D., and Herzberg, O. (2002) "Dissociative phosphoryl transfer in PEP mutase catalysis: structure of the enzyme/sulfopyruvate complex and kinetic properties of mutants" *Biochemistry 41*, 10270-10276.

Lord, R. C., and Yu, N. T. (1970) "Laser-excited Raman spectroscopy of biomolecules. I. Native lysozyme and its constituent amino acids" *J. Mol. Biol. 50*, 509-524.

Ludwig, M. L., and Matthews, R. G. (1997) "Structure-based perspectives on B_{12}-dependent enzymes" *Annu. Rev. Biochem. 66*, 269-313.

Marquardt, J. L., Brown, E. D., Lane, W. S., Haley, T. M., Ichikawa, Y., Wong, C. H., and Walsh, C. T. (1994) "Kinetics, stoichiometry, and identification of the reactive thiolate in the inactivation of UDP-GlcNAc enolpyruvoyl transferase by the antibiotic fosfomycin" *Biochemistry 33*, 10646-10651.

Mayer, R. J., and Que, L., Jr. (1984) "^{18}O studies of pyrogallol cleavage by catechol 1,2-dioxygenase" *J. Biol. Chem. 259*, 13056-13060.

McIntire, W. S., Wemmer, D. E., Chistoserdov, A., and Lidstrom, M. E. (1991) "A new cofactor in a prokaryotic enzyme: tryptophan tryptophylquinone as the redox prosthetic group in methylamine dehydrogenase" *Science 252*, 817-824.

McQueney, M. S., Lee, S. L., Swartz, W. H., Ammon, H. L., Mariano, P. S., and Dunaway-Mariano, D. (1991) "Evidence for an intramolecular, stepwise reaction pathway for PEP phosphomutase catalyzed phosphorus-carbon bond formation" *J. Org. Chem. 56*, 7121-7130.

Michaud-Soret, I., Andersson, K. K., Que, L., Jr., and Haavik, J. (1995) "Resonance Raman studies of catecholate and phenolate complexes of recombinant human tyrosine hydroxylase" *Biochemistry 34*, 5504-5510.

Minor, W., Steczko, J., Stec, B., Otwinowski, Z., Bolin, J. T., Walter, R., and Axelrod, B. (1996) "Crystal structure of soybean lipoxygenase L-1 at 1.4 A resolution" *Biochemistry 35*, 10687-106701.

Mulliez, E., Fontecave, M., Gaillard, J., and Reichard, P. (1993) "An iron-sulfur center and a free radical in the active anaerobic ribonucleotide reductase of *Escherichia coli*" *J. Biol. Chem. 268*, 2296-2299.

Nakashita, H., Watanabe, K., Hara, O., Hidaka, T., and Seto, H. (1997) "Studies on the biosynthesis of bialaphos. Biochemical mechanism of C-P bond formation: discovery of phosphonopyruvate decarboxylase which catalyzes the formation of phosphonoacetaldehyde from phosphonopyruvate" *J. Antibiot. (Tokyo) 50*, 212-219.

Neese, F., Zumft, W. G., Antholine, W. E., and Kroneck, P. M. H. (1996) "The purple mixed-valence CuA center in nitrous-oxide reductase: EPR of the ^{63}Cu-, ^{65}Cu-, and Both ^{65}Cu- and ^{15}N histidine-enriched enzyme and a molecular orbital interpretation" *J. Am. Chem. Soc. 118*, 8692-8699.

Nelson, M. J. (1987) "The nitric oxide complex of ferrous soybean lipoxygenase-1. Substrate, pH, and ethanol effects on the active-site iron" *J. Biol. Chem. 262*, 12137-12142.

Ohlendorf, D. H., Weber, P. C., and Lipscomb, J. D. (1987) "Determination of the quaternary structure of protocatechuate 3,4-dioxygenase from *Pseudomonas aeruginosa*" *J. Mol. Biol. 195*, 225-227.

Ormö, M., deMarê, F., Regnström, K., Aberg, A., Sahlin, M., Ling, J., Loehr, T. M., Sanders-Loehr, J., and Sjöberg, B. M. (1992) "Engineering of the iron

site in ribonucleotide reductase to a self-hydroxylating monooxygenase" *J. Biol. Chem. 267*, 8711-8714.

Ortiz de Montellano, P. R. (1995) *Cytochrome P450: Structure, Mechanism, and Biochemistry*, Plenum Press, New York.

Ortiz de Montellano, P. R., and De Voss, J. J. (2002) "Oxidizing species in the mechanism of cytochrome P450" *Nat. Prod. Rep. 19*, 477-493.

Orville, A. M., Chen, V. J., Kriauciunas, A., Harpel, M. R., Fox, B. G., Mèunck, E., and Lipscomb, J. D. (1992) "Thiolate ligation of the active site Fe^{2+} of isopenicillin N synthase derives from substrate rather than endogenous cysteine: spectroscopic studies of site-specific Cys $\rightarrow$ Ser mutated enzymes" *Biochemistry 31*, 4602-4612.

Orville, A. M., and Lipscomb, J. D. (1997) "Cyanide and nitric oxide binding to reduced protocatechuate 3,4-dioxygenase: insight into the basis for order-dependent ligand binding by intradiol catecholic dioxygenases" *Biochemistry 36*, 14044-10455.

Orville, A. M., and Lipscomb, J. D. (1993) "Simultaneous binding of nitric oxide and isotopically labeled substrates or inhibitors by reduced protocatechuate 3,4-dioxygenase" *J. Biol. Chem. 268*, 8596-8607.

Palmer, G. (1979) in *The Porphyrins* (Dolphin, D. E., Ed.), Academic Press, New York.

Palmer, G. (2000) in *Physical methods in bioinorganic chemistry: spectroscopy and magnetism* (Que, L., Jr., Ed.), University Science Books, Sausalito, Calif. USA.

Pavel, E. G., Zhou, J., Busby, R. W., Gunsior, M., Townsend, C. A., and Solomon, E. I. (1998) "Circular Dichroism and Magnetic Circular Dichroism spectroscopic studies of the non-heme ferrous active site in clavaminate synthase and its interaction with α-ketoglutarate cosubstrate" *J. Am. Chem. Soc. 120*, 743-753.

Paz, M. A., Fluckiger, R., Boak, A., Kagan, H. M., and Gallop, P. M. (1991) "Specific detection of quinoproteins by redox-cycling staining" *J. Biol. Chem. 266*, 689-692.

Peisach, J., and Blumberg, W. E. (1974) "Structural implications derived from the analysis of electron paramagnetic resonance spectra of natural and artificial copper proteins" *Arch. Biochem. Biophys. 165*, 691-708.

Prescott, A. G., and Lloyd, M. D. (2000) "The iron(II) and 2-oxoacid-dependent dioxygenases and their role in metabolism" *Nat. Prod. Rep. 17*, 367-383.

Price, J. C., Barr, E. W., Glass, T. E., Krebs, C., and Bollinger, J. M., Jr. (2003) "Evidence for hydrogen abstraction from C1 of taurine by the high-spin Fe(IV) intermediate detected during oxygen activation by taurine: α-ketoglutarate dioxygenase (TauD)" *J. Am. Chem. Soc. 125*, 13008-13009.

Price, J. C., Barr, E. W., Tirupati, B., Bollinger, J. M., Jr., and Krebs, C. (2003) "The first direct characterization of a high-valent iron intermediate in the reaction of an α-ketoglutarate-dependent dioxygenase: A high-spin Fe(IV) complex in taurine/α-ketoglutarate dioxygenase (TauD) from *Escherichia coli*" *Biochemistry 42*, 7497-7508.

Pyrz, J. W., Roe, A. L., Stern, L. J., and Que, L., Jr. (1985) "Model studies of iron-tyrosinate proteins" *J. Am. Chem. Soc. 107*, 614-620.

Que, L., Jr. (1988) *Biological Applications of Raman Spectroscopy*, Vol. 3, Wiley, New York.

Que, L., Jr. (2000) "One motif--many different reactions" *Nat. Struct. Biol. 7*, 182-184.

Ramsey, A. J., Daubner, S. C., Ehrlich, J. I., and Fitzpatrick, P. F. (1995) "Identification of iron ligands in tyrosine hydroxylase by mutagenesis of conserved histidinyl residues" *Protein. Sci. 4*, 2082-2086.

Reginato, N., McCrory, C. T. C., Pervitsky, D., and Li, L. (1999) "Synthesis, X-ray crystal structure, and solution behavior of $Fe(NO)_2(1\text{-}MeIm)_2$: implications for nitrosyl non-heme-iron complexes with $g = 2.03$" *J. Am. Chem. Soc. 121*, 10217-10218.

Roach, P. L., Clifton, I. J., Hensgens, C. M., Shibata, N., Schofield, C. J., Hajdu, J., and Baldwin, J. E. (1997) "Structure of isopenicillin N synthase complexed with substrate and the mechanism of penicillin formation" *Nature 387*, 827-830.

Rocklin, A. M., Tierney, D. L., Kofman, V., Brunhuber, N. M. W., Hoffman, B. M., Christoffersen, R. E., Reich, N. O., Lipscomb, J. D., and Que, L., Jr.

(1999) "Role of the nonheme Fe(II) center in the biosynthesis of the plant hormone ethylene" *Proc. Natl. Acad. Sci. USA 96*, 7905-7909.

Rogers, T. O., and Birnbaum, J. (1974) "Biosynthesis of fosfomycin by *Streptomyces fradiae*" *Antimicrob. Agents. Chemother. 5*, 121-132.

Rohde, J. U., In, J. H., Lim, M. H., Brennessel, W. W., Bukowski, M. R., Stubna, A., Münck, E., Nam, W., and Que, L., Jr. (2003) "Crystallographic and spectroscopic characterization of a nonheme Fe(IV)-O complex" *Science 299*, 1037-1039.

Ryle, M. J., Liu, A., Muthukumaran, R. B., Ho, R. Y., Koehntop, K. D., McCracken, J., Que, L., Jr., and Hausinger, R. P. (2003) "O_2- and α-ketoglutarate-dependent tyrosyl radical formation in TauD, an α-keto acid-dependent non-heme iron dioxygenase" *Biochemistry 42*, 1854-1862.

Ryle, M. J., Padmakumar, R., and Hausinger, R. P. (1999) "Stopped-flow kinetic analysis of Escherichia coli taurine/α-ketoglutarate dioxygenase: interactions with α-ketoglutarate, taurine, and oxygen" *Biochemistry 38*, 15278-15286.

Sahlin, M., Gräslund, A., and Ehrenberg, A. (1986) "Determination of relaxation time for a free radical from microwave saturation studies." *J. Magn. Reson. 67*, 135-137.

Salama, S., Stong, J. D., Neilands, J. B., and Spiro, T. G. (1978) "Electronic and resonance Raman spectra of iron(III) complexes of enterobactin, catechol, and *N*-methyl-2,3-dihydroxybenzamide" *Biochemistry 17*, 3781-3785.

Sato, N., Uragami, Y., Nishizaki, T., Takahashi, Y., Sazaki, G., Sugimoto, K., Nonaka, T., Masai, E., Fukuda, M., and Senda, T. (2002) "Crystal structures of the reaction intermediate and its homologue of an extradiol-cleaving catecholic dioxygenase" *J. Mol. Biol. 321*, 621-636.

Seidel, H. M., Freeman, S., Seto, H., and Knowles, J. R. (1988) "Phosphonate biosynthesis: isolation of the enzyme responsible for the formation of a carbon-phosphorus bond" *Nature 335*, 457-458.

Senda, T., Sugiyama, K., Narita, H., Yamamoto, T., Kimbara, K., Fukuda, M., Sato, M., Yano, K., and Mitsui, Y. (1996) "Three-dimensional structures of free form and two substrate complexes of an extradiol ring-cleavage type dioxygenase, the BphC enzyme from *Pseudomonas sp*. strain KKS102" *J. Mol. Biol. 255*, 735-752.

Seto, H., Hidaka, T., Kuzuyama, T., Shibahara, S., Usui, T., Sakanaka, O., and Imai, S. (1991) "Studies on the biosynthesis of fosfomycin. 2. Conversion of 2-hydroxypropyl-phosphonic acid to fosfomycin by blocked mutants of *Streptomyces wedmorensis*" *J. Antibiot. (Tokyo) 44*, 1286-1288.

Seto, H., and Kuzuyama, T. (1999) "Bioactive natural products with carbon-phosphorus bonds and their biosynthesis" *Nat. Prod. Rep. 16*, 589-596.

Siegmund, H. U., and Kaufman, S. (1991) "Hydroxylation of 4-methylphenylalanine by rat liver phenylalanine hydroxylase" *J. Biol. Chem. 266*, 2903-2910.

Sjöberg, B. M., Reichard, P., Gräslund, A., and Ehrenberg, A. (1977) "Nature of the free radical in ribonucleotide reductase from *Escherichia coli*" *J. Biol. Chem. 252*, 536-541.

Smith, J. J., Thomson, A. J., Proudfoot, A. E., and Wells, T. N. (1997) "Identification of an Fe(III)-dihydroxyphenylalanine site in recombinant phosphomannose isomerase from *Candida albicans*" *Eur. J. Biochem. 244*, 325-333.

Sofia, H. J., Chen, G., Hetzler, B. G., Reyes-Spindola, J. F., and Miller, N. E. (2001) "Radical SAM, a novel protein superfamily linking unresolved steps in familiar biosynthetic pathways with radical mechanisms: functional characterization using new analysis and information visualization methods" *Nucleic Acids Res. 29*, 1097-1106.

Solomon, E. I., Brunold, T. C., Davis, M. I., Kemsley, J. N., Lee, S.-K., Lehnert, N., Neese, F., Skulan, A. J., Yang, Y.-S., and Zhou, J. (2000) "Geometric and electronic structure/function correlations in non-heme iron enzymes" *Chem. Rev. 100*, 235-349.

Solomon, E. I., Zhou, J., Neese, F., and Pavel, E. G. (1997) "New insights from spectroscopy into the structure/function relationships of lipoxygenases" *Chem. Biol. 4*, 795-808.

Sono, M., Roach, M. P., Coulter, E. D., and Dawson, J. H. (1996) "Heme-containing 0xygenases" *Chem. Rev. 96*, 2841-2887.

Stubbe, J., and van der Donk, W. A. (1998) "Protein radicals in enzyme catalysis" *Chem. Rev. 98*, 705-762.

Thornburg, L. D., Lai, M. T., Wishnok, J. S., and Stubbe, J. (1993) "A non-heme iron protein with heme tendencies: an investigation of the substrate specificity of thymine hydroxylase" *Biochemistry 32*, 14023-14033.

Tomasi, A., and Iannone, A. (1993) in *Biological Magnetic Resonance* (Berliner, L. J., and Reuben, J., Eds.) pp 353-384, Plenum Press, New York.

Tsuruoka, T., Miyata, A., and Yamada, Y. (1978) "Two kinds of mutants defective in multiple carbohydrate utilization isolated from in vitro fosfomycin-resistant strains of *Escherichia coli* K--12" *J. Antibiot. (Tokyo) 31*, 192-201.

Unkrig, V., Neugebauer, F. A., and Knappe, J. (1989) "The free radical of pyruvate formate-lyase. Characterization by EPR spectroscopy and involvement in catalysis as studied with the substrate-analogue hypophosphite" *Eur. J. Biochem. 184*, 723-728.

Valegård, K., Terwisscha van Scheltinga, A. C., Dubus, A., Ranghino, G., Oster, L. M., Hajdu, J., and Andersson, I. (2004) "The structural basis of cephalosporin formation in a mononuclear ferrous enzyme" *Nat. Struct. Mol. Biol. 11*, 95-101.

Valegård, K., van Scheltinga, A. C., Lloyd, M. D., Hara, T., Ramaswamy, S., Perrakis, A., Thompson, A., Lee, H. J., Baldwin, J. E., Schofield, C. J., Hajdu, J., and Andersson, I. (1998) "Structure of a cephalosporin synthase" *Nature 394*, 805-809.

Waite, J. H., Housley, T. J., and Tanzer, M. L. (1985) "Peptide repeats in a mussel glue protein: theme and variations" *Biochemistry 24*, 5010-5014.

Waite, J. H., and Rice-Ficht, A. C. (1989) "A histidine-rich protein from the vitellaria of the liver fluke *Fasciola hepatica*" *Biochemistry 28*, 6104-6110.

Wallar, B. J., and Lipscomb, J. D. (1996) "Dioxygen activation by enzymes containing binuclear non-heme iron clusters" *Chem. Rev. 96*, 2625-2657.

Wang, L., Erlandsen, H., Haavik, J., Knappskog, P. M., and Stevens, R. C. (2002) "Three-dimensional structure of human tryptophan hydroxylase and its implications for the biosynthesis of the neurotransmitters serotonin and melatonin" *Biochemistry 41*, 12569-12574.

Westrich, L., Heide, L., and Li, S. M. (2003) "CloN6, a novel methyltransferase catalysing the methylation of the pyrrole-2-carboxyl moiety of clorobiocin" *Chembiochem 4*, 768-773.

Whittaker, M. M., Kersten, P. J., Nakamura, N., Sanders-Loehr, J., Schweizer, E. S., and Whittaker, J. W. (1996) "Glyoxal oxidase from *Phanerochaete chrysosporium* is a new radical-copper oxidase" *J. Biol. Chem. 271*, 681-687.

Whittaker, M. M., and Whittaker, J. W. (1990) "A tyrosine-derived free radical in apogalactose oxidase" *J. Biol. Chem. 265*, 9610-9613.

Wolfe, M. D., and Lipscomb, J. D. (2003) "Hydrogen peroxide-coupled cis-diol formation catalyzed by naphthalene 1,2-dioxygenase" *J. Biol. Chem. 278*, 829-835.

Wolgel, S. A., Dege, J. E., Perkins-Olson, P. E., Jaurez-Garcia, C. H., Crawford, R. L., Münck, E., and Lipscomb, J. D. (1993) "Purification and characterization of protocatechuate 2,3-dioxygenase from *Bacillus macerans*: a new extradiol catecholic dioxygenase" *J. Bacteriol. 175*, 4414-4426.

Woolum, J. C., Tiezzi, E., and Commoner, B. (1968) "Electron spin resonane of iron-nitric oxide complexes with amino acids, peptides and proteins" *Biochim. Biophys. Acta. 160*, 311-320.

Woschek, A., Wuggenig, F., Peti, W., and Hammerschmidt, F. (2002) "On the transformation of (*S*)-2-hydroxypropylphosphonic acid into fosfomycin in *Streptomyces fradiae*--a unique method of epoxide ring formation" *Chembiochem 3*, 829-835.

Zhang, Y., Pavlosky, M. A., Brown, C. A., Westre, T. E., Hedman, B., Hodgson, K. O., and Solomon, E. I. (1992) "Spectroscopic and theoretical description of the electronic structure of the $S = 3/2$ nitrosyl complex of non-heme iron enzymes" *J. Am. Chem. Soc. 114*, 9189-9191.

Zhang, Z., Barlow, J. N., Baldwin, J. E., and Schofield, C. J. (1997) "Metal-catalyzed oxidation and mutagenesis studies on the iron(II) binding site of 1-aminocyclopropane-1-carboxylate oxidase" *Biochemistry 36*, 15999-16007.

Zhang, Z., Ren, J., Harlos, K., McKinnon, C. H., Clifton, I. J., and Schofield, C. J. (2002) "Crystal structure of a clavaminate synthase-Fe(II)-2-oxoglutarate-

substrate-NO complex: evidence for metal centered rearrangements" *FEBS Lett. 517*, 7-12.

Zhang, Z., Ren, J., Stammers, D. K., Baldwin, J. E., Harlos, K., and Schofield, C. J. (2000) "Structural origins of the selectivity of the trifunctional oxygenase clavaminic acid synthase" *Nat. Struct. Biol. 7*, 127-133.

Zhang, Z., Ren, J. S., Clifton, I. J., and Schofield, C. J. (2004) "Crystal structure and mechanistic implications of 1-aminocyclopropane-1-carboxylic acid oxidase-the ethylene-forming enzyme" *Chem. Biol. 11*, 1383-1394.

Zhao, Z., Liu, P., Murakami, K., Kuzuyama, T., Seto, H., and Liu, H.-w. (2002) "Mechanistic studies of HPP epoxidase: configuration of the substrate governs its enzymatic fate" *Angew. Chem. Int. Ed. 41*, 4529-4532.

Vita

Feng Yan was born in Hefei, Anhui, China on November 16, 1975, the son of Zhijian Yan and Yanming Zhang. After completing his work at Hefei No. 1 High School, in 1990, he was recommended for admission to Tsinghua University, Beijing, China, waived of the national admission exam. He graduated from Tsinghua University with B.S. degree in Chemistry in 1997, as the top one student of the class. In the following year, Feng entered the Graduate School of The University of Minnesota, Minneapolis, and joined the research group of Dr. Hung-wen (Ben) Liu there. While at UMN, he completed two years of teaching assistantship. In 2001, he moved with Dr. Liu and other group members to Austin and continued his graduate studies at Department of Chemistry and Biochemistry of The University of Texas. His work on the enzyme HppE in fosfomycin biosynthesis has resulted in a few co-authored research articles.

Permanent address: 7600 Wood Hollow Drive, APT 916, Austin, TX 78731

This dissertation was typed by Feng Yan.